MEASUREMENTS AND PREDICTIONS OF TURBULENT FLOW AND HEAT TRANSFER IN TRAPEZOIDAL DUCTS

by

Mahmoud Mohamad A. Khalifa

A thesis
presented to the University of Manitoba
in partial fulfillment of the
requirements for the degree of
Doctor of Philosophy
in
Mechanical Engineering Department

Winnipeg, Manitoba

(c) Mahmoud Mohamad A. Khalifa, 1986

Permission has been granted to the National Library of Canada to microfilm this thesis and to lend or sell copies of the film.

The author (copyright owner) has reserved other publication rights, and neither the thesis nor extensive extracts from it may be printed or otherwise reproduced without his/her written permission.

L'autorisation a été accordée à la Bibliothèque nationale du Canada de microfilmer cette thèse et de prêter ou de vendre des exemplaires du film.

L'auteur (titulaire du droit d'auteur) se réserve les autres droits de publication; ni la thèse ni de longs extraits de celle-ci ne doivent être imprimés ou autrement reproduits sans son autorisation écrite.

ISBN 0-315-33995-0

MEASUREMENTS AND PREDICTIONS OF TURBULENT FLOW AND HEAT TRANSFER IN TRAPEZOIDAL DUCTS

BY

MAHMOUD MOHAMAD A. KHALIFA

A thesis submitted to the Faculty of Graduate Studies of the University of Manitoba in partial fulfillment of the requirements of the degree of

DOCTOR OF PHILOSOPHY

© 1986

Permission has been granted to the LIBRARY OF THE UNIVERSITY OF MANITOBA to lend or sell copies of this thesis, to the NATIONAL LIBRARY OF CANADA to microfilm this thesis and to lend or sell copies of the film, and UNIVERSITY MICROFILMS to publish an abstract of this thesis.

The author reserves other publication rights, and neither the thesis nor extensive extracts from it may be printed or otherwise reproduced without the author's written permission.

ACKNOWLEDGEMENTS

The auther wishes to express his deep gratitude and appreciation to his supervisor, Professor Dr. A. C. Trupp, Mechanical Engineering Department, for his precious guidance, and sincere help through the completion of this thesis. Thanks are also due to Mr. W. Barrett for the assistance during the course of the experimental work, and Mr. H. Weiss for drafting most of the figures.

The funding for the present research was provided by the Natural Sciences and Engineering Research Council of Canada through a grant to Dr. A. C. Trupp, and their support is gratefully acknowledged.

ABSTRACT

Fully developed turbulent isothermal air flows through a symmetric trapezoidal duct of 60° acute angle and 0.77 aspect ratio were investigated experimentally for Reynolds numbers of 37,000 to 116,000. The measurements included local wall shear stresses, axial pressure gradient, mean axial velocities, the Reynolds stresses (except $\rho\overline{vw}$) and the secondary velocities. The secondary flow pattern was found to consist of four flow cells per symmetric half of the trapezoidal duct. Maximum secondary velocities of about 2% of the average mean axial velocity were observed. The effects of the secondary flow currents on the distributions of mean axial velocity, turbulent kinetic energy and wall shear stress were clearly evident.

A two-equation turbulence model (k-ϵ) was used to predict the fluid flow and heat transfer characteristics under fully developed turbulent flow conditions. The six, non-linear, elliptic equations for stream function, axial vorticity, mean axial velocity, turbulent kinetic energy, turbulence kinetic energy dissipation rate and temperature were solved by the general elliptic finite difference procedure of Gosman et al. [1] using Seale's vorticity source model [2]. Predictions were made and are presented for the present tra-

pezoidal duct for Reynolds number in the range 20,000 to 200,000. The flow structure of Rodet's trapezoidal duct [3] (acute angle ϕ = 75°, aspect ratio a/b = 0.536) was also predicted. Results are also presented for the Chiranjivi & Sankara Rao trapezoidal duct [4] (acute angle ϕ = 70°, aspect ratio a/b = 0.28). The model constants used for these two predictions were identical to that used for the present trapezoidal duct. The predicted flow characteristics are shown to be in reasonable agreement with the available experimental data.

In addition to the fluid flow, heat transfer predictions were made and are presented for the three trapezoidal ducts. For these solutions the thermal boundary condition was axially uniform heat input with constant peripheral wall temperature. The predicted results provide the cross-sectional distribution of air temperature, the distributions of local heat flux and the average Nusselt numbers for the investigated range. The available experimental and analytical heat transfer data are compared with the present predictions. The agreement is seen to be reasonable.

LIST OF TABLES

Table		Page
1	Uncertainties in Experimental Measurements	143
2	Near-wall Velocity Distributions (Re=99,000)	144
3	Relationships Between The Turbulence Intensities	145
4	Comparisons of the k-ϵ Model Constants of The Present Work With Those Employed by Others	147
5	Coefficients in the General Elliptic Differential Equation (6.1)	148

LIST OF FIGURES

Figure		Page
1	Cross-Section of Trapezoidal Duct Test Section	149
2a	General Cross-Section of Trapezoidal Duct	150
2b	Shape of the Present Trapezoidal Duct Relative to [3] , [4] and [5]	150
3	Primary Flow Cell for the Analytical Model	151
4a	Side Elevation View of Test Rig	152
4b	Traversing Mechanism Assembly	153
5a	Measurement Grid for X-Probe	154
5b	Measurement Grid for Pitot-tube, Single Hot-wire and 45° Slanting Wire	155
6	Friction Factor vs Reynolds Number for the Trapezoidal Ducts	156
7	Wall Shear Stress Distributions for Bottom Wall	157
8	Wall Shear Stress Distributions for Top Wall	158
9	Wall Shear Stress Distributions for Inclined Wall	159

10 Contour Plots of Axial Velocity 160

11 Contour Plots of Axial Velocity 161

12a Mean Velocity Distributions Near Bottom Wall; Re = 99,000 162

12b Mean Velocity Distributions Near Top Wall; Re = 99,000 163

12c Mean Velocity Distributions Near Inclined Wall; Re = 99,000 164

13 Distributions of $(\overline{u^2})^{1/2}/\overline{u^*}$ Via Single Hot-wire; Re = 99,000 165

14 Distributions of $(\overline{v^2})^{1/2}/\overline{u^*}$; Re = 99,000 166

15 Distributions of $(\overline{w^2})^{1/2}/\overline{u^*}$; Re = 99,000 167

16 Distributions of $(\overline{u^2})^{1/2}/\overline{u^*}$ at z/b =0.5 Using Different Probes; Re = 79,000 168

17 Distributions of $(\overline{u^2})^{1/2}/\overline{u^*}$ at z/b =0.124 Using Different Probes; Re = 99,000 169

18 Distributions of $(\overline{u^2})^{1/2}/\overline{u^*}$ Along Duct Symmetry Line; Re=99,000 170

19 Distributions of $(\overline{v^2})^{1/2}/\overline{u^*}$ Along Duct Symmetry Line; Re=99,000 171

20 Distributions of $(\overline{w^2})^{1/2}/\overline{u^*}$ Along Duct Symmetry Line; Re=99,000 172

21 Contours of $(\overline{u^2})^{1/2}/\overline{u^*}$; Re=99,000 173

22 Contours of $(\overline{v^2})^{1/2}/\overline{u^*}$; Re=99,000 174

23 Contours of $(\overline{w^2})^{1/2}/\overline{u}^*$; Re=99,000 175

24 Contours of $\overline{uv}/(\overline{u}^*)^2$; Re=99,000 176

25 Distributions of Shear Stress $\rho\overline{uv}$; Re=99,000. . . 177

26 Contours of $\overline{uw}/(\overline{u}^*)^2$; Re=99,000 178

27 Distributions of Shear Stress $\rho\overline{uw}$; Re=99,000 . . 179

28 Distributions of Primary Shear Stress Along Duct Symmetry Line (y=0); Re=99,000 180

29 Distributions of k Normal to Walls; Re=99,000 . . 181

30 Contour Plots of $k/(\overline{u}^*)^2$. 182

31 Relationships Between u^+ and k^+, v^+ and w^+ for the Rectangular Domain: $0 \leq y/a \leq 1$, $0 \leq z/b \leq 1$; Re= 99,000. 183

32 Distributions of $\overline{W}$ for Three Horizontal Traverses; Re=99,000 184

33 Distributions of $\overline{V}$ for Three Vertical Traverses; Re=99,000 185

34 Secondary Flow Pattern in a Trapezoidal Duct; Re= 99,000. 186

35 Finite Difference Grid For Numerical Predictions 187

36 Finite Difference Area of Integration 188

37 Predictions of $\overline{U}/U_b$ Using Different Grid Systems at z/b =0.5; Re = 99,000 189

38 Predictions of $k/(\bar{u}^*)^2$ Using Different Grid Systems at $z/b = 0.406$; Re = 99,000 190

39 Comparison of Predicted and Measured $\bar{U}/U_b$ Along Horizontal Traverses; Re = 99,000 191

40 Comparison of Predicted and Measured $\bar{U}/U_b$; Re=99,000 192

41 Variation of Maximum Axial Velocity ($\bar{U}_{max}$) With Reynolds Number 193

42 Comparison of Predicted and Measured $k/(\bar{u}^*)^2$ Along Horizontal Traverses; Re=99,000 . . 194

43 Comparison of Predicted and Measured $k/(\bar{u}^*)^2$; Re = 99,000 195

44 Contour Plots of Stream Function Ψ and Axial Vorticity ω; Re=99,000 196

45 Comparison of Predicted and Measured Secondary Flow Component $\bar{V}$; Re = 99,000 197

46 Comparison of Predicted and Measured Secondary Flow Component $\bar{W}$; Re = 99,000 198

47 Contour Plots of Secondary Velocities; Re=99,000. 199

48 Contour Plots of Temperature Distribution T*; Re=99,000 200

49 Comparison of Predicted and Measured Local Wall Shear Stress for Bottom Wall; Re = 116,000 201

50 Comparison of Predicted and Measured Local Wall Shear Stress for Top Wall; Re = 116,000 202

51 Comparison of Predicted and Measured Local Wall Shear Stress for Inclined Wall; Re = 116,000 203

52 Local Heat Flux Distribution Along The Bottom Wall; Re = 99,000 204

53 Local Heat Flux Distribution Along The Top Wall; Re = 99,000 205

54 Local Heat Flux Distribution Along The Inclined Wall; Re = 99,000 206

55 Comparison of Predicted and Measured Friction Factors 207

56 Average Nusselt Number vs Reynolds Number 208

57 Effect of Reynolds Number on $\overline{U}/U_b$ 209

58 Effect of Reynolds Number on $k/(\overline{u}^*)^2$ 210

59 Effect of Reynolds Number on T^* 211

60 Contour Plots of $\Psi/(\rho U_b D_h)x1000$ 212

61 Effect of Reynolds Number on $(\overline{V}/U_b)$ 213

62 Effect of Reynolds Number on $(\overline{W}/U_b)$ 214

63 Effect of Reynolds Number on $(\overline{V}/u^*)$ 215

64 Effect of Reynolds Number on $(\overline{W}/u^*)$ 216

65 Effect of Reynolds Number on Local Wall Shear Stress 217

66 Effect of Reynolds Number on Local Wall Heat Flux 218

67 Comparison of Friction Factors for Three Trapeziodal Ducts 219

68 Comparison of Nusselt Number for Three Trapeziodal Ducts 220

69 Comparison of Nusselt Number With Experiment [4] 221

70 Contour Plots of $\overline{U}/\overline{U}_{max}$ x 1000; C′= 0.045, Re=240,000. 222

71 Contour Plots of $\overline{U}/\overline{U}_{max}$ x 1000; C′= 0.055, Re=240,000. 223

72 Contour Plots of $2k/(\overline{U}_{max})^2$ x 10000; Re=240,000 224

73 Contour Plots of $k/(\overline{u}^*)^2$ and $\overline{U}/U_b$ for the Duct of [4]; Re=100,000 225

74 Comparison of Local Friction Velocity With Experiment [3]; Re=240,000 226

75 Local Wall Shear Stress and Heat Flux for the Duct of [4]; Re=100,000 227

NOMENCLATURE

a,b,c,d	Trapezoidal Duct Dimensions; See Figs. 2a and 1
a_ϕ, b_φ	Finite Difference Equation Coefficients
A,B	Universal Law of The Wall Constants
C,D	Coefficients of Intensity Correlations (see Table 3)
C1,C2,C_μ,C′,C″	Turbulence Model Constants
C_p	Constant Pressure Specific Heat
D_h	Equivalent Hydraulic Diameter
f	Friction Factor , $f=8\bar{\tau}_w/(\rho U_b^2)$
i	Fluctuating Component of Enthalpy
I	Mean (time-average) Enthalpy
k	Mean Turbulent Kinetic Energy; $(u^2+v^2+w^2)^{1/2}/2$
k^+	Dimensionless Turbulent Kinetic Energy; $k/(\bar{u}^*)^2$
l	Turbulence Mixing Length
m	Mass Flow Rate
n	Anisotropy Factor , Equation (5.4a)

Nu	Average Nusselt number; $Nu=\dot{q}_{av} D_h/(\lambda(T_w-T_b))$
p	Pressure
p*	Jayatillake Function , Equation (5.19)
Pr	Prandtl Number , $\mu C_p/\lambda$
Pr_t	Turbulent Prandtl Number
$\dot{q}$	Local Heat Flux at The Wall
$\dot{q}_{av}$	Average of Local Heat Fluxes Over All Walls
Re	Reynolds Number Based on U_b and D_h
s	Distance Along Inclined wall; See Fig. 1
S	Source Term , Equation (3.14a)
t	Fluctuating Component of Temperature (also time)
T_b	Mean Temperature (time-average)
T_w	Average Mean Temperature Over Primary Flow Cell (bulk temperature)
T	Wall Temperature
T*	$(T_w - \overline{T})/(T_w - T_b)$
u,v,w	Fluctuating Components of The Velocities in The x,y and z Directions Respectively

u^+, v^+, w^+	Dimensionless Turbulence Intensities; $(\overline{u^2})^{1/2}/\bar{u}^*, (\overline{v^2})^{1/2}/\bar{u}^*, (\overline{w^2})^{1/2}/\bar{u}^*$
u^*	Local Friction Velocity , $(\tau/\rho)^{1/2}$
$\bar{u}^*$	Average Friction Velocity; $(\bar{\tau}_w/\rho)^{1/2}$
$\bar{U}$	Axial Mean Velocity (time-average)
U_b	Average Mean Axial Velocity Over Primary Flow Cell (bulk velocity)
$\bar{U}_{sec}$	Resultant of $\bar{V}$ and $\bar{W}$, $(\bar{V}^2+\bar{W}^2)^{1/2}$
U^+	Dimensionless Velocity, $\bar{U}/u^*$
$\bar{V}, \bar{W}$	Mean Velocities in the y and z Directions (secondary velocities)
x	Axial Coordinate
y,z	Horizontal and Vertical Directions, See Fig. 1
z^+	Dimensionless Distance From (and normal to) a Wall, zu^*/ν
z	Normal Distance From The Wall to Surface of no Shear
μ	Fluid Laminar Dynamic Viscosity
μ_t	Isotropic Eddy Viscosity
ν	Kinematic Viscosity, μ/ρ
λ	Fluid Thermal Conductivity
ρ	Fluid Density

τ	Local Wall Shear Stress
$\bar{\tau}_w$	Average of Local Wall Shear Stresses Over All Walls
ϕ	Corner Angle of Trapezoidal Duct; See Fig. 2a
Φ	Parameter in The General Elliptic Equation (6.1)
ϵ	Dissipation Rate of Turbulence Kinetic Energy
κ	Von-Karman Constant
$\sigma_\varepsilon, \sigma_k$	Turbulence Model Constants (see Table 2)
ξ	Convergence Criterion
Ψ	Stream Function Defined by Equation (3.7)
ω	Axial Vorticity Defined by Equation (3.6)
σ	Standard Deviation (%); See Table 3

Subscripts

b	Bulk
h	Hydraulic
i,j	Finite Difference Indices (directions)
max	Maximum

-	Overbar Designates Time Averaging

Superscript	
+	Non-dimensionalized

CONTENTS

ACKNOWLEDGEMENTS iv

ABSTRACT v

LIST OF TABLES vii

LIST OF FIGURES viii

NOMENCLATURE xiv

page

INTRODUCTION 1

1.1 Motivation 1
1.2 Scope and Objectives 3

LITERATURE REVIEW 5

2.1 Introduction 5
2.2 Review of Experimental Work 6
2.2.1 Trapezoidal Ducts 6
2.2.2 Other Non-Circular Ducts 7
2.3 Review of Theoretical Work 10
2.3.1 Trapezoidal Ducts 10
2.3.2 Other Non-Circular Ducts 11
2.4 Turbulence Models 13
2.4.1 General 13
2.4.2 Survey of Existing Turbulence Models . . . 13
2.4.3 Choice of k - ϵ Model 15

GOVERNING EQUATIONS 17

3.1 Continuity and Reynolds Equations 17
3.2 Stream Function and Axial Vorticity Equations 20
3.3 Turbulent Kinetic Energy Equation 21
3.4 Turbulence Energy Dissipation Rate Equation . . 22
3.5 Enthalpy Equation 23
3.6 Governing Equations in Ψ Form 23

EXPERIMENTAL FACILITY AND MEASUREMENTS 26

4.1 Test Rig 26
4.2 Test Section 26
4.3 Traversing Mechanism 27

4.4 Instrumentation 27
4.5 Experimental Results and Discussion 29
4.5.1 General 29
4.5.2 Accuracy of Measurements 30
4.5.3 Friction Factors 32
4.5.4 Local Wall Shear Stress 34
4.5.5 Mean Axial Velocity 36
4.5.6 Reynolds Stresses 38
4.5.7 Turbulent Kinetic Energy 43
4.5.8 Secondary Velocities 45

THE ANALYTICAL MODEL 48

5.1 Vorticity Source Term Modelling 48
5.2 Closure of k, ϵ and $\overline{T}$ Equations 52
5.3 Boundary Conditions 53
5.3.1 Stream Function (Ψ) 53
5.3.2 Axial Vorticity (ω) 53
5.3.3 $\overline{U}$, k, ϵ and $\overline{T}$ 53
5.4 Summary of Equations to be Solved 56
5.4.1 Transport Equations 56
5.4.2 Algebraic Equations 58
5.4.3 Boundary Conditions 59
5.4.4 Model Constants 60

THE NUMERICAL PROCEDURE 61

6.1 Introduction 61
6.2 The Finite Difference Equations 61
6.2.1 Convection Term 62
6.2.2 Diffusion Term 65
6.2.3 Source Term 67
6.2.4 The Complete Finite-Difference Equation 67
6.3 Stability of the Successive Substitution Formula 68
6.3.1 General 68
6.3.2 Modifications of k and ϵ Source Terms . . 69
6.4 Iterative Technique 70
6.5 Convergence Criterion 70
6.6 Initial Conditions 71
6.7 The Grid Spacing 71

RESULTS AND DISCUSSION OF THE NUMERICAL PROCEDURE 73

7.1 General 73
7.2 Mean Axial Velocity Distribution 74
7.3 Mean Turbulent Kinetic Energy Distribution . . 75
7.4 Vorticity and Stream Function Distributions . . 76
7.5 Secondary Velocities 76
7.6 Temperature Distribution 77
7.7 Wall Shear Stress 78
7.8 Wall Heat Flux 79
7.9 Friction Factor and Nusselt Number 79
7.10 Effect of Reynolds Number 80

PREDICTIONS OF OTHER TRAPEZOIDAL DUCTS 82

8.1 General 82
8.2 Friction Factor and Nusselt Number 82
8.3 Mean Axial Velocity and Turbulent Kinetic Energy 84
8.4 Local Friction Velocity and Heat Flux 85

CONCLUSIONS AND RECOMMENDATIONS FOR FUTURE WORK 87

REFERENCES 89

APPENDIX A: DERIVATION OF EQUATION FOR SOURCE OF VORTICITY IN A TRAPEZOIDAL DUCT 98

APPENDIX B: COMPUTER CODE FOR TRAPEZOIDAL DUCTS 106

NOMENCLATURE OF THE COMPUTER PROGRAM 109

TABLES 1 - 5 143-148

FIGURES 1 - 75 149-227

CHAPTER 1

INTRODUCTION

1.1 MOTIVATION

Turbulent flows in ducts of non-circular cross-section are often encountered in engineering practice. Examples are flows in heat exchangers, ventilation and air-conditioning systems, nuclear reactors, turbomachinery, open channels, canals and rivers. The flow in such ducts is accompanied by secondary motions in the plane perpendicular to the streamwise direction. If these ducts are straight, the secondary motion is caused by turbulence and it is called secondary motion of Prandtl's second kind. In curved ducts, where centrifugal forces act at right angles to the main flow direction, this motion is pressure induced and is said to be of Prandtl's first kind. This first kind also exists in curved circular ducts and for laminar flow.

For straight ducts, Prandtl and Nikuradse were probably the first to describe the differences between flow in a circular pipe (rectilinear) and a square duct (helical). The effect of the secondary flow on the lines of constant velocity is to transport these lines in the direction of the secondary flow. Although the turbulence driven secondary velocity is only of the order of 2% of the streamwise bulk

velocity, this motion can have important consequences. By transporting high momentum fluid in the core region towards the corners, it causes bulging of the axial velocity contours towards the corners of the duct.

A detailed investigation of secondary velocities and their effects on the turbulence structure and overall bulk values for friction factor and Nusselt number is important. Also the growing interest in developing multi-passage tubes for compact heat exchangers encourages the investigation of turbulent flow and heat transfer characteristics in non-circular ducts. A literature survey (Chapter 2) on turbulent flow and heat transfer through straight non-circular ducts has shown that trapezoidal ducts have not received much attention either experimentally or analytically. The present research evolved from a desire to obtain turbulent flow data for this duct. It involves an experimental and analytical investigation of the turbulence structure and secondary flows in fully developed turbulent flow in a symmetric trapezoidal duct. This duct represents a complicated secondary flow pattern geometry. Hence, detailed experimental data (including secondary flow measurements) should be extremely useful as a test case in regard to development of numerical prediction schemes. This could lead to better design concepts and confirmation of mathematical models of turbulence.

1.2 SCOPE AND OBJECTIVES

The experimental study described herein concerns the fully developed, turbulent, adiabatic air flow structure in a trapezoidal duct with 60° acute angle and aspect ratio a/b =0.77. The Pitot tube and hot wire measurements were conducted on the test section shown in Fig. 1. The measurements which include axial static pressure drop, axial velocity, local wall shear stress, secondary velocities and Reynolds stresses (except $\rho\overline{vw}$) were made mainly at Reynolds numbers (based on equivalent hydraulic diameter) of 79,000 and 99,000.

For the analytical work, a two-equation turbulence model (k-ϵ) along with an algebraic model for Reynolds stresses was used for prediction of fully developed turbulent flow and heat transfer in trapezoidal ducts. The six coupled, non-linear, elliptic equations for axial vorticity, stream function, turbulent kinetic energy, kinetic energy dissipation rate, mean axial velocity and enthalpy were solved by means of the general elliptic finite difference procedure of Gosman et al. [1]. The algebraic model for the vorticity source adopted the procedure outlined by Seale [2]. The analytical model was applied to predict the fully developed turbulent flow characteristics for the present trapezoidal duct. The results were in reasonable agreement with the experimental measurements. With the same model constants, the analytical model was applied to predict the fully developed

turbulent flow and heat transfer in two other trapezoidal ducts.

CHAPTER 2

LITERATURE REVIEW

2.1 INTRODUCTION

Information about the flow and temperature fields in the complex geometrical configurations found in compact heat exchangers, nuclear reactors, air conditioning systems, etc. is of major interest to engineers. Over the past two decades, a considerable number of experimental and numerical investigations have been carried out on turbulent flow in straight non-circular ducts. The flow cross-section for each of these ducts is usually symmetric in two or more parts; each symmetric part being called a primary flow cell. Due to symmetry there can be no net transfer of momentum or energy across the boundaries of a primary flow cell. For the same reason secondary flows cannot cross a primary flow cell boundary. In terms of secondary flow, non-circular ducts may be placed into three classes according to the number of secondary flow cells in each primary flow cell. These classes are :

Class 1- One cell per primary flow cell as in square ducts, equilateral triangular ducts, etc.

Class 2- Two cells per primary flow cell as in rectangular ducts, internally finned tubes, etc.

Class 3- Three or more cells per primary flow cell as in trapezoidal ducts, isosceles triangular ducts, etc. The following is a brief presentation of the experimental and numerical work available in the literature for different secondary flow geometries.

2.2 REVIEW OF EXPERIMENTAL WORK

2.2.1 Trapezoidal Ducts

For symmetric trapezoidal ducts of the type shown in Fig. 2a, the shape of any family member can be specified by ϕ and the ratio a/b. As an example, for ϕ =60° the limiting cases are the equilateral triangular duct (a/b= 0) and infinite parallel plates ($a/b \longrightarrow \infty$). Nikuradse {[5],1930} was the first to deal with turbulent flow in a trapezoidal duct. He noted that the isovels in this duct tended to bulge towards the corners. He postulated four cells of secondary flow per primary flow cell. About 30 years later, Rodet {[3], 1960} and (still later) Chiranjivi and Sankara Rao {[4], 1971} did some experimental work in trapezoidal ducts. Rodet's experimental data is the only flow stucture data. His trapezoidal duct was characterised by ϕ =75° and a/b =0.536. He used the hot wire anemometry system in his measurements. He determined the local wall shear stresses and the cross-sectional distributions of mean axial velocity and Reynolds stresses, however he did not attempt to measure the secondary velocities. The experimental data of Chiranjivi and Sankara Rao

were confined to bulk heat transfer only. Their duct was characterised by ϕ =70° and a/b =0.28. Water and glycerol-water mixtures were used as test fluids. Heat entered only through the base of their trapezoidal duct with the other three sides being insulated. The duct base was kept at constant temperature and heat transfer measurements were made under both laminar and turbulent flow conditions. The shape of the present duct relative to [3] , [4] and [5] is shown in Fig. 2b.

2.2.2 Other Non-Circular Ducts

Square ducts have been studied the most extensively {e.g. Brundrett and Baines [6]; Launder and Ying [7]; and Gessner et al. [8]}. Rectangular ducts have also been studied by several investigators; for example, by Hoagland [9], Leutheusser [10], Gessner and Jones [11, 12] and Melling and Whitelaw [13]. Other duct configurations which have been investigated experimentally include :

- triangular array rod bundles; Trupp [14]
- wall subchannel of a rod bundle; Rehme [106]
- square-pitch rod cluster; Hooper [107]
- closely-spaced rod arrays; Hooper and Rehme [108]
- equilateral triangular duct; Aly et al. [15] and Altemani and Sparrow [17]
- isosceles triangular duct; Cremers and Eckert [16]
- two square interconnected sub-channels; Lyall [18]
- circular pipe with one or two eccentric rods; Kacker [19]

- interior sub-channel of a bare rod bundle; Carajilescov and Todreas [20]
- simulated rod bundle; Seale [21]
- internally finned tube; Said [22]

For all previous investigators, Hoagland [9] was the first to measure the secondary velocities by a hot wire anemometer. Maximum secondary velocities were found to be about 1 to 1.5% of the centre line axial velocity and occurred near the walls in the corner region. His rectangular duct was of class 1 (aspect ratio 1:1) and class 2 (aspect ratio 2:1 or 3:1) geometry. Hoagland's hot wire technique was employed later in a square duct by Brundrett & Baines [6] to measure secondary velocities as well as other turbulence quantities. They suggested that the production of axial vorticity (which was responsible for secondary flow) was associated with the relative vicinity of the fluid particles to the duct walls. They contributed also that the generation of axial vorticity is mainly due to normal stress term gradients in the differential equation. Gessner & Jones [11, 12] used a hot wire technique to examine the Reynolds number effect on secondary flow. They indicated that the secondary flow decreases slightly with increasing Reynolds number when non-dimensionlized by the centre line axial velocity. They examined the Reynolds equation along a secondary flow streamline. They concluded that the differences between Reynolds stresses and static pressure gradients in the plane of

the cross-section cause secondary flow. Launder & Ying [7] used the hot wire system to measure secondary flow in rough and smooth square ducts. They found that the secondary velocities when normalized with the average friction velocity are independent of duct roughness. They also concluded that the secondary velocities, when normalized with the friction velocity are sufficiently independent of Reynolds number. Using a laser-Doppler anemometer, Melling & Whitelaw [13] measured the secondary velocities in a rectangular duct. Their results agree qualitatively with the previous hot wire anemometer results of the same duct. Their secondary flow results did not satisfy continuity exactly. They argued that their error in secondary velocities measurements is quantifiable, unlike that arising from hot wire measurements.

In addition to class 1 or class 2 geometries, secondary flow was measured in only two class 3 geometries. The first case was by Lyall [18] in two square interconnected subchannels using a hot wire anemometer. Maximum secondary velocities of about 3.5% of the local axial mean velocity were recorded near the gap region. The pattern of secondary flow was different in the gap regions of the two similar subchannels. The secondary flow results were considered inadequate. He estimated that secondary flow convection exceeds turbulent diffusion when the ratio of the secondary velocity to axial velocity exceeds about 0.001. The second class 3 geometry is the simulated rod bundle by Seale [21]. He used the

procedure developed by Mojola [104] to get the secondary velocities from a hot wire anemometer. He detected three large and two small secondary flow cells in each symmetric part of his duct. Maximum secondary velocities were about 1.5% of the bulk axial velocity.

Measurements of turbulence characteristics in closely-spaced rod arrays were reported by Hooper and Rehme [108]. Techniques for resolving secondary flow velocities to within ±1% of the local axial velocity failed to detect significant non-zero mean secondary flow components. The long length scales of the axial and azimuthal turbulent velocity components, relative to the gap width, emphasized the anisotropy of the turbulent transport processes in the rod gap.

2.3 REVIEW OF THEORETICAL WORK

2.3.1 Trapezoidal Ducts

Most of the analytical work for trapezoidal ducts has so far been devoted to fully developed laminar flow. Theoretical results for friction factor and Nusselt number for trapezoidal ducts for the range of $30° < \phi < 90°$ and $0 < a/b < \infty$ have been documented by Shah and London [23].

Theoretical work in fully developed turbulent flow in trapezoidal ducts appears to have been very limited. Some numerical predictions of fully developed turbulent flow in a trapezoidal duct was reported by Nakayama et al. {[24],

1983}. His trapezoidal duct was characterised by ϕ =75° and a/b =0.536 i.e. Rodet's duct [3]. He employed the k-ϵ model along with the algebraic stress model of Launder and Ying [7] for vorticity production. He claimed that the algebraic stress model, when coupled with the k-ϵ model leads to reasonably satisfactory predictions when compared with experimental data. A comparison of the present predictions with some of his predictions is shown later in Chapter 8.

2.3.2 Other Non-Circular Ducts

One of the first calculations of secondary flow in straight non-circular ducts was carried out by Wilson et al. [28] in a square duct. Subsequently, square ducts were studied by Launder and Ying [25], Naot et al. [26], Emery et al. [27], Gosman & Rapley [29] and Nakayama [30]. Rectangular ducts have been studied numerically by Gosman & Rapley [29], Nakayama [30] and Zhou [31]. Developing flow in a square duct and developed flow in a paratially roughened rectangular duct have been investigated by Demuren & Rodi [88]. Other duct configurations which have been explored numerically include, the equilateral triangular duct {Aly et al. [15]; Gosman & Rapley [32]}, isosceles triangular duct by Rapley & Gosman [33], triangular array rod bundles {Aly [34]; Trupp & Aly [35]; Carajilescov & Todreas [20]; Gosman & Rapley [29]}, internally finned tube {Ivanovic [36]; Said [22]}, and simulated rod bundles by Seale [21].

For the calculations of turbulent flow, there are in general, two numerical schemes used with a suitable modelling of Reynolds stresses. These two schemes are primitive variable method developed by Patankar and Spalding [77] and stream-function/vorticity method which was made accessible by the book by Gosman et al. [1]. From the mathematical point of view the two methods are equivalent and have advantages and disadvantages.

The vorticity source term modelling in non-circular ducts involving turbulence-driven secondary motion was reviewed by Demuren and Rodi [88]. They showed the different proposals to calculate the Reynolds stress terms $(\overline{v^2})^{1/2}$, $(\overline{w^2})^{1/2}$ and $\overline{vw}$. They introduced a more refined form of the model of Launder, Reece and Rodi [59]. Their model form included the secondary velocity gradient terms in the Reynolds-stress equations. All the previous investigators except for Seale [2, 21] used the Launder and Ying model (or Launder&Ying with modifications) in conjunction with the primitive variables or stream-function/vorticity method to predict secondary flow. Seale [2] showed that the method originated by Launder and Ying [7] is sometimes unsatisfactory from the point of view of convergence and stability of the numerical solution of the vorticity equation. Difficulties tend to arise when the geometry is complicated or of class 3 geometry.

2.4 TURBULENCE MODELS

2.4.1 General

From an engineering point of view there is no need to consider the details of turbulence. Usually the engineer is concerned only with the time-average effects of turbulent flow. The process of time averaging of the turbulent flow conservation equations, causes statistical correlations involving fluctuating velocities and temperatures to appear in these equations. Since there is no direct way of knowing the magnitudes of these terms; their effect must be approximated or modelled in terms of measurable or calculable quantities. Thus a model of turbulence is a set of equations which when solved with the mean flow equations, allows calculation of the relevant correlations and closely simulates the behaviour of real fluids.

2.4.2 Survey of Existing Turbulence Models

Reviews of these models have been published by Launder and Spalding [37, 38, 39], Bradshaw [40], Harlow [41], Rodi and Spalding [42] and Reynolds [43]. A study of turbulence models [43] classifies them according to the number of turbulence quantities which appear as dependent variables of differential equations. This classification is presented below.

Zero-equation models

These models do not employ equations for turbulent quantities. The models of this group relate the turbulent shear stress to the mean flow velocity gradient at each point. All models of this class use the eddy-viscosity concept of Boussinesq. Examples of this type are : the mixing length hypothesis of Prandtl (1925), Von-Karman mixing length model (1930) and the eddy viscosity model of Trubchikov (1934).

One-equation models

This class involves one turbulence quantity as the dependent variable of a differential equation. Several one-equation models focus attention on the turbulence kinetic energy k as the dependent variable. Examples of this class of models are : Prandtl and Wiegkardt {[44], 1945}, Bradshaw et al. {[45], 1967} and Nee and Kovasznay {[46], 1968}.

Two-equations models

These models involve two turbulent quantities appearing as dependent variables of differential equations as : k - w model of Kolmogorov {[47], 1942} where w is known as the frequency($k^{1/2}/l$) and l is an algebraic length scale, k - kl model of Ng and Spalding {[48], 1972}, k - l model of Spalding {[49], 1967b}, k - ϵ model of Harlow and Nakayama

{[50], 1968} and of Jones and Launder {[51], 1972}, k -W model of Llegbusi and Spalding [53] where W is the equation of vorticity fluctuations.

Multi-equations models

These models involving partial differential equations for some or all components of the turbulent stress tensor. Some proponents of these models are : Chou {[54], 1945}, Rotta {[55], 1951}, Davidov {[56], 1961}, Hanjalic and Launder [57], Naot et al. [58], and Launder et al. [59].

2.4.3 Choice of k - ϵ Model

Zero-equation models are much better in predicting integral properties of the flow than in predicting local details. Predictions of turbulent boundary layer separation by these models were not very successful [60]. One-equation models have been used by several investigators, e.g. square duct [7], equilateral triangular duct [15] and rod bundles [35]. The limitations of the one-equation models arise from the algebraic equation of calculating turbulence length scale l. In recirculating flows, the convective transport is important, and so the length scale should be calculated from a transport equation rather than algebraic formulae. Also in fully developed duct flows, complex cross-sections give rise to large diffusive effects on l which cannot be accounted for by algebraic formulae. There are several vari-

ables adopted by different researchers to determine the length scale such as $k^{1/2}$, ϵ, l, kl, and k/l^2. The turbulence energy dissipation rate, ϵ, has been favoured by more investigators than any other. This is because the exact equation for ϵ can be derived and ϵ itself appears directly as an unknown in the equation for k.

CHAPTER 3

GOVERNING EQUATIONS

3.1 CONTINUITY AND REYNOLDS EQUATIONS

In the trapezoidal duct, symmetry permits the flow cross-section to be subdivided into two primary flow cells. No net mass, momentum or energy is transferred across any boundary of the cell. A knowledge of the flow properties in either one of the two cells is sufficient to describe the entire flow field. The primary flow cells and Cartesian coordinate system used in the present investigation are shown in Fig. 3. The equations governing the distributions of the mean velocity components pertinent to the flow prediction for fully developed steady flow of an incompressible fluid are outlined below.

The mass conservation equations for the mean and fluctuating components are :

$$\frac{\partial \bar{V}}{\partial y} + \frac{\partial \bar{W}}{\partial z} = 0, \qquad (3.1)$$

$$\frac{\partial u}{\partial x} + \frac{\partial v}{\partial y} + \frac{\partial w}{\partial z} = 0 \qquad (3.2)$$

The Reynolds equations with negligible body forces are :

x-direction

$$\rho\left(\bar{V}\frac{\partial\bar{U}}{\partial y} + \bar{W}\frac{\partial\bar{U}}{\partial z}\right) = -\frac{\partial\bar{p}}{\partial x} + \mu\left(\frac{\partial^2\bar{U}}{\partial y^2} + \frac{\partial^2\bar{U}}{\partial z^2}\right) - \rho\left(\frac{\partial\overline{uv}}{\partial y} + \frac{\partial\overline{uw}}{\partial z}\right) \qquad (3.3)$$

y-direction

$$\rho\left(\bar{V}\frac{\partial\bar{V}}{\partial y} + \bar{W}\frac{\partial\bar{V}}{\partial z}\right) = -\frac{\partial\bar{p}}{\partial y} + \mu\left(\frac{\partial^2\bar{V}}{\partial y^2} + \frac{\partial^2\bar{V}}{\partial z^2}\right) - \rho\left(\frac{\partial\overline{v^2}}{\partial y} + \frac{\partial\overline{vw}}{\partial z}\right) \qquad (3.4)$$

z-direction

$$\rho\left(\bar{V}\frac{\partial\bar{W}}{\partial y} + \bar{W}\frac{\partial\bar{W}}{\partial z}\right) = -\frac{\partial\bar{p}}{\partial z} + \mu\left(\frac{\partial^2\bar{W}}{\partial y^2} + \frac{\partial^2\bar{W}}{\partial z^2}\right) - \rho\left(\frac{\partial\overline{vw}}{\partial y} + \frac{\partial\overline{w^2}}{\partial z}\right) \qquad (3.5)$$

Where the over-bar designates time average.

The function of the various terms are more easily understood if the axial momentum equation is rearranged in the following form :

$$\underbrace{\rho\left(\bar{V}\frac{\partial\bar{U}}{\partial y} + \bar{W}\frac{\partial\bar{U}}{\partial z}\right)}_{\text{Convection Terms}} - \underbrace{\mu\left(\frac{\partial^2\bar{U}}{\partial y^2} + \frac{\partial^2\bar{U}}{\partial z^2}\right) + \rho\left(\frac{\partial\overline{uv}}{\partial y} + \frac{\partial\overline{uw}}{\partial z}\right)}_{\text{Diffusion Terms}} + \underbrace{\frac{\partial\bar{p}}{\partial x}}_{\text{Source Term}} = 0 \qquad (3.3a)$$

Convection terms of equation (3.3a) represent the change in the axial momentum of a small fluid particle due to convection by secondary flows. The diffusion terms represent the change in axial momentum due to viscous and Reynolds shear stresses. The source term represents the change in axial momentum due to the axial pressure gradient. Its magnitude is constant over the cross-section as can be verified by differentiating equations (3.3), (3.4) and (3.5) with respect to x.

The boundary conditions for the Reynolds equations are (see Fig. 3) :

I) Along the bottom and top walls (y axis),

$\overline{U} = \overline{V} = \overline{W} = 0$ due to no slip condition.

II) Along the inclined wall,

$\overline{U} = \overline{V} = \overline{W} = 0$ due to no slip condition.

III) Along the symmetry line (y= 0), equation (3.4) should vanish since there can be no net momentum transfer in the y-direction across this boundary. Thus $\overline{V}$=0 and consequently $(\partial\overline{V}/\partial z) = 0 = (\partial^2\overline{V}/\partial z^2)$. Since $\overline{V}$ has opposite signs on each side of this symmetry line, $\partial^2\overline{V}/\partial y^2 = 0$. Also due to symmetry $(\partial\overline{p}/\partial y) = 0 = (\partial\overline{v^2}/\partial y)$. Hence by applying these simplifications, equation (3.4) reduces to $\partial\overline{vw}/\partial z = 0$. Upon integration, and using the boundary condition $\overline{vw} = 0$ at the bottom or top wall, it can be readily shown that $\overline{vw} = 0$ along the symmetry line. On this same boundary, $\partial\overline{V}/\partial y$ and $\partial\overline{uv}/\partial y$ may have finite values since $\overline{V}$ and $\overline{uv}$ have an anti-symmetric distribution about this symmetry line. For this reason and the fact that $\overline{W}$ may have finite values along the symmetry line except at the walls, it is not possible to obtain a simple theoretical distribution for $\overline{uw}$ at this boundary from equation (3.3).

3.2 STREAM FUNCTION AND AXIAL VORTICITY EQUATIONS

The axial vorticity ω is defined by :

$$\omega = \frac{\partial \bar{W}}{\partial y} - \frac{\partial \bar{V}}{\partial z} \tag{3.6}$$

The 'in-plane' components of the velocity vector, $\bar{V}$ and $\bar{W}$, the secondary velocities, are replaced by the introduction of the stream function Ψ defined by :

$$\partial\Psi/\partial z = \rho\bar{V}, \tag{3.7a}$$

$$\partial\Psi/\partial y = -\rho\bar{W} \tag{3.7b}$$

substituting (3.7) into (3.6), the stream function equation can be written in the form :

$$\frac{\partial}{\partial y}\left(\frac{1}{\rho}\frac{\partial\Psi}{\partial y}\right) + \frac{\partial}{\partial z}\left(\frac{1}{\rho}\frac{\partial\Psi}{\partial z}\right) = -\omega \tag{3.8}$$

where ω represents the source term in this equation.

The equation governing the conservation of axial vorticity can be obtained by differentiating the time average momentum equations in the y and z directions (differentiate y-direction equation with respect to z and z-direction equation with respect to y) and combine to eliminate the pressure gradient terms. Upon simplification, this yields :

$$\bar{V}\frac{\partial\omega}{\partial y} + \bar{W}\frac{\partial\omega}{\partial z} = \frac{\partial^2}{\partial y\partial z}(\overline{v^2}-\overline{w^2}) - \left(\frac{\partial^2\overline{vw}}{\partial y^2} - \frac{\partial^2\overline{vw}}{\partial z^2}\right) + \nu\left(\frac{\partial^2\omega}{\partial y^2} + \frac{\partial^2\omega}{\partial z^2}\right) \tag{3.9}$$

Terms on the left side of equation (3.9) represent the convection of axial vorticity by the secondary velocities.This process tends to make the vorticity constant along the secondary flow streamlines. The last terms on the right side represent the diffusion of vorticity by viscous effects and tend to make the vorticity uniform over the duct cross-section by diffusing it from high to low regions of intensity. The first two terms on the right side may represent either production or dissipation of axial vorticity depending on the local turbulence field.

3.3 TURBULENT KINETIC ENERGY EQUATION

The transport equation for the mean turbulent kinetic energy has been derived exactly from the Navier-Stokes equations by several authors; see for example [80]. The adopted modelled form of the k-equation is equivalent to that used by Launder and Ying [25], Emmons [96], Tatchell [91], Seale [94] and several others :

$$\underbrace{\{\rho\bar{V}\frac{\partial \bar{k}}{\partial y} + \rho\bar{W}\frac{\partial \bar{k}}{\partial z}\}}_{\text{Convection Term}} = \underbrace{\{\frac{\partial}{\partial y}(\mu\frac{\partial \bar{k}}{\partial y} - \rho\overline{vk'}) + \frac{\partial}{\partial z}(\mu\frac{\partial \bar{k}}{\partial z} - \rho\overline{wk'})\}}_{\text{Diffusion Term}}$$

$$\underbrace{-(\rho\overline{uv}\frac{\partial \bar{U}}{\partial y} + \rho\overline{uw}\frac{\partial \bar{U}}{\partial z})}_{\text{Production Term}} \underbrace{-\rho\epsilon}_{\text{Dissipation Term}} \qquad (3.10)$$

where,

(a) Convection term : represents convection of the mean turbulent kinetic energy by secondary velocities.

(b) Diffusion term : represents energy diffusion by viscous and turbulence effects.

(c) Production term : represents the rate of production of turbulent energy by the mean flow.

(d) Dissipation term : represents the rate of dissipation of k by molecular viscosity.

3.4 TURBULENCE ENERGY DISSIPATION RATE EQUATION

The transport equation for the turbulence energy dissipation rate as constructed by Hanjalic and Launder [57] may be written in the form :

$$\underbrace{\{\rho\bar{V}\frac{\partial\bar{\epsilon}}{\partial y} + \rho\bar{W}\frac{\partial\bar{\epsilon}}{\partial z}\}}_{\text{Convection Term}} = \underbrace{\{\frac{\partial}{\partial y}(\mu\frac{\partial\bar{\epsilon}}{\partial y} - \rho\overline{v\epsilon'}) + \frac{\partial}{\partial z}(\mu\frac{\partial\bar{\epsilon}}{\partial z} - \rho\overline{w\epsilon'})\}}_{\text{Diffusion Term}}$$

$$\underbrace{-C1\epsilon/k(\rho\overline{uv}\frac{\partial\bar{U}}{\partial y} + \rho\overline{uw}\frac{\partial\bar{U}}{\partial z})}_{\text{Generation Term}} \underbrace{-C2\rho\epsilon^2/k}_{\text{Dissipation Term}} \qquad (3.11)$$

where C1 and C2 are constants.

The roles of the terms in equation (3.11) are similar to those terms in equation (3.10).

3.5 ENTHALPY EQUATION

Neglecting the kinetic heating and viscous dissipation, the enthalpy conservation equation may be written in the form :

$$\underbrace{\{\rho V\frac{\partial \bar{h}}{\partial y} + \rho W\frac{\partial \bar{h}}{\partial z}\}}_{\text{Convection Term}} = \underbrace{\{\frac{\partial}{\partial y}(\frac{\mu}{Pr}\frac{\partial \bar{h}}{\partial y} - \rho\overline{vh'}) + \frac{\partial}{\partial z}(\frac{\mu}{Pr}\frac{\partial \bar{h}}{\partial z} - \rho\overline{wh'})\}}_{\text{Diffusion Term}}$$

$$\underbrace{-\rho U\frac{\partial \bar{h}}{\partial x}}_{\text{Source Term}} \qquad (3.12)$$

3.6 GOVERNING EQUATIONS IN Ψ FORM

Equations (3.3), (3.8), (3.9), (3.10), (3.11) and (3.12) may be expressed in terms of the stream function Ψ in the following form :

Axial momentum equation :

$$\{\frac{\partial}{\partial y}(\bar{U}\frac{\partial \bar{\Psi}}{\partial z}) - \frac{\partial}{\partial z}(\bar{U}\frac{\partial \bar{\Psi}}{\partial y})\} - \mu\{\frac{\partial^2 \bar{U}}{\partial y^2} + \frac{\partial^2 \bar{U}}{\partial z^2}\} + \rho\{\frac{\partial \overline{uv}}{\partial y} + \frac{\partial \overline{uw}}{\partial z}\} + \frac{\partial \bar{p}}{\partial x} = 0 \qquad (3.13)$$

Axial vorticity equation :

$$\{\frac{\partial}{\partial y}(\omega\frac{\partial \bar{\Psi}}{\partial z}) - \frac{\partial}{\partial z}(\omega\frac{\partial \bar{\Psi}}{\partial y})\} - \{\frac{\partial}{\partial y}(\frac{\partial(\mu\omega)}{\partial y}) + \frac{\partial}{\partial z}(\frac{\partial(\mu\omega)}{\partial z})\} + S_w = 0 \qquad (3.14)$$

where S_w is the axial vorticity source term :

$$S_w = -\rho \frac{\partial^2}{\partial y \partial z}(\overline{v^2}-\overline{w^2}) + \rho\left(\frac{\partial^2 \overline{vw}}{\partial y^2} - \frac{\partial^2 \overline{vw}}{\partial z^2}\right) = 0 \qquad (3.14a)$$

Stream function equation :

$$\frac{\partial}{\partial y}\left(\frac{\partial \Psi}{\partial y}\right) + \frac{\partial}{\partial z}\left(\frac{\partial \Psi}{\partial z}\right) + \rho\omega = 0 \qquad (3.15)$$

Turbulent kinetic energy equation :

$$\left\{\frac{\partial}{\partial y}\left(k\frac{\partial \Psi}{\partial z}\right) - \frac{\partial}{\partial z}\left(k\frac{\partial \Psi}{\partial y}\right)\right\} - \left\{\frac{\partial}{\partial y}\left(\mu\frac{\partial k}{\partial y} - \rho\overline{vk'}\right) + \frac{\partial}{\partial z}\left(\mu\frac{\partial k}{\partial z} - \rho\overline{wk'}\right)\right\}$$

$$+ \rho\left(\overline{uv}\frac{\partial \overline{U}}{\partial y} + \overline{uw}\frac{\partial \overline{U}}{\partial z}\right) + \rho\epsilon = 0 \qquad (3.16)$$

Turbulence energy dissipation rate equation :

$$\left\{\frac{\partial}{\partial y}\left(\epsilon\frac{\partial \Psi}{\partial z}\right) - \frac{\partial}{\partial z}\left(\epsilon\frac{\partial \Psi}{\partial y}\right)\right\} - \left\{\frac{\partial}{\partial y}\left(\mu\frac{\partial \epsilon}{\partial y} - \rho\overline{v\epsilon'}\right) + \frac{\partial}{\partial z}\left(\mu\frac{\partial \epsilon}{\partial z} - \rho\overline{w\epsilon'}\right)\right\}$$

$$+C1\rho\epsilon/k\left(\overline{uv}\frac{\partial \overline{U}}{\partial y} + \overline{uw}\frac{\partial \overline{U}}{\partial z}\right) + C2\rho\epsilon^2/k = 0 \qquad (3.17)$$

Temperature (enthalpy) equation :

$$\{\frac{\partial}{\partial y}(\bar{T}\frac{\partial \Psi}{\partial z}) - \frac{\partial}{\partial z}(\bar{T}\frac{\partial \Psi}{\partial y})\} - \{\frac{\partial}{\partial y}(\frac{\mu}{Pr}\frac{\partial \bar{T}}{\partial y} - \frac{\rho\overline{vt}}{C_p}) + \frac{\partial}{\partial z}(\frac{\mu}{Pr}\frac{\partial \bar{T}}{\partial z} - \frac{\rho\overline{wt}}{C_p})\}$$

$$+ \rho\bar{U}\frac{\partial \bar{T}}{\partial x} = 0 \qquad (3.18)$$

The boundary conditions for these equations are discussed in detail in Section (5.3)

CHAPTER 4

EXPERIMENTAL FACILITY AND MEASUREMENTS

4.1 TEST RIG

The fan for the test rig (Fig. 4a) was a CML Northern Blower size 7, class 11, width SWSI, Arr.9, SQ industrial fan with type LS wheel. It was belt driven by a 1HP, 1725 rpm, 3/60/208V GEC electric motor. Room air entered the fan through a bellmouth, and volumetric control was provided through a parallel blade damper on the discharge side. The fan discharge was connected via a flexible neoprene coupling (for no transmission of any detectable vibration) to a transition piece where the flow cross-section was gradually changed from rectangular to trapezoidal over a 0.91 m length. Following transition, the air flow was allowed to develop naturally in test sections A and B (plywood construction) before entering test section C (precision acrylic).

4.2 TEST SECTION

The cross-section of the duct is shown in Fig. 1. It was estimated that variations in the side-wall lengths were less than ± 0.25 mm and ± 1.0 mm for the acrylic and wooden sections respectively. The measuring station was located 3.0 cm

inside the open end of the duct. This location corresponded to a distance of 102 equivalent hydraulic diameters from the test section entrance.

4.3 TRAVERSING MECHANISM

Measurements were made on the basis of a Cartesian coordinate system (see Figs. 5a,b). Accurate positioning of either a Pitot tube or a hot wire probe in the test plane was achieved by means of a DISA 55H01 traversing mechanism (see Fig. 4b). The entire mechanism was mounted on a cross-slide table which allowed motion in the axial direction. It was estimated that absolute probe positions could be determined to within ± 0.05 mm and ± 0.1 mm in the vertical and horizontal directions respectively. Relative positional accuracy was of course much better since resolutions were 0.01 mm and 0.02 mm in the z and y directions respectively.

4.4 INSTRUMENTATION

Mean axial velocity ($\bar{U}$) and wall shear stress (τ) measurements were made using a Pitot tube and a Betz projection manometer which had a range of 0-300 mm H2O and an accuracy of ± 0.1 mm H2O. The Pitot tube had an outside diameter of 1.067 mm, and was made from stainless steel tubing having an inside to outside diameter ratio of 0.6. A static pressure tube with outside diameter of 1.24 mm and 4 holes drilled on the circumference at 1.43 cm from the sealed end was used to

measure the static pressure in the cross-section plane of the duct.

Turbulence measurements were made using DANTEC constant temperature linearized hot wire anemometry. The anemometry system consisted of two sets of 55D05 anemometers and a 55M10 anemometer, 55D10 linearizers and 55D25 auxiliary units. The ancillary equipment consisted of a 55D31 digital D.C. voltmeter, a 55D35 r.m.s. voltmeter and 52B25 turbulence processor. The miniature probes included a 55P11 single wire, a 55P61 X-probe and a 55P12 45° slanting probe.

Measurements of axial velocity fluctuations and secondary velocities were made using the M-system. The axial velocity fluctuations by the 55D05 system were in good agreement with that taken by the 55M10 system.

Measurements of secondary velocity components $\overline{V}$ and $\overline{W}$ were made using both X-wire and 45° slanting wire. Full descriptions of the equations for direct measurements are shown by both Gerrard [69] and Said [22]. Precautions were taken in the experimental procedures for measuring the tiny secondary velocities. For X-wire measurements, each channel was checked at a fixed point in the cross-section after a few measurements to eliminate problems of wire mismatch and drift. However, X-wire measurements were influenced by transverse velocity gradients. To eliminate these potential problems for the X-wire, special traverses were made using a

45° slanting probe. The measurements by a slanting wire were taken for the cross-section with the wire in (say) position 1 (45° with the axial direction). The channel voltage was checked at a fixed point after a few measurements in case of channel drift. Later, the wire was rotated 180°(position 2), and the cross-section was scanned another time with the same care as taken for position 1. The two readings for each position allowed the secondary velocity ($\overline{V}$ or $\overline{W}$) to be calculated. In addition, using the advantage of the anti-symmetric distribution of $\overline{V}$, separate point measurements for $\overline{V}$ (only) were taken at symmetric points on opposite sides of the trapezoidal duct using the slanting 45° hot wire. This procedure was previously used successfully by Gerrard [69].

4.5 EXPERIMENTAL RESULTS AND DISCUSSION

4.5.1 General

Detailed measurements were conducted in the primary flow cell shown in Fig. 3 at Reynolds numbers of 79,000 and 99,000. Hot wire and Pitot tube measurements were taken at about 95 locations. Figures 5a,b show the nodes of the measurement grids. Figure 5a represents the nodes of the measurement grids for the X-probe. Figure 5b represents the nodes of the measurement grids for the Pitot tube, single wire, 45° slanting wire and some results (secondary velocities) of the X-wire. All experimental data have been documented in a Department of Mechanical Engineering internal

report [64]. The distributions of turbulence quantities along normals to the walls are compared (where possible) with other ducts (pipe, square duct, equilateral triangular duct).

4.5.2 Accuracy of Measurements

A study about error analysis in experimental data by Kline [101] showed the obligation of an uncertainty analysis in record experiments. He defines uncertainty as a possible value that the error in a particular measurement may have. An error in a measurement is the difference between the true and observed value. An error is a fixed number but an uncertainty is a statistical variable. Errors can be classified into three classes: Accidental errors, fixed errors, and mistakes. Accidental errors are those which cause repeated readings to differ without apparent reason. They arise from instrument friction and time lag. Fixed errors are those which cause repeated readings to be in error by the same amount and generally arise from mechanical design of the equipment. Mistakes are completely erroneous reading of scales. Large mistakes can be eliminated before the results are calculated, but smaller mistakes will remain in the data since there is no means of locating and then eliminating them. The source of the uncertainties in the final result is:

1) The calibration uncertainty
2) The signal generating system

3) The approximations involved in the equations which were applied to describe the device behaviour.

Concerning the present results, using the technique given by Kline and McClintock [102] and a guide given by Yavuzkurt [105] for uncertainty analysis of hot wire data, the estimated error (20:1 odds) for several results is presented in Table 1. The analysis does not take into account errors due to high intensity turbulence.

It is worthwhile to point out (as is known by all hot wire experimenters) that the error in hot wire measurements is very sensitive to misalignment of the probe to the flow direction, incorrect wire angle, dirt buildup on wire, operational errors due to temperature changes, unmatched channels, etc. However, for repeated runs of the experiment, the relative behaviour of the variables show little deviation. The accuracy of the trends of the data will thus be much better than the accuracy of the absolute values. The most practical way for establishing trend accuracy is to examine the repeatability of the results (of the same probe or different probes or combination thereof). The trend accuracy for each result is presented along with the experimental results in the following sections.

Due to the complications adopted in measuring secondary velocities, a completely thorough assessment of the errors in $\overline{V}$ and $\overline{W}$ components was almost impossible. However, a

rough calculations of the uncertainty (excluding the possible position error for the measurement by a slant wire) show that for secondary velocity of about 1% the uncertainty was about 50%, while for 0.5% and 2% secondary velocities it was about 72% and 22% respectively. On the other hand, the accuracy may also be gauged roughly by two methods. The first by testing for conservation of mass at selected traverses. The main limitation here is the unknown secondary velocity profiles close to the walls. The second way is by comparing the measurements of X-probe with that of the 45° slanting probe. It is difficult to quantify what degree of agreement is typical; the reader can form an opinion when the data are presented in Section (4.5.8). At this time, the agreement of the trends by both probes will also be discussed.

4.5.3 Friction Factors

Friction factors for each Reynolds number were calculated using the axial pressure measurements at 20 static pressure taps/piezometer rings spanning the length of the last half of the test section. For all Reynolds numbers, pressure decreased linearly with axial distance. The fully developed axial pressure gradient for each Reynolds number was determined from a straight line least-squares fit to the data. Friction factors were then computed using U_b via Pitot tube to an accuracy estimated to be within 4%. A least-squares fit of straight lines to the data at eight Reynolds numbers gave the following expression :

$$f = 0.1976\ (Re)^{-0.214} \qquad (4.1)$$

Equation (4.1) is capable of describing the experimental data with a standard deviation (σ) of about 2% of the range average.

The present results are shown in Fig. 6 which also includes the experimental data of Rodet [3] and the Nikuradse [5] data line. Relative to pipe flow, the present data lie typically about 8% below the standard correlation shown in Fig. 6 for circular pipe. In this respect, the present results are consistent with reported results for other non-circular ducts. Leutheusser [10] for square ducts and Carlson and Irvine [64] for isosceles triangular ducts, found that friction factors were significantly lower than predicted by the hydraulic diameter rule.

Figure 6 also shows the predictions for the present duct and Rodet's duct by the method proposed by Malak et al. [92]. The present results generally fall slightly below the line of Malak et al. by an average of about 2.5% which is within the experimental accuracy. According to Malak et al. friction factors for the present duct and for Rodet's duct fall within 2% of each other, whereas Nikuradse's duct lies between the two. This outcome stems from the fact that the fRe products for the three ducts are almost equal under fully developed laminar flow conditions. As shown in Fig. 6,

Rodet's data are in good agreement with the prediction of Malak et al. This, in turn, explains the good consistency between the present data and that of Rodet, despite substantial differences in duct cross-sectional shape. On the other hand, the data of Nikuradse's duct is noticably above the predictions of Malak et al., but only at the lower Reynolds numbers. Overall, the present results appear to be consistent with expectations and with the limited experimental data for other trapezoidal ducts.

4.5.4 Local Wall Shear Stress

The shear stresses on the walls of the primary flow cell were found by Preston tube using the calibration proposed by Patel [65]. The technique is applicable to any flow in which the velocity distribution for the wall region can be described by the inner law of the wall. Several investigators [66, 64, 10] have established the validity of the technique for measuring wall shear in pipe and square duct flows.

The measured distributions of the axial component of wall shear at two Reynolds numbers are shown in Figs. 7, 8, and 9. Each distribution has been normalized by the overall average value. The average shear stress values obtained by integrating the local shear stress distributions were within 3% of the corresponding values obtained from axial pressure gradient measurements.

For the individual walls, the average wall shear stress on the top wall was about 12% higher than the overall average whereas the bottom wall and the inclined wall were about 1.5% and 3% lower than the overall average respectively. A similar deviation of the top wall has been noted in the work of Nikuradse [5]. There the average shear stress of the top wall was 10% above the overall average whereas the bottom wall and the inclined wall were about 2% and 4% lower than the overall average respectively. On the other hand, the average shear stress of the three walls of Rodet's trapezoidal duct were approximately equal to the overall average. This outcome is in keeping with one of the roles of secondary flow, namely, to tend to equalize the wall shear stress around the entire duct perimeter. The cause of the deviations of the present data and Nikuradse data is not known. As shown later numerically (Section 7.7), the average of the top wall is about 9% above, while the inclined wall is 2% lower than the overall average. The average of the bottom wall shear stress is equal to the overall average.

The secondary flow effect on the local distribution of wall shear stress is evident by the small dip near the top ($s/d \simeq 0.4$) of the inclined wall and from the flatness of the distributions for the top and bottom walls respectively.

4.5.5 Mean Axial Velocity

The mean axial velocity measurements at the test section were measured using both Pitot tube and hot wire anemometry at each of the grid points shown in Fig. 5b. Bulk velocities (U_b) were obtained by numerical integration of the mean axial velocity fields. In evaluating U_b, the region near the wall was handled by assuming appropriate empirical shaping near the solid boundaries.

All mean velocity calculations were based on actual properties in the tunnel and included density corrections for variations in relative humidity. No corrections were made for velocity gradient or turbulence effects, although the wall proximity correction suggested by Ower and Pankhurst [67] was applied. It is estimated that the mean axial velocities are accurate to within about 1% and 2% for Pitot tube and single hot wire respectively. For the same nominal mass flow rate through the duct, the U_b values from the Pitot tube traverse were about 2% higher than the U_b from the single hot wire probe traverse. But as shown in Fig. 10, when each is normalized by its own U_b, the distributions of $\bar{U}/U_b$ were very similar. Also isovel plots of $\bar{U}/U_b$ for different mass flow rates were found to be essentially independent of Reynolds number as shown in Fig. 11. There was however, a slight tendency for the profiles to become flatter with increasing Reynolds number. For example, for Re = 79,000 the ratio $\bar{U}_{max}/U_b$ was about 1.22 and this value decreased

slightly to about 1.21 for Re = 99,000. The effect of Reynolds number on $\overline{U}_{max}/U_b$ for a wide range of Reynolds numbers will be explored numerically in Section (7.2).

A close examination of Figs. 10 and 11 shows some distortions to the contours towards the corners. These distortions are caused by secondary flow shown later in Section (4.5.8). Similar distortions were present for the trapezoidal ducts of Nikuradse [5] and Rodet [3] and other non-circular ducts [2, 6, 9]. The present result indicate that, there is flow toward the corners of the duct and away from the midwalls which decrease the axial velocity in the core region and increase it near the corners. It is concluded that the secondary motions, which are connected to the turbulent fluctuations in non-circular ducts, are responsible for this redistribution.

The velocity distributions near the three walls have been tested by a Pitot tube traverses at selected locations normal to each wall. The results of the traverses are demonstrated by plotting velocity profiles normal to each wall in terms of dimensionless coordinates U^+ and z^+. The plots shown in Figs. 12a, 12b and 12c are based on local friction velocity. Values of A and B were determined by least-squares fit (LSF) of straight lines using only the data points located in the linear portion of each distribution. The results are summarized in Table 2. As can be seen from Figs. 12a, 12b and 12c, logarithmic velocity distributions do in-

deed exist and the coefficients do not differ much from the conventional values of turbulent pipe flow. Hence if one excludes the immediate corner regions (where the flow is influenced by the presence of both walls) all the profiles conformed to a 'log-law' behaviour for the near wall regions for the present class 3 geometry. The LSF constants in Table 1 are used later in the computer program. The differences between the predictions using these constants and the standard log law constants were found to be negligible.

4.5.6 Reynolds Stresses

The experimental data for the three normal Reynolds stresses and the $\overline{uw}$ and $\overline{uv}$ shear stresses are presented in this section. In view of the large volume of experimental data and the Reynolds number similarty, the results presented here are mostly for one Reynolds number test. The rest of the results, once again, are documented in the internal report [63]. The $\overline{v^2}$, $\overline{w^2}$, $\overline{uv}$ and $\overline{uw}$ data have been corrected for tangential cooling effects as suggested by Lawn [62]. All results have been normalized by the average friction velocity, $\overline{u^*}$, to facilitate comparisons with other data.

The distributions of turbulence intensities are shown in Figs. 13($(\overline{u^2})^{1/2}/\overline{u^*}$), 14($(\overline{v^2})^{1/2}/\overline{u^*}$) and 15($(\overline{w^2})^{1/2}/\overline{u^*}$). For the horizontal traverse at z/b=0.5, the turbulence levels are small in the core region of the duct and they increase monotonically as the traverses approach the inclined

wall. This pattern is fairly standard. For the traverses nearer to the bottom or top wall, the patterns are more complicated and are influenced by secondary flow. Although each traverse is exactly parallel to a horizontal wall, at y/c = 0 turbulence levels are relatively high because of the secondary flow from the wall to the core region. As y/c increased, the turbulence intensities decrease (rather than hold constant) and then bottom-out corresponding to where the secondary flow moves into the corner, having brought low turbulent fluid from the core region. However, as the traverses finally approachs the inclined wall, the normal stress distributions consistently register an increasing trend entering the high turbulence production zone near the inclined wall. Also it was found (as expected) that $(\overline{u^2})^{1/2}/\overline{u}^*$ is generally larger than $(\overline{v^2})^{1/2}/\overline{u}^*$ and $(\overline{w^2})^{1/2}/\overline{u}^*$. As mentioned in Section (4.5.2), the trend accuracy for turbulence measurements is usually reasonably accurate. It can be determined by repeating the measurements of the same parameter several times by the same wire or by different wires. The trend accuracy determined this way for the normal stresses are considered to be within 10% as (for example) shown in Figs. 16 and 17.

The distributions of turbulence intensities along the duct symmetry line are presented and compared to the results of corresponding traverses for pipe [68], square duct [6] and equilateral triangular duct [34]. The comparisons are

shown in Figs. 18, 19 and 20. The distributions for the present data lie between the square duct and pipe flow and are very similar to the results for the equilateral triangular duct. In general, the present turbulence intensities exceed their counterparts for pipe flow by roughly about 15%. Part of this may be attributable to the fact that the local friction velocities for each end of the symmetry line are 4 to 5% higher than the duct average friction velocity (see Figs. 7 and 8). The remainder may partly be due to the secondary flow which moves fluid from each wall towards the central region thus causing turbulence intensities at a given location to be higher than would otherwise be.

The contour plots for the Reynolds normal stresses are shown in Figs. 21, 22 and 23. These contours clearly indicate the distortion in the turbulence field due to secondary flow. The three normal stress contours are qualitatively similar to those obtained by Rodet [3] in a trapezoidal duct characterised by $\phi = 75°$ and $a/b = 0.536$. Relationships between the turbulence intensities and turbulent kinetic energy will be described in Section (4.5.7).

Turning next to the Reynolds shear stresses, the trend accuracy for shear stresses based on the measurements at different Reynolds number by different probes are considered to be within 12%. No data were gathered for $\overline{\rho vw}$, however this shear stress is known from theory to be zero along the symmetry line ($y/c = 0$) and is expected elsewhere to be

small. As shown in Fig. 24, the shear stress ρuv was also found to be essentially zero along the symmetry line. This agrees with the theoretical conclusion that $\rho\overline{uv}$ acting on the xz plane at y/c = 0, must be zero since $\overline{uv}/(\overline{u}^*)^2$ (like $\overline{V}$) has an antisymmetric distribution on each side of the symmetry plane. The contour map for $\overline{uv}$ contains both positive and negative regions. The split is roughly left-right. The $\overline{uv}$ distribution is mainly similar to that obtained by Rodet [3].

Further information on $\overline{uv}$ is given in Fig. 25 which shows the distributions of $\overline{uv}/(\overline{u}^*)^2$ along three vertical traverses. The vertical traverse at y/c = 0.236 undergoes an alternating sign change across the duct height. This is likely associated with secondary flow.

The contour map of the shear stress $\overline{uw}$ in the primary flow cell is shown in Fig. 26. Like the $\overline{uv}$ map, it contains both positive and negative regions but the split is roughly top-bottom. Attention is also drawn to evidence of secondary flow from the bulges towards the top corner.

For fluid in the central region or adjacent to the top or bottom wall, $\rho\overline{uw}$ is the primary shear stress. As expected along the duct symmetry line (y/c= 0), this normalized shear stress varies (see Fig. 26) monotonically from roughly -1 to +1. For fluid adjacent to the inclined wall, the primary shear stress on a surface parallel to this wall would be a

mixture of $\rho\overline{uv}$ and $\rho\overline{uw}$. Contour values shown in Fig. 24 of $\overline{uv}/(\overline{u}^*)^2$ of about 0.7 and in Fig. 26 of $\overline{uw}/(\overline{u}^*)^2$ of about 0.3, are consistent with this expectation.

Three vertical traverses of $\overline{uw}/(\overline{u}^*)^2$ are shown in Fig. 27. One of these is the duct symmetry line (y/c= 0) over which the variation is slightly non-linear and ranges from about -1.1 to 0.8. A linear variation from -1 to +1 is, of course, characteristic along a diameter of fully developed pipe flow. For non-circular ducts, departures from linearity along a symmetry line are not uncommon and dimensionless magnitudes may readily exceed unity (e.g. square duct [6]). Departures here from unity and from linearity are due to both secondary flow and to the $\overline{uv}$ distribution (Fig. 24). Along the duct symmetry line, the axial momentum equation (3.3) becomes (neglecting the viscous term) :

$$\overline{W}\frac{\partial\overline{U}}{\partial z} = -\frac{1}{\rho}\frac{\partial\overline{p}}{\partial x} + \frac{\partial\overline{uv}}{\partial y} + \frac{\partial\overline{uw}}{\partial z} ,$$

where the pressure gradient term is a constant for fully developed flow. Hence the gradient of $\overline{uw}$ along the symmetry line, depends on the modifications to this pressure gradient constant by the local values of $\overline{W}\partial\overline{U}/\partial z$ and $\partial\overline{uv}/\partial y$. Concerning the latter, although $\overline{uv}$ is zero along the symmetry line, $\partial\overline{uv}/\partial y$ is non-zero since $\overline{uv}$ has an antisymmetric distribution about the symmetry line. Based on Fig. 24, peak values for $\overline{uv}/(\overline{u}^*)^2$ are about -0.5 near the top wall but only about -0.14 near the bottom wall. Hence along y/c= 0, $\partial\overline{uv}/\partial y$ val-

ues are likely to be quite different for these two regions. On the other hand, based on the known secondary flow pattern, the term $\overline{W}\partial\overline{U}/\partial z$ has a single polarity and should be of about the same magnitude for points equidistant from each wall. Hence it appears that the $\overline{uv}$ distribution exerts the asymmetric effect on $\overline{uw}$ along the z-direction.

Comparison of $\overline{uw}/(\overline{u}^*)^2$ with pipe [68], square [6] and equilateral triangular [34] ducts is shown in Fig. 28. The present results for the bottom wall are higher than for pipe flow, while the results for the top wall generally agree with pipe flow. Seale [21] found a similar agreement with pipe flow in his measurements in a simulated rod bundle. There is a considerable difference between the present data (particularly top wall) and square duct flow. The traverses normal to the bottom wall are higher than for the equilateral triangular duct while that for the top wall are lower. Considering the comparisons of the present shear stress with that of Rodet [3], there is a difference between the two maps of $\overline{uw}/(\overline{u}^*)^2$ near the inclined wall. This difference may be attributable to the difference in aspect ratio.

4.5.7 Turbulent Kinetic Energy

The mean turbulent kinetic energy $\{k= (\overline{u^2}+\overline{v^2}+\overline{w^2})/2\ )\}$ was computed at each node of the measurement grid. Comparisons of $k/(\overline{u}^*)^2$ with other investigators is presented in Fig. 29. The traverses are from the wall to the surface of no shear

(assumed coincident with the maximum axial velocity position). The result for each of the three walls takes almost a parabolic shape with $k/(\overline{u}^*)^2 \simeq 1$ at the centre region and $\simeq 4$ at the wall region. In general, the results are between the square duct flow and pipe flow and agree best with the equilateral triangular duct.

Contour plots showing the distribution of $k/(\overline{u}^*)^2$ in the primary flow cell are shown in Fig. 30 for two Reynolds numbers. Clear indications of secondary flow can be seen from the strong distortions of the contours toward the corners of the trapezoidal duct. These indicate that there are four secondary flow cells in the primary flow cell. The results shown in Fig. 30 are qualitatively similar to those obtained by Rodet [3] for his duct.

The relationship between the turbulence intensities and mean turbulent kinetic energy is of considerable practical interest particularly for secondary flow modelling. Relationships for the type described by Alshamani [71, 72] were obtained. The values for the coefficients of linear equations and the standard deviation for all cases are included in Table 3. Some typical results together with LSF lines are shown in Fig. 31. It appears, in general, that including the points near the inclined wall in the process of LSF increases significently the standard deviation. However, the change in the coefficients of the linear equations is not significent. Also, using local friction velocities in normalization

would increase the standard deviation but the LSF line would not change significently. As can be seen from Table 3, the coefficients for the case Re = 99,000 and the range of points $0 \leq y/a \leq 1$ and $0 \leq z/b \leq 1$ are closest to that found by Seale [2] for a simulated rod bundle geometry. In general, a linear relationship between the mean turbulent kinetic energy and turbulence intensities do exist. The similarity between the present coefficients and that of simulated rod bundle implies that the vorticity source model of Seale [2] may be capable of handling other class 3 geometries.

4.5.8 Secondary Velocities

The present work included direct measurements of $\overline{V}$ and $\overline{W}$ by X-probe and a slanting 45° probe. The data have been normalized by the average mean axial velocity, U_b. Like other secondary flow geometries, the present data seem to scale reasonably on either U_b or $\overline{u}^*$. Also the distributions of $\overline{V}/U_b$ and $\overline{W}/U_b$ via X-probe showed good consistency at the two main Reynolds numbers as shown in reference [63].

Figure 32 shows the z-direction component of the secondary flow ($\overline{W}$) for three horizontal traverses. For the traverse at z/b =0.182, for example, the data shows an upflow near the duct symmetry line, a downflow in the mid-span region and a second upflow near the inclined wall. As drawn, the line faired through the data does not strictly satisfy conservation of mass. To comply with continuity, the zero

position would have to be lowered to about - 0.2%, or (alternatively) $\overline{W}/U_b$ must reach about 3% adjacent to the inclined wall. Otherwise, considering the small quantities being measured, the agreement between the 45° slanting probe and the X-probe is quite reasonable except near the inclined wall where the X-probe consistently gave lower values. This is likely due to error induced on the separated wires by the steep axial velocity gradients near the wall.

Axial velocity gradient errors associated with the X-probe can also be seen in Fig.33 which shows the $\overline{V}/U_b$ distributions for three vertical traverses each with three sets of measurements. The X-probe generally registered too high near the top wall and too low near the bottom wall. Again, the faired lines do not completely satisfy continuity as drawn, however near-wall secondary flows may be under estimated. Overall, the three data sets show considerable scatter, but there is general agreement in trend.

Figure 34 shows the resultant secondary flow ($\overline{U}_{sec}$) in the primary flow cell cross-section at Re = 99,000. The construction is based on $\overline{V}$ and $\overline{W}$ via the 45° slanting probe using the rotation technique for each component. Each arrow indicates the magnitude (see scale) and direction ; location corresponds to the centre of the arrow. Four counter-rotating cells of secondary flow can be seen with the pattern shown in the inset to Fig. 34. This pattern is precisely that inferred by Nikuradse [5] based on the distortions seen

in his measured axial velocity distribution. Flow from the highest axial momentum region (maximum $\bar{U}$; located at y/c = 0, z/b $\simeq$ 0.48) is convected into each corner where it splits for the return flow. For the flow into the 60° corner, the largest observed secondary velocity was about 1.6% of U_b. The global maximum was indicated to be just under 2.2 % of U_b and this was located adjacent to the inclined wall. Compared to other class 3 geometries, this maximum value is a little larger than that found by Seale [21] for a simulated rod bundle (about 1.5% of U_b), but smaller than that determined by Lyall [18] for two square interconnected sub-channels (about 3.5% of local axial velocity).

CHAPTER 5

THE ANALYTICAL MODEL

In Chapter 3, the momentum equations in the y and z directions were replaced by a stream function Ψ and the axial vorticity ω (thus eliminating the in-plane pressure gradient). Providing suitable closures are made for Reynolds stresses and turbulent heat fluxes, the flow and heat transfer characteristics may be obtained by solving equations (3.13) to (3.18).

5.1 VORTICITY SOURCE TERM MODELLING

To calculate the secondary velocities $\overline{V}$ and $\overline{W}$ a means must be prescribed to determine the Reynolds stresses in the axial vorticity source term (equation (3.14a)). A number of investigators [6, 15, 35] have shown that the shear stress term in equation (3.14a) are negligible with respect to the normal stress terms. Several proposals have been made for simulating vorticity source via the normal stresses.

Launder and Ying [7] derived a model for the stresses $(\overline{v^2} - \overline{w^2})$ and $(\overline{vw})$ by simplifying the transport equations for these stresses given in model form by Hanjalic and Launder [57]. From these differential equations, algebraic expressions for the above stresses were obtained by neglecting the convection and diffusion terms (assumption of local equilib-

rium) and by further neglecting all secondary velocity gradients. The algebraic stress relations of Launder and Ying are :

$$\overline{v^2} - \overline{w^2} = -C''k/\epsilon(\overline{uw}\ \partial\bar{U}/\partial z - \overline{uv}\ \partial\bar{U}/\partial y) \qquad (5.1)$$

$$2\overline{vw} = C''k/\epsilon(\overline{uw}\ \partial\bar{U}/\partial y + \overline{uv}\ \partial\bar{U}/\partial z) \qquad (5.2)$$

where C'' is an empirical constant. The primary shear stresses components $\overline{uv}$ and $\overline{uw}$ were calculated from a standard eddy - viscosity model as :

$$-\rho\overline{uv} = \mu_{t,y}\ \partial\bar{U}/\partial y, \qquad (5.3)$$

$$-\rho\overline{uw} = \mu_{t,z}\ \partial\bar{U}/\partial z \qquad (5.4)$$

where $\mu_{t,y}$ and $\mu_{t,z}$ are the turbulent (eddy) viscosity in y and z directions respectively. By defining the anisotropy factor,

$$n = \mu_{t,z}/\mu_{t,y}\ , \qquad (5.4a)$$

substituting in equation (5.4) yields :

$$-\rho\overline{uw} = n\ \mu_{t,y}\ \partial\bar{U}/\partial y \qquad (5.4b)$$

Later $\mu_{t,y}$ will be written simply as μ_t. The isotropic eddy viscosity (μ_t) is related to the turbulence kinetic energy (k) and its dissipation rate (ϵ) by the Prandtl-Kolmogorov formula :

$$\mu_t = C_\mu\ \rho\ k^2/\epsilon \qquad (5.5)$$

where C_μ is an empirical constant which was assigned the value described by the standard k - ϵ model [75].

Seale [2], in a recent review of predicted secondary flows in several non-circular ducts by the Launder and Ying model, claimed that this method of generating secondary flow is unsatisfactory especially for multi-cells geometries. He proposed an algebraic model for calculating the source of axial vorticity without the need for the precise calculation of the Reynolds stresses. After examining the measurements of Brundrett and Baines [6] in a square duct, Aly et al. [15] in a triangular duct, sub-channels of a simulated rod bundles [70] and based upon Alshamani's [71,72] investigations, he neglected shear stress term and developed an expression for the difference in the normal stresses in terms of turbulent kinetic energy (k) as :

$$v^{+2} - w^{+2} = a'k^{+2} + b'k^{+} + c' \qquad (5.6)$$

where a', b' and c' are constants determined experimentally. Based on the experimental evidence of Laufer [68] in a circular pipe and of Aly et al. [15] along the mid-wall plane of the triangular duct, Seale [2] assumed that k varies parabolically in non-circular ducts with normal distance from the wall. The distribution of $k/(\overline{u}^*)^2$ for the present trapezoidal duct along the normals of the three walls shows (fairly well) a parabolic distribution as in Fig. 29. Seale presented an expression to describe this distribution from

the wall to the region of maximum mean velocity in the duct as :

$$k^+ = ki^+ + (kw^+ - ki^+)(1 - \frac{z}{\hat{z}_{max}})^2 \qquad (5.7)$$

The substitution of equation (5.7) into equations (5.6) and (3.14a) yield the following algebraic equation for the source of axial vorticity :

$$S_w = 8C' \frac{\rho(\overline{u^*})^2}{(\hat{z}_{max})^2} . kc^+ \; m \; z \; z \; z \; \frac{\delta \hat{z}}{\delta y} \qquad (5.8)$$
$$L \; P \; N$$

where C′ and m are empirical constants. A detailed derivation of equation (5.8) along with the empirical constants for the present trapezoidal duct is presented in Appendix A.

Regarding the present predictions, the two preceding models were both tried. For small C″, the predicted secondary flow pattern (either two or three cells) did not agree with experimental finding. For higher C″ values (i.e values to produce strong enough secondary flows), convergence was not achieved.

However, on the other hand, reasonable results were obtained by using Seale's model. Some difficulties were faced in defining the surface of no-shear from the present experi-

mental data. A modified form of Seale's model was developed. The details of this modifications are presented in Appendix A.

5.2 CLOSURE OF k, ε AND $\bar{T}$ EQUATIONS

The turbulent diffusion terms $\overline{vk'}$, $\overline{wk'}$, $\overline{v\epsilon'}$, $\overline{w\epsilon'}$, $\overline{vt}$ and $\overline{wt}$ appearing in equations (3.16), (3.17) and (3.18) are represented by a single gradient diffusion approach as follows:

$$\overline{vk'}(\rho\sigma_k) = -\mu_t \delta k/\delta y \quad , \quad \overline{wk'}(\rho\sigma_k) = -n\mu_t \delta k/\delta z \; ; \qquad (5.9)$$

$$\overline{v\epsilon'}(\rho\sigma_\varepsilon) = -\mu_t \delta \epsilon/\delta y \quad , \quad \overline{w\epsilon'}(\rho\sigma_\varepsilon) = -n\mu_t \delta \epsilon/\delta z \; ; \qquad (5.10)$$

$$\overline{vt}(\rho Pr_t) = -\mu_t \delta \bar{T}/\delta y \quad , \quad \overline{wt}(\rho Pr_t) = -n\mu_t \delta \bar{T}/\delta z \qquad (5.11)$$

where σ_k and σ_ε are empirical constants, Pr_t is the turbulent Prandtl number. Pr_t was regarded as a uniform constant over the field of flow. It was given the value of 0.9 as recommended by Launder and Spalding [73]. Based on computer optimization of the above reference σ_k was taken to equal 1, while σ_ε was determined via the following equation :

$$\sigma_\varepsilon = (\kappa^2/C_\mu^{1/2})/(C2-C1) \qquad (5.12)$$

where κ is the Von-Karman constant, C1, C2 and C_μ are constants which have been given the standard values as recommended by several investigators [73, 74, 75].

5.3 BOUNDARY CONDITIONS

5.3.1 Stream Function (Ψ)

For the solid walls and the symmetry line of the primary flow cell (Fig. 3), the stream function is constant. This constant was set equal to zero.

5.3.2 Axial Vorticity (ω)

At the symmetry line, it can be shown that the vorticity must be zero. At the solid walls, the vorticity was obtained from :

$$\omega_p = -2(\Psi_n - \Psi_p)/(3\rho(z_n - z_p)^2) \qquad (5.13)$$

Equation (5.13) was derived by Gosman et al. [1] on the assumption, that the secondary velocity increases linearly with the normal distance from the wall. Note, p is the node on the boundary; n is the node next to the boundary.

5.3.3 $\bar{U}$, k, ϵ and $\bar{T}$

a) At the symmetry line

Along the symmetry line, the gradients of each of these variables in the direction normal to the line of symmetry is zero. These conditions may be written as :

$$\eth k/\eth y = 0 = \eth \epsilon/\eth y$$

$$\eth \bar{U}/\eth y = 0 = \eth \bar{T}/\eth y \qquad (5.14)$$

Equations (5.14) were satisfied by setting the value of the variable at the right and left of the symmetry line to be equal.

b) Near the walls

The form of the k - ϵ model presented in Chapter 3 is valid only for fully developed turbulent flows. Close to the walls there is a region where the local Reynolds number of turbulence ($k^2/\epsilon\nu$) is so small that viscous effects predominate over turbulent ones. There are two methods of accounting for this region: The first is the low Reynolds number modelling method and the second is the wall function method. The method used here is the wall function method. Wall functions have been proposed and used by many authors including Spalding [76], Wolfshtein [78], and Patankar and Spalding [77]. It is based on the notion of one-dimensional flow and local turbulence equilbrium. These conditions give rise to the familiar logarithmic law of the wall velocity distribution :

$$U_n = u^* [A \ln z_n^+ + B] \qquad (5.15)$$

where u* is the local friction velocity, A and B are constants, z_n^+ is the normalized normal distance from the wall ($z_n u^*/\nu$), and n is the node adjacent to the wall which was designed to be located beyond the viscous sublayer for the Reynolds number range involved. The local friction velocity u* is given by :

$$u^* = (\tau/\rho)^{1/2} \qquad (5.15a)$$

where the local shear stress (τ) was calculated from the turbulence field data at the second string of nodes (m) in the fluid by using an explicit form of the log law :

$$\tau = \rho C_\mu^{1/4} k_m^{1/2} U_m / \{A \ln(C_\mu^{1/4} k_m^{1/2} |z_m - z_p| / \nu) + B\} \quad (5.15b)$$

The constants A and B were taken as A = 2.44, B = 5.0. These values of A and B are those recommended by Hinze [79] on the basis that they are good average values when compared to the experimental data obtained by various investigators and with the present experimental data in Section (4.5.5).

The boundary conditions for the turbulent kinetic energy (k) and its dissipation rate (ϵ) were specified also at the near wall node as:

$$k_n = (u^*)^2 / C_\mu^{1/2} \quad (5.16)$$

$$\epsilon_n = (u^*)^3 / (\kappa z) \quad (5.17)$$

where κ is the Von-Karman constant, z is the normal distance from the wall and n denotes the node adjacent to the wall. Equations (5.16) and (5.17) were obtained by the assumption of local equilibrium at the near wall region (assuming convection and diffusion to be zero and equating the production of turbulent energy to its dissipation).

The heat transfer field was solved for the case of constant axial wall heat flux per unit length with a constant

peripheral wall temperature. A similar form to the universal velocity profile has been used for the temperature profile near the wall which is :

$$T_n - T_w = \pm \dot{q}\, Pr_t \{ U/u^* + P^* \}/(\rho\, C_p\, u^*) \qquad (5.18)$$

where $\dot{q}$ is the heat flux into or from the wall and P* is a function accounting for the resistance of the viscous sublayer to heat transfer relative to that for the fully developed turbulent region {Jayatilleke [81]}. P* is given by :

$$P^* = 9.24\ ((Pr/Pr_t)^{3/4} - 1\ ) \qquad (5.19)$$

5.4 SUMMARY OF EQUATIONS TO BE SOLVED

5.4.1 Transport Equations

a) Axial momentum equation

$$\{\frac{\partial}{\partial y}(\bar{U}\frac{\partial \Psi}{\partial z}) - \frac{\partial}{\partial z}(\bar{U}\frac{\partial \Psi}{\partial y})\} - \{\frac{\partial}{\partial y}((\mu+\mu_t)\frac{\partial \bar{U}}{\partial y}) + \frac{\partial}{\partial z}((\mu+\mu_t)\frac{\partial \bar{U}}{\partial z})\} + \frac{\partial \bar{p}}{\partial x} = 0 \qquad (5.20)$$

b) Axial vorticity equation

$$\{\frac{\partial}{\partial y}(\omega\frac{\partial \Psi}{\partial z}) - \frac{\partial}{\partial z}(\omega\frac{\partial \Psi}{\partial y})\} - \{\frac{\partial}{\partial y}(\mu\frac{\partial \omega}{\partial y}) + \frac{\partial}{\partial z}(\mu\frac{\partial \omega}{\partial z})\} - \rho\frac{\partial^2}{\partial y \partial z}(\overline{v^2}-\overline{w^2}) + \rho(\frac{\partial^2}{\partial y^2} - \frac{\partial^2}{\partial z^2})(\overline{vw}) = 0 \qquad (5.21)$$

c) Stream function equation

$$\frac{\partial}{\partial y}\left(\frac{\partial \Psi}{\partial y}\right) + \frac{\partial}{\partial z}\left(\frac{\partial \Psi}{\partial z}\right) + \rho\omega = 0 \qquad (5.22)$$

d) Turbulent kinetic energy equation

$$\left\{\frac{\partial}{\partial y}\left(k\frac{\partial \Psi}{\partial z}\right) - \frac{\partial}{\partial z}\left(k\frac{\partial \Psi}{\partial y}\right)\right\} - \left\{\frac{\partial}{\partial y}\left(\left(\mu+\frac{\mu_t}{\sigma_K}\right)\frac{\partial k}{\partial y}\right)\right.$$

$$\left.+\frac{\partial}{\partial z}\left(\left(\mu+\frac{\mu_t}{\sigma_K}\right)\frac{\partial k}{\partial z}\right)\right\} - \mu_t\left\{\left(\frac{\partial \bar{U}}{\partial y}\right)^2 + \left(\frac{\partial \bar{U}}{\partial z}\right)^2\right\} + \rho\epsilon = 0 \qquad (5.23)$$

e) Turbulence energy dissipation rate equation

$$\left\{\frac{\partial}{\partial y}\left(\epsilon\frac{\partial \Psi}{\partial z}\right) - \frac{\partial}{\partial z}\left(\epsilon\frac{\partial \Psi}{\partial y}\right)\right\} - \left\{\frac{\partial}{\partial y}\left(\left(\mu+\frac{\mu_t}{\sigma_\varepsilon}\right)\frac{\partial \epsilon}{\partial y}\right)\right.$$

$$\left.+\frac{\partial}{\partial z}\left(\left(\mu+\frac{\mu_t}{\sigma_\varepsilon}\right)\frac{\partial \epsilon}{\partial z}\right)\right\} - C1\mu_t\frac{\epsilon}{k}\left\{\left(\frac{\partial \bar{U}}{\partial y}\right)^2 + \left(\frac{\partial \bar{U}}{\partial z}\right)^2\right\} + C2\rho\frac{\epsilon^2}{k} = 0 \qquad (5.24)$$

f) Temperature equation

$$\{\frac{\partial}{\partial y}(\bar{T}\frac{\partial \bar{\Psi}}{\partial z}) - \frac{\partial}{\partial z}(\bar{T}\frac{\partial \bar{\Psi}}{\partial y})\} - \{\frac{\partial}{\partial y}((\frac{\mu}{Pr}+\frac{\mu_t}{Pr_t})\frac{\partial \bar{T}}{\partial y}) + \frac{\partial}{\partial z}((\frac{\mu}{Pr}+\frac{\mu_t}{Pr_t})\frac{\partial \bar{T}}{\partial z})\} + \rho \bar{U}\frac{\partial \bar{T}}{\partial x} = 0 \qquad (5.25)$$

5.4.2 Algebraic Equations

a) Turbulent (eddy) viscosity :

$$\mu_t = C_\mu \rho k^2/\epsilon \qquad (5.26)$$

b) Source term for vorticity equation :

$$\frac{\partial^2}{\partial y \partial z}(\bar{v}^2 - \bar{w}^2) = 8C' \frac{\rho(\bar{u}^*)^2}{(\hat{z}_{max})^2} . kc^+ mz_L z_P z_N \frac{\partial \hat{z}}{\partial y} \qquad (5.27)$$

where ,

$$z_P = 1 - \hat{z}/\hat{z}_{max} \quad , \quad z_L = 1 - z/\hat{z}_{max} \quad ,$$

$$z_N = \{1 + z_M + (kw^+ - z_M)z_L^2\} - \{(1-z_L^2)(kw^+ - z_M)\} \quad , \qquad (5.28)$$

$$z_M = 1 - m z_p^2 \quad ,$$

$kc^+ = 1$, $m = 2.4$

c) Source term for axial momentum equation :

$$\partial\bar{p}/\partial x = -4\,\bar{\tau}_w/D_h \qquad (5.29)$$

d) Source term for temperature equation :

$$\partial\bar{T}/\partial x = \dot{q}_{av}/(\dot{m}\,C_p)\ .\ \text{wetted perimeter} \qquad (5.30)$$

e) Friction factor :

$$f = 8\,\bar{\tau}_w/\,(\rho U_b{}^2) \qquad (5.31)$$

5.4.3 Boundary Conditions

1) Symmetry line :

$$\Psi = 0 = \omega \quad ,$$

$$\bar{V} = 0 \quad ,$$

$$\partial\bar{U}/\partial y = 0 = \partial\bar{T}/\partial y \quad , \qquad (5.32)$$

$$\partial k/\partial y = 0 = \partial\epsilon/\partial y$$

2) Solid walls :

$$\Psi = 0 \qquad (5.33)$$

$$\omega_p = -2(\Psi_n - \Psi_p)/3\rho/(z_n - z_p)^2 \qquad (5.34)$$

where p is the wall node and n is the node adjacent to the wall in the normal direction.

$$U_n = u^* (A \ln z^+ + B) \qquad (5.35)$$

where

$$z^+ = u^* (z_n - z_p)/\nu$$

$$k_n = u^{*2}/C_\mu^{1/2} \quad , \qquad (5.36)$$

$$\epsilon_n = u^{*3} /(\kappa z) \quad , \qquad (5.37)$$

$$T_n = T_w + q\{U/u^* + P^*\}/(\rho\, C_p\, u^*) \qquad (5.38)$$

where ,

$$P^* = 9.24\ \{(Pr/Pr_t)^{3/4} - 1\}$$

and

$$u^{*2} = C_\mu^{1/4} k_m^{1/2} U_m / \{A \ln\{\rho C_\mu^{1/4} k_m^{1/2} (z_m - z_p)/\mu\} + B\}$$

5.4.4 Model Constants

$C_\mu = 0.09$, $\sigma_k = 1$, $C1 = 1.44$, $C2 = 1.92$, $\sigma_\varepsilon = 1.167$

$C' = 0.045$, $\kappa = 0.41$, $Pr_t = 0.9$, $A = 2.44$, $B = 5.0$

All the constants compared with other investigators constants are summarized in Table 4.

CHAPTER 6

THE NUMERICAL PROCEDURE

6.1 INTRODUCTION

Equations (5.20) to (5.25) may be written in the form :

$$a_\phi \left\{\frac{\delta}{\delta y}\left(\Phi\frac{\delta\Psi}{\delta z}\right)-\frac{\delta}{\delta z}\left(\Phi\frac{\delta\Psi}{\delta y}\right)\right\} - \left\{\frac{\delta}{\delta y}\left(b_{\phi,y}\frac{\delta\Phi}{\delta y}\right)+\frac{\delta}{\delta z}\left(b_{\phi,z}\frac{\delta\Phi}{\delta z}\right)\right\}+S_\phi=0 \quad (6.1)$$

The representative symbols in this equation are identified for each equation in Table 5. In order to solve these non-linear differential equations they are approximated to a set of algebraic equations by integration over finite areas. A non uniform Cartesian coordinate grid was adopted over the primary flow cell. The grid is shown in Fig. 35.

6.2 THE FINITE DIFFERENCE EQUATIONS

The integration of the different terms of the differential equations was performed over the area enclosed by the dotted line rectangle in Fig. 36. The sides of this rectangle lie midway between the neighbouring grid lines. The double integration over the domain shown in Fig. 36 yields :

$$a_\phi \int_{z,s}^{z,n} \int_{y,w}^{y,e} \left\{ \frac{\partial}{\partial y}\left(\Phi \frac{\partial \Psi}{\partial z}\right) - \frac{\partial}{\partial z}\left(\Phi \frac{\partial \Psi}{\partial y}\right) \right\} dydz -$$

Convection Term (Ic)

$$\int_{z,s}^{z,n} \int_{y,w}^{y,e} \left\{ \frac{\partial}{\partial y}\left(b_{\phi,y} \frac{\partial \Phi}{\partial y}\right) + \frac{\partial}{\partial z}\left(b_{\phi,z} \frac{\partial \Phi}{\partial z}\right) \right\} dydz$$

Diffusion Term (Id)

$$+ \int_{z,s}^{z,n} \int_{y,w}^{y,e} S_\phi dydz = 0 \qquad (6.2)$$

Source Term (Is)

The integrals for each term appearing in equation (6.2) are evaluated in the following sub-sections.

6.2.1 Convection Term

The following assumptions are considered to hold for integration of the convection term :

i) The function Φ is uniform within each rectangle and has the value of node P.

ii) The value of the stream function at the corner of the rectangle is equal to the average of the values on the four neighbouring nodes.

iii) The value of the function at interfaces e, w, n, or s must take the value possessed by the fluid upstream of the specific face (upwind differencing practice).

The convection term (Ic) of equation (6.2) can be broken to four separate integrals to give :

$$Ic = \int_{z,s}^{z,n} \{\Phi e(\frac{\delta\Psi}{\delta z})_e - \Phi w(\frac{\delta\Psi}{\delta z})_w\} dz - \int_{y,w}^{y,e} \{\Phi n(\frac{\delta\Psi}{\delta y})_n - \Phi s(\frac{\delta\Psi}{\delta y})_s\} dy \qquad (6.3)$$

Since the four terms are similar, only the first term will be considered here.

$$Ic1 = \int_{z,s}^{z,n} \Phi e(\frac{\delta\Psi}{\delta z})_e \, dz \qquad (6.4)$$

For well-behaved functions for Φ and Ψ there exists an average value of Φe which is Φe such that :

$$\Phi e = \frac{\int_{z,s}^{z,n} \Phi e(\frac{\delta\Psi}{\delta z})_e \, dz}{\int_{z,s}^{z,n} (\frac{\delta\Psi}{\delta z})_e \, dz} \simeq \frac{Ic1}{(\Psi ne - \Psi se)} \qquad (6.5)$$

Hence Ic1 can be written in the form :

$$Ic1 = \Phi e \, (\Psi ne - \Psi se) \qquad (6.6)$$

Where Φe, Ψne and Ψse can be expressed according to the above stated assumptions. The application of upwind scheme into equation(6.6) means that the value of Φ at the interface is equal to the value of Φ at the grid point on the upwind side of the face. Thus :

$$\Phi e = \Phi_P \quad \text{if} \quad (\Psi ne - \Psi se) > 0 \qquad (6.7a)$$

$$\Phi e = \Phi_E \quad \text{if} \quad (\Psi ne - \Psi se) < 0 \qquad (6.7b)$$

The conditional statements (6.7a,b) on Ic1 term can be written in the following form :

$$Ic1 \simeq \Phi_E \left\{\frac{(\Psi ne-\Psi se)-|\Psi ne-\Psi se|}{2}\right\}+\Phi_p \left\{\frac{(\Psi ne-\Psi se)+|\Psi ne-\Psi se|}{2}\right\} \quad (6.8)$$

Making use of assumption (ii), one can write :

$$\Psi se \simeq \frac{\Psi_{SE} + \Psi_E + \Psi_P + \Psi_S}{4} \quad (6.9)$$

The other three terms of equation (6.3) can be obtained by a similar treatment. Assembling and arranging the various terms give :

$$Ic = A_E (\Phi_P - \Phi_E) + A_W (\Phi_P - \Phi_W) + A_N (\Phi_P - \Phi_N) + A_S (\Phi_P - \Phi_S) \quad (6.10)$$

Where the coefficients A are :

$$A_E = \frac{a\phi}{8}\{(\Psi_{SE} + \Psi_S - \Psi_{NE} - \Psi_N) + |\Psi_{SE} + \Psi_S - \Psi_{NE} - \Psi_N|\},$$

$$A_W = \frac{a\phi}{8}\{(\Psi_{NW} + \Psi_N - \Psi_{SW} - \Psi_S) + |\Psi_{NW} + \Psi_N - \Psi_{SW} - \Psi_S|\},$$

$$A_N = \frac{a\phi}{8}\{(\Psi_{NE} + \Psi_E - \Psi_{NW} - \Psi_W) + |\Psi_{NE} + \Psi_E - \Psi_{NW} - \Psi_W|\}, \quad (6.11)$$

and,

$$A_S = \frac{a\phi}{8}\{(\Psi_{SW} + \Psi_W - \Psi_{SE} - \Psi_E) + |\Psi_{SW} + \Psi_W - \Psi_{SE} - \Psi_E|\}.$$

6.2.2 Diffusion Term

The diffusion term of equation (6.2) can be integrated to give :

$$Id = -\int_{z,s}^{z,n} \{(b_{\phi,y})_e \left(\frac{\partial\Phi}{\partial y}\right)_e - (b_{\phi,y})_w \left(\frac{\partial\Phi}{\partial y}\right)_w\} dz -$$

$$\int_{y,w}^{y,e} \{(b_{\phi,z})_n \left(\frac{\partial\Phi}{\partial z}\right)_n - (b_{\phi,z})_s \left(\frac{\partial\Phi}{\partial z}\right)_s\} dy \qquad (6.12)$$

The four terms of equation (6.12) are similar, therefore only one integral will be considered.

$$Id1 = \int_{z,s}^{z,n} (b_{\phi,y})_e \left(\frac{\partial\Phi}{\partial y}\right)_e dz \qquad (6.13)$$

Assuming piecewise linear profiles for $(b_{\phi,y})_e$ and Φ between the grid nodes P and E the values of equation (6.13) will be :

$$(b_{\phi,y})_e = \frac{(b_{\phi,y})_E + (b_{\phi,y})_P}{2} , \qquad (6.13a)$$

$$\left(\frac{\partial\Phi}{\partial y}\right)_e = \frac{(\Phi_P - \Phi_E)}{(y_E - y_P)} \quad \text{and} \qquad (6.13b)$$

$$z_n - z_s = (z_N - z_S)/2 \qquad (6.13c)$$

The factor 1/2 in equation (6.13c) arises from the assumption of the interfaces being midway between grid nodes N and S. The integration of equation (6.13) will be :

$$Id1 = \frac{\{b_{\phi,y})_E + b_{\phi,y})_W\}}{4} \cdot \frac{(z_N - z_S)}{(y_E - y_P)} \cdot (\Phi_E - \Phi_P) \qquad (6.14)$$

The other terms (Id2, Id3 and Id4) may be evaluated in a similar manner; assembling and arranging yields :

$$Id = B_E (\Phi_E - \Phi_P) + B_W (\Phi_W - \Phi_P) + B_N (\Phi_N - \Phi_P) + B_S (\Phi_S - \Phi_P) \qquad (6.15)$$

where:

$$B_E = \frac{\{b_{\phi,y})_E + b_{\phi,y})_P\}}{4} \cdot \frac{(z_N - z_S)}{(y_E - y_P)},$$

$$B_W = \frac{\{b_{\phi,y})_W + b_{\phi,y})_P\}}{4} \cdot \frac{(z_N - z_S)}{(y_P - y_W)},$$

$$B_N = \frac{\{b_{\phi,z})_N + b_{\phi,z})_P\}}{4} \cdot \frac{(y_E - y_W)}{(z_N - z_P)}, \qquad (6.16)$$

and,

$$B_S = \frac{\{b_{\phi,z})_S + b_{\phi,z})_P\}}{4} \cdot \frac{(y_E - y_W)}{(z_P - z_S)}.$$

6.2.3 Source Term

To evaluate source terms for the differential transport equations, the different parameters inside the integrals will be assumed constant within the control volume and assumed to have the value at node P. The validity of this assumption depends mainly on grid size; the finer the better. The source term of equation (6.2) can be integrated to give:

$$Is = \int_{z,s}^{z,n} \int_{y,w}^{y,e} S_{\phi} \, dy \, dz = S_{\phi,P} \cdot V_P \qquad (6.17)$$

where,

$$V_P = \frac{(y_E - y_W).(z_N - z_S)}{4} \qquad (6.18)$$

6.2.4 The Complete Finite-Difference Equation

Assembling equations (6.10), (6.15) and (6.17) to obtain the successive-substitution formula which may be written in the form :

$$\Phi_P = C_E \Phi_E + C_W \Phi_W + C_N \Phi_N + C_S \Phi_S - Is/\Sigma AB \qquad (6.19)$$

where,

$$
\begin{aligned}
C_E &= (A_E + B_E)/\Sigma AB \quad , \\
C_W &= (A_W + B_W)/\Sigma AB \quad , \\
C_N &= (A_N + B_N)/\Sigma AB \quad , \\
C_S &= (A_S + B_S)/\Sigma AB \quad , \\
\Sigma AB &= A_E + A_W + A_N + A_S + B_E + B_W + B_N + B_S
\end{aligned}
\tag{6.20}
$$

The A,s and B,s are given by equations (6.11) and (6.16) respectively.

6.3 STABILITY OF THE SUCCESSIVE SUBSTITUTION FORMULA

6.3.1 General

The conditions for convergence of an iterative solution of equations of the form of (6.19) have been specified in Gosman et al. [1] and by Said [22]. The convergence may be procured if the following conditions are satisfied:

(1) the sum of the moduli of the C,s must be less than or equal to unity at every node of the grid;

(2) this sum must be less than unity on at least one grid node; and

(3) the C,s and Is must not vary too greatly from one cycle of iteration to another. The first stability criterion

is satisified by using upwind differences for the convective terms. For the second criterion, the boundary conditions may be represented by an equation of the form ΦP = constant. This equation may be thought of as one in which the sum of C,s is zero. Hence the stability condition (2) is satisfied. For the third stability condition, the variations of the C,s and Is can always be made as small as desired by using under-relaxation or by modifying the source term. Usually this stability condition can be fulfilled by experience.

6.3.2 Modifications of k and ϵ Source Terms

In order to fulfill the stability criterion number three the modified k and ϵ successive substitution formulae may be written as:

$$k_P = \frac{C_E k_E + C_W k_W + C_N k_N + C_S k_S + \mu_{t,P} \frac{V_p}{\Sigma AB} \{ (\frac{\delta \bar{U}}{\delta y})^2 + (\frac{\delta \bar{U}}{\delta z})^2 \}}{\{1+\rho \epsilon_P V_P / (k_P \Sigma AB)\}} \qquad (6.21)$$

$$\epsilon_P = \frac{C_E \epsilon_E + C_W \epsilon_W + C_N \epsilon_N + C_S \epsilon_S + C1 \mu_{t,P} \{ (\frac{\delta \bar{U}}{\delta y})^2 + (\frac{\delta \bar{U}}{\delta z})^2 \}}{\{1+\rho C2 \epsilon_P V_P / (k_P \Sigma AB)\} / \{V_P \epsilon_P / (k_P \Sigma AB)\}} \qquad (6.22)$$

6.4 ITERATIVE TECHNIQUE

The transport equations are solved by using a point iterative method. This method is known as the Gauss Seidel method. To accelerate the convergence, the different updated values of the dependent variable at a certain node are used, for the next node, as soon as they become available. This method is preferred over block methods for its simplicity. A provision for under-relaxation was included in the procedure for all dependent variables. This took the form:

$$\overset{N}{\Phi i,j} = \overset{N-1}{\Phi i,j} + R_{\phi}(\overset{N}{\Phi i,j} - \overset{N-1}{\Phi i,j}) \qquad (6.23)$$

where $\overset{N}{\Phi i,j}$ is the value of the dependent variable at iteration number N, $\overset{N-1}{\Phi i,j}$ is the value at the same node in the previous iteration (N-1). R_{ϕ} is the under-relaxation factor. R_{ϕ} was taken usually as 0.7 for all variables.

6.5 CONVERGENCE CRITERION

The convergence criterion used was chosen such that the maximum fractional change of the parameter Φ in the field from one iteration to the next should not exceed a prescribed value. This criterion was of the form:

$$\left| \frac{\overset{N}{\Phi i,j} - \overset{N-1}{\Phi i,j}}{\overset{N}{\Phi i,j}} \right|_{max} \leq \xi$$

where ξ was taken as 0.001 for both the vorticity and stream function, and 0.0001 for the other parameters.

6.6 INITIAL CONDITIONS

The initial values of ω and Ψ were assumed to be zero everywhere. The initial values for $\overline{U}$, k, ϵ and $\overline{T}$ were assumed to have the distributions with secondary flow suppressed. The initial conditions for $\overline{U}$, k, ϵ and $\overline{T}$ solutions with no secondary flow were average values of these variables.

6.7 THE GRID SPACING

A non-uniform grid system has been employed. The grid distribution was arranged in such a way that the grid points were closely spaced adjacent to the walls with expanding step size in the direction away from these walls. The first string of nodes in the fluid was always beyond the viscous sublayer. Solutions with grid spacings 35x25, 31x21 and 26x16, in y and z directions respectively, were obtained. The solutions from the three grid systems were compared (for example) with the experimental results of $\overline{U}$ and k in Figs. 37 and 38 respectively. As shown in the figures, the solutions from the two grid systems 35x25 and 31x21 are very close and agree reasonable with the measurements. The computer time for one run of the 35x25 grid system was about 36 minutes while that for the 31x21 grid was about 13 minutes.

Because of this large difference, the 31x21 grid was used for all subsequent computations.

CHAPTER 7

RESULTS AND DISCUSSION OF THE NUMERICAL PROCEDURE

7.1 GENERAL

The solutions were obtained by employing the computation scheme described in Chapter 6. An isotropic eddy viscosity (n=1) was assumed. The predicted results for the present trapezoidal duct (ϕ=60°, a/b=0.77) are compared with the corresponding experimental results. The Reynolds number range was 20,000 to 200,000. Heat transfer results are presented for the case of constant axial wall heat flux with constant peripheral temperature. The wall temperature was taken as 100°C. The fluid was air at standard pressure and Pr=0.712. The properties of air were taken at the inlet bulk temperature (25°C). The grid nodes were non-uniform and consisted of a 31x21 mesh (Fig. 35) in the y and z directions respectively. All calculations were performed on the AMDAHL 470/V7 computer at the University of Manitoba. Details of the computer program are given in Appendix B.

7.2 MEAN AXIAL VELOCITY DISTRIBUTION

Figure 39 presents a comparison between predicted and measured mean axial velocities along two horizontal traverses. As may be seen from the figure, the agreement seems to be good at the symmetry line and near the inclined wall. However, for the central portions, the magnitude of predicted velocities are higher than the measurements by up to about 8%. However, the flatness in the velocity distribution due to secondary flow is obvious for the traverse at z/b=0.166.

Mean axial velocity distributions of $\bar{U}/U_b$ contours are presented in Fig. 40 along with the experimental results. The agreement is fairly reasonable when viewed in terms of percentage differences. The maximum difference is shown to be typically about 4% in the core region and about 8% in the corner regions. However, compared to the experimental contours, the predicted contours do not penetrate sufficiently into the corners. In fact, the model constant C′ is responsible for these small penetrations. At one stage, a higher value of C′ was used but the secondary flow magnitude appeared to be too strong compared to the experimental evidence. Also the shear stress agreement (for higher C′) with experiment is underestimated near the symmetry line and overestimated in the mid-span region (see Figs. 49 and 50). Thus, the value of C′=0.045 (as was used by Seale [21]) was chosen as the best value to give reasonable agreement for all variables with the experiment.

The effect of Reynolds number on the predicted ratio $\bar{U}_{max}/U_b$ has been examined in Fig. 41. It is noted that the duct maximum velocity normalized with the duct average bulk velocity U_b decreases with Reynolds number. For most of the experimental points, the predictions are 2% higher than the experimental values. These results are consistent with the experimental results of Nikuradse in reference [101] for flow in smooth circular tube.

7.3 MEAN TURBULENT KINETIC ENERGY DISTRIBUTION

The distributions of $k/(\overline{u^*})^2$ along two horizontal traverses are shown in Fig. 42. For the two traverses, the agreement seems to be satisfactory particularly in the core and near the inclined wall regions. However, these traverses are typical for other traverses in the duct cross-section. The well known pattern of k distribution for the traverse near the horizontal wall is as expected. This pattern has been described in connection with turbulence intensities in Section (4.5.6).

Comparison of the computed turbulent kinetic energy contours with the experimental data is shown in Fig. 43 for a Reynolds number of 99,000. The maximum difference is shown to be typically about 15% in the core region of the duct and about 28% in the wall and corner regions. The agreement between the two contours is less than the agreement in isovels contours in Fig. 40. It is evident that the penetration of

the contours towards the corners is much larger than that of the axial velocity in Fig. 40. This situation has been noted for other non-circular ducts {for example, Wilson et al. [28], Launder and Ying [7], Seale [21] and Brundrett and Baines [6]}.

7.4 VORTICITY AND STREAM FUNCTION DISTRIBUTIONS

The vorticity and stream function contours are represented in Fig. 44. The contours indicate a large vortex near the bottom wall, a smaller one near the top wall and two small cells close to the inclined wall. These contours indicate a secondary flow pattern similar to the one experimentally observed in Fig. 34.

7.5 SECONDARY VELOCITIES

The predicted secondary velocities are compared to the experimental data in Figs. 45 and 46 for $\overline{V}$ and $\overline{W}$ components respectively. For $\overline{V}$ component, the three traverses show a flow to the left near the bottom wall. The traverses at y/c=0.189 and 0.672 show flow to the left near th top wall. However, the traverse at y/c=0.378 is out of phase with the experimental data near the top wall. For the second component $\overline{W}$ the traverses at z/b=0.182 and 0.364 show upflow near the symmetry line, a downflow in the mid-span region and then upflow again near the inclined wall. For the third traverse the flow is down near the symmetry line and up near

the top corner. The overall agreement for the two components is reasonable especially when viewed in terms of trend-line accuracy. However, certain deficiencies are evident; for example near the duct walls. This may be attributed to an error of the measurements in this region due to wall effect.

Figure 47 presents the predicted secondary velocity contours. These contours show a maximum value of the secondary velocity component $\overline{V}$ in the return flow near the bottom wall of about 1.8% of the average bulk velocity U_b. The maximum value of the second component $\overline{W}$ is 1.5% of U_b and exists in the return flow at the mid wall bisector near the top wall. These values are comparable with the measurements.

7.6 TEMPERATURE DISTRIBUTION

The predicted isotherms (T*) are presented in Fig. 46. The left hand part of the figure represents contours with secondary flow suppressed from the calculation scheme. The effect of secondary flow on the temperature field was inferred from the distortions of the isotherms in the right hand part of Fig.48. As may be seen, the dimensionless temperature distributions resemble those of $\overline{U}/U_b$.

7.7 WALL SHEAR STRESS

The predicted wall shear stress distributions along the three walls of the trapezoidal duct are compared with the experimental results in Figs. 49, 50 and 51. As may be seen in the figures, the value of $C'=0.035$ gives better agreement than the other values. As mentioned in Section (7.2) the value $C'=0.045$ gives more bulging in the distributions of $k/(\overline{u*})^2$ and $\overline{U}/U_b$ and is not significantly worse for the shear stress agreement. Along the bottom wall the maximum difference between the measurements and predictions is about 8%. This maximum difference exists at $y/c \simeq 0.45$. For the top wall the agreement is fairly satisfactory. With respect to the inclined wall the dip in the distribution is shifted to the left. This makes a maximum difference of about 11% between the experiment and calculations. Because the sign of the vorticity source term largely affects the sign of the secondary flow at a point, and because the direction of the secondary flow controls the position of the dip, it is concluded that the latter discrepancy in the inclined wall may be partially attributed to the method of vorticity source term modelling. However, the overall agreement for the shear stress is fairly reasonable.

With regard to the individual average shear stress of the walls, the average of the top wall is about 9% above the overall average whereas the inclined wall was 2% lower than the overall average. The average of the bottom wall was equal the overall average.

7.8 WALL HEAT FLUX

The local heat flux distribution around the periphery of the duct is presented in Figs. 52, 53 and 54. The distribution of wall heat flux as predicted without secondary flow is superimposed on the above distributions. These distributions are qualitatively similar to the predicted pattern for local wall shear stress. As shown in the above figures, suppression of the secondary flows from the computation scheme increases the variation of the heat flux around the walls of the duct.

7.9 FRICTION FACTOR AND NUSSELT NUMBER

Predicted average friction and Nusselt numbers were correlated using least-squares fit of straight lines for 10 values of f and Nu. Each least-squares fit line is capable of describing the data with a standard deviation of about 0.3% of the range average. Figure 55 shows the comparison of the friction factor numerical correlation with the experimental correlation and the correlation line for friction factor in smooth circular tubes. The predicted friction factors are from 2-7% higher than the present experiment and within 4% of pipe flow.

Concerning Nusselt number, Fig. 56 shows the numerical prediction correlation of Nu versus Re along with correlations for circular tube of Dittus-Boelter [82] and Petukhov-

Popov [83]. Also Fig. 56 includes the experimental data line of Altemani and Sparrow [17] in an unsymmetrically heated triangular duct. The present predictions are 5% higher than Petukhov-Popov correlation and 12% lower than Dittus-Boelter correlation. Also the present predictions are about 12% higher than the experimental data of Altemani and Sparrow [17].

It is concluded that the present predictions of f and Nu are consistent with the existing correlations.

7.10 EFFECT OF REYNOLDS NUMBER

The effect of Reynolds number on the predicted flow structure and local heat transfer characteristics is described below.

The dependence of the average friction factor and Nusselt number on the Reynolds number is described by the following correlations:

$$f \propto Re^{-0.20}, \qquad (7.1)$$

$$Nu \propto Re^{0.80} \qquad (7.2)$$

As expected, friction factor decreased with Re, while Nusselt number increased with Re.

Figures 57, 58 and 59 present the distributions of $\overline{U}/U_b$, $k/(\overline{u^*})^2$ and T^* along horizontal traverses respectively. It is evident from the three figures that the distributions be-

come progressively flatter in the core region as Re increases. However, the change is very small in the corner and wall regions.

A contour plot of stream function Ψ for two different Reynolds numbers is shown in Fig. 60. It can be seen that the large cell near the bottom wall grows in strength and extent as Re increases from 40,000 to 160,000. The cell near the top wall grows in strength but decreases in extent; the latter by almost the same amount of the increase of the bottom cell. There is no significant change either in strength or extent for the two cells adjacent to the inclined wall.

The secondary velocity components normalized by Ub are examined in Figs. 61 and 62 for Reynolds number effect. In addition to shifts as indicated above, there is generally some increase of secondary flow magnitude with Reynolds number. However, this dependence becomes small as the Reynolds number becomes high as shown by the small differences between Reynolds numbers of 120,000 and 200,000. The secondary velocity components normalized by the average friction velocity $\overline{u}^*$ are shown in Figs. 63 and 64. The same behaviour with Reynolds number occurs.

The normalized (with circumferential average value) local wall shear stresses and local wall heat fluxes were found to be roughly independent of Reynolds number. Figures 65 (bottom wall) and 66 (inclined wall) are chosen to illustrate this finding.

CHAPTER 8

PREDICTIONS OF OTHER TRAPEZOIDAL DUCTS

8.1 GENERAL

As mentioned in Chapter 2, the only flow structure data in trapezoidal ducts is due to Rodet [3]. Also the data of Chiranjivi and Sankara Rao [4] were confined to bulk heat transfer only. Converged solutions were obtained for the two ducts using the same model constants that were used for the present trapezoidal duct. Comparisons have been made with the available experimental data.

8.2 FRICTION FACTOR AND NUSSELT NUMBER

Figure 67 shows the correlation between average friction factor f and Reynolds number Re for the three trapezoidal ducts. The lines were obtained by a least-squares fit of straight lines for seven cases for both Rodet's duct [3] and the duct of Chiranjivi and Sankara Rao [4]. The three lines are capable of describing the numerical prediction data with a maximum standard deviation of about 0.4% of the range average. The numerical finite difference predictions of f for Rodet's duct overestimate his experimental data points by a maximum value of 9%. The three lines of f lie below the standard correlation shown in Fig. 67 by a maximum of about 7%. This deviation is common in other non-circular ducts.

For the heat transfer, the correlation of Nu with Re is shown in Fig. 68 along with the Dittus-Boelter [82] and Petukhov-Popov [83] correlations for smooth circular tubes. The standard deviation of Nu line is within 0.2% of the range average. As expected (like f vs Re correlation) the difference between the correlations of the three ducts are small. The experimental data correlation of Chiranjivi and Sankara Rao [4] is presented in Fig. 69. As shown in this figure the difference between the exponent of Re for the present prediction (0.777) and their exponent (0.4) is large. Also their correlation does not agree with circular tube correlations as shown in the figure. This may be attributed to either the low Reynolds number (15,300) under which their experiment was done or to the difference between the numerical prediction boundary condition and their condition of asymmetrical heating. However, it has been already established by several investigators [17, 84, 85, 86, 87] that the average Nusselt number values do not change appreciably with the kind of boundary conditions applied. Hence it is concluded that the sizeable difference between the present predictions of Nu for the Chiranjivi and Sankara Rao duct and their experimental work is due to the small Reynolds number under which their experiment was conducted. The present predictions for their duct agree with the Dittus-Boelter correlation to within 12% and with the Petukhov-Popov correlation to within 4%.

8.3 MEAN AXIAL VELOCITY AND TURBULENT KINETIC ENERGY

The predicted isovels and turbulent kinetic energy for Rodet's trapezoidal duct are plotted along with his experimental data in Figs. 70, 71 and 72. The isovels shown in Figs. 70 and 71 are for two different C′. The isovels show reasonable agreement with his experimental data. The difference between the two contours of mean axial velocity is less than about 1% in the core region and about 7% near the walls and corners. It is noted for C′=0.045 (Fig. 70) that the bulging of the predicted contours is less than that which exists in the experimental contours particularly near the inclined wall. Hence the value of C′=0.045 apparently is not high enough to cause the same bulging as the experiment. However, whereas using a higher value of C′=0.055 does give more bulging in the velocity contours as shown in Fig. 71, the overall agreement with the experimental data looks little better than in Fig. 70.

The mean turbulent kinetic energy are compared in Fig. 72 for C′=0.045. Qualitatively, the agreement is reasonable. Some quantative disagreement is noted near the walls where predictions underestimate the measurements by about 13%. The difference between the two contours is about 4% in the core region. As shown in Fig. 72, the predictions of k show four cells of secondary flow and this agrees with the experimental pattern. In general, the level of agreement shown in Fig. 72 is considered to be fair.

The predicted isovels and turbulent kinetic energy for the duct of Chiranjivi and Sankara Rao [4] are documented in Fig. 73. Generally the distributions do not differ much from those of other trapezoidal ducts.

8.4 LOCAL FRICTION VELOCITY AND HEAT FLUX

A comparison between the predicted local friction velocity u^* (normalized by the overall average $\bar{u}^*$) for Rodet's duct and his calculations is shown in Fig. 74. Rodet's calculations were based on his measured axial velocity using the universal law of the wall. The present predictions underestimate his calculations near the corners and the midwall bisector by a maximum of about 9%. Also, there is a deviation between the two distributions of the inclined wall. This disagreement may be partly attributed to his extrapolation of the axial velocities near the walls. However, the distributions display substantially the same variations as Rodet's calculations. The average wall shear stress for bottom and top walls is about 2% and 8% lower than the overall average respectively while the inclined wall is about 3% higher than the overall average. Figure 74 includes the predictions of Nakayama et al. [24] using a different vorticity source model. The present predictions are closer to Rodet's calculations particularly for bottom and top walls. However, the dip position of the inclined wall of Nakayama et al. agrees with Rodet's data better than

the present predictions. The distributions of the local heat flux are quite similar to that of the local friction velocity.

For the purpose of possible future comparisons with experiments, the local wall shear stress and heat flux for the duct of Chiranjivi and Sankara Rao [4] are presented in Fig. 75. The qualitative features of the distributions do not differ much from those of other trapezoidal ducts.

CHAPTER 9

CONCLUSIONS AND RECOMMENDATIONS FOR FUTURE WORK

The following conclusions are drawn from the experimental and numerical results. They are applicable to fully developed turbulent flows in trapezoidal ducts for the Reynolds number range of 20,000 to 200,000.

(i) The secondary flow pattern in trapezoidal ducts was confirmed experimentally by direct measurements of $\overline{V}$ and $\overline{W}$ components. The pattern consists of four counter-rotating cells of secondary flow per symmetric half of the duct. The pattern is such that the flow is directed from the high axial momentum region at the centre of the duct towards the corners along approximately the corners bisectors. The return flow is along the three walls and then back to the core region. Maximum secondary velocity components are barely larger than 2% of U_b.

(ii) The flow structure is clearly influenced by the presence of secondary flows. The bulging of turbulent kinetic energy contour towards the corners is more pronounced than on the axial velocity and temperature fields.

(iii) The distributions of $\overline{uw}/(\overline{u^*})^2$ along the duct symmetry line range basically from -1 to +1 in almost linear fashion. The vertical traverses of $\overline{uv}/(\overline{u^*})^2$ undergoes an alternating sign change across the duct height due to secondary flow. These characteristics are consistent with Rodet [3] for a trapezoidal duct of ϕ=75° and a/b=0.536.

(iv) Numerical predictions were made using the k-ϵ turbulence model coupled with Seale's [2] model for vorticity source term. The overall level of agreement between numerical predictions and available experimental data was considered satisfactory.

(v) The effect of ϕ and a/b on the average friction factor and Nusselt number is small over the range of $60° \leq \phi \leq 75°$ and $0.28 \leq a/b \leq 0.77$.

(vi) For heat transfer predictions, the isotherms are qualitatively similar to isovels. The local heat flux distribution along the walls is affected by the secondary flow currents.

Since the trapezoidal duct is akin to the annular sector duct, the author recommends studing fully developed flows in annular sector ducts. This will help to understand the flow and heat transfer characteristics in multi-passage tubes. In view of the present work, it was found that the solution of the vorticity equation is sensitive to $\hat{z}$ line; therefore this line should be defined with caution in the corner of an obtuse angle. Also the vorticity boundary condition near the inclined wall should be handled carefully. It is recommended that more general and simple vorticity source models should be tested in complicated ducts (multi-cells geometries).

REFERENCES

1. Gosman, A.D., Pun, W.M., Runchal, A.K., Spalding, D.B., and Wolfshtein, M. "Heat and Mass Transfer in Recirculating Flows" Academic Press, 1969.

2. Seale, W.J. "Turbulence Generated Secondary Flows in Ducts of Non-circular Cross-section" J. Mech. Eng. Sci., Vol. 24, No.3, pp. 119-127, 1982.

3. Rodet, E. "Etude de l'Ecoulement d'un Fluide dans un Tunnel Prismatique De Section Trapezoidale" Publ. Sci. et Tech. du Min. de L'Air, No. 369, 1960.

4. Chiranjivi, C. and Sankara Rao, P.S. "Laminar and Turbulent Forced Convection Heat Transfer in a Symmetric Trapezoidal Channel" Indian Journal of Technology, Vol. 9, pp. 416-420, 1971.

5. Nikuradse, J. "Untersuchungen uber turbulente Stromungen in ncht kreisformigen" Rohren.Ing.-Archiv 1, 306-332, 1930.

6. Brundrett, E. & Baines, W.D. "The Production and Diffusion of Vorticity in Duct Flow" J. Fluid Mech., Vol. 19, pp. 375-394, 1964.

7. Launder, B.E. & Ying, W.M. "Secondary Flows in Ducts of Square Cross-section" J. Fluid Mech., Vol. 54, pp. 289-295, 1972.

8. Gessner, F.B., Po., J.K. and Emery, A.F. "Measurements of Developing Turbulent Flow in a Square Duct" Symposium on Turbulent Shear Flows, Univ. Park, Pennsylvania, Vol. 1, pp. 9.1-9.10, April 1977.

9. Hoagland, L.C. "Fully Developed Turbulent Flow in Straight Rectangular Ducts -Secondary Flow, its Causes and Effect on the Primary Flow" Ph.D. Thesis, MIT, 1960.

10. Leutheusser, H.J. "Turbulent Flow in Rectangular Ducts" ASCE, J. Hydraulics Division, Vol. 89, No. HY3, pp. 1-19, 1963.

11. Gessner, F.B. "Turbulence and Mean Flow Characteristics of Fully Developed Flow in Rectangular Channels" Ph.D Thesis, Purdue University, 1964.

12. Gessner, F.B. & Jones, J.B. "On Some Aspects of Fully Developed Turbulent Flow in Rectangular Channels" J. Fluid Mech., Vol. 23, pp. 689-713, 1965.

13. Melling, A. & Whitelaw, J.H. "Turbulent Flow in a Rectangular Duct" J. Fluid Mech., Vol. 78, pp. 289-315,1976.

14. Trupp, A.C. "The Structure of Turbulent Flow in Triangular Array Rod Bundles" Ph.D. Thesis, University of Manitoba, Winnipeg, Canada, 1973.

15. Aly, A.M.M., Trupp, A.C. & Gerrard, A.D. "Measurements and Predictions of Fully Developed Turbulent Flow in an Equilateral Triangular Duct" J. Fluid Mech., Vol. 85, pp. 57-83, 1978.

16. Cremers, C.J. & Eckert, E.R.G. "Hot-wire Measurements of Turbulence Correlations in a Triangular Duct" Trans. ASME, 84E, J. Appl. Mech., Vol. 4, pp. 609-614, 1962.

17. Altemani, C.A.C. & Sparrow, E.M. "Turbulent Heat Transfer and Fluid Flow in an Unsymmetrically Heated Triangular Duct" Trans. of the ASME, J. Heat Transfer, Vol. 102, pp. 590-597, Nov. 1980.

18. Lyall, H.G. "Measurement of Flow Distribution and Secondary Flow in Ducts Composed of Two Square Interconnected Sub-Channels" Symposium on Internal Flows, University of Salford, Apr. 20-22, pp. E16-E23, 1971.

19. Kacker, S.C. "Some Aspects of Fully Developed Turbulent Flow in Non-circular Ducts" J. Fluid Mech., Vol. 57, Part 3, pp. 583-602, 1973.

20. Carajilescov, P. & Todreas, N.E. "Experimental and Analytical Study of Axial Turbulent Flows in an Interior Sub-channel of a Bare Rod Bundle" Trans. ASME, J. Heat Transfer, Vol. 98, pp. 262-268, 1976.

21. Seale, W.J. "Measurements and Predictions of Fully Developed Turbulent Flow in a Simulated Rod Bundle" J. Fluid Mech., Vol. 123, pp. 399-423, 1982.

22. Said, M.N.A.A. "Predictions and Measurements of Fully Developed Turbulent Flow in Longitudinal Internally Finned Tubes" Ph.D. Thesis, University of Manitoba, Winnipeg, Canada, 1981.

23. Shah, R.K. & London, A.L. Laminar Flow Forced Convection in Ducts" Advances in Heat Transfer, Supplement 1, Academic Press, 1978.

24. Nakayama, A., Chow, W.L. and Sharma, D. "Calculation of Fully Developed Turbulent Flows in Ducts of Arbitrary Cross-section" J. Fluid Mech., Vol. 128, pp. 199-217, 1983.

25. Launder, B.E. & Ying, W.M. Prediction of Flow and Heat Transfer in Ducts of Square Cross-section" Proc. Instn. Mech. Engrs., Vol. 187, pp. 455-461, 1973.

26. Naot, D., Shavit, A. and Wolfshtein "Numerical Calculation of Reynolds Stresses in a Square Duct With Secondary Flow" Warme und Stoffubertragung 7, pp. 151-161, 1974.

27. Emery, A.F., Neighbors, P.K. and Gessner, F.B. "The Numerical Prediction of Developing Turbulent Flow and Heat Transfer in a Square Duct" Trans. of the ASME, J. of Heat Transfer, Vol. 102, pp. 51-57, Feb. 1980.

28. Wilson, N.W., Azad, R.S. and Trupp, A.C. An Analysis of the Effect of Secondary Flows on the Longitudinal Velocity Distribution in Square Ducts" Symp. Internal Flows, University of Salford, Paper 11, April 1971.

29. Gosman, A.D. & Rapley, C.W. "Fully Developed Flow in Passages of Arbitrary Cross-section" in C. Taylor & K. Morgan (eds), Recent Advances in Numerical Methods in Fluids, Pineridge Press, Swansea, UK, 1980.

30. Nakayama, A. "Three-dimensional Flow Within Conduits of Arbitrary Geometrical Configurations" Ph.D. Thesis, University of Illinois at Urbana-Champaign, 1981.

31. Zhou, Z. "A Comparison of Turbulent Flow Predictions For Rectangular Ducts Using Five Vorticity Source Models" M.Sc. Thesis, The University of Manitoba, Winnipeg, Canada, 1985.

32. Gosman, A.D. & Rapley, C.W. "A Prediction Method for Fully Developed Turbulent Flow Through Non-circular Passages" Numerical Methods in Laminar and Turbulent Flows (eds. C. Taylor et al.), Pentech, 1978.

33. Rapley, C.W. & Gosman, A.D. "The Prediction of Turbulent Flow and Heat Transfer in a Narrow Isosceles Triangular Duct" Int. J. Heat and Mass Transfer, Vol. 27, pp. 253-262, 1984.

34. Aly, A.M.M. "Turbulent Flows in Equilateral Triangular Ducts and Rod Bundle Sub-channels" Ph.D. Thesis, The University of Manitoba, Winnipeg, Canada, 1977.

35. Trupp, A.C. & Aly, A.M.M. "Predicted Secondary Flows in Triangular Array Rod Bundles" ASME J. Fluid Eng., Vol. 101, pp. 354-363, 1979.

36. Ivanovic, M. "Prediction of Flow and Heat Transfer in Internally Finned Tubes" Ph.D. Thesis, University of Minnesota, July, 1978.

37. Launder, B.E. & Spalding, D.B. "Mathematical Models of Turbulence" Academic Press, London, 1972.

38. Launder, B.E. & Spalding, D.B. "The Numerical Computation of Turbulent Flows" Computer Methods in Applied Mechanics and Engineering, Vol. 3, pp. 269-289, 1974.

39. Launder, B.E. & Spalding, D.B. "Turbulence Models and Their Applications to the Prediction of Internal Flows" Symposium on Internal Flows, University of Salford, April 1971.

40. Bradshaw, P. "The Understanding and Prediction of Turbulent Flow" Aeronautical J., Vol. 76, pp. 403-418, July 1972.

41. Harlow, F.H. "Turbulence Transport Modelling" Published by AIAA, New York, 1973.

42. Rodi, W. & Spalding, D.B. "A Two-parameter Model of Turbulence, and its Application to Free Jets" Warme-und Stoffubertragung, B.3, S. 85-95, Springer-Verlag, 1970.

43. Reynolds, W.C. "Computation of Turbulent Flows" Annual Review of Fluid Mechanics, Vol. 8,, pp. 183-208, 1970.

44. Prandtl, L. & Wiegkardt, K. "Uber eim neues Formelsystem fur die asgebildete Turbulenz" Nachr. Akad. Wiss. Gottingen, Math.-Phys.KL, p. 6, 1945.

45. Bradshaw, P., Ferriss, D.H. and Atwell, N.P. "Calculation of Boundary Layer Development Using the Turbulent Energy Equation" J. Fluid Mech. Vol. 28, pp. 593-616, 1967.

46. Nee, V.W. & Kovasznay, L.S.G. "Simple Phenomenological Theory of Turbulent Shear Flows" The Physics of Fluids 12, 3, p. 473, 1969.

47. Kolmogorov, A.N. "Equations of Turbulent Motion of an Incompressible Fluid" Itv. Ak. Nauk SSR, Seria fizicheska VI 1942, pp. 56-58, No. 1 2(1942)

48. Ng., K.H. and Spalding, D.B. "Some Applications of a Model of Turbulence to Boundary Layers Near Walls" Physics of Fluids, Vol. 15, pp. 20-30, 1972.

49. Spalding, D.B. "The Calculation of the Length Scale of Turbulence in Some Turbulent Boundary Layers Remote from Walls" Imperial College, Heat Transfer Section Rep. TWF/TN/31.

50. Harlow, F.H. & Nakayama, P.I. "Transport of Turbulence Energy Decay Rate" Los Alamos Sci. Lab. Univ. California Rep. LA-3854, 1968.

51. Jones, W.P. & Launder, B.E. "The Prediction of Laminarisation With a 2-Equation Model of Turbulence" Int. J. Heat Mass Transfer Vol. 15, p. 301, 1972.

52. Rotta, J. "Recent attempts to Develop a Generally Applicable Calculation Method for Turbulent Shear Flow Layers" Proceedings of AGARD Conference on Turbulent Shear Flows, London, 1971.

53. Llegbusi, J.O. & Spalding, D.B. "An Improved Version of the k-W Model of Turbulence" ASME J. of Heat Transfer, Vol. 107, pp. 63-69, Feb. 1985.

54. Chou, P.Y. "On the Velocity Correlations and the Solution of the Equations of Turbulent Flactuations" Quart. Appl. Math. Vol. 3, p. 38, 1945.

55. Rotta, J. "Statistische Theorie nichthonogener Turbulenz" Zeitsch fur Physik, 129, 547, and 131,51, (1951).

56. Davidov, B.I. "On the Statistical Dynamics of an Incompressible Turbulent Fluid" Dokl. AN SSSR 136, 47, (1961).

57. Hanjalic, K. & Launder, B.E. "A Reynolds Stress Model of Turbulence and its Applications to Thin Shear Flows" J. Fluid Mech., Vol. 52, pp. 609-638, 1972.

58. Naot, D., Shavit, H. and Wolfshtein, M. "Numerical Calculation of Reynolds Stresses in a Square Duct With Secondary Flow" Warme und Stoffubertragung 7, pp. 151-161, 1974.

59. Launder, B.E., Reece, G.J. and Rodi, W. "Progress in the Development of a Reynolds Stress Turbulence Closure" J. Fluid Mech. Vol. 68, 537-566, 1975.

60. Reynolds, W,C. "Computation of Turbulent Flows - State - of- The - Art" Report MD-27, Thermo-Sciences Division, Department of Mechanical Engineering, Stanford University, 1970.

61. DANTIC "Probe Manual" DANTIC Electromedical A/S, Herlev, Denmark.

62. Lawn, C.J. "Turbulence Measurements with Hot-wires at B.N.L." Central Elec. Gen. Board, Berkley Nuclear Labs. Rep. RD/B/M1277, 1969.

63. Khalifa, M.M.A. & Trupp, A.C. "Turbulent Flow Characteristics in a Trapezoidal Duct - Experimental Results" Dept. of Mech. Eng., University of Manitoba, Report No. ER25.39, June 1985.

64. Carlson, C.W. & Irvine, T.F. "Fully Developed Pressure Drop in Triangular Shaped Ducts" Trans. ASME, J. Heat Trans., Vol. 83, pp. 441-444, 1961.

65. Patel, V.C. "Calibration of the Preston Tube and Limitations on It,s Use in Pressure Gradients" J. Fluid Mech., Vol. 25, pp. 185-208, 1965.

66. Preston, J.H. "The Determination of the Local Skin Friction by Means of Surface Pitot Tube" Journal of the Royal Aeronautical Society, Vol. 58, pp. 109-121, 1954.

67. Ower, F. & Pankhurst, R.C. "The Measurements of Air Flow" Pergamon Press, 1966.

68. Laufer, J. "The Structure of Turbulence in Fully Developed Pipe Flow" NACA Rep. 1174, 1954.

69. Gerrard, A.D. "Turbulent Flow in an Equilateral Triangular Duct" M.Sc. Thesis, University of Manitoba, 1976.

70. Rehme, K. "Experimentelle Untersuchungen der turbulenten Stromung in einem Wandkanal eines Stabbundles" Kernforschungszentrum, KFK 2441, 1977.

71. Alshamani, K.M.M. "Relationships Between Turbulent Intensities in Turbulent Pipe and Channel Flows" Aero. J., Vol. 83, 159-191, 1979.

72. Alshamani, K.M.M. Correlations Among Turbulent Shear Stress, Turbulent Kinetic Energy, and Axial Turbulence Intensity" AIAA J., Vol. 16, 859-861, 1978.

73. Launder, B.E. & Spalding, D.B. "The Numerical Computation of Turbulent Flows" Comput. Meth. Appl. Mech. Eng. Vol. 3, p. 269, 1974.

74. Rodi, W. 1980 "A New Algebraic Relation for Calculating the Reynolds Stresses" Z. angew. Math. Mech. 56, T219-T221, 1976.

75. Rodi, W. "Turbulence Models and Their Application in Hydraulics" Intl Assn for Hydraul. Res., Delft, The Netherlands, 1980.

76. Spalding, D.B. "Monograph on Turbulent Boundary Layers" Report No. TWF/TN/33, Mech. Eng. Dept. Imperial College, 1967.

77. Patankar, S.V. & Spalding, D.B. "Heat and Mass Transfer in Boundary Layers" Intertext Books, London, 1970.

78. Wolfshtein, M. "The Velocity and Temperature Distribution in One-Dimensional Flow with Turbulence Augmentation and Pressure Gradient" Int. J. Heat Mass Transfer, Vol. 12, pp. 301-318, 1969.

79. Hinze, J.O. "Turbulence" 2nd edition,, McGraw Hill, 1975.

80. Kays, W.M. "Convective Heat and Mass Transfer" 2nd edition,, McGraw Hill, 1980.

81. Jayatilleke, C.L.V. "The Influence of Prandtl Number and Surface Roughness on the Resistance of the Laminar Sub-layer to Momentum and Heat Transfer" Progress in Heat and Mass Transfer, International Journal of Heat and Mass Transfer, Vol. 1, pp. 193-329, Pergamon Press, 1969.

82. Eckert, E.R.G. & Drake, R.M. "Heat and Mass Transfer" 2nd edition,, McGraw Hill, 1959.

83. Petukhov, B.S. "Heat Transfer and Friction in Turbulent Pipe Flow with Variable Physical Properties" Advances in Heat Transfer, Vol. 6, Academic Press,, pp. 503-564, 1972.

84. Patankar, S.V. & Acharya, S. "Development of a Turbulence Model for Rectangular Passages" Transaction of the CSME, Vol. 8, No. 3, 1984.

85. Novotny, J.L., McComas, S.T., Sparrow, E.M. and Eckert, E.R.G. "Heat Transfer for Turbulent Flow in Rectangular Ducts With Two Heated and Two Unheated Walls" AICHE J., Vol. 10, No. 4,, pp. 466-470, 1964.

86. Sparrow, E.M., Lloyd, J.R. and Hixon, C.W. "Experiments on Turbulent Heat Transfer in an Asymmetrically Heated Rectangular Duct" Trans. of the ASME, J. Heat Transfer, 88, pp. 170-174, 1966.

87. Knowles, G.R. & Sparrow, E.M. "Local and Average Heat Transfer Characteristics for Turbulent Airflow in an Asymmetrically Heated Tube" ASME J. of Heat Transfer, Vol. 101, pp. 635-641, 1979.

88. Demuren, A.O. & Rodi, W. "Calculation of Turbulence - Driven Secondary Motion in Non-circular Ducts" J. Fluid Mech., Vol. 140, pp. 189-222, 1984.

89. Patanker, S.V. & Spalding, D.B. "A Calculation Procedure for Heat, Mass and Momentum Transfer in 3D Parabolic Flows" Int. J. Heat Mass Transfer Vol. 15, 1787-1806, 1972.

90. Tatchell, D.G. "Convective Processes in Confined, Three Dimensional Boundary Layers" Ph.D. Thesis, University of London, 1975.

91. Patankar, S.V. "Numerical Heat Transfer and Fluid Flow" McGraw-Hill, 1980.

92. Malak, J., Hejna, J. and Schmid, J. "Pressure Losses and Heat Transfer in Non-circular Channels with Hydraulic Smooth Walls" Int. J. Heat Mass Transfer, Vol. 18, pp. 139-149, 1975.

93. Seale, W.J. "Turbulent Diffusion of Heat Between Connected Flow Passeges Part 2: Predictions Using the ($k-\epsilon$) Turbulence Model" Nucl. Engng. Des., Vol. 54, 197-209, 1979.

94. Hatton, A.P. & Quarmby, A. "The Effect of Axially Varying and Unsymmetrical Boundary Conditions on Heat Transfer With Turbulent Flow Between Parallel Plates" Int. J. Heat Mass Transfer, Vol. 6, pp.903-914, 1963.

95. Emmons, H. "Shear Flow Turbulence" Proc. 2nd U.S. National Congress Appl. Mech., pp. 1-12, 1954.

96. Bart, J. & Harlow, F.H. "Transport Equations in Turbulence" The Physics of Fluids, Vol. 13, No. 11, Nov. 1970.

97. Ibragimov, M.H., Petrishchev, V.S. and Sabelev, G.I. "Calculation of Heat Transfer in Turbulent Flow With Allowance For Secondary Flow" Int. J. Heat Mass Transfer, Vol. 14, pp. 1033-1037, 1971.

98. Date, A.W. "Prediction of Fully Developed Flow in a Tube Containing a Twisted Tape" Int. J. Heat Mass Transfer, Vol. 17, pp. 845-859, 1974.

99. Jones, W.P. and Launder, B.E. "The Calculation of Low - Reynolds number Phenomena With a Two - Equation Model of Turbulence" Int. J. Heat Mass Transfer, Vol. 16, pp. 1119-1130, 1973.

100. Knudsen, J. & Katz, D. "Fluid Dynamics and Heat Transfer" McGraw-Hill Chemical Engineering Series,, p. 149, 1958.

101. Kline, S.J. "The Purposes of Uncertainty Analysis" J. of Fluids Engineering, ASME, Vol. 107/153, 1985.

102. Kline, S.J. and McClintock, F.A. "Describing Uncertainties in Single Sample Experiments" Mechanical Engineering, pp. 3-8, Jan. 1953.

103. Thornton-Trump, A.B. "Error Analysis of a Hot-wire Anemometer and Processing Circuit" University of Manitoba, Department of Mechanical Enginnering Publication , ER 25.14, July 1971.

104. Mojola, O.O. "A Hot-wire Method for Three-dimensional Shear Flows" DISA Information No. 16, pp. 11-14, 1974.

105. Yavuzkurt, S. "A Guide to Uncertainty Analysis of Hot-wire Data" J. of Fluids Engineering, ASME, Vol. 106/181, June 1984.

106. Rehme, K. "The Structure of Turbulent Flow Through a Wall Subchannel of a Rod Bundle" Nucl. Engng. Des., Vol. 45, pp. 311-323, 1978.

107. Hooper, J.D. "Developed Single Phase Turbulent Flow Through a Square-pitch Rod Cluster" Nucl. Engng. Des. Vol. 60, pp. 365-379, 1980.

108. Hooper, J.D. and Rehme, K. "Large-scale Structural Effects in Developed Turbulent Flow Through Closely-spaced Rod Arrays" J. Fluid Mech., Vol. 145, pp. 305-337, 1984.

APPENDIX A

DERIVATION OF EQUATION FOR SOURCE OF VORTICITY IN A TRAPEZOIDAL DUCT

The assumed expression for the kinetic energy distribution equation (5.7) is re-written here as:

$$k^+ = ki^+ + (kw^+ - ki^+)\left(1 - \frac{z}{\hat{z}_{max}}\right)^2 \qquad (A.1)$$

Where,

$$ki^+ = kc^+\left\{1 - m\left(1 - \frac{z}{\hat{z}_{max}}\right)^2\right\} , \qquad (A.2)$$

$k^+ = k/(\overline{u^*})^2$,

$\overline{u^*}$= friction velocity based on mean wall shear stress ,

kw^+= value of k^+ at the wall; taken as 4.0 ,

kc^+= value of k^+ at duct centre; taken as 1.0 ,

m = a constant ,

z = normal distance from any wall of the duct ,

$\hat{z}$ = normal distance from any wall to surface of no shear ,

$\hat{z}_{max}$ = maximum value of z for the concerned wall.

It is important to note that the surface of no-shear is assumed to be coincident with the position of the maximum streamwise velocity in the direction normal to the concerned wall. Based on the present measurements the position of the surface of no shear is shown by dashed lines in Fig. (A.1).

After suppressing the shear stress term from vorticity source term equation (3.14a) equation (5.6) was substituted into it, and the source of axial vorticity becomes:

$$S_\omega = C'\rho(\overline{u^*})^2 \frac{\delta}{\delta y \delta z}(k^{+2} + 2k^+) \qquad (A.3)$$

Defining the following dimensionless parameters:

$$z_L = 1 - z/\hat{z}_{max} \quad , \qquad (A.4)$$

$$z_P = 1 - \hat{z}/\hat{z}_{max}$$

for a given psition (y,z) in Fig. (A.1); z_L is a function of z only and z_P is a function of y only. So z should be a function of y only. Substituting equations (A.2) and (A.4) into equation (A.1) yield:

$$k^+ = z_M + (kw^+ - z_M)(z_L)^2 \qquad (A.5)$$

where Z_M is defined later by equation (A.13b)

now $$\frac{\delta z_L}{\delta z} = -1/\hat{z}_{max} \quad , \qquad (A.6)$$

and $$\frac{\delta z_P}{\delta y} = -\frac{\delta z}{\delta y} \cdot 1/\hat{z}_{max} \quad ,$$

so substituting (A.6) into (A.3) gives:

$$S_{\dot{w}} = C' \frac{\rho(\overline{u^*})^2}{(\hat{z}_{max})^2} \cdot \frac{\delta z}{\delta y} \frac{\delta^2}{\delta z \, \delta z}_{L \; P} (k^{+2}+2k^{+}) \qquad (A.7)$$

now

$$\frac{\delta^2}{\delta z \, \delta z}_{L \; P} (k^{+2} + 2k^{+}) = \frac{\delta}{\delta z}_{P} \{2k^{+} \frac{\delta k^{+}}{\delta z}_{L} + 2 \frac{\delta k^{+}}{\delta z}_{L}\}$$

$$= 2\{(k^{+}+1) \frac{\delta}{\delta z}_{P} (\frac{\delta k^{+}}{\delta z}_{L}) + \frac{\delta k^{+}}{\delta z}_{L} \cdot \frac{\delta k^{+}}{\delta z}_{P}\} \qquad (A.8)$$

and

$$k^{+} = z_{M} + (kw^{+} - z_{M}) z_{L}^2 \quad ,$$

$$\frac{\delta k^{+}}{\delta z}_{L} = 2(kw^{+} - z_{M}) z_{L} \quad , \qquad (A.9)$$

$$\frac{\delta}{\delta z}_{P} (\frac{\delta k^{+}}{\delta z}_{L}) = \frac{\delta}{\delta z}_{P} (2kw^{+} z_{L} - 2 z_{M} z_{L})$$

$$= -2 z_{L} \frac{\delta z}{\delta z}_{P} M$$

$$= -2 z_{L} \frac{\delta}{\delta z}_{P} (1 - m z_{P}^2) k c^{+}$$

$$= 4 k c^{+} m z_{L} z_{P}$$

hence

$$(k^{+}+1)\frac{\partial}{\partial z}\left(\frac{\partial k^{+}}{\partial z}\right)_{P}=4kc^{+}mz_{L}z_{P}\{1+z_{M}+(kw^{+}-z_{M})z_{L}^{2}\} \qquad (A.10)$$

and

$$\left(\frac{\partial k^{+}}{\partial z}\right)_{P}=\frac{\partial}{\partial z}\{z_{M}+(kw^{+}-z_{M})z_{L}^{2}\}$$

$$=\frac{\partial}{\partial z}\{kc^{+}(1-mz_{P}^{2})+kw^{+}z_{L}^{2}-kc^{+}(1-mz_{P}^{2})z_{L}^{2}\}$$

$$=-2mkc^{+}z_{P}+2mkc^{+}z_{P}z_{L}^{2}$$

$$=-2mkc^{+}z_{P}(1-z_{L}^{2}) \qquad (A.11)$$

hence

$$\left(\frac{\partial k^{+}}{\partial z}\right)_{L}\cdot\left(\frac{\partial k^{+}}{\partial z}\right)_{P}=-4mkc^{+}z_{L}z_{P}(kw^{+}-z_{M})(1-z_{L}^{2}) \qquad (A.12)$$

Substituting (A.12) into (A.8) gives:

$$\frac{\partial^{2}}{\partial z_{L}\,\partial z_{P}}(k^{+2}+k^{+})=8mkc^{+}z_{L}z_{P}z_{N} \qquad (A.13)$$

where,

$$z_N = \{1+z_M+(kw^+-z_M)z_L^2\} - \{(1-z_L^2)(kw^+-z_M)\} \quad ;(A.13a)$$

$$z_M = (1 - mz_P^2) \qquad (A.13b)$$

By substituting (A.13) into (A.7) the final form of the vorticity source can be written as:

$$S_w = 8C' \frac{\rho(\bar{u}^*)^2}{(\hat{z}_{max})^2} . kc^+ m z_L z_P z_N \frac{\delta\hat{z}}{\delta y} \qquad (A.14)$$

To match the computational results with the measurements, the constants C' and m were taken as 0.045 and 2.4 respectively.

As may be seen in Fig. (A.1), there is a region of points in the primary flow cell have two different vorticity source magnitudes. This overlaping of points in the top part of the primary flow cell is mainly due to the obtuse angle of the trapezoidal duct. The magnitude of the vorticity source at a point is taken from the calculation of the closest wall to that point. The bisector of the obtuse angle is taken as a divider for the regions near the top and inclined walls. Following the above features, there was no converged solution for the vorticity and stream function equations. By considering the bisector of the obtuse angle as a $\hat{z}$ line for the top wall and the top part of the inclined wall (as shown

in Fig. A.2) the convergence of the ω and Ψ equations was achieved. This alteration for geometries with a corner angle greater than 90° seems to be necessary modification to the procedure of the vorticity source modelling of Seale [2].

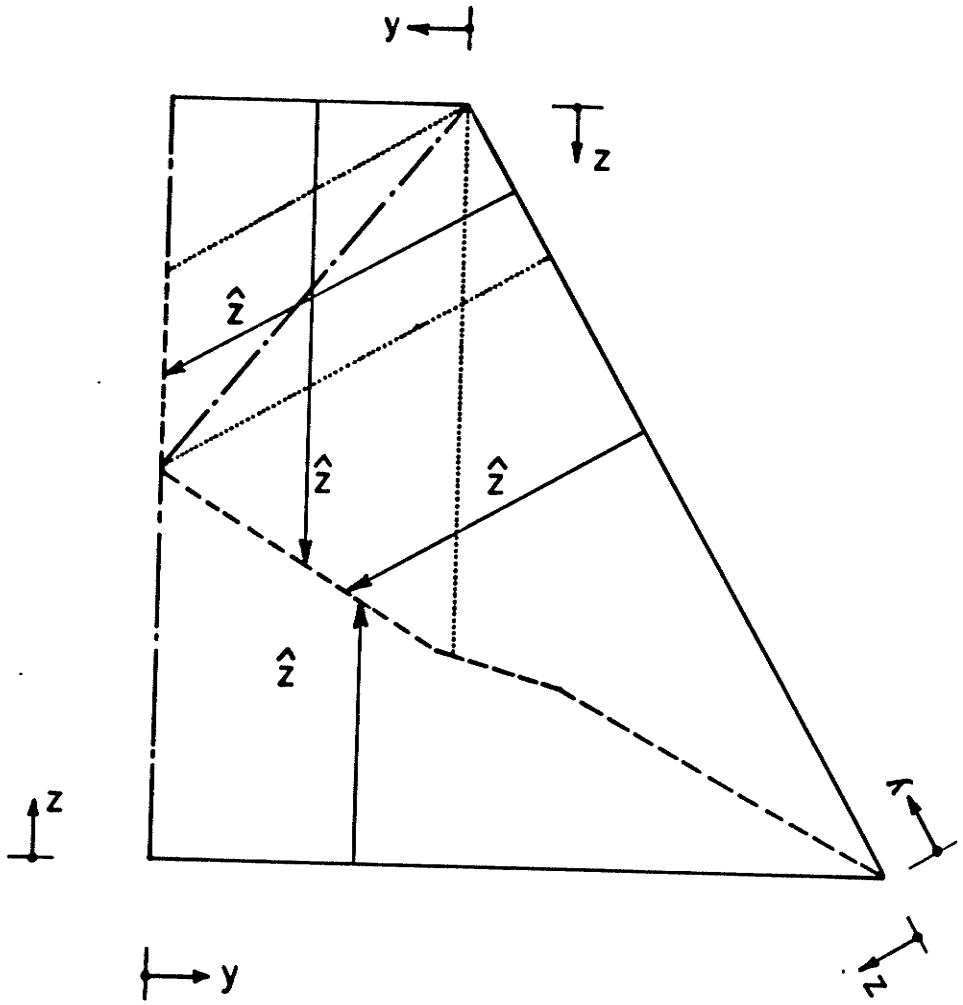

Fig. A.1 The Surface of no Shear and $\hat{z}$ Lines for the Present Duct (Experiment).

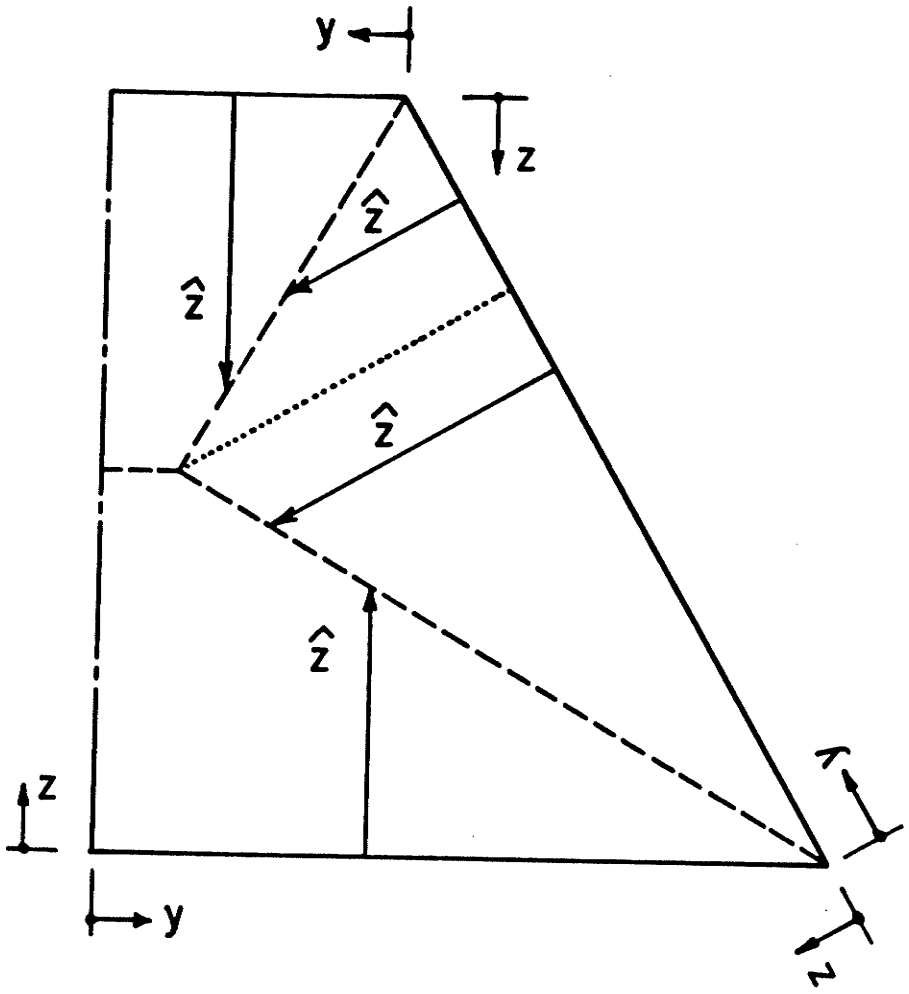

Fig. A.2 The Surface of no Shear and $\hat{z}$ Lines for the Present Duct (Analytical Model).

APPENDIX B

COMPUTER CODE FOR TRAPEZOIDAL DUCTS

In order to predict the flow and heat transfer characteristics the set of equations summarized in section (5.4) must be solved. A computer program was developed for this purpose. The block diagram of the code is presented in Fig. B.1, and the input data are defined as:

FORTRAN SYMBOL	MEANING
M	Grid Number in y-Direction
N	Grid Number in z-Direction
DEQ	Equivalent Hydraulic Diameter
ROW	Fluid Density
RE	Reynolds Number
AMU	Fluid Dynamic Viscosity
ANU	Fluid Kinematic Viscosity
CMU	C_μ
CE1	C1
CE2	C2
CAPA	κ
A,B	Law of The Wall Constants
ROWCMU	$\rho C_\mu^{1/4}$
SIGMU	σ_U
SIGMK	σ_k
SIGME	σ_ε
AA,BB,TH	Trapezoidal Duct Dimensions and Acute Angle Respectively.

RLW	Under-relaxation Factor For ω
RLEP	,, ,, ,, Ψ
RLK	,, ,, ,, k
RLE	,, ,, ,, ϵ
RLU	,, ,, ,, $\bar{U}$
RLT	,, ,, ,, $\bar{T}$
CRW	Convergence Criterion For ω
CREP	,, ,, ,, Ψ
CRK	,, ,, ,, k
CRE	,, ,, ,, ϵ
CRU	,, ,, ,, $\bar{U}$
CRT	,, ,, ,, $\bar{T}$
ASS	C′
XM	m
XKC	$kc,^{+}$
IM	Control Number
	=1 Secondary Flow Suppressed
	=2 Secondary Flow Included
JF	Control Number
	=1 Initial Values of $\bar{U}$,k, ϵ
	are Avearage values
	=2 Initial Values are the
	Stored Solutions With IM=1
IMAX	Maximum Number of Iterations
	For Ψ, ω, $\bar{U}$, k, ϵ Equations.
IMAXT	Maximum Number of Iterations
	For $\bar{T}$ Equation
IPRINT	Number of Iterations Between

	Print Out of Results
TW	Duct Wall Temperature
PR	Fluid Prandtl Number
PRT	Turbulent Prandtl Number
AMR	AMU/PR
CK	Thermal Cnductivity of Fluid
PF	P-function of Jayatilleke [81]
ICOUNT	Number of Iterations For $\bar{U}$, k, ϵ, ω, Ψ
ITEMP	Number of Iterations For $\bar{T}$

The nomenclature of the computer program is presented in Table (B.1).

TABLE (B.1)

NOMENCLATURE OF THE COMPUTER PROGRAM

FORTRAN SYMBOLS	MEANING
Y(I), Z(J)	Grid Specifications
BEF(I,J)	
BWF(I,J)	
BNF(I,J)	
BSF(I,J)	Coefficients of The Numerical
AE(I,J)	Procedure (Chapter 6)
AW(I,J)	
AN(I,J)	
AS(I,J)	
VP(I,J)	$\int_A \int dydz$ {Equation (6.18)}
U(I,J)	Axial Velocity
V(I,J)	Secondary Velocity Components
W(I,J)	
TKE(I,J)	Turbulent Kinetic Energy
TED(I,J)	Turbulence Dissipation
EPS(I,J)	Stream Function
OMEG(I,J)	Vorticity
T(I,J)	Temperature
VORSOR(I,J)	Vorticity Source

VSEC(I,J)	Total Secondary Velocity
TOWT(I)	Local Shear Stress For Top Wall
TOWB(I)	Local Shear Stress For Bottom Wall
TOWI(I)	Local Shear Stress For Inclined Wall
QT(I)	Local Heat Flux For Top Wall
QB(I)	Local Heat Flux For Bottom Wall
QI(I)	Local Heat Flux For Inclined Wall
T*(I,J)	Dimensionless Temperature
RSWF(I,J)	Local Residual of ω
RSEPF(I,J)	" " Ψ
RSKF(I,J)	" " k
RSEF(I,J)	" " ϵ
RSUF(I,J)	" " $\bar{U}$
RSTF(I,J)	" " $\bar{T}$
UFT(I)	Local Friction Velocity For Top Wall
UFB(I)	Local Friction Velocity For Bottom Wall
UFI(I)	Local Friction Velocity For Inclined WAll
DUY(I,J)	$\{ \partial(\ )/\partial y\}_{i,j}$
DUZ(I,J)	$\{ \partial(\ )/\partial z\}_{i,j}$

F1(I,J)	
F2(I,J)	Temporary Storage Locations
F3(I,J)	
F4(I,J)	
DPDX	$\partial\bar{p}/\partial x$
DTDX	$\partial\bar{T}/\partial x$

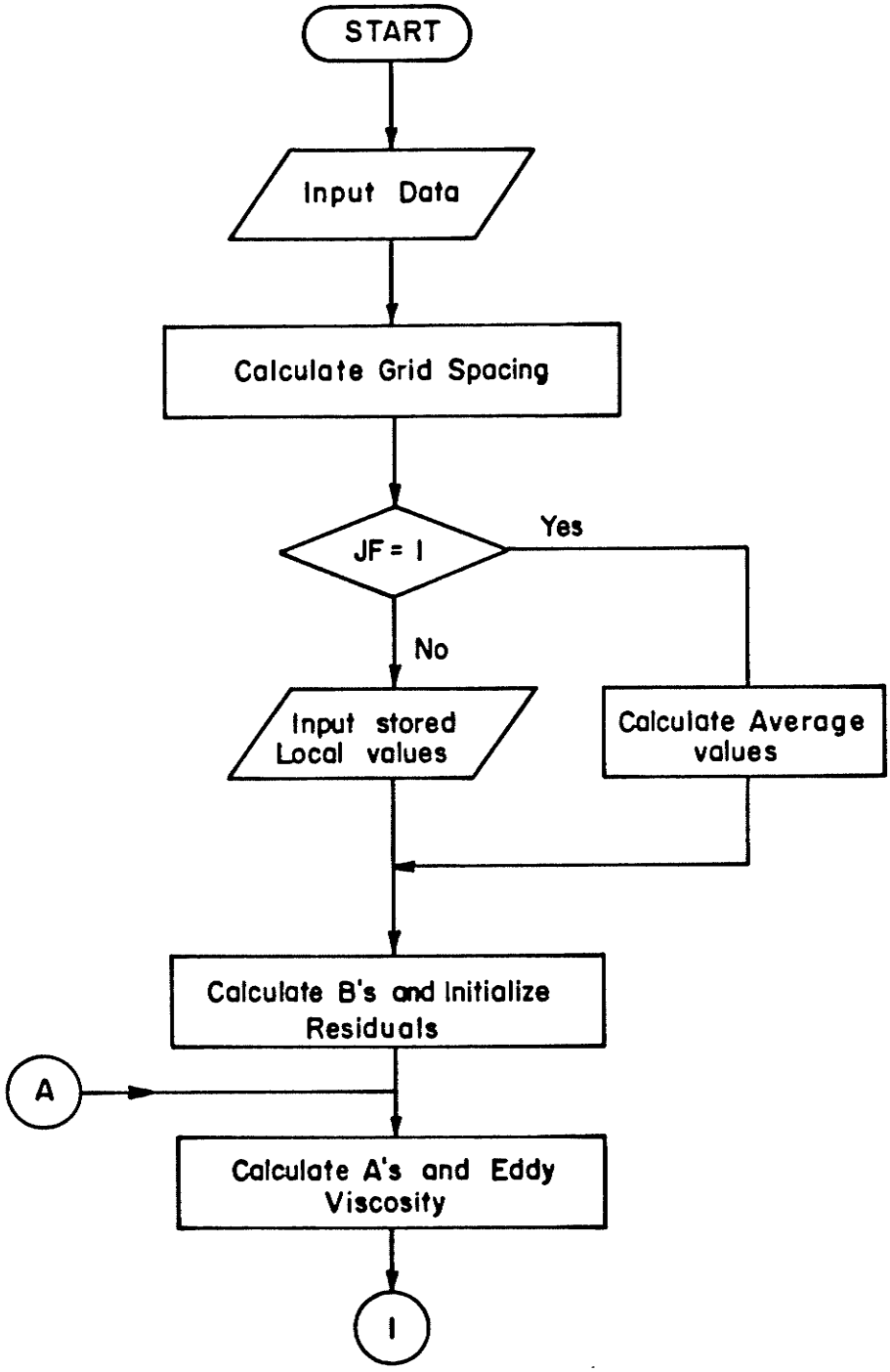

Fig. B.1 Block Diagram of the Computer Code

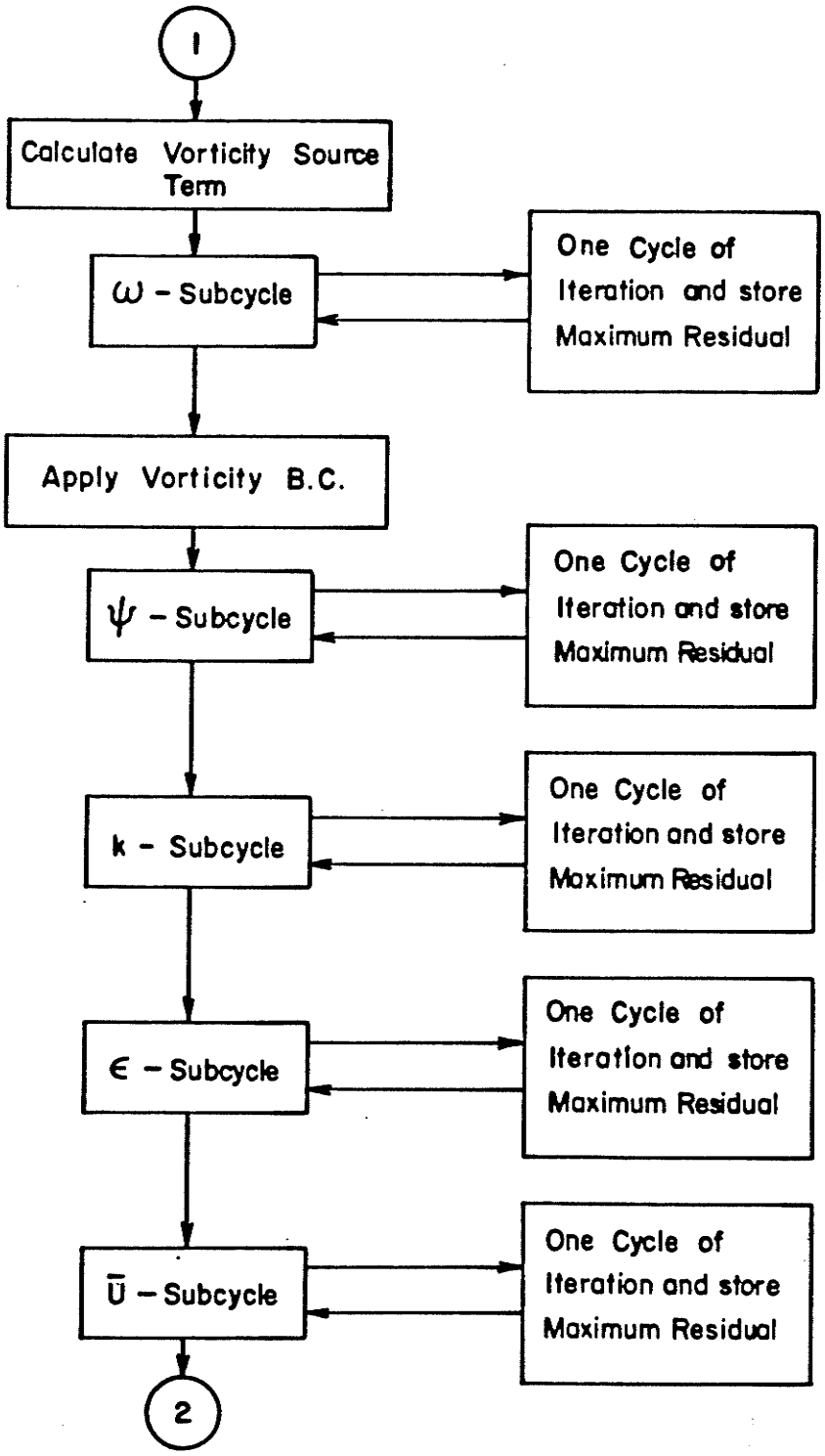

Fig. B.1 Continued

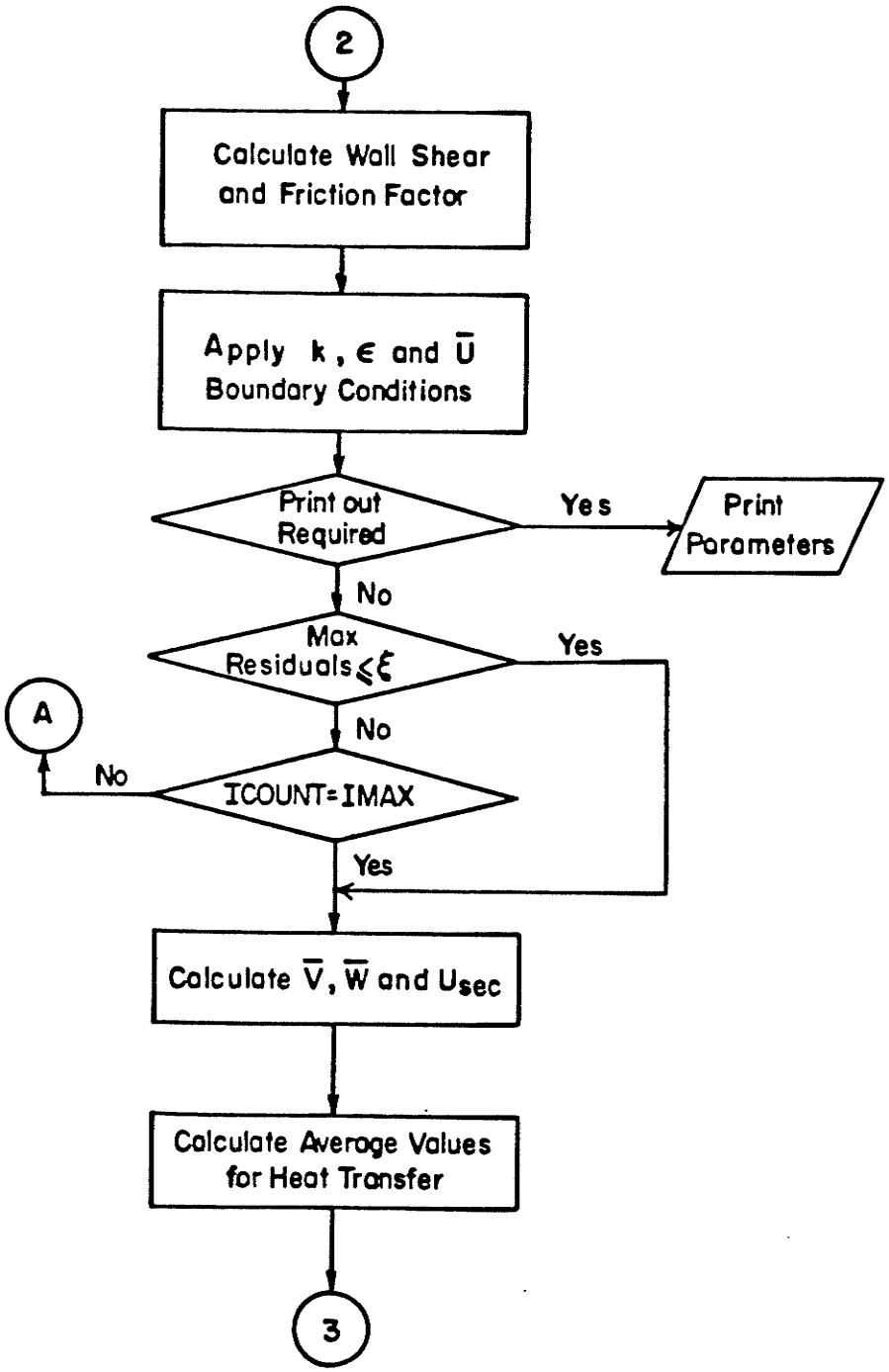

Fig. B.1 Continued

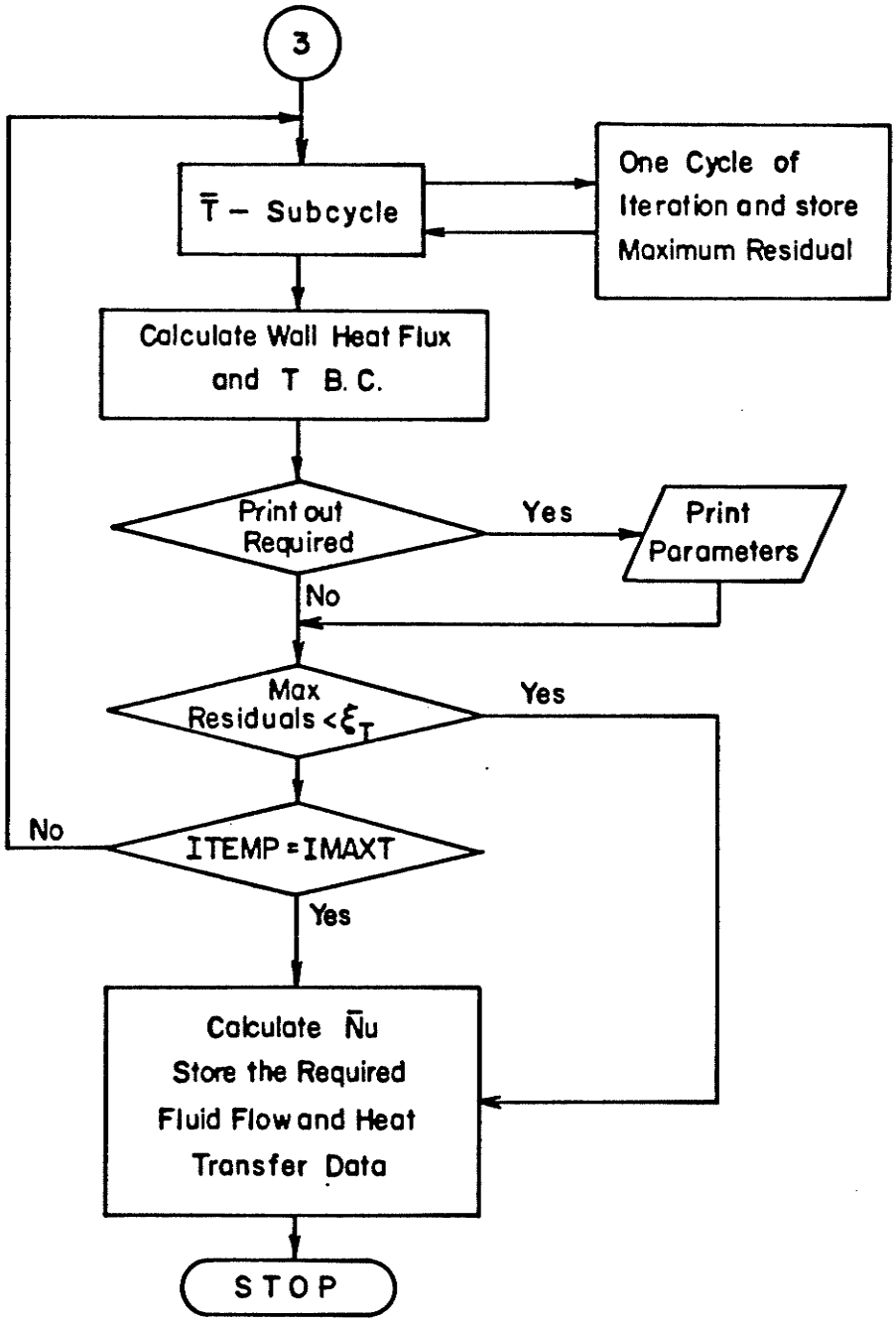

Fig. B.1 Continued

```
C----------MAHMOUD MOHAMED ATTIA KHALIFA----------------------
      DIMENSION AE(41,41),AW(41,41),AN(41,41),AS(41,41),AMUT(41,41),
     *BEF(41,41),BWF(41,41),BNF(41,41),BSF(41,41),AL(41,41),
     *DA(41,41),DAT(41,41),DUY(41,41),DUZ(41,41),DUS(41,41),EPS(41,41)
      DIMENSION F1(41,41),F2(41,41),F3(41,41),F4(41,41),OMEG(41,41),
     *OM(40),RSEF(41,41),RSKF(41,41),QT(20),QB(41),QI(40),QI1(40),
     *RSWF(41,41),RSEPF(41,41),RSUF(41,41),RSTF(41,41),
     *S(40),SP(40),XSS(40),ZPT(20),ZPB(41),T(41,41),
     *TED(41,41),TKE(41,41),QI2(40),
     *TOWB(41),TOWT(20),TOWI(40)
      DIMENSION U(41,41),UFB(41),UFT(20),UFI(40),
     *UO(41,41),TW1(40),UF1(40),TW2(40),UF2(40)
      DIMENSION V(41,41),VP(41,41),VSEC(41,41),VORSOR(41,41),
     *VSBUA(41,41),W(41,41)
      DIMENSION Y(41),YRAT(41,41),YSTR(41),Z(41),ZRAT(41,41),
     *ZSTR(41),ZPLUSP(41),ZT(41),YT(41)
C----------------CHAPTER-1- DATA AND CONSTANTS -----------------
      DATA A,B/2.439,5.0/
      DATA AA,BB,CC,TH/.02539,.066,.0635,60.0/
      DATA M,N/31,21/
      DATA RE,ROW/98914.93,1.1657/
      DATA CMU,CE1,CE2,CAPA/.09,1.44,1.92,.41/
      DATA ASS,XM,XKC/0.03500,2.4,1.0/
      DATA RLW,RLEP,RLE,RLK,RLU/0.7,0.7,0.7,0.7,0.7/
      DATA SIGMK,SIGMU/1.0,1.0/
      DATA JF,IM/2,2/
      DATA IMAX,ITMAX,IPRINT,IRPRNT/6000,1000,2000,300/
      DATA CRW,CREP,CRK,CRE,CRU/0.001,0.001,0.001,0.001,0.001/
      DATA PR,PRT,CP,TBAV,TW,QAV/.712,.9,1005.,25.,100.,+10.0/
      DATA RLT,CRT/.5,.001/
C-----------------------------------------------------------------
      AMU=185.325*1.0E-7
      N1=N-1
      N2=N-2
      N3=N-3
      N4=N-4
      N5=N-5
      N6=N-6
      TH=TH*3.1415926/180.0
      SI=SIN(TH)
      CO=COS(TH)
      TA=TAN(TH)
      DEQ=2.0*BB*(AA+CC)/(AA+CC+BB/SI)
      AREA = BB*(AA+CC)
      CAREA=AREA/2.0
      CWTPR =AA+CC+BB/SI
      UBAV = RE * AMU / (ROW * DEQ)
      AMASS = ROW * UBAV * CAREA
      ANU = AMU / ROW
      SIGME = CAPA * CAPA / ((CE2 - CE1) * SQRT(CMU))
C-----------------------------------------------------------------
      PRINT 500, M,N,AA,BB,CC,TH,DEQ,RE,UBAV,ROW,AMU
      PRINT 502, CMU,CE1,CE2,SIGMK,SIGME,SIGMU,CAPA
      PRINT 503, ASS,XM,XKC
      PRINT 504, A,B
      PRINT 506, CRW,CREP,CRK,CRE,CRU
      PRINT 508, RLW,RLEP,RLK,RLE,RLU
      PRINT 510, AREA,CAREA
C--------------  CHAPTER-2--GRID--NODES-------------------------
      Y(1) = 0.0
      Z(1) = 0.0
C-------- GRID NODES FOR N=25 , M=35  -------------------------
      IF(N.NE.25) GO TO 9
      DZ=BB/(N-1)
```

```
      DO 4 J=2,N
      Z(J)=Z(J-1)+DZ
    4 CONTINUE
      L=M-N1
      DY1=AA/(L-1)
      K=L+1
      DO 5 I=2,K
      Y(I) = Y(I-1) + DY1
    5 CONTINUE
      K=K+1
      M=M+1
      DO 7 I=K,M
      J=M-(I-1)
      Y(I)=Y(I-1)+(Z(J+1)-Z(J))/TA
    7 CONTINUE
    9 CONTINUE
C-----------GRID NODES FOR N=21,M=31 -------------------------
      IF(N.NE.21) GO TO 127
      Z(2)=.018181818*BB
      Z(3)=2.0*Z(2)
      Z(4)=Z(3)+1.5*Z(2)
      Z(5)=Z(4)+1.5*(Z(4)-Z(3))
C     Z(6)=Z(5)+2.0*(Z(5)-Z(4))
      DZ=(BB-2.0*Z(5))/(N-9)
      K=N-4
      DO 123 J=6,K
      Z(J)=Z(J-1)+DZ
  123 CONTINUE
C     Z(N4)=Z(N5)+Z(6)-Z(5)
      Z(N3)=Z(N4)+Z(5)-Z(4)
      Z(N2)=Z(N3)+Z(4)-Z(3)
      Z(N1)=Z(N2)+Z(3)-Z(2)
      Z(N)=Z(N1)+Z(2)
      L=M-N1
      DY1=AA/(L-1)
      K=L+1
      DO 126 I=2,K
      Y(I)=Y(I-1)+DY1
  126 CONTINUE
      K=K+1
      M=M+1
      DO 128 I=K,M
      J=M-(I-1)
      Y(I)=Y(I-1)+(Z(J+1)-Z(J))/TA
  128 CONTINUE
  127 CONTINUE
      YFLAG = (Y(M) -(CC+DY1))/(CC+DY1)
      ZFLAG = (Z(N) - BB)/BB
      PRINT ,YFLAG,ZFLAG
      IF((ABS(YFLAG) .GT. 0.0001) .OR. (ABS(ZFLAG) .GT. 0.0001)) GO
     *TO 9999
      M1=M-1
      M2=M-2
      M3=M-3
      M4=M-4
      M5=M-5
      M6=M-6
      L=M-N1
C-----------------------------------------------------------------
      DO 35 J=1,N
      DO 35 I=2,M
      YSTR(I) =(Y(I)-DY1) /CC
      ZSTR(J) = Z(J)/BB
   35 CONTINUE
```

```
      XSS(L)=0.0
      LXX=L+1
      DO 39 I=LXX,M
      XSS(I)=(Y(I)-Y(I-1))/CO+XSS(I-1)
   39 CONTINUE
      DO 108 I=LXX,M
      XSS(I)=XSS(I)/(BB/SI)
  108 CONTINUE
      PRINT 512
      PRINT 514
      WRITE(6,516) (Y(I),I=1,M)
      PRINT 518
      PRINT 520
      WRITE(6,517) (Z(J),J=1,N)
      PRINT 548
      WRITE(6,*) (YSTR(I),I=2,M)
      PRINT 550
      WRITE(6,*) (ZSTR(J),J=1,N)
      PRINT 551
      WRITE(6,*) (XSS(I),I=L,M)
C-----------------------------------------------------------------
      DO 11 J=1,41
C     K=M-(J-1)
      DO 11 I=1,41
      OMEG(I,J) = 0.0
      EPS(I,J) = 0.0
      TKE(I,J) = 0.0
      TED(I,J) = 0.0
      U(I,J) = 0.0
      V(I,J) = 0.0
      W(I,J) = 0.0
      VSEC(I,J)=0.0
      AMUT(I,J) = 0.0
      VP(I,J) = 0.0
      VORSOR(I,J) = 0.0
      AE(I,J) = 0.0
      AW(I,J) = 0.0
      AN(I,J) = 0.0
      AS(I,J) = 0.0
      F1(I,J)=0.0
      F2(I,J)=0.0
      F3(I,J)=0.0
      F4(I,J)=0.0
      T(I,J) =0.0
   11 CONTINUE
      DO 10 I=1,41
      TOWB(I)=0.0
      UFB(I)=0.0
   10 CONTINUE
      DO 14 I=1,20
      TOWT(I)=0.0
      UFT(I)=0.0
   14 CONTINUE
      DO 16 K=1,40
      TOWI(K)=0.0
      UFI(K)=0.0
      UF1(K)=0.0
      UF2(K)=0.0
      TW2(K)=0.0
      TW1(K)=0.0
   16 CONTINUE
C---------      ASSUMED INITIAL GUESS -------------------------
      IF(JF.EQ.2) GO TO 37
      UFAV = 1.2000
```

```
      UFAVB=UFAV
      UFAVT=UFAV
      UFAVI=UFAV
      TOWAV = ROW * UFAV**2
      DPDX =4.0*TOWAV/DEQ
      TKT=UFAV**2/SQRT(CMU)
      TKB=TKT
      TKI=TKT
      TKEI=(TKT+TKB+TKI)/3.0
      TDT=UFAV**3/(CAPA*(Z(N)-Z(N1)))
      TDB=UFAV**3/(CAPA*Z(2))
      ZPLUS=UFAV*Z(2)/ANU
      UINT=UFAV*(A*ALOG(ZPLUS)+B)
      UINB=UINT
C-----------------------------------------------------------------
      TEDI=(TDT+TDB)/2.0
      UIN=(UINT+UINB)/2.0
C-----------------------------------------------------------------
      DO 13 I=1,M1
      UFB(I) = UFAV
      TOWB(I)=TOWAV
   13 CONTINUE
      UFB(M)=0.0
      TOWB(M)=0.0
      DO 15 I=1,L
      UFT(I)=UFAV
      TOWT(I)=TOWAV
   15 CONTINUE
      DO 17  J=2,N
      K=M-(J-1)
      UFI(K)=UFAV
      TOWI(K)=TOWAV
   17 CONTINUE
      UFI(M)=0.0
      TOWI(M)=0.0
      X1=(Z(2)-Z(1))/SI
      X2=(Z(3)-Z(2))/SI
      UFI(M1)=UFI(M2)*X1/(X1+X2)
      TOWI(M1)=ROW*UFI(M1)**2
      DO 19 J=2,N1
      K=M-J
      DO 19 I=1,K
      U(I,J) = UBAV
      TKE(I,J) = TKEI
      TED(I,J)=TEDI/2.0
   19 CONTINUE
      DO 12 I=1,M
      U(I,1)=0.0
   12 CONTINUE
      DO 21 I=1,L
      U(I,N)=0.0
   21 CONTINUE
      DO 23 J=1,N1
      I=M-(J-1)
      U(I,J)=0.0
   23 CONTINUE
      DO 24 J=3,N
      I=M-(J-1)
      S(I)=(Y(I+1)-Y(I))*SI
      SP(I)=S(I)*UFAV/ANU
   24 CONTINUE
      PRINT 521,ZPLUS
      L1=L+1
      PRINT 523
```

```
      WRITE(6,*) (SP(I),I=L,M2)
      PRINT 525
      WRITE(6,*) (TED(I,2),I=2,M2)
      PRINT 527
      WRITE(6,*) (TED(I,N1),I=2,L)
      PRINT 529, UFAV,TOWAV,DPDX,TKEI,TEDI
C-----------------------------------------------------------------
      IF(JF.EQ.1) GO TO 44
 37   READ(13,*) U,TKE,TED,TOWB,TOWT,TOWI,UFB,UFT,UFI,UF1,UF2,
     *DPDX,UFAV,TOWAV
      PRINT 699
      WRITE(6,*) DPDX,UFAV,TOWAV
      PRINT 720
      CALL RR(U,M,N)
      PRINT 700
      CALL RR(TKE,M,N)
      PRINT 710
      CALL RR(TED,M,N)
      WRITE(6,*) (TOWB(I),I=2,M)
      WRITE(6,*) (TOWT(I),I=2,L)
      DO 26 J=1,N
      K=M-(J-1)
      WRITE(6,*) TOWI(K)
 26   CONTINUE
      ZPLUS=UFAV*Z(2)/ANU
 44   CONTINUE
C------------- CALCULATION  OF B,S  FOR OMEGA AND EPS----------
      DO 29 J=2,N1
      K=M-J
      DO 29 I=2,K
      BEF(I,J) = 0.25 * (Z(J+1)-Z(J-1)) / (Y(I+1)-Y(I))
      BWF(I,J) = 0.25 * (Z(J+1)-Z(J-1)) / (Y(I)-Y(I-1))
      BNF(I,J) = 0.25 * (Y(I+1)-Y(I-1)) / (Z(J+1) - Z(J))
      BSF(I,J) = 0.25 * (Y(I+1)-Y(I-1)) / (Z(J) - Z(J-1))
      VP(I,J) = 0.25 * (Y(I+1)-Y(I-1)) * (Z(J+1)-Z(J-1))
 29   CONTINUE
C-----------------------------------------------------------------
      SUMDA = 0.0
      DO 32 J=2,N
      K=M-(J-1)
      DO 32 I=3,K
      DA(I,J) = (Y(I)-Y(I-1)) * (Z(J)-Z(J-1))
      SUMDA = SUMDA + DA(I,J)
 32   CONTINUE
C----------------TRIANGLES--ALONG--INCLINED--WALL---------------
      SUMDT=0.0
      DO 30 J=2,N
      K=M-(J-1)
      I=K
      DAT(I,J)=0.5*(Z(J)-Z(J-1))*(Y(I+1)-Y(I))
      SUMDT=SUMDT+DAT(I,J)
 30   CONTINUE
      SUMDA=SUMDA+SUMDT
      PRINT 522, SUMDA
      ROWCMU = ROW * CMU**0.25
C---------------- MAIN LOOP OF ITERATIONS ---------------------
      ICOUNT = 0
 900  ICOUNT = ICOUNT + 1
C---------      INITIALIZATION OF RESIDUALS -----------------
      RSWM = 0.0
      RSEPM = 0.0
      RSKM = 0.0
      RSEM = 0.0
      RSUM = 0.0
```

```
      DO 38 J=1,N
      K=M-(J-1)
      DO 38 I=1,K
      F1(I,J) = 0.0
      F2(I,J) = 0.0
      F3(I,J) = 0.0
      F4(I,J) = 0.0
      DUY(I,J) = 0.0
      DUZ(I,J) = 0.0
   38 CONTINUE
      DO 33 J=1,N
      OMEG(1,J)=-OMEG(3,J)
      EPS(1,J)=-EPS(3,J)
      OMEG(2,J)=0.0
      EPS(2,J)=0.0
      TKE(1,J)=TKE(3,J)
      TED(1,J)=TED(3,J)
      U(1,J)=U(3,J)
      T(1,J)=T(3,J)
   33 CONTINUE
      IF(IM .EQ. 1) GO TO 43
C--------- A'S CALCULATIONS ----------------------------------
      DO 40 J=2,N1
      K=M-J
      DO 40 I=2,K
      AEF=EPS(I+1,J-1)+EPS(I,J-1)-EPS(I+1,J+1)-EPS(I,J+1)
      AE(I,J)=(AEF+ABS(AEF))/8.0
      AWF=EPS(I-1,J+1)+EPS(I,J+1)-EPS(I-1,J-1)-EPS(I,J-1)
      AW(I,J)=(AWF+ABS(AWF))/8.0
      ANF=EPS(I+1,J+1)+EPS(I+1,J)-EPS(I-1,J+1)-EPS(I-1,J)
      AN(I,J)=(ANF+ABS(ANF))/8.0
      ASF=EPS(I-1,J-1)+EPS(I-1,J)-EPS(I+1,J-1)-EPS(I+1,J)
      AS(I,J)=(ASF+ABS(ASF))/8.0
   40 CONTINUE
   43 CONTINUE
C--------- EDDY VISCOSITY ( MUT ) -----------------------------
      DO 42 J=2,N1
      K=M-J
      DO 42 I=1,K
      IF(TED(I,J) .EQ. 0.0) GO TO 45
      AMUT(I,J) = CMU * ROW * (TKE(I,J)**2) / TED(I,J)
      GO TO 42
   45 AMUT(I,J) = 0.0
   42 CONTINUE
C--------- COEFFICIENT FOR THE VORTICITY SOURCE TERM ------------
      DO 49 J=1,N
      K=M-J
      DO 49 I=2,K
      YRAT(I,J) = (Y(I) - Y(I-1)) / (Y(I+1) - Y(I))
   49 CONTINUE
      DO 52 J=2,N1
      K=M-J
      DO 52 I=1,K
      ZRAT(I,J) = (Z(J) - Z(J-1)) / (Z(J+1) - Z(J))
   52 CONTINUE
C-------- DU BY DZ AT INTERIOR NODES AND WALLS BISECTOR ----------
      DO 54 J=2,N1
      K=M-J
      DO 54 I=1,K
      DUZ(I,J) = ((U(I,J+1) - U(I,J)) * ZRAT(I,J) + (U(I,J) - U(I,
     *J-1)) / ZRAT(I,J)) / (Z(J+1) - Z(J-1))
   54 CONTINUE
C------------  DUY AT INTERIOR  NODES  ----------------------------
      DO 56 J=2,N1
```

```
      K=M-J
      DO 56 I=2,K
      DUY(I,J) = ((U(I+1,J) - U(I,J)) * YRAT(I,J) + (U(I,J) - U(I-1,
     *J)) / YRAT(I,J)) / (Y(I+1) - Y(I-1))
   56 CONTINUE
C--------- DUY AND DUZ AT.    HORIZONTAL   WALLS ------------------
      DO 58 I=1,M1
      DUZ(I,1) =( U(I,2)-U(I,1)) / (Z(2) - Z(1))
   58 CONTINUE
      DUZ(M,1)=0.0
      DO 60 I=1,M
      DUY(I,1) = 0.0
   60 CONTINUE
      DO 62 I=1,L
      DUZ(I,N)=(U(I,N)-U(I,N1))/(Z(N)-Z(N1))
      DUY(I,N)=0.0
   62 CONTINUE
C
C------------- AT  INCLINED WALL   ----------------------------
      DO 65 J=2,N1
      K=M-(J-1)
      K1=K-1
      DUY(K,J)=(U(K,J)-U(K1,J))/(Y(K)-Y(K1))
   65 CONTINUE
      DO 68 J=2,N1
      K=M-(J-1)
      DUZ(K,J)=(U(K,J)-U(K,J-1))/(Z(J)-Z(J-1))
   68 CONTINUE
C--------- F2: COEFFICIENT FOR K & E SOURCE TERM ---------------
      DO 70 J=1,N
      K=M-(J-1)
      DO 70  I=1,K
      DUYSQ = DUY(I,J)**2
      DUZSQ = DUZ(I,J)**2
      F2(I,J) = (DUYSQ + DUZSQ) / SIGMU
   70 CONTINUE
      IF(IM.NE.2) GO TO 431
      DD=BB/SI
      EE=DD/2.0
      GG=EE/2.0
      FF=BB
      ZCIMAX=FF/2.0
      HH=DD-GG
      DY=AA-GG+DY1
      ZCBMAX=FF/2.0
      ZCTMAX=EE*SI
      AL1=-30.0*3.1415926/180.0
      AL2=-AL1
      AL3=-2.0*AL1
C     WRITE(6,*) DY,DY1
C-------------------------------------------------------------
C     DLS=10*3.1415926/180.0
C     DIS=DD/2.0*TAN(DLS)
C     DIS1=DIS*C0
C     ZCBMAX=BB/2.-DIS1
C     ZCIMAX=ZCBMAX
C     ZCTMAX=BB-ZCBMAX
C     EE=ZCIMAX/SIN(TH-DLS)
C     GG=ZCIMAX/TAN(TH-DLS)
C     HH=DD-GG
C     DY=AA-EE*COS(TH+DLS)+DY1
C     AL1=-30.*3.1415926/180.
C     AL2=-AL1
C     AL3=TH+DLS
```

```
C-------------------------------------------------------
      DO 409 J=1,N
      DO 409 I=1,M
      YT(I)=Y(I)-DY
      ZT(J)=Z(J)-ZCBMAX
  409 CONTINUE
      DO 800 J=1,N
      K=M-(J-1)
      DO 800 I=1,K
      IF(YT(I).LE.0.0) GO TO 802
      AL(I,J)=ATAN(ZT(J)/YT(I))
  802 CONTINUE
  800 CONTINUE
      DO 804 J=1,N
      K=M-(J-1)
      DO 804 I=1,K
      IF(Z(J).LE.ZCBMAX) GO TO 808
      IF(YT(I).GE.0.0) GO TO 806
      AL(I,J)=3.1415926+ATAN(ZT(J)/YT(I))
  806 CONTINUE
  808 CONTINUE
      IF(Z(J).GT.ZCBMAX) GO TO 810
      IF(YT(I).GE.0.0) GO TO 812
      AL(I,J)=-(3.1415926-ATAN(ZT(J)/YT(I)))
  812 CONTINUE
  810 CONTINUE
  804 CONTINUE
      DO 814 J=1,N
      K=M-(J-1)
      DO 814 I=1,K
      IF(YT(I).NE.0.0) GO TO 816
      IF(Z(J).GT.ZCBMAX) GO TO 818
      AL(I,J)=-3.1415926/2.0
  818 CONTINUE
  816 CONTINUE
      IF(YT(I).NE.0.0) GO TO 820
      IF(Z(J).LE.ZCBMAX) GO TO 822
      AL(I,J)=3.1415926/2.0
  822 CONTINUE
  820 CONTINUE
  814 CONTINUE
C     CALL VV(AL,M,N)
      DO 413 J=1,N
      K=M-(J-1)
      DO 413 I=1,K
C-----------------------BOTTOM WALL---------------------------
      IF(AL(I,J).GE.AL1) GO TO 415
      ZCB=ZCBMAX*(CC+DY1-Y(I))/(CC+DY1-DY)
      IF(Y(I).LE.(DY+DY1)) ZCB=ZCBMAX
      ZL=1.0-Z(J)/ZCBMAX
      ZP=1.0-ZCB/ZCBMAX
      ZM=1.0-XM*ZP**2
      ZN=1.0+ZM+(4.0-ZM)*ZL**2-(1.0-ZL**2)*(4.0-ZM)
      ZN=ABS(ZN)
      DZCBDY=-ZCBMAX/(CC+DY1-DY)
      IF(Y(I).LE.(DY+DY1)) DZCBDY=0.0
      VORSOR(I,J)=8.*ASS*XM*XKC*TOWAV*ZL*ZP*ZN*DZCBDY/ZCBMAX**2
      SO=VORSOR(I,J)
C     WRITE(6,*) I,J,ZM,ZL,ZP,ZN,SO
  415 CONTINUE
C-----------------------TOP WALL-----------------------------
      IF(AL(I,J).LE.AL3) GO TO 417
      ZCT=ZCTMAX*(AA+DY1-Y(I))/(AA+DY1-DY)
      IF(Y(I).LE.(DY+DY1)) ZCT=ZCTMAX
```

```
      ZTT=BB-Z(J)
      ZL=1.0-ZTT/ZCTMAX
      ZP=1.0-ZCT/ZCTMAX
      ZM=1.0-XM*ZP**2
      ZN=1.0+ZM+(4.0-ZM)*ZL**2-(1.0-ZL**2)*(4.0-ZM)
      ZN=ABS(ZN)
      DZCTDY=+ZCTMAX/(AA+DY1-DY)
      IF(Y(I).LE.(DY+DY1)) DZCTDY=0.0
      VORSOR(I,J)=8.*ASS*XM*XKC*TOWAV*ZL*ZP*ZN*DZCTDY/ZCTMAX**2
      SO=VORSOR(I,J)
C     WRITE(6,*) I,J,ZM,ZL,ZP,ZN,SO
  417 CONTINUE
C-------------------------INCLINED WALL  (1-ST PART)-----------
      IF(AL(I,J).LE.AL2.OR.AL(I,J).GT.AL3) GO TO 419
      ZI1=(Y(K)-Y(I))*SI
      ZIV=ZI1*CO
      YI1=DD-(ZIV+Z(J))/SI
      ZCI1=ZCIMAX*YI1/GG
      ZL=1.0-ZI1/ZCIMAX
      ZP=1.0-ZCI1/ZCIMAX
      ZM=1.0-XM*ZP**2
      ZN=1.0+ZM+(4.0-ZM)*ZL**2-(1.0-ZL**2)*(4.0-ZM)
      ZN=ABS(ZN)
      DZCIDY=-ZCIMAX/GG
      VORSOR(I,J)=8.*ASS*XM*XKC*TOWAV*ZL*ZP*ZN*DZCIDY/ZCIMAX**2
      SO=VORSOR(I,J)
C     WRITE(6,*) I,J,ZM,ZL,ZP,ZN,SO
  419 CONTINUE
C-------------------------INCLINED WALL (SECOND PART)----------
      IF(AL(I,J).GT.AL2.OR.AL(I,J).LT.AL1) GO TO 440
      ZI=(Y(K)-Y(I))*SI
      YI2=Z(J)/SI+ZI/TAN(TH)
      ZCI2=ZCIMAX*YI2/HH
      ZI2=(Y(K)-Y(I))*SI
      ZL=1.0-ZI2/ZCIMAX
      ZP=1.0-ZCI2/ZCIMAX
      ZM=1.0-XM*ZP**2
      ZN=1.0+ZM+(4.0-ZM)*ZL**2-(1.0-ZL**2)*(4.0-ZM)
      ZN=ABS(ZN)
      DZCIDY=+ZCIMAX/HH
      VORSOR(I,J)=8.*ASS*XM*XKC*TOWAV*ZL*ZP*ZN*DZCIDY/ZCIMAX**2
      SO=VORSOR(I,J)
C     WRITE(6,*) I,J,ZM,ZL,ZP,ZN,SO
  440 CONTINUE
  413 CONTINUE
C     GO TO 1112
C--------- VORTICITY SUBCYCLE ---------------------------------
      DO 200 J=2,N1
      K=M-J
      DO 200 I=3,K
      CE=AE(I,J)+2.0*AMU*BEF(I,J)
      CW=AW(I,J)+2.0*AMU*BWF(I,J)
      CN=AN(I,J)+2.0*AMU*BNF(I,J)
      CS=AS(I,J)+2.0*AMU*BSF(I,J)
      SGMAB=CE+CW+CN+CS
      SOURCE = VP(I,J) * VORSOR(I,J)
      OMEGA =(CE* OMEG(I+1,J) + CW* OMEG(I-1,J) + CN* OMEG(I,J+1)
     *+ CS* OMEG(I,J-1)+SOURCE)/SGMAB
C--------------------- CALCULATE RESIDUALS ---------------------
      IF(ABS(OMEG(I,J)).GT.ABS(OMEGA)) GO TO 201
      IF(ABS(OMEGA).LT.0.000001) GO TO 202
      RSW=1.0-ABS(OMEG(I,J)/OMEGA)
      GO TO 203
  201 IF(ABS(OMEG(I,J)).LT.0.000001) GO TO 202
```

```
584.         RSW=1.0-ABS(OMEGA/OMEG(I,J))
585.      203 RSWF(I,J)=RSW
586.         IF(ABS(RSW) .GT. ABS(RSWM)) RSWM=RSW
587.      202 OMEG(I,J) = RLW * OMEGA + (1.0 - RLW) * OMEG(I,J)
588.      200 CONTINUE
589. C--------- THE VORTICITY BOUNDARY VALUES ----------------------
590. C-------------- HORIZONTAL WALLS -------------------------------
591.         DO 204 I=2,M2
592.         OMEG(I,1) = -2.*EPS(I,2)/(3.*ROW*Z(2)**2)
593.      204 CONTINUE
594.         Y1=Y(M2)-Y(M3)
595.         Y2=Y(M1)-Y(M3)
596.         OMEG(M1,1)=OMEG(M3,1)+(OMEG(M2,1)-OMEG(M3,1))*Y2/Y1
597.         DO 206 I=2,L
598.         OMEG(I,N)= -2.*EPS(I,N1)/(3.*ROW*(Z(N)-Z(N1))**2)
599.      206 CONTINUE
600. C--------------   INCLINED WALL --------------------------------
601.         DO 208 J=2,N1
602.         I=M-(J-1)
603.         S(I)=(Y(I)-Y(I-1))*SI
604.         OM(I)=-2.*EPS(I-1,J)/(3.*ROW*S(I)**2)
605.  208   CONTINUE
606.         DO 207 J=3,N1
607.         I=M-(J-1)
608.         X2=(Y(I)-Y(I-1))*CO
609.         X1=(Z(J)-Z(J-1))*SI
610.         OMEG(I,J)=(OM(I)*X1+OM(I+1)*X2)/(X1+X2)
611.      207 CONTINUE
612.         Y1=(Z(4)-Z(2))/SI
613.         Y2=(Z(4)-Z(3))/SI
614.         OMEG(M1,2)=OMEG(M3,4)+(OMEG(M2,3)-OMEG(M3,4))*Y1/Y2
615.         OMEG(M,1)=OMEG(M1,2)
616. C--------------------- STREAM FUNCTION SUBCYCLE -----------------
617. C
618.         DO 250 J=2,N1
619.         K=M-J
620.         DO 250 I=3,K
621. C       DO 250 II=2,K
622. C       I=K-II+2
623.         SGMB=2.0*(BEF(I,J)+BWF(I,J)+BNF(I,J)+BSF(I,J))
624.         SOURCE = OMEG(I,J) * VP(I,J) * ROW
625.         EPSI =(2.0*(BEF(I,J)*EPS(I+1,J)+BWF(I,J)*EPS(I-1,J)+
626.        *BNF(I,J)*EPS(I,J+1)+BSF(I,J)*EPS(I,J-1))+SOURCE)/SGMB
627. C------------------ CALCULATE EPSI,RESIDUALS --------------------
628.         IF(ABS(EPS(I,J)).GT.ABS(EPSI)) GO TO 253
629.         IF(ABS(EPSI).LT.0.00001) GO TO 252
630.         RSEP=1.0-ABS(EPS(I,J)/EPSI)
631.         GO TO 254
632.      253 IF(ABS(EPS(I,J)).LT.0.001) GO TO 252
633.         RSEP=1.0-ABS(EPSI/EPS(I,J))
634.      254 RSEPF(I,J)=RSEP
635.         IF(ABS(RSEP) .GT. ABS(RSEPM)) RSEPM=RSEP
636.      252 EPS(I,J) = RLEP * EPSI + (1.0 - RLEP) * EPS(I,J)
637.      250 CONTINUE
638.         IF(ICOUNT.NE.50) GO TO 1404
639.         CALL VV(VORSOR,M,N)
640. C       CALL RR(OMEG,M,N)
641. C       CALL RR(EPS,M,N)
642.     1404 CONTINUE
643.      431 CONTINUE
644. C------------   CLEAR LOCATIONS F3 AND F4   --------------------
645.         DO 256 J=1,N
646.         K=M-(J-1)
647.         DO 256 I=1,K
```

```
      F3(I,J) = 0.0
      F4(I,J) = 0.0
  256 CONTINUE
C---------------- COEFFICIENT FOR K EQUATION ------------------
      DO 260 J=2,N1
      K=M-J
      DO 260 I=2,K
      IF(TKE(I,J) .EQ. 0.0) GO TO 260
      F4(I,J) = ROW * VP(I,J) * TED(I,J) / TKE(I,J)
  260 CONTINUE
C
C----------------------- K SUBCYCLE ---------------------------
C
      DO 262 J=3,N2
      K=M1-J
      DO 262 I=2,K
      CE=AE(I,J)+BEF(I,J)*(2.0*AMU+(AMUT(I,J)+AMUT(I+1,J))/SIGMK)
      CW=AW(I,J)+BWF(I,J)*(2.0*AMU+(AMUT(I,J)+AMUT(I-1,J))/SIGMK)
      CN=AN(I,J)+BNF(I,J)*(2.0*AMU+(AMUT(I,J)+AMUT(I,J+1))/SIGMK)
      CS=AS(I,J)+BSF(I,J)*(2.0*AMU+(AMUT(I,J)+AMUT(I,J-1))/SIGMK)
      SGMABK = CE+CW+CN+CS
      TKEY=(CE*TKE(I+1,J)+CW*TKE(I-1,J)+CN*TKE(I,J+1)+CS*TKE(I,J-1)
     *+AMUT(I,J)*F2(I,J) * VP(I,J))/(F4(I,J)+SGMABK)
C------------------ CALCULATE K RESIDUALS ----------------------
      IF(TKE(I,J).GT.TKEY) GO TO 261
      IF(TKEY.LT.0.000001) GO TO 264
      RSK=1.0-TKE(I,J)/TKEY
      GO TO 263
  261 IF(TKE(I,J).LT.0.00001) GO TO 264
      RSK=1.0-TKEY/TKE(I,J)
  263 RSKF(I,J)=RSK
      IF(ABS(RSK) .GT. ABS(RSKM)) RSKM=RSK
  264 TKE(I,J) = RLK * TKEY + (1.0 - RLK) * TKE(I,J)
  262 CONTINUE
C
C     **** DISSIPATION SOURCE TERM STORED IN LOCATION F3 ****
C
      DO 270 J=2,N1
      K=M-J
      DO 270 I=2,K
      F3(I,J) = CE1 * CMU * TKE(I,J) * F2(I,J) * VP(I,J) * ROW
  270 CONTINUE
C
C---------------------- DISSIPATION SUBCYCLE -------------------
C
      DO 272 J=3,N2
      K=M1-J
      DO 272 I=2,K
      CE=AE(I,J)+BEF(I,J)*(2.0*AMU+(AMUT(I,J)+AMUT(I+1,J))/SIGME)
      CW=AW(I,J)+BWF(I,J)*(2.0*AMU+(AMUT(I,J)+AMUT(I-1,J))/SIGME)
      CN=AN(I,J)+BNF(I,J)*(2.0*AMU+(AMUT(I,J)+AMUT(I,J+1))/SIGME)
      CS=AS(I,J)+BSF(I,J)*(2.0*AMU+(AMUT(I,J)+AMUT(I,J-1))/SIGME)
      SGMABE =CE+CW+CN+CS
      TEDN=(CE*TED(I+1,J)+CW*TED(I-1,J)+CN*TED(I,J+1)+CS*TED(I,J-1)
     *+F3(I,J))/(CE2*F4(I,J)+SGMABE)
      IF(TEDN .LT. 0.0) WRITE(6,*) ICOUNT,I,J,CE,CW,CN,CS
      IF(TEDN .LT. 0.0) CALL RR(F3,M,N)
      IF(TEDN .LT. 0.0) CALL RR(F4,M,N)
      IF(TEDN .LT. 0.0) GO TO 399
C
C----------------- CALCULATE DISS. RESIDUALS ------------------
      IF(TED(I,J).GT.TEDN) GO TO 271
      IF(TEDN.LT.0.000001) GO TO 274
      RSE=1.0-TED(I,J)/TEDN
```

```
      GO TO 273
  271 IF(TKE(I,J).LT.0.00001) GO TO 274
      RSE=1.0-TEDN/TED(I,J)
  273 RSEF(I,J)=RSE
      IF(ABS(RSE) .GT. ABS(RSEM)) RSEM=RSE
  274 TED(I,J) = RLE * TEDN + (1.0 - RLE) * TED(I,J)
  272 CONTINUE
C--------- AXIAL VELOCITY (U) SUBCYCLE -------------------------
      DO 280 J=3,N2
      K=M1-J
      DO 280 I=2,K
      CE=AE(I,J)+BEF(I,J)*(2.0*AMU+(AMUT(I,J)+AMUT(I+1,J))/SIGMU)
      CW=AW(I,J)+BWF(I,J)*(2.0*AMU+(AMUT(I,J)+AMUT(I-1,J))/SIGMU)
      CN=AN(I,J)+BNF(I,J)*(2.0*AMU+(AMUT(I,J)+AMUT(I,J+1))/SIGMU)
      CS=AS(I,J)+BSF(I,J)*(2.0*AMU+(AMUT(I,J)+AMUT(I,J-1))/SIGMU)
      SGMABU =CE+CW+CN+CS
      U(I,J)=(CE*U(I+1,J)+CW*U(I-1,J)+CN*U(I,J+1)+CS*U(I,J-1)
     *+DPDX*VP(I,J))/SGMABU
      AAE=AE(I,J)
      AAW=AW(I,J)
      AAN=AN(I,J)
      AAS=AS(I,J)
      IF(U(I,J).LT.0.0) CALL RR(U,M,N)
      IF(U(I,J).LT.0.0) WRITE(6,*) ICOUNT,I,J,CE,CW,CN,CS
      IF(U(I,J).LT.0.0) PRINT, DPDX,SGMABU
      IF(U(I,J).LT.0.0) PRINT,AAE,AAW,AAN,AAS
  280 CONTINUE
C----------------- CALCULATE U RESUDIALS -------------------------
      DO 328 J=2,N1
      K=M-J
      DO 328 I=2,K
      IF(ICOUNT.EQ.1) GO TO 314
      RSU=0.0
      RSUF(I,J)=0.0
      IF(UO(I,J).GT.U(I,J)) GO TO 316
      IF(U(I,J).LT.0.00001) GO TO 318
      RSU=1.0-UO(I,J)/U(I,J)
      GO TO 330
  316 IF(UO(I,J).LT.0.00001) GO TO 318
      RSU=1.0-U(I,J)/UO(I,J)
  330 RSUF(I,J)=RSU
      IF(ABS(RSU).GT.ABS(RSUM)) RSUM=RSU
  318 U(I,J) = RLU * U(I,J)+ (1.0 - RLU) * UO(I,J)
  314 UO(I,J)=U(I,J)
  328 CONTINUE
C--------- CALCULATE  LOCAL  WALL SHEAR STRESSES ---------------
C----------------------  TOP WALL  -----------------------------
      DO 296 I=2,L
      RWMUK=ROWCMU*SQRT(TKE(I,N2))
      ZDPLS=RWMUK*(Z(N)-Z(N2))/AMU
      UPLS=A*ALOG(ZDPLS)+B
      TOWT(I)=RWMUK*U(I,N2)/UPLS
      UFT(I)=SQRT(TOWT(I)/ROW)
      ZPT(I)=UFT(I)*(Z(N)-Z(N1))/ANU
 296  CONTINUE
C----------------------- BOTTOM  WALL  --------------------
      DO 294 I=2,M3
      RWMUK=ROWCMU*SQRT(TKE(I,3))
      ZDPLS=RWMUK*(Z(3)-Z(1))/AMU
      UPLS=A*ALOG(ZDPLS)+B
      TOWB(I)=RWMUK*U(I,3)/UPLS
      UFB(I)=SQRT(TOWB(I)/ROW)
      ZPB(I)=UFB(I)*(Z(2)-Z(1))/ANU
  294 CONTINUE
```

```
776.        Y1=Y(M2)-Y(M3)
777.        Y2=Y(M2)-Y(M4)
778.        TOWB(M2)=(TOWB(M4)*Y1/Y2-TOWB(M3))/(Y1/Y2-1.0)
779.        UFB(M2)=SQRT(TOWB(M2)/ROW)
780.        ZPB(M2)=UFB(M2)*Z(2)/ANU
781.        X1=Y(M)-Y(M1)
782.        X2=Y(M)-Y(M2)
783.        TOWB(M1)=TOWB(M2)*X1/X2
784.        UFB(M1)=SQRT(TOWB(M1)/ROW)
785.        TOWB(M)=0.0
786. C-------------  U, K AND E BOUNDARY CONDITIONS -----------------
787. C-------------------------BOTTOM WALL  --------------------------
788.        DO 306 I=2,M2
789.        ZDPLS=UFB(I)*(Z(2)-Z(1))/ANU
790.        U(I,2)=UFB(I)*(A*ALOG(ZDPLS)+B)
791.        TKE(I,2)=UFB(I)*UFB(I)/SQRT(CMU)
792.        TED(I,2)=UFB(I)*UFB(I)*UFB(I)/(CAPA*(Z(2)-Z(1)))
793.    306 CONTINUE
794.        UFB(M)=0.0
795.        TKE(M,1)=0.0
796.        TED(M,1)=0.0
797. C---------  TOP WALL  ------------------------------------------
798.        DO 308 I=2,L
799.        ZDPLS=UFT(I)*(Z(N)-Z(N1))/ANU
800.        U(I,N1)=UFT(I)*(A*ALOG(ZDPLS)+B)
801.        TKE(I,N1)=UFT(I)*UFT(I)/SQRT(CMU)
802.        TED(I,N1)=UFT(I)*UFT(I)*UFT(I)/(CAPA*(Z(N)-Z(N1)))
803.    308 CONTINUE
804. C---------------INCLINED WALL SHEAR STRESS AND BOUNDARY CONDITIONS---
805.        DO 298 J=2,N2
806.        I=M-J
807.        RWMUK=ROWCMU*SQRT(TKE(I-1,J))
808.        XX1=(Y(I+1)-Y(I-1))*SI
809.        ZDPLS=RWMUK*XX1/AMU
810. C      IF(J.GT.(N-10).AND.J.LT.(N-5)) GO TO 1604
811.        UPLS=A*ALOG(ZDPLS)+B
812. C      GO TO 1608
813. C1604 UPLS=A*ALOG(ZDPLS)+7.5
814. C1608 CONTINUE
815.        TW1(I-1)=RWMUK*U(I-1,J)/UPLS
816.        UF1(I-1)=SQRT(TW1(I-1)/ROW)
817.    298 CONTINUE
818. C-----GET SHEAR STRESS BY INTERPOL TO USE FOR U,K,E BOUN. COND.---
819.        DO 307 J=2,N3
820.        I=M-J
821.        X1=(Y(I-1)-Y(I-2))*CO
822.        X2=(Z(J+1)-Z(J))/SI-(Y(I+1)-Y(I-1))*CO+(Y(I)-Y(I-1))*CO
823.        TW2(I-1)=(TW1(I-1)*X1+TW1(I-2)*X2)/(X1+X2)
824.        UF2(I-1)=SQRT(TW2(I-1)/ROW)
825.        S(I-1)=(Y(I)-Y(I-1))*SI
826.        SP(I-1)=UF2(I-1)*S(I-1)/ANU
827. C      IF(J.GT.(N-10).AND.J.LT.(N-5)) GO TO 1600
828.        U(I-1,J+1)=UF2(I-1)*(A*ALOG(SP(I-1))+B)
829. C      GO TO 1602
830. C1600 U(I-1,J+1)=UF2(I-1)*(A*ALOG(SP(I-1))+2.5)
831. C1602 CONTINUE
832.        TKE(I-1,J+1)=UF2(I-1)*UF2(I-1)/SQRT(CMU)
833.        TED(I-1,J+1)=UF2(I-1)*UF2(I-1)*UF2(I-1)/(CAPA*S(I-1))
834.    307 CONTINUE
835.        S(M2)=(Y(M1)-Y(M2))*SI
836.        R1=(Z(3)-Z(2))*SI+(Y(M2)-Y(M3))*CO
837.        R2=R1+(Z(4)-Z(3))*SI+(Y(M3)-Y(M4))*CO
838.        UF2(M2)=(UF2(M4)*R1/R2-UF2(M3))/(R1/R2-1.0)
839.        TW2(M2)=ROW*UF2(M2)*UF2(M2)
```

```
      SP(M2)=UF2(M2)*S(M2)/ANU
      TW2(L)=(TW2(L+1)+TOWT(L))/2.0
      UF2(L)=SQRT(TW2(L)/ROW)
      S(L)=(Y(L+1)-Y(L))*SI
      SP(L)=S(L)*UF2(L)/ANU
C---------ACTUAL NODES OF INC. WALL SHEAR STRESS-------------
      DO 310 J=2,N3
      I=M-J
      Y1=(Y(I)-Y(I-2))*CO
      Y2=(Z(J+1)-Z(J))/SI-(Y(I+1)-Y(I-1))*CO
      TOWI(I)=(TW1(I-1)*Y1+TW1(I-2)*Y2)/(Y1+Y2)
      UFI(I)=SQRT(TOWI(I)/ROW)
  310 CONTINUE
      R11=(Z(3)-Z(2))/SI
      R22=R11+(Z(4)-Z(3))/SI
      UFI(M1)=(UFI(M3)*R11/R22-UFI(M2))/(R11/R22-1.0)
      TOWI(M1)=ROW*UFI(M1)*UFI(M1)
      UFI(L)=UFT(L)
      TOWI(L)=TOWT(L)
      UFI(M)=0.0
      TOWI(M)=0.0
      TOWI(L+1)=(TOWI(L)+TOWI(L+2))/2.0
      UFI(L+1)=SQRT(TOWI(L+1)/ROW)
C---------------- AT THE MIDWALL BISECTOR ----------------------
      DO 288 J=2,N1
      U(1,J)=U(3,J)
      TKE(1,J)=TKE(3,J)
      TED(1,J)=TED(3,J)
  288 CONTINUE
C-----  CALCULATE AVERAGE WALL SHEAR STRESS AND FRICTION VELOC.-
C-------------------   BOTTOM    WALL
      SUMB = 0.0
      DO 300 I=3,M
      TOWMB = (TOWB(I) + TOWB(I-1)) / 2.0
      SUMB = SUMB + TOWMB * (Y(I) - Y(I-1))
  300 CONTINUE
      TOWAVB=SUMB/CC
      UFAVB=SQRT(TOWAVB/ROW)
C-------------------   TOP       WALL   ------------------------
      SUMT=0.0
      DO 302 I=3,L
      TOWMT=(TOWT(I)+TOWT(I-1))/2.0
      SUMT=SUMT+TOWMT*(Y(I)-Y(I-1))
  302 CONTINUE
      TOWAVT=SUMT/AA
      UFAVT=SQRT(TOWAVT/ROW)
C-------------------   INCLINED  WALL   ------------------------
      SUMI=0.0
      TOWI(M)=TOWB(M)
      DO 304 J=1,N1
      K=M-(J-1)
      I=K
      TOWM=(TOWI(I)+TOWI(I-1))/2.0
      SUMI=SUMI+TOWM*(Y(I)-Y(I-1))/CO
  304 CONTINUE
      TOWAVI=SUMI/(BB/SI)
      UFAVI=SQRT(TOWAVI/ROW)
      TOWAV = (SUMB+SUMT+SUMI)/CWTPR
      UFAV = SQRT(TOWAV / ROW)
      ZPLUS=UFAV*Z(2)/ANU
C---------  CALCULATE  DP/DX  ---------------------------------
      DPDX = 4.0 * TOWAV / DEQ
C--------------- AVERAGE BULK VELOCITY CALCULATION -----------
      SUM = 0.0
```

```
      DO 290 J=2,N
      K=M-(J-1)
      DO 290 I=3,K
      UAV = (U(I,J) + U(I-1,J) + U(I-1,J-1) + U(I,J-1)) / 4.0
      DV = UAV * DA(I,J)
      SUM = SUM + DV
  290 CONTINUE
      SUMT=0.0
      DO 292 J=2,N
      K=M-(J-1)
      I=K
      UAV=(U(I,J)+U(I+1,J-1)+U(I,J-1))/3.0
      DV=UAV*DAT(I,J)
      SUMT=SUMT+DV
  292 CONTINUE
      SUM=SUM+SUMT
      UB = SUM / CAREA
      UR = UBAV/UB
C--------- CORRCTN OF U EVERYWHERE IN ORDER TO SATISFY CONT EQ --
      DO 312 J=1,N
      K=M-(J-1)
      DO 312 I=1,K
      U(I,J) = U(I,J) * UBAV / UB
  312 CONTINUE
C-----------------------------------------------------------------
      IFREQ = ICOUNT / IRPRNT
      IFREQ = IFREQ * IRPRNT
      IF(ICOUNT .NE. IFREQ) GO TO 326
      PRINT 524, ICOUNT
      PRINT 526, RSWM,RSEPM,RSKM,RSEM,RSUM
C     CALL RR(RSWF,M,N)
C     CALL RR(RSEPF,M,N)
C     CALL RR(OMEG,M,N)
C     CALL RR(EPS,M,N)
  326 IF(ABS(RSWM) .LE. CRW .AND. ABS(RSEPM) .LE. CREP .AND. ABS(RSK
     *M) .LE. CRK .AND. ABS(RSEM) .LE. CRE .AND. ABS(RSUM) .LE. CRU)
     *GO TO 399
C-----------------------------------------------------------------
      IFREQ = ICOUNT / IPRINT
      IFREQ = IFREQ * IPRINT
      IF(ICOUNT .NE. IFREQ) GO TO 340
  399 CONTINUE
      IF(IM .EQ. 1) GO TO 395
C--------- SECONDARY VELOCITIES --------------------------------
      DO 360 J=1,N
C     K=M-(J-1)
      DO 360 I=1,M
      DUY(I,J) = 0.0
      DUZ(I,J) = 0.0
  360 CONTINUE
C---------------    DEPS BY DY ---------------------------------
      DO 362 J=2,N1
      K=M-J
      DO 362 I=2,K
      DUY(I,J) = ((EPS(I+1,J) - EPS(I,J)) * YRAT(I,J) + (EPS(I,J) -
     *EPS(I-1,J)) / YRAT(I,J)) / (Y(I+1) - Y(I-1))
  362 CONTINUE
C---------           DEPS BY DZ ---------------------------------
      DO 364 J=2,N1
      K=M-J
      DO 364 I=3,K
      DUZ(I,J) = ((EPS(I,J+1) - EPS(I,J)) * ZRAT(I,J) + (EPS(I,J) -
     *EPS(I,J-1)) / ZRAT(I,J)) / (Z(J+1) - Z(J-1))
  364 CONTINUE
```

```
      DO 374 J=2,N1
      K=M-J
      DO 374 I=2,K
      V(I,J) = (1.0 / ROW) * DUZ(I,J)
      W(I,J) = -(1.0 / ROW) * DUY(I,J)
      VSEC(I,J) = SQRT(V(I,J)**2 + W(I,J)**2)
374   CONTINUE
C     PRINT 618
C     CALL RR(OMEG,M,N)
C     PRINT 624
C     CALL RR(EPS,M,N)
395   CONTINUE
340   IF(ABS(RSWM) .LE. CRW .AND. ABS(RSEPM) .LE. CREP .AND. ABS(RSK
     *M) .LE. CRK .AND. ABS(RSEM) .LE. CRE .AND. ABS(RSUM) .LE. CRU)
     *GO TO 899
      IF(ICOUNT .LT. IMAX) GO TO 900
899   CONTINUE
      PRINT 730,UFAV,TOWAV,DPDX
      PRINT 524, ICOUNT
      PRINT 526, RSWM,RSEPM,RSKM,RSEM,RSUM
      CALL SS(ICOUNT,RSWM,RSEPM,RSKM,RSEM,RSUM,UB,UR,DPDX,
     *UFAV,UFB,UFT,UFI,TOWAV,TOWB,TOWT,TOWI,ZPT,ZPB,SP,M,N)
      IF(IM.EQ.1) GO TO 345
      PRINT 618
      CALL RR(OMEG,M,N)
      PRINT 624
      CALL RR(EPS,M,N)
345   CONTINUE
      PRINT 630
      CALL RR(U,M,N)
      PRINT 626
      CALL RR(TKE,M,N)
      PRINT 628
      CALL RR(TED,M,N)
      PRINT 632
      CALL RR(AMUT,M,N)
      IF(JF.NE.1) GO TO 350
      WRITE(13,*) U,TKE,TED,TOWB,TOWT,TOWI,UFB,UFT,UFI,UF1,UF2,
     *DPDX,UFAV,TOWAV
350   CONTINUE
C--------- SECONDARY VELOCITIES --------------------------------
      DO 760 J=1,N
C     K=M-(J-1)
      DO 760 I=1,M
      DUY(I,J) = 0.0
      DUZ(I,J) = 0.0
760   CONTINUE
C---------------    DEPS BY DY ---------------------------------
      DO 762 J=2,N1
      K=M-J
      DO 762 I=2,K
      DUY(I,J) = ((EPS(I+1,J) - EPS(I,J)) * YRAT(I,J) + (EPS(I,J) -
     *EPS(I-1,J)) / YRAT(I,J)) / (Y(I+1) - Y(I-1))
762   CONTINUE
C---------          DEPS BY DZ ---------------------------------
      DO 764 J=2,N1
      K=M-J
      DO 764 I=3,K
      DUZ(I,J) = ((EPS(I,J+1) - EPS(I,J)) * ZRAT(I,J) + (EPS(I,J) -
     *EPS(I,J-1)) / ZRAT(I,J)) / (Z(J+1) - Z(J-1))
764   CONTINUE
      DO 774 J=2,N1
      K=M-J
      DO 774 I=2,K
```

```
      V(I,J) = (1.0 / ROW) * DUZ(I,J)
      W(I,J) = -(1.0 / ROW) * DUY(I,J)
      VSEC(I,J) = SQRT(V(I,J)**2 + W(I,J)**2)
  774 CONTINUE
      VMAX =0.0
      WMAX = 0.0
      SECMAX = 0.0
      DO 388 J=2,N1
      K=M-J
      DO 388 I=2,K
      V(I,J) = V(I,J) / UBAV * 100.0
      W(I,J) = W(I,J) / UBAV * 100.0
      VSBUA(I,J) = VSEC(I,J) / UBAV*100.0
      IF(ABS(W(I,J)) .GT. ABS(WMAX)) WMAX=W(I,J)
      IF(ABS(V(I,J)) .GT. ABS(VMAX)) VMAX=V(I,J)
      IF(VSBUA(I,J) .GT. SECMAX) SECMAX=VSBUA(I,J)
  388 CONTINUE
      PRINT 564
      CALL RR(V,M,N)
      PRINT 566
      CALL RR(W,M,N)
      PRINT 570
      CALL RR(VSBUA,M,N)
      PRINT 568,VMAX,WMAX,SECMAX
C-----------------------------------------------------------------
C------------------HEAT TRANSFER PREDICTIONS----------------------
C-----------------------------------------------------------------
      AMR=AMU/PR
      CK=25.63*1.0E-3
      PF=9.4*((PR/PRT)**0.75-1.0)
C---------------INITIAL BOUNDARY CONDIONS-----------------------
      DO 901 J=3,N2
      K=M1-J
      DO 901 I=2,K
      T(I,J)=TBAV
  901 CONTINUE
C-------------------------AT THE WALLS--------------------------
      DO 905 I=2,L
      T(I,N)=TW
  905 CONTINUE
      DO 907 I=2,M
      T(I,1)=TW
  907 CONTINUE
      DO 909 J=2,N1
      I=M-(J-1)
      T(I,J)=TW
  909 CONTINUE
C------------ASSUME THAT Q(I) IS PROPORTIONAL TO TOW(I)---------
      DO 902 I=2,L
      QT(I)=QAV*TOWT(I)/TOWAV
  902 CONTINUE
      DO 903 I=2,M
      QB(I)=QAV*TOWB(I)/TOWAV
  903 CONTINUE
      DO 904 J=2,N2
      I=M-J
      QI2(I-1)=QAV*TW2(I-1)/TOWAV
  904 CONTINUE
      R1=(Z(3)-Z(2))*SI+(Y(M2)-Y(M3))*CO
      R2=R1+(Z(4)-Z(3))*SI+(Y(M3)-Y(M4))*CO
      QI2(M2)=(QI2(M4)*R1/R2-QI2(M3))/(R1/R2-1.0)
      DO 956 I=2,L
      XXTB=ROW*CP*UFT(I)/(PRT*(U(I,N1)/UFT(I)+PF))
      T(I,N1)=TW-QT(I)/XXTB
```

```
1096.    956 CONTINUE
1097.        DO 957 I=2,M2
1098.        YYTB=ROW*CP*UFB(I)/(PRT*(U(I,2)/UFB(I)+PF))
1099.        T(I,2)=TW-QB(I)/YYTB
1100.    957 CONTINUE
1101.        DO 959 J=2,N3
1102.        I=M-J
1103.        XYIB=ROW*CP*UF2(I-1)/(PRT*(U(I-1,J+1)/UF2(I-1)+PF))
1104.        T(I-1,J+1)=TW-QI2(I-1)/XYIB
1105.    959 CONTINUE
1106.        DTDX=QAV*CWTPR/(AMASS*CP)
1107. C----------------------CONSTANT COEFFICIENTS FOR TEM CYCLE-------
1108.        DO 910 J=2,N1
1109.        K=M-J
1110.        DO 910 I=2,K
1111.        BEF(I,J)=AE(I,J)+BEF(I,J)*(2.0*AMR+(AMUT(I,J)+AMUT(I+1,J))/PRT)
1112.        BWF(I,J)=AW(I,J)+BWF(I,J)*(2.0*AMR+(AMUT(I,J)+AMUT(I-1,J))/PRT)
1113.        BNF(I,J)=AN(I,J)+BNF(I,J)*(2.0*AMR+(AMUT(I,J)+AMUT(I,J+1))/PRT)
1114.        BSF(I,J)=AS(I,J)+BSF(I,J)*(2.0*AMR+(AMUT(I,J)+AMUT(I,J-1))/PRT)
1115.        F1(I,J)=BEF(I,J)+BWF(I,J)+BNF(I,J)+BSF(I,J)
1116.    910 CONTINUE
1117. C--------------------TEMPERATURE CYCLE--------------------------
1118.        ITEMP=0.0
1119.   1985 ITEMP=ITEMP+1
1120.        RSTM=0.0
1121.        DO 986 J=3,N2
1122.        K=M1-J
1123.        DO 986 I=2,K
1124.        SOURCE=+ROW*U(I,J)*DTDX*VP(I,J)
1125.        TEM=(BEF(I,J)*T(I+1,J)+BWF(I,J)*T(I-1,J)+BNF(I,J)*T(I,J+1)+
1126.       *BSF(I,J)*T(I,J-1)-SOURCE)/F1(I,J)
1127. C---------------CALCULATE   RESIDUALS----------------------
1128.        IF(TEM.EQ.0.0) GO TO 916
1129.        RST=1.0-T(I,J)/TEM
1130.        RSTF(I,J)=RST
1131.        IF(ABS(RST).GT.ABS(RSTM)) RSTM=RST
1132.    916 T(I,J)=RLT*TEM+(1.-RLT)*T(I,J)
1133.    986 CONTINUE
1134. C-----------------TEMPERATURE BOUNDARY CONDITIONS---------------
1135.        DO 915 I=2,L
1136.        XXTB=ROW*CP*UFT(I)/(PRT*(U(I,N1)/UFT(I)+PF))
1137.        T(I,N1)=TW-QT(I)/XXTB
1138.    915 CONTINUE
1139.        DO 924 I=2,M2
1140.        YYTB=ROW*CP*UFB(I)/(PRT*(U(I,2)/UFB(I)+PF))
1141.        T(I,2)=TW-QB(I)/YYTB
1142.    924 CONTINUE
1143.        T(M1,1)=TW
1144.        DO 960 J=2,N3
1145.        I=M-J
1146.        XYIB=ROW*CP*UF2(I-1)/(PRT*(U(I-1,J+1)/UF2(I-1)+PF))
1147.        T(I-1,J+1)=TW-QI2(I-1)/XYIB
1148.    960 CONTINUE
1149.        DO 926 J=1,N
1150.        T(1,J)=T(3,J)
1151.    926 CONTINUE
1152. C------------------------CALCULATE LOCAL HEAT FLUX-------------
1153.        DO 952 I=2,L
1154.        XXT=ROW*CP*UFT(I)/(PRT*(U(I,N2)/UFT(I)+PF))
1155.        QT(I)=(-T(I,N2)+TW)*XXT
1156.    952 CONTINUE
1157. C------------------BOTTOM WALL---------------------------------
1158.        DO 958 I=2,M3
1159.        YYT=ROW*CP*UFB(I)/(PRT*(U(I,3)/UFB(I)+PF))
```

```
1160.       QB(I)=(-T(I,3)+TW)*YYT
1161.   958 CONTINUE
1162.       Y1=Y(M2)-Y(M3)
1163.       Y2=Y(M2)-Y(M4)
1164.       QB(M2)=(QB(M4)*Y1/Y2-QB(M3))/(Y1/Y2-1.0)
1165.       X1=Y(M)-Y(M1)
1166.       X2=Y(M1)-Y(M2)
1167.       QB(M1)=(QB(M2)*X1+QB(M)*X2)/(X1+X2)
1168.       QB(M)=0.0
1169. C----------------------INCLINED WALL-----------------------
1170.       DO 932 J=2,N2
1171.       I=M-J
1172.       XYI=ROW*CP*UF1(I-1)/(PRT*(U(I-1,J)/UF1(I-1)+PF))
1173.       QI1(I-1)=(TW-T(I-1,J))*XYI
1174.   932 CONTINUE
1175.       DO 954 J=2,N3
1176.       I=M-J
1177.       X1=(Y(I-1)-Y(I-2))*CO
1178.       X2=(Z(J+1)-Z(J))/SI-(Y(I+1)-Y(I-1))*CO+(Y(I)-Y(I-1))*CO
1179.       QI2(I-1)=(QI1(I-1)*X1+QI1(I-2)*X2)/(X1+X2)
1180.   954 CONTINUE
1181.       R1=(Z(3)-Z(2))*SI+(Y(M2)-Y(M3))*CO
1182.       R2=R1+(Z(4)-Z(3))*SI+(Y(M3)-Y(M4))*CO
1183.       QI2(M2)=(QI2(M4)*R1/R2-QI2(M3))/(R1/R2-1.0)
1184.       QI2(L)=(QI2(L+1)+QT(L))/2.0
1185. C---------QI(I) AT ORIGINAL NODES ON THE INCL. WALL-----------
1186.       DO 962 J=2,N3
1187.       I=M-J
1188.       Y1=(Y(I)-Y(I-2))*CO
1189.       Y2=(Z(J+1)-Z(J))/SI-(Y(I+1)-Y(I-1))*CO
1190.       QI(I)=(QI1(I-1)*Y1+QI1(I-2)*Y2)/(Y1+Y2)
1191.   962 CONTINUE
1192.       R11=(Z(3)-Z(2))/SI
1193.       R22=R11+(Z(4)-Z(3))/SI
1194.       QI(M1)=(QI(M3)*R11/R22-QI(M2))/(R11/R22-1.0)
1195.       QI(L)=QT(L)
1196.       QI(M)=0.0
1197.       QI(L+1)=(QI(L)+QI(L+2))/2.0
1198. C---------------CALCULATE AVERAGE HEAT FLUX AND NUSLET NUM._____
1199. C----------------------BOTTOM  WALL--------------------------
1200.       SUMB = 0.0
1201.       DO 940 I=3,M
1202.       QMB = (QB(I) + QB(I-1)) / 2.0
1203.       SUMB = SUMB + QMB * (Y(I) - Y(I-1))
1204.   940 CONTINUE
1205.       QAVB=SUMB/CC
1206. C--------------------- TOP  WALL ------------------------
1207.       SUMT=0.0
1208.       DO 942 I=3,L
1209.       QMT=(QT(I)+QT(I-1))/2.0
1210.       SUMT=SUMT+QMT*(Y(I)-Y(I-1))
1211.   942 CONTINUE
1212.       QAVT=SUMT/AA
1213. C-------------------   INCLINED  WALL   -----------------
1214.       SUMI=0.0
1215.       QI(L)=QT(L)
1216.       DO 944 J=1,N1
1217.       K=M-(J-1)
1218.       I=K
1219.       QMI=(QI(I)+QI(I-1))/2.0
1220.       SUMI=SUMI+QMI*(Y(I)-Y(I-1))/CO
1221.   944 CONTINUE
1222.       QAVI=SUMI/(BB/SI)
1223.       QAV = (SUMB+SUMT+SUMI)/CWTPR
```

```
1224.       DTDX=QAV*CWTPR/(AMASS*CP)
1225. C-----------------AVERAGE TEM CALCULATIONS-----------------
1226.       SUM = 0.0
1227.       DO 927 J=2,N
1228.       K=M-(J-1)
1229.       DO 927 I=3,K
1230.       TUAV = (T(I,J)*U(I,J) + T(I-1,J)*U(I-1,J)+
1231.      *T(I-1,J-1)*U(I-1,J-1)+T(I,J-1)*U(I,J-1))/4.0
1232.       DV = TUAV * DA(I,J)
1233.       SUM = SUM + DV
1234.   927 CONTINUE
1235.       SUMT=0.0
1236.       DO 928 J=2,N
1237.       K=M-(J-1)
1238.       I=K
1239.       TUAV=(T(I,J)*U(I,J)+T(I+1,J-1)*U(I+1,J-1)+
1240.      *T(I,J-1)*U(I,J-1))/3.0
1241.       DV=TUAV*DAT(I,J)
1242.       SUMT=SUMT+DV
1243.   928  CONTINUE
1244.       SUM=SUM+SUMT
1245.       TB = SUM*ROW/AMASS
1246.       TR = TBAV/TB
1247. C---------CCORRCTN OF T EVERYWHERE IN ORDER TO PREVENT TEM DREF.-
1248.       DO 930 J=2,N1
1249.       K=M-J
1250.       DO 930 I=2,K
1251.       T(I,J) = T(I,J) * TBAV / TB
1252.   930 CONTINUE
1253. C---------------------CHECK CONVERGENCE----------------------
1254.       IFREQ = ITEMP / IRPRNT
1255.       IFREQ = IFREQ * IRPRNT
1256.       IF(ITEMP .NE. IFREQ) GO TO 950
1257.       PRINT 854, ITEMP
1258.       PRINT 856, RSTM
1259.   950 IF(ABS(RSTM) .LE. CRT) GO TO 955
1260.       IF(ITEMP .LT. ITMAX) GO TO 1985
1261.   955 CONTINUE
1262.       PRINT 854, ITEMP
1263.       PRINT 856, RSTM
1264. C-----------------PRINT OUT OF CONVERGED SOLUTION--------------
1265.       H=ABS(QAV/(TW-TB))
1266.       XN=H*DEQ/CK
1267.       PRINT 871,QAV,TB,TW,H,XN,DTDX
1268.       PRINT 873
1269.       CALL RR(T,M,N)
1270. C---------------------------------------------------------------
1271.       DO 993 J=2,N1
1272.       K=M-J
1273.       DO 993 I=2,K
1274.       T(I,J)=(TW-T(I,J))/(TW-TB)
1275.   993 CONTINUE
1276.       PRINT 994
1277.       CALL RR(T,M,N)
1278. C---------------------------------------------------------------
1279.       DO 890 J=1,N
1280.       K=M-(J-1)
1281.       DO 890 I=1,K
1282.       F1(I,J)=EPS(I,J)/(ROW*UBAV*DEQ)*1000.0
1283.       F2(I,J)=OMEG(I,J)/UFAV*DEQ
1284.       F3(I,J)=U(I,J)/UBAV
1285.       F4(I,J)=TKE(I,J)/UFAV**2
1286.   890 CONTINUE
1287.       WRITE(14,*) ((F1(I,J),I=1,M),J=1,N)
```

```
1288.       WRITE(14,*) ((F2(I,J),I=1,M),J=1,N)
1289.       WRITE(14,*) ((F3(I,J),I=1,M),J=1,N)
1290.       WRITE(14,*) ((F4(I,J),I=1,M),J=1,N)
1291.       WRITE(14,*) ((V(I,J),I=1,M),J=1,N)
1292.       WRITE(14,*) ((W(I,J),I=1,M),J=1,N)
1293. C--------- FRICTION FACTOR CALCULATION -------------------------
1294.       FF = 8.0 * TOWAV / (ROW * UBAV**2)
1295.       PRINT 532, FF,H,XN
1296.       PRINT 534, AMASS,QAV
1297. C-----------------------------------------------------------------
1298.       DO 376 I=2,M
1299.       TOWB(I) = TOWB(I) / TOWAV
1300.       UFB(I) = UFB(I) / UFAV
1301.    376 CONTINUE
1302.       DO 378 I=2,L
1303.       TOWT(I)=TOWT(I)/TOWAV
1304.       UFT(I)=UFT(I)/UFAV
1305.    378  CONTINUE
1306.       DO 380 J=1,N
1307.       K=M-(J-1)
1308.       I=K
1309.       TOWI(I)=TOWI(I)/TOWAV
1310.       UFI(I)=UFI(I)/UFAV
1311.    380 CONTINUE
1312. C-----------------------------------------------------------------
1313.       DO 421 I=2,M
1314.       QB(I) = QB(I) / QAV
1315.    421 CONTINUE
1316.       DO 423 I=2,L
1317.       QT(I)=QT(I)/QAV
1318.    423  CONTINUE
1319.       DO 542 J=1,N
1320.       K=M-(J-1)
1321.       I=K
1322.       QI(I)=QI(I)/QAV
1323.    542 CONTINUE
1324. C-----------------------------------------------------------------
1325.       PRINT 560
1326.       CALL RR(F3,M,N)
1327.       PRINT 558
1328.       CALL RR(F4,M,N)
1329.       PRINT 544
1330.       WRITE(6,*) (TOWT(I),I=2,L)
1331.       PRINT 540
1332.       WRITE(6,*) (TOWI(I),I=L,M)
1333.       PRINT 538
1334.       WRITE(6,*) (TOWB(I),I=2,M)
1335.       PRINT 552
1336.       WRITE(6,*) (QT(I),I=2,L)
1337.       PRINT 554
1338.       WRITE(6,*) (QI(I),I=L,M)
1339.       PRINT 556
1340.       WRITE(6,*) (QB(I),I=2,M)
1341. C-----------------------------------------------------------------
1342. C-----------------------------------------------------------------
1343.    512 FORMAT(//40X,'THE NODAL DISTANCE IN THE Y - DIRN. (METER) :'/)
1344.    518 FORMAT(//40X,'THE NODAL DISTANCE IN THE Z - DIRN. (METER) :'/)
1345.    500 FORMAT('1',40X,'**** INPUT VALUES ****'///44X,'M  =',I4/44X,
1346.       *'N  =',I4/44X,'AA     =',F9.6,2X,'(METER)'/44X,'BB    =',F9.6,2X,
1347.       *'(METER)'/44X,'CC     =',F9.6,2X,'(METER)'/44X,'TH    =',F9.6,2X,
1348.       *'(RAD)'/44X,'DEQ  =',F9.6,2X,'(METER)'/44X,'RE  =',E10.2
1349.       */44X,'UBAV  =',F12.5,2X,'(M/SEC)'/44X,'ROW =',F8.5,2X,'(KG/CU.M)'/
1350.       *44X,'AMU =',E12.5,2X,'(KG/M SEC)'/)
1351.    502 FORMAT(//40X,'CONSTANT  VALUES :'/44X,'CMU =',F7.3/44X,'CE1 =',
```

```
1352.       *F7.3/44X,'CE2 =',F7.3/44X,'SIGMK =',F7.3/44X,'SIGME =',F7.3/44X,
1353.       *'SIGMU =',F7.3/44X,'CAPA =',F8.4/)
1354.    871 FORMAT(//40X,'HEAT TRANSFER RESULTS:'/44X,'QAV =',E12.5/44X,
1355.       *'TB  =',F7.3/44X,'TW  =',F7.3/44X,'H   =',F7.3/44X,'XN  =',
1356.       *E12.5/44X,'DTDX=',F7.3/)
1357.    503 FORMAT(//40X,'CONSTANT  VALUES :'/44X,'ASS =',F9.6/44X,'XM  =',
1358.       *F7.3/44X,'XKC =',F7.3/)
1359.    578 FORMAT(///10X,'? DY1 OR DY2 OR DZ IS WRONG ?XXX'///)
1360.    508 FORMAT( 40X,'UNDER RELAXATION FACTORS :'/46X,'RLW  =',F7.4/46X,
1361.       *'RLEP  =',F7.4/46X,'RLK  =',F7.4/46X,'RLE  =',F7.4/46X,
1362.       *'RLU  =',F7.4/)
1363.    529 FORMAT(//40X,'ASSUMED INITIAL AND BOUNDARY VALUES ARE :'/44X,
1364.       *'UFAV =',E12.5/44X,'TOWAV =',E12.5/44X,'DPDX  =',
1365.       *E12.5/44X,'TKEI  =',E12.5/44X,'TEDI  =',E12.5/)
1366.    730 FORMAT(//40X,'FINAL VALUES OF UFAV,TOWAV,DPDX :'/44X,
1367.       *'UFAV =',E12.5/44X,'TOWAV =',E12.5/44X,'DPDX  =',E12.5/)
1368.    525 FORMAT(//40X,'ASSUMED DISSIPTN. I.V. (TED(I,2)) :'/)
1369.    527 FORMAT(//40X,'ASSUMED DISSIPTN. I.V. (TED(I,N1)) :'/)
1370. C  531 FORMAT(//40X,'ASSUMED DISSIPTN. I.V. (TED(K,J)) :'/)
1371.    524 FORMAT(///51X,'ICOUNT  =',2X,I5//)
1372.    526 FORMAT(  4X,'RSWM=',E13.6,9X,'RSEPM=',E13.6,9X,'RSKM=',
1373.       *E13.6,9X,'RSEM=',E13.6,9X,'RSUM=',E13.6)
1374.    854 FORMAT(///51X,'ITEMP   =',2X,I5//)
1375.    856 FORMAT(  50X,'RSTM=',E13.6)
1376. C  536 FORMAT(/40X,'UFB  DIST. NORMALIZED BY UFAV ')
1377. C  542 FORMAT(/40X,'UFT  DIST.  NORMALIZED  BY UFAV ')
1378.    538 FORMAT(/40X,'TOWB DIST. NORMALIZED  BT TOWAV ')
1379.    544 FORMAT(/40X,'TOWT DIST. NORMALIZED  BY TOWAV ')
1380.    552 FORMAT(/40X,'QT(I) DIST. NORMALIZED  BY QAV ')
1381.    554 FORMAT(/40X,'QI(I) DIST. NORMALIZED  BY QAV ')
1382.    556 FORMAT(/40X,'QB(I) DIST. NORMALIZED  BY QAV ')
1383.    522 FORMAT(/40X,'SUMDA :',E14.6,2X,'(SQ. M.)')
1384.    540 FORMAT(/40X,'TOWI(I) DIST. NORMALIZED  BT TOWAV ')
1385. C  546 FORMAT(/40X,'UFI(I) DIST. NORMALIZED  BT UFAV ')
1386.    532 FORMAT( /30X,'F.F.=',E14.6,4X,'H   =',E14.6,4X,'XN  =',E14.6)
1387.    514 FORMAT( 1X,'      I=',4X,'1',13X,'2',13X,'3',13X,'4',13X,'5',13X,'
1388.       *6',13X,'7',13X,'8'/)
1389.    516 FORMAT(5X,8(1E11.4,3X)/5X,8(1E11.4,3X)/5X,8(1E11.4,3X)/)
1390.    517 FORMAT(5X,11E11.4/5X,11E11.4)
1391.    520 FORMAT( 1X,'      J=',3X,'1',10X,'2',10X,'3',10X,'4',10X,'5',10X,'
1392.       *6',10X,'7',10X,'8',10X,'9',10X,'10',10X,'11'/)
1393.    568 FORMAT(/45X,'VMAX =',E12.5,2X,'(% UB)'/45X,'WMAX =',E12.5,2X,
1394.       *'(% UB)'/45X,'SECMAX =',E12.5,2X,'(% UB)'/)
1395.    506 FORMAT(/40X,'CONVERGIENCE FACTORS :'/44X,'CRW =',F7.4/44X,
1396.       *'CREP=',F7.4/44X,'CRK =',F7.4/44X,'CRE =',F7.4/44X,'CRU =',F7.4/)
1397.    558 FORMAT(/40X,'THE T.K.E. DISTBN. NORMALIZED BY (UFAV SQ) :'/)
1398.    560 FORMAT(/40X,'THE AXIAL VEL. DISTBN. NRMALIZED BY UBAV :'/)
1399.    873 FORMAT(/40X,'THE AIR TEMP. DISTBUTION  (DEG.CELS. :'/)
1400.    994 FORMAT(/40X,'THE DIMENSIONLESS AIR TEMPERA. T*      :'/)
1401.    564 FORMAT(/40X,'THE VEL. DISTBN. IN Y - DIRN. (V/UB) :'/)
1402.    566 FORMAT(/40X,'THE VEL. DISTBN. IN Z - DIRN. (W/UB) :'/)
1403.    570 FORMAT(/40X,'THE SECONDARY VELOCITY - %AGE OF UBAV :'/)
1404.    548 FORMAT (/40X,'DISTANCE FROM MIDWALL BISECTOR NORMALIZED BY DUCT
1405.       * LENGTH UNDER CONSIDERATION (Y*)'/)
1406.    550 FORMAT (/40X,'DISTANCE FROM BOTTOM  WALL  NORMALIZED BY TRAP.
1407.       * HIGHT  (BB)'/)
1408.    551 FORMAT (/40X,'DIST. FROM TOP OF INC. WALL NORM. BY (BB/SI)')
1409.    510 FORMAT(/40X,'DUCT CROSS SECTN. AREA :',E14.6,2X,'(SQ. M)',/40X,
1410.       *'SOLUTION DOMAIN AREA   :',E14.6,2X,'(SQ. M)')
1411. C  528 FORMAT(//40X,'THE VORTICITY RESIDUALS :'/)
1412. C  530 FORMAT(//40X,'THE STREAM FUNCTION RESIDUALS :'/)
1413. C  535 FORMAT(//40X,'THE TURBL. K.E.     RESIDUALS :'/)
1414. C  731 FORMAT(//40X,'THE TURB. DISSIP.   RESIDUALS :'/)
1415. C  533 FORMAT(//40X,'THE AXIAL. VELOC.   RESIDUALS :'/)
```

```
1416.    521 FORMAT(//40X,'THE DIMNSNLESS  DISTANCE FROM THE HORIZ WALL :'
1417.       *,/45X,'ZPLUS=',E12.5//)
1418.    523 FORMAT(//40X,'THE DIMNSLESS  DIST. FROM THE INCLINED WALL :'/)
1419.    504 FORMAT(/40X,'LAW OF THE WALL CONSTANTS :'/45X,'A  =',F10.4/45X,
1420.       *'B  =',F10.4/)
1421.    534 FORMAT(/30X,'MASS RATE OF FLOW (KG/SEC) :',E12.4,4X,
1422.       *'QAV(WATT/SQ.M/M):',E14.6)
1423.  C 556 FORMAT(/40X,'THE TEMP DIST. (T/TBAV)   :'/)
1424.  C 556 FORMAT(/40X,'       K / UF**2 :'/)
1425.    618 FORMAT( //40X,'OMEGA(1/SEC)'/)
1426.    699 FORMAT( //11X,'  DP/DX  &  UFAV  &  TOWAV CPRIME=ZERO'/)
1427.    624 FORMAT( //40X,'EPSI (KG/M SEC)'/)
1428.    626 FORMAT( //40X,'K (SQ.M/SQ.SEC)'/)
1429.    628 FORMAT( //40X,'DISS (M.SQ/SEC**3)'/)
1430.    630 FORMAT( //40X,'U (M/SEC)'/)
1431.    632 FORMAT( //40X,'MUT  (KG/M SEC) :'/)
1432.    700 FORMAT( //40X,'K (SQ.M/SQ.SEC)CPRIME=ZERO'/)
1433.    710 FORMAT( //40X,'DISS (M**2/SEC**3) CPRIME=ZERO'/)
1434.    720 FORMAT( //40X,'U (M/SEC) CPRIME=ZERO'/)
1435.  C 421 FORMAT( //40X,'AL(I,J) FROM NEW ORIGIN'/)
1436.  C 423 FORMAT( //40X,'VORTICI SOURCE BY SEALS APPROX'/)
1437.        GO TO 1112
1438.   9999 CONTINUE
1439.        WRITE(6,578)
1440.   1112 STOP
1441.        END
1442.  C-------------------------------------------------------------
1443.        SUBROUTINE RR(PHI,M,N)
1444.        REAL PHI(41,41)
1445.        N1=N-1
1446.        PRINT 580
1447.        DO 402 J=2,N1
1448.        K=M-J
1449.        PRINT 582,J,(PHI(I,J),I=2,K)
1450.    402 CONTINUE
1451.    580 FORMAT( 1X,'(J)  I=',4X,'2',13X,'3',13X,'4',13X,'5',13X,'6',13X,'
1452.       *7',13X,'8',13X,'9'//)
1453.    582 FORMAT(1X,I2,4X,8(1E11.4,3X)/7X,8(1E11.4,3X)/7X,8(1E11.4,3X)/
1454.       *7X,8(1E11.4,3X)/7X,4(1E11.4,3X)//)
1455.        RETURN
1456.        END
1457.  C-------------------------------------------------------------
1458.        SUBROUTINE VV(PHI,M,N)
1459.        REAL PHI(41,41)
1460.        N1=N-1
1461.        PRINT 700
1462.        DO 710 J=1,N
1463.        K=M-(J-1)
1464.        PRINT 715,J,(PHI(I,J),I=1,K)
1465.    710 CONTINUE
1466.    700 FORMAT( 1X,'(J)  I=',4X,'1',13X,'2',13X,'3',13X,'4',13X,'5',13X,'
1467.       *6',13X,'7',13X,'8'//)
1468.    715 FORMAT(1X,I2,4X,7(1E14.7,3X)/7X,7(1E14.7,3X)/7X,7(1E14.7,3X)/
1469.       *7X,7(1E14.7,3X)/7X,7(1E14.7,3X)/7X,1(1E14.7,3X)//)
1470.        RETURN
1471.        END
1472.  C-------------------------------------------------------------
1473.        SUBROUTINE SS(ICOUNT,RSWM,RSEPM,RSKM,RSEM,RSUM,UB,UR,DPDX,
1474.       *UFAV,UFB,UFT,UFI,TOWAV,TOWB,TOWT,TOWI,ZPT,ZPB,SP,M,N)
1475.        DIMENSION UFB(41),UFT(20),UFI(40),TOWB(41),TOWT(20),TOWI(40),
1476.       *SP(40),ZPT(20),ZPB(41)
1477.        L=M-(N-1)
1478.        M1=M-1
1479.        M2=M-2
```

```
      L1=L+1
      PRINT 584,ICOUNT
      PRINT 586,RSWM,RSEPM,RSKM,RSEM,RSUM
      PRINT 588,UB,UR
      PRINT 590,UFAV,TOWAV,DPDX
      PRINT 592
      WRITE(6,*) (UFB(I),I=2,M)
      PRINT 594
      WRITE(6,*) (UFT(I),I=2,L)
      PRINT 595
      WRITE(6,*) (UFI(I),I=L,M)
      PRINT 596
      WRITE(6,*) (TOWB(I),I=2,M)
      PRINT 598
      WRITE(6,*) (TOWT(I),I=2,L)
      PRINT 593
      WRITE(6,*) (TOWI(I),I=L,M)
      PRINT 602
      WRITE(6,*) (ZPT(I),I=2,L)
      PRINT 603
      WRITE(6,*) (ZPB(I),I=2,M2)
      PRINT 604
      WRITE(6,*) (SP(I),I=L,M2)
  584 FORMAT(///51X,'ICOUNT  =',2X,I5//)
  586 FORMAT( 4X,'RSWM=',E13.6,9X,'RSEPM=',E13.6,9X,'RSKM=',E13.6,9X,'
     *RSEM=',E13.6,9X,'RSUM=',E13.6//)
  590 FORMAT(/40X,'UFAV=',E12.5,2X,'(M/SEC)'//40X,'TOWAV=',E12.5,2X,
     *'(N/SQ M)'//40X,'DPDX=',E12.5,2X,'(PA/M)'/)
  596 FORMAT(/40X,'TOWB(I) DIST. ALONG BOTTOM SURFACE (N/SQ.M)'/)
  598 FORMAT(/40X,'TOWT(I) DIST.ALONG TOP SURFACE (N/SQ.M)'/)
  592 FORMAT(/40X,'UFB(I) DIST. ALONG BOTTOM SURFACE (M/SEC)'/)
  594 FORMAT(/40X,'UFT(I) DIST. ALONG TOP SURFACE (M/SEC)'/)
  602 FORMAT(/40X,'THE DIM.LESS NORMAL DIST. FROM THE TOP.  WALL'/)
  603 FORMAT(/40X,'THE DIM.LESS NORMAL DIST. FROM THE BOTTO.WALL'/)
  604 FORMAT(/40X,'THE DIM.LESS NORM. DIST. FROM THE INCLI.  WALL'/)
  588 FORMAT(40X,'UB = ',E12.5,2X,'(M/SEC)'//40X,'UR =',E12.5//)
  595 FORMAT(/40X,'UFI(I) DIST. ALONG INCLINED SURFACE (M/SEC)'/)
  593 FORMAT(/40X,'TOWI(I) DIST. ALONG INCLINED SURFACE (N/SQ.M)'/)
      RETURN
      END
$ENTRY
/*
```

```
C-----------------LAUNDER YOUNG VORTICITY MODEL-----------------C
C---------      F1: THE NORMAL STRESSES ------------------------
C---------      F4: THE SHEAR STRESSES -------------------------------
C--------- F2: COEFFICIENT FOR K & E SOURCE TERM ----------------
      DO 70 J=2,N1
      K=M-J
      DO 70  I=2,K
      DUYSQ = X*DUY(I,J)**2
      DUZSQ = DUZ(I,J)**2
      F2(I,J) = (DUYSQ + DUZSQ) / SIGMU
      IF(IVORT .EQ. 1) GO TO 70
      IF(TED(I,J) .EQ. 0.0) GO TO 72
      FACTOR = CPRIME * AMUT(I,J) * TKE(I,J) / TED(I,J)
      GO TO 74
   72 FACTOR = 0.0
   74 CONTINUE
      IF(INORML .EQ. 1) GO TO 76
      F1(I,J) = FACTOR * (DUZSQ - DUYSQ)
   76 CONTINUE
      IF(ISHEAR .EQ. 1) GO TO 70
      F4(I,J) = FACTOR * DUY(I,J) * DUZ(I,J)*(X+1.0)/2.0
   70 CONTINUE
C---------------------------------------------------------------
      IF(IVORT .EQ. 1) GO TO 100
      IF(INORML .EQ. 1) GO TO 110
C     **** CLEAR LOCATIONS DUY AND DUZ ****
      DO 75  J=1,N
      K=M-(J-1)
      DO 75  I=1,K
      DUY(I,J) = 0.0
      DUZ(I,J) = 0.0
   75 CONTINUE
C-------------NOTE: F3 HER IS THE DERIVATIVE OF F1 WITH RESPE TO Z
C   F3 AT INTERIOR NODES
      DO 77 J=2,N1
      K=M-J
      DO 77 I=2,K
      F3(I,J) = ((F1(I,J+1) - F1(I,J)) * ZZ(I,J) + (F1(I,J) - F1
     *(I,J-1)) / ZZ(I,J)) / (Z(J+1) - Z(J-1))
   77 CONTINUE
C----------------------BOUNDARY VALUES-------------------------
C-------------------------F3 AT HORIZONTAL WALLS-----------------
C     DO 81  I=2,M2
C     F3(I,1) = (F1(I,2) - F1(I,1)) / (Z(2) - Z(1))
C 81  CONTINUE
C     DO 78 I=2,L
C     F3(I,N)=(F1(I,N)-F1(I,N1))/(Z(N)-Z(N1))
C 78  CONTINUE
C--------------------------F3 AT INCLINED WALL--------
C     DO 80 J=2,N1
C     K=M-(J-1)
C     F3(K,J)=(F1(K,J)-F1(K,J-1))/(Z(J)-Z(J-1))
C 80  CONTINUE
C     F3(M,1)=F3(M1,1)
C----------2ND DERIV. OF F1 WITH RESPECT TO Y----------
C----------------DUY AT INTERIOR NODES -------------------------
      DO 82 J=2,N1
      K=M-J
      DO 82 I=2,K
      DUY(I,J) = ((F3(I+1,J) - F3(I,J)) * YY(I,J) + (F3(I,J) - F3
     *(I-1,J)) / YY(I,J)) / (Y(I+1) - Y(I-1))
   82 CONTINUE
C---------------------AT INCLINED WALL--------------------
C     DO 88 J=2,N1
```

```
543. C      K=M-(J-1)
544. C      K1=K-1
545. C      DUY(K,J)=(F3(K,J)-F3(K1,J))/(Y(K)-Y(K1))
546. C 88   CONTINUE
547. C----------------------AT MID HORIZONTAL BISECTOR---------------
548. C      DO 90 J=2,N1
549. C      DUY(2,J)=0.0
550. C   90 CONTINUE
551. C----------------------ATCHORIZONTAL  WALLS--------------------
552. C      DO 84 I=2,M
553. C      DUY(I,1)=0.0
554. C   84 CONTINUE
555. C      DO 86 I=2,L
556. C      DUY(I,N)=0.0
557. C 86   CONTINUE
558. C-------------------------CLEAR LOCATION F1--------------------
559.        DO 92  J=1,N
560.        K=M-(J-1)
561.        DO 92  I=1,K
562.        F1(I,J) = 0.0
563.    92  CONTINUE
564. C---------VORT.SOURCE TERM (NORMAL STRESSES)STORED IN F1 LOCN. ---
565.        DO 94 J=1,N
566.        K=M-(J-1)
567.        DO 94 I=1,K
568.        F1(I,J) = DUY(I,J)
569.     94 CONTINUE
570.    110 CONTINUE
571. C----------------------------CLEAR LOCATIONS DUY ---------------
572.        DO 96  J=1,N
573.        K=M-(J-1)
574.        DO 96  I=1,K
575.        DUY(I,J) = 0.0
576.        IF(INORML .EQ. 1) F1(I,J) = 0.0
577.    96  CONTINUE
578.        IF(ISHEAR .EQ. 1) GO TO 150
579. C--------- VORTICITY SOURCE (SHEAR STRESS) CALCULATIONS --------
580.        DO 98 J=2,N1
581.        K=M-J
582.        DO 98 I=2,K
583.        DUZ(I,J) = ((F4(I,J+1) - F4(I,J)) * ZZ(I,J) + (F4(I,J) - F4
584.       *(I,J-1)) / ZZ(I,J)) / (Z(J+1) - Z(J-1))
585.     98 CONTINUE
586. C-------------------------BOUNDARY VALUES ----------------------
587. C------------------------------DUZ AT INCLINED WALL----------
588. C      DO 106 J=2,N1
589. C      K=M-(J-1)
590. C      DUZ(K,J)=(F4(K,J)-F4(K,J-1))/(Z(J)-Z(J-1))
591. C106   CONTINUE
592. C--------------------DUZ AT HORIZONTAL WALLS ----------------------
593. C      DO 104 I=2,M1
594. C      DUZ(I,1)=(F4(I,2)-F4(I,1))/Z(2)
595. C 104  CONTINUE
596. C      DO 107 I=2,L
597. C      DUZ(I,N)=(F4(I,N)-F4(I,N1))/(Z(N)-Z(N1))
598. C 107  CONTINUE
599. C      DUZ(M,1)=0.0
600. C----------------DUY AT INTERIOR NODES ----------------------
601.        DO 108 J=2,N1
602.        K=M-J
603.        DO 108 I=2,K
604.        DUY(I,J) = ((F4(I+1,J) - F4(I,J)) * YY(I,J) + (F4(I,J) - F4
605.       *(I-1,J)) / YY(I,J)) / (Y(I+1) - Y(I-1))
606.    108 CONTINUE
```

```
C--------------------------BOUNDARY VALUES----------------------
C-----DUY AT INCLINED WALL--------
C      DO 117 J=2,N1
C      K=M-(J-1)
C      K1=K-1
C      DUY(K,J)=(F4(K,J)-F4(K1,J))/(Y(K)-Y(K1))
C117   CONTINUE
C-------------------DF4/DY AT HORIZONTIAL WALLS=0.0-------------
C-------------------------------------------------------------------
C---------------------CLEAR LOCATIONS F3 AND F4 -----------
       DO 119 J=1,N
       K=M-(J-1)
       DO 119 I=1,K
       F3(I,J) = 0.0
       F4(I,J) = 0.0
   119 CONTINUE
       DO 121 J=2,N1
       K=M-J
       DO 121 I=2,K
       F4(I,J) = ((DUZ(I,J+1) - DUZ(I,J)) * ZZ(I,J) + (DUZ(I,J) -
      *DUZ(I,J-1)) / ZZ(I,J)) / (Z(J+1) - Z(J-1))
   121 CONTINUE
       DO 124 J=2,N1
       K=M-J
       DO 124 I=2,K
       F3(I,J) = ((DUY(I+1,J) - DUY(I,J)) * YY(I,J) + (DUY(I,J) -
      *DUY(I-1,J)) / YY(I,J)) / (Y(I+1) - Y(I-1))
   124 CONTINUE
C-----F4C, F3 AT INCLINED WALL--------
C      DO 130 J=2,N1
C      K=M-(J-1)
C      K1=K-1
C      F4(K,J)=(DUZ(K,J)-DUZ(K,J-1))/(Z(J)-Z(J-1))
C      F3(K,J)=(DUY(K,J)-DUY(K1,J))/(Y(K)-Y(K1))
C130   CONTINUE
C----------F4 AT HORIZONTAL WALLS-----
C      DO 113 I=1,M1
C      F4(I,1)=(DUZ(I,2)-DUZ(I,1))/Z(2)
C 113 CONTINUE
C      DO 112 I=1,L
C      F4(I,N)=(DUZ(I,N)-DUZ(I,N1))/(Z(N)-Z(N1))
C 112 CONTINUE
C-------------------------F3 AT HORIZONTAL WALLS=0.0-------------
   150 CONTINUE
C-----------------------CLEAR LOCATION DUDZ-------------------
       DO 132 J=1,N
       K=M-(J-1)
       DO 132 I=1,K
       DUZ(I,J) = 0.0
   132 CONTINUE
C--------  THE  VORT. SOURCE TERM : (NORMAL + SHEAR STRESSES) ----
C----- THE VOR. SOURSE TERM IS (SHEAR STRESS ONLY) STORED IN DUZ LOC.-
       DO 134 J=2,N1
       K=M-J
       DO 134 I=2,K
       IF(ISHEAR .EQ. 1) GO TO 136
       DUZ(I,J) = F3(I,J) - F4(I,J)
   136 VORSOR(I,J) =  F1(I,J) + DUZ(I,J)
   134 CONTINUE
```

Table 1

Uncertainties in Experimental Measurements

Result	Uncertainty ±(%)	Result	Uncertainty ±(%)
U Pitot	1	$\sqrt{\overline{u^2}}$	12
U Hot-wire	2	$\sqrt{\overline{v^2}}$	14
f	4	$\sqrt{\overline{w^2}}$	14
τ	4	$\overline{uw}$	16
U_b	2	$\overline{uv}$	20

Table 2

Near-Wall Velocity Distributions (Re = 99,000)

Form: $U^+ = A \ln z^+ + B$

Wall	Top	Inclined	Bottom
A	2.25	2.36	2.26
B	6.32	6.34	6.48
Max. z^+ in range	700	700	400
No. of data points	66	37	60
No. of traverses	3	3	4
Std. Dev. (%)*	2.08	2.56	0.88

* Standard deviations are based on the differences between the experimental U^+ values and the U^+ values from the LSF equation for the same z^+, and are expressed as a percentage of the average U^+ in the range based on the LSF equation.

Table 3

Relationships Between the Turbulence Intensities

Form: Parameter = C u^+ + D

Parameter	k^+			v^+			w^+		
Coefficients	C	D	σ(%)*	C	D	σ(%)*	C	D	σ(%)*
Alshamani [7 2] Pipe Flow Channel Flow	2.24 2.25	-1.13 -1.3	—— ——	0.515 0.55	scatter 0.11	—— ——	0.339 0.383	0.408 scatter	—— ——
Seale [2] ** Simulated Rod Bundle	2.40	-1.44	——	0.587	0.167	——	0.303	0.441	——
Present Results Re = 99,000 o< y/a < 1, 65 points	2.55	-1.49	4.04	0.602	0.210	3.8	0.328	0.513	3.43
Re = 79,000 o< y/a < 1, 65 points	2.48	-1.54	4.92	0.626	0.088	4.48	0.383	0.369	4.04
** Re = 99,000 o< y/a < 1, 65 points	2.42	-1.34	8.55	0.598	0.208	4.6	0.338	0.471	7.16
** Re = 79,000 o< y/a < 1, 65 points	2.35	-1.389	10.46	0.622	.089	4.63	0.391	0.338	6.47
Re = 99,000 Re = 79,000 o< y/a < 1, 130 points	2.54	-1.55	5.65	0.623	0.135	5.65	0.360	0.434	4.9

Table 3 (continued)

Present Results, Re = 99,000 o< y/c < 1, 98 points	2.53	-1.44	5.96	0.527	0.310	7.39	0.363	0.497	7.87
Re = 79,000 o< y/c < 1, 98 points	2.52	-1.58	4.74	0.578	0.149	7.04	0.445	0.309	6.84
Re = 99,000 Re = 79,000 o< y/c < 1, 196 points	2.55	-1.55	6.46	0.560	0.217	8.14	0.408	0.396	8.05

* Standard deviations are based on the differences between the experimental values of the parameter and the values from the LSF equation for the same u^+, and are expressed as a percentage of the average value of the parameter in the range based on the LSF equation.

** k^+, u^+, v^+, w^+ are based on local friction velocity.

Table 4

Comparison of the k-ε Model Constants of the Present Work

With Those Employed by Others

Investigator(s)	C_1	C_2	C_μ	C'	σ_ε	σ_k	κ	P_{rt}
Present Work	1.44	1.92	0.09	0.045	1.167	1.0	0.41	0.9
Seale [93], 1979	1.44	1.92	0.09	0.045	1.3	1.0	0.41	0.9
Said [22], 1981	1.44	1.92	0.09	—	1.167	1.0	0.41	0.9
Gosman & Rapley [29], 1980	1.44	1.92	0.09	—	1.22	1.0	0.42	—
Gosman & Rapley [32], 1978	1.55	2.0	0.09	—	1.185	1.0	0.40	—
Nabayama et al. [24], 1983	1.44	1.92	0.09	—	1.3	0.9	0.41	—
Tatchell [90], 1975	1.47	1.92	0.09	—	1.3	1.0	0.42	0.9
Launder & Spalding [38], 1974	1.44	1.92	0.09	—	1.3	1.0	—	—
Date [98], 1974	1.55	2.0	0.09	—	1.3	1.0	0.4	—
Jones & Launder [99], 1973	1.45	2.0	0.09	—	1.3	1.0	0.42	—
Jones & Launder [51], 1972	1.55	2.0	0.09	—	1.3	1.0	—	—

Table 5

Coefficients in the General Elliptic Differential Equation (6.1)

Equation	ϕ	a_ϕ	$b_{\phi,y}$	$b_{\phi,z}$	S_ϕ
(5.21)	ω	1	μ	μ	$-\rho\left\{\frac{\partial^2}{\partial y \partial z}(\bar{v}^2 - \bar{w}^2)\right\}$
(5.22)	ψ	0	1	1	$\rho\omega$
(5.20)	$\bar{U}$	1	$\mu+\mu t$	$\mu+\mu t$	$\frac{\partial \bar{P}}{\partial x} = -4\,\bar{\tau}_w/D_h$
(5.23)	k	1	$\mu + \frac{\mu t}{\sigma_k}$	$\mu + \frac{\mu t}{\sigma_k}$	$-\mu t\left\{(\frac{\partial \bar{U}}{\partial y})^2 + (\frac{\partial \bar{U}}{\partial z})^2\right\} + \rho\varepsilon$
(5.24)	ε	1	$\mu + \frac{\mu t}{\sigma_\varepsilon}$	$\mu + \frac{\mu t}{\sigma_\varepsilon}$	$-C_1 \frac{\varepsilon}{k} \mu t\left\{(\frac{\partial \bar{U}}{\partial y})^2 + (\frac{\partial \bar{U}}{\partial z})^2\right\} + \rho C_2 \frac{\varepsilon^2}{k}$
(5.25)	$\bar{T}$	1	$\frac{\mu}{P_r} + \frac{\mu t}{P_{rt}}$	$\frac{\mu}{P_r} + \frac{\mu t}{P_{rt}}$	$\rho\bar{U}\frac{\partial \bar{T}}{\partial X}$

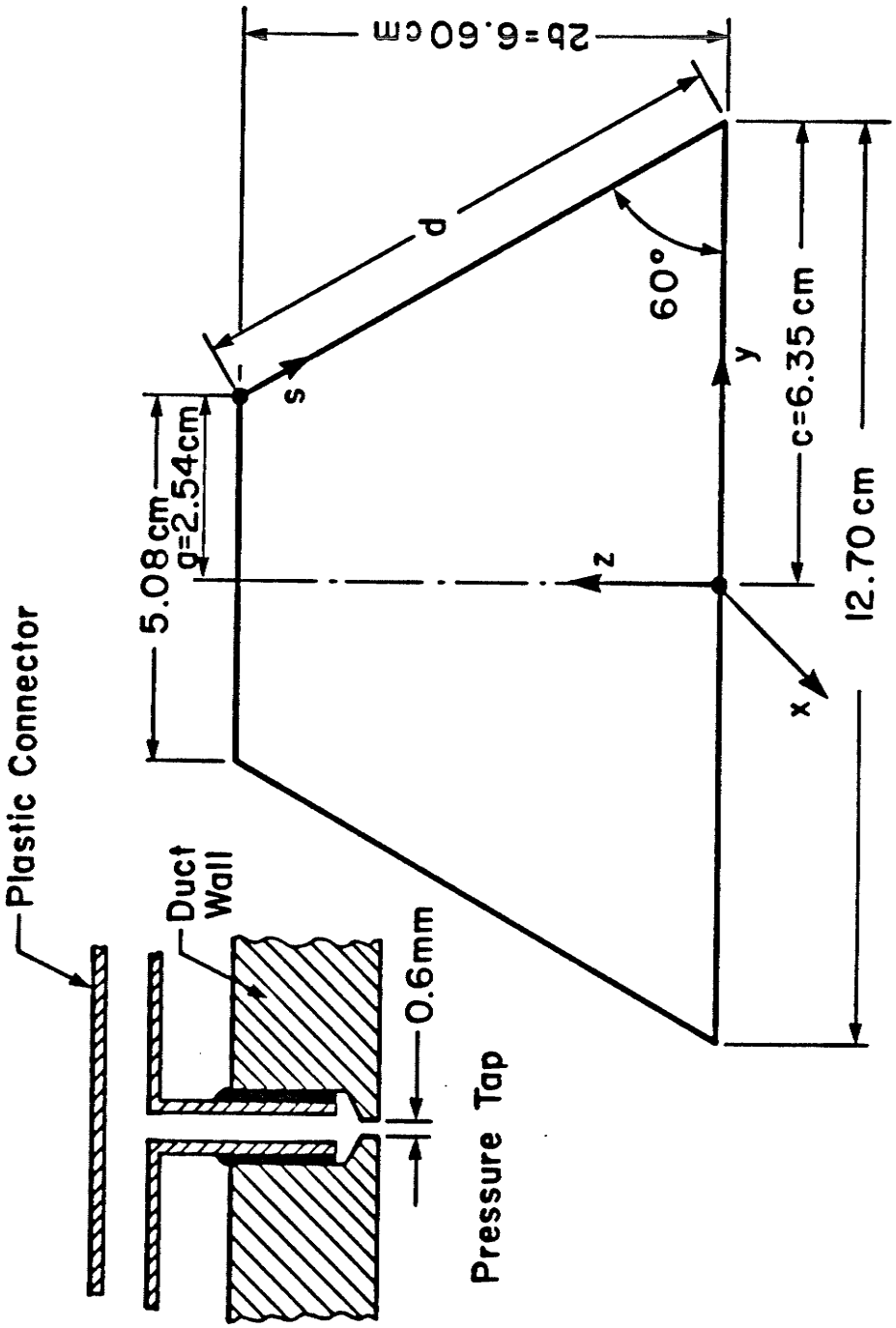

Fig. 1: Cross-section of Trapezoidal Duct Test Section.

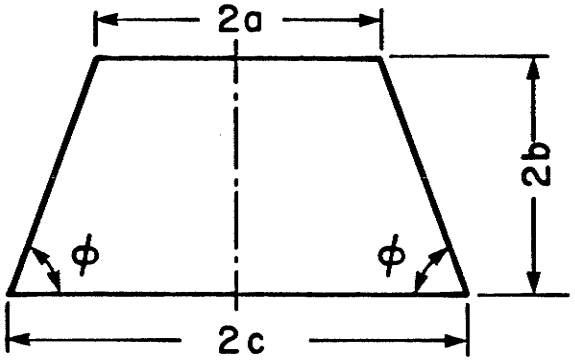

Fig. 2a: General Cross-section of Trapezoidal Duct.

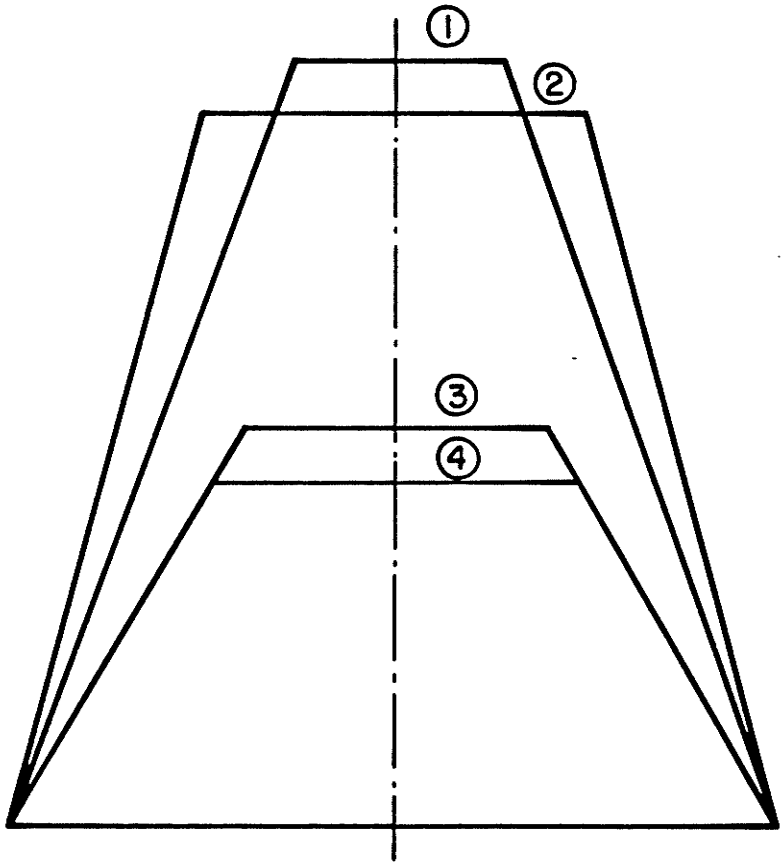

Duct. No.	ϕ (Deg.)	a/b	a/c
1. Chiranjivi & Sankara Rao	70	0.280	0.280
2. Rodet	75	0.536	0.500
3. Present Duct	60	0.770	0.400
4. Nikuradse	≃ 60	1.02	0.48

Fig. 2b: Shape of the Present Trapezoidal Duct Relative to [3], [4] and [5].

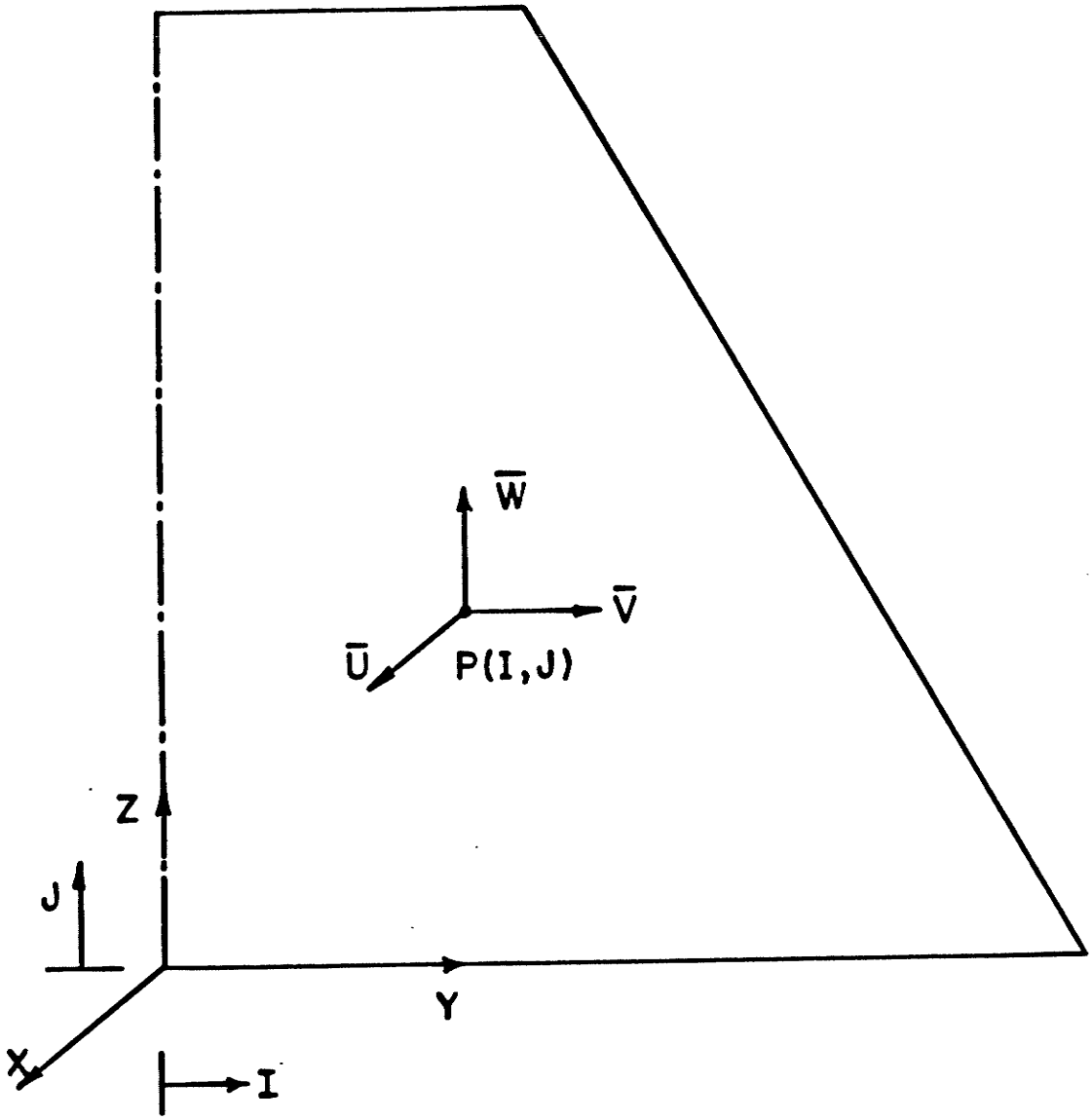

Fig. 3: Primary Flow Cell for the Analytical Model.

1. Centrifugal fan/damper
2. Electric Motor/drive
3. Canvas Coupling
4. Transition
5. Test section A (Wood)
6. Test section B (Wood)
7. Test section C (Acrylic)

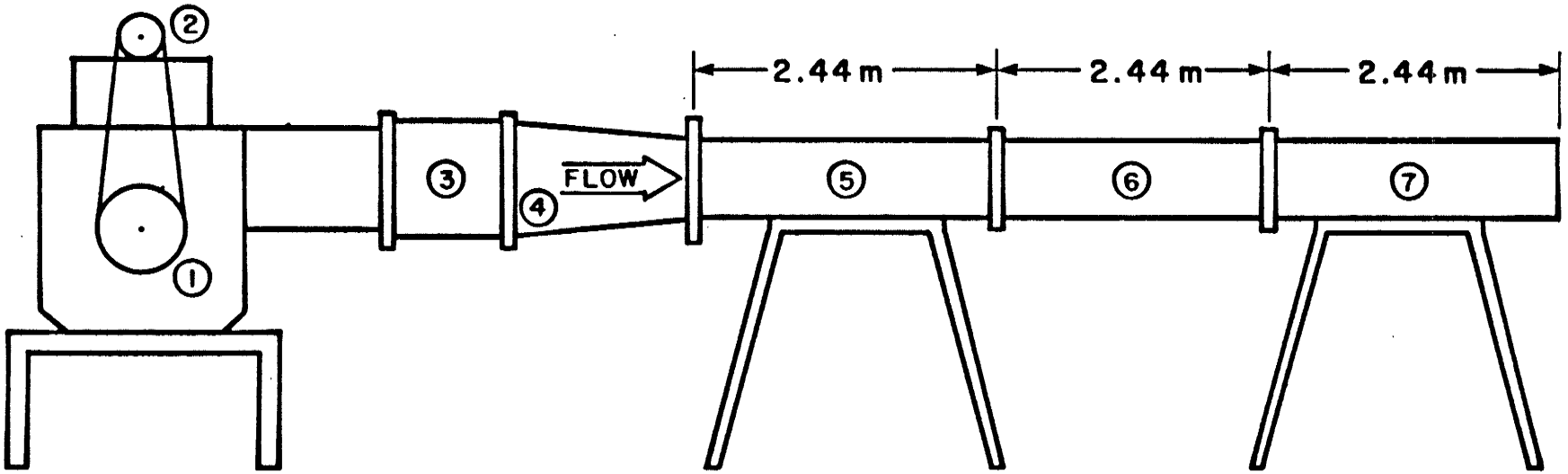

Fig. 4a: Side Elevation View of Test Rig.

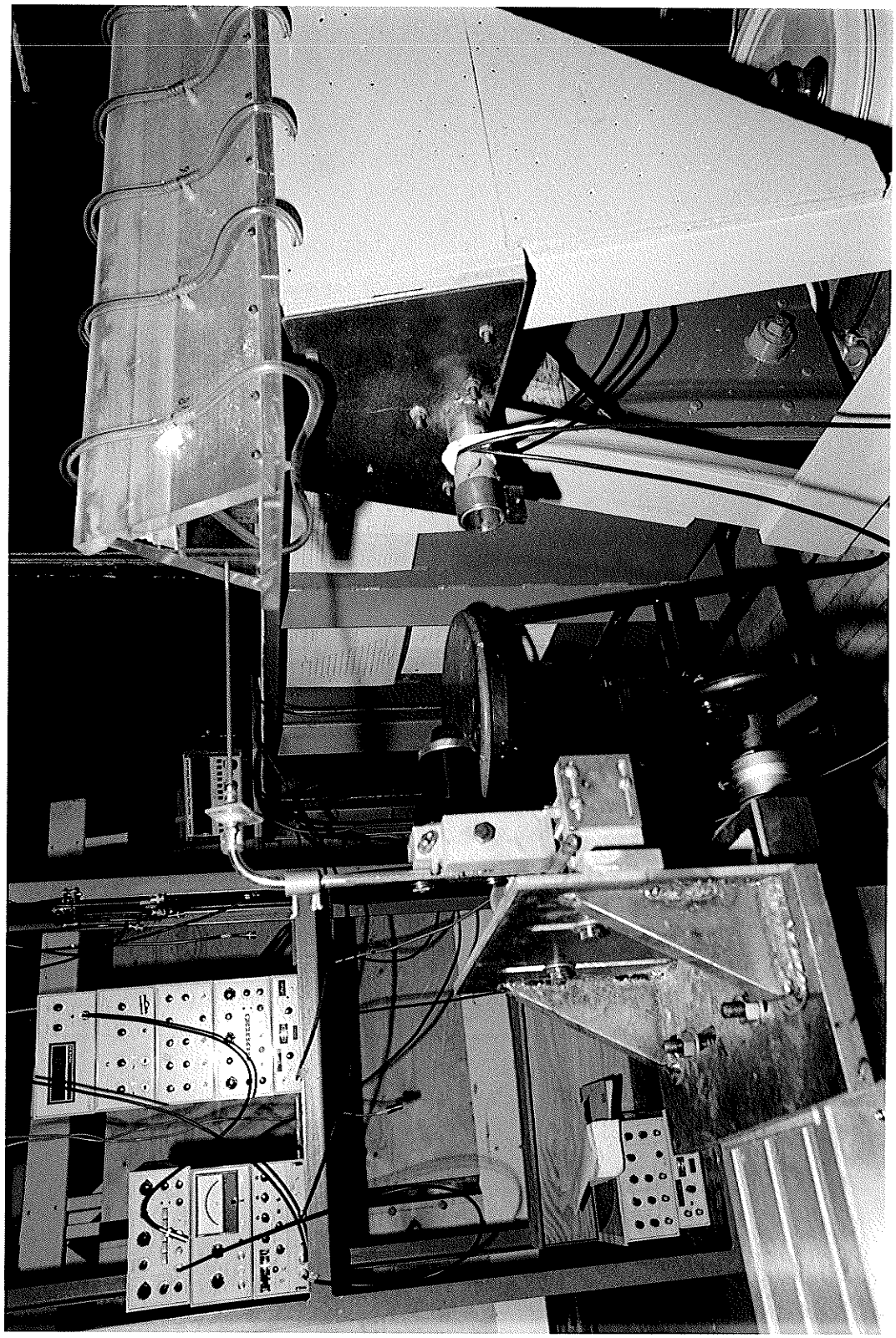

Fig. 4b: Traversing Mechanism Assembly.

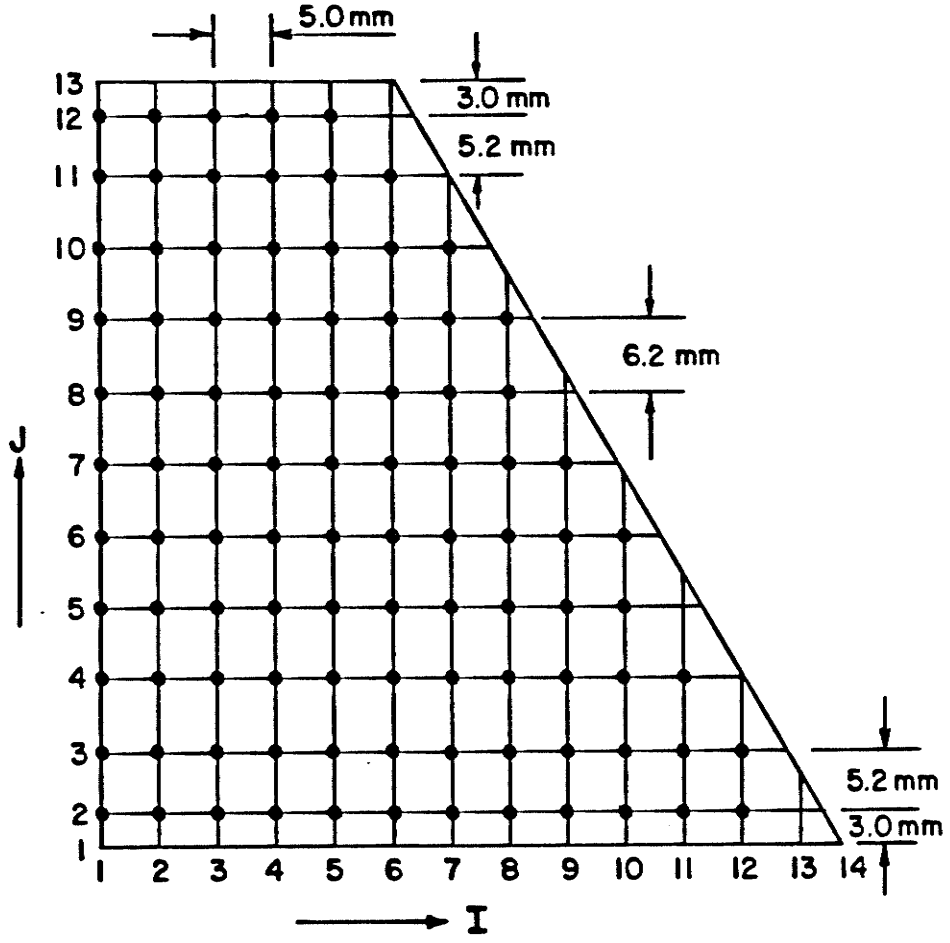

Fig. 5a: Measurement Grid for X-probe.

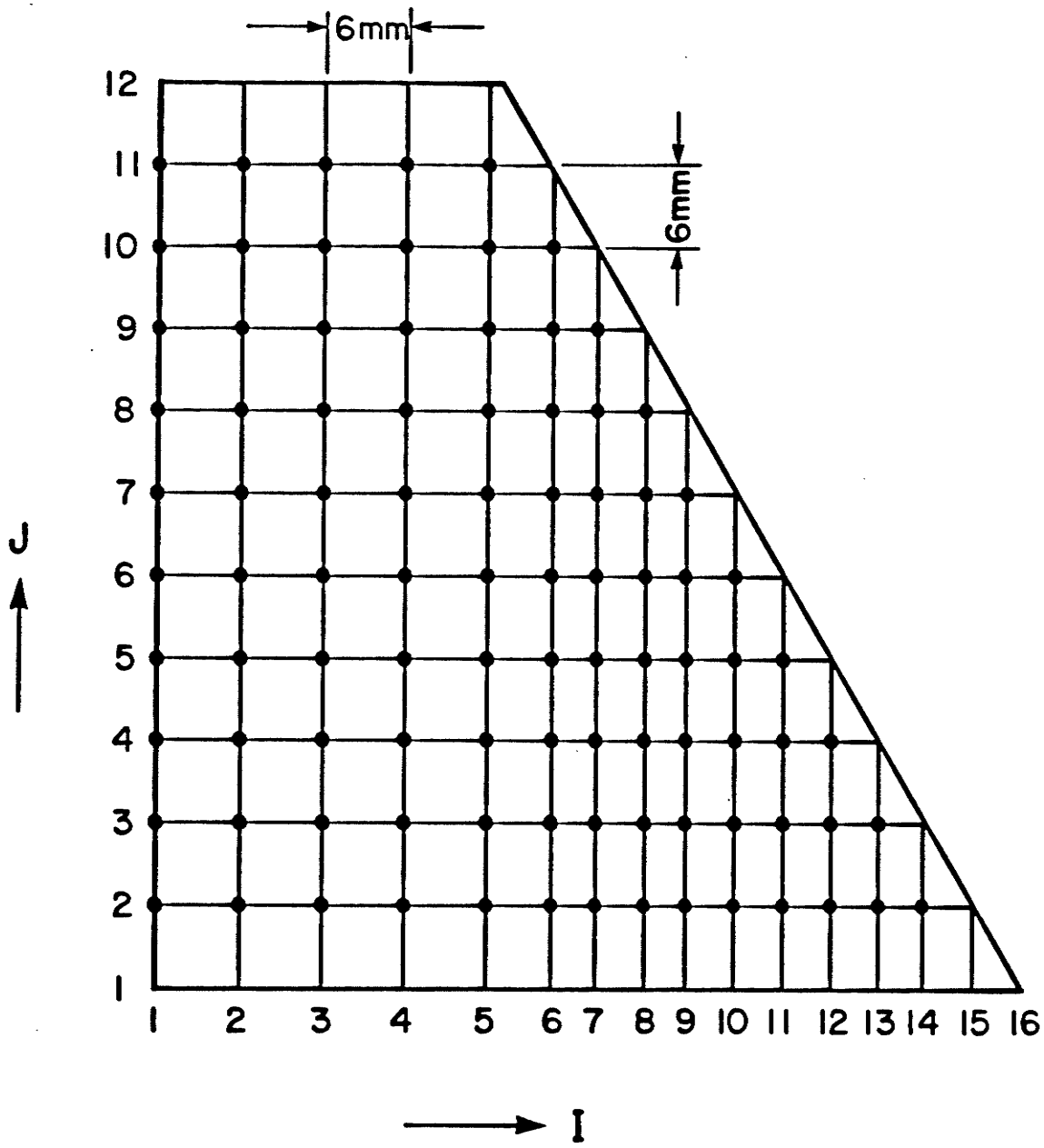

Fig. 5b: Measurement Grid for Pitot-tube, Single Hot-wire, and 45° Slanting Wire.

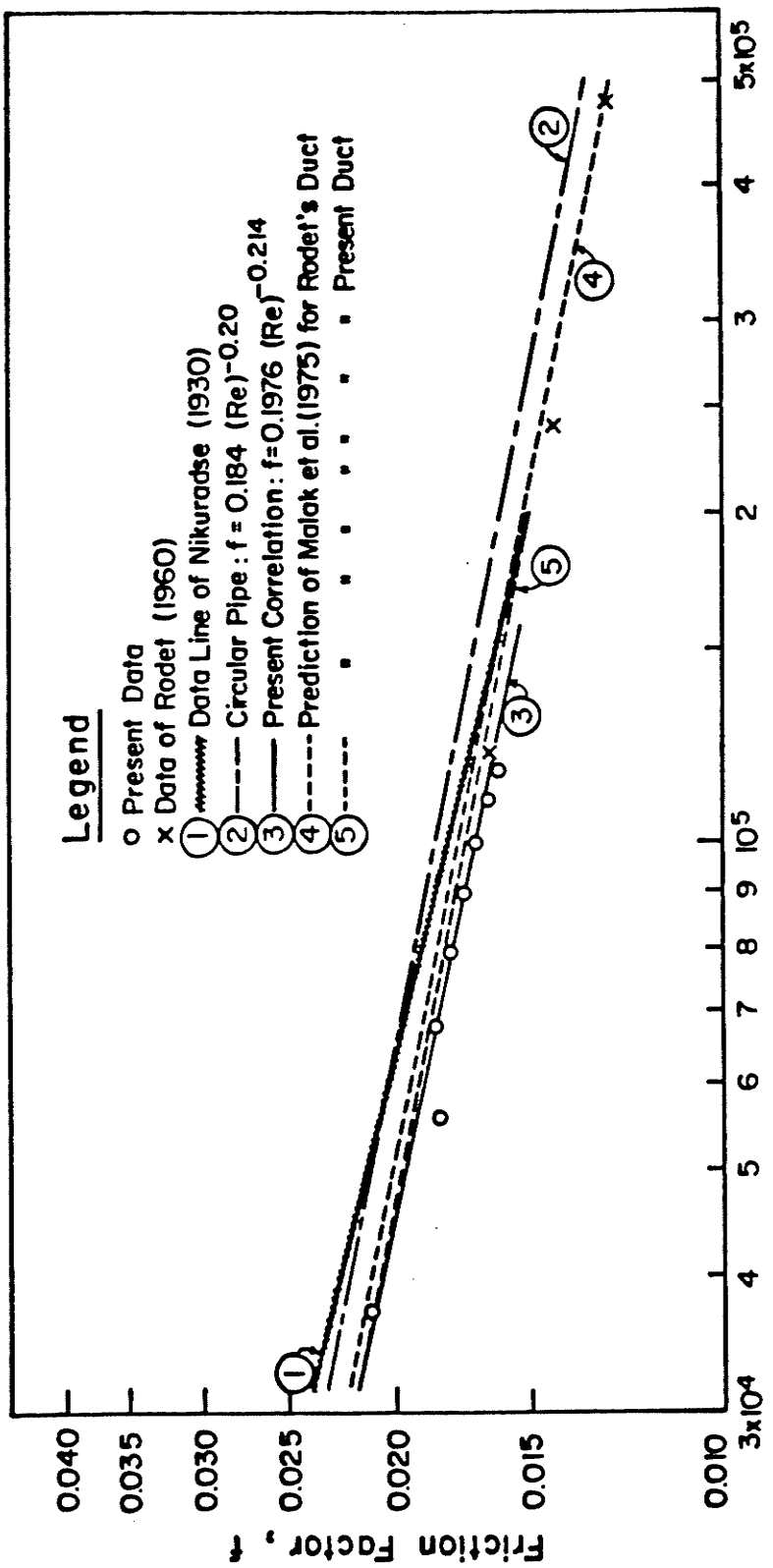

Fig. 6: Friction Factor vs Reynolds Number for the Trapezoidal Ducts

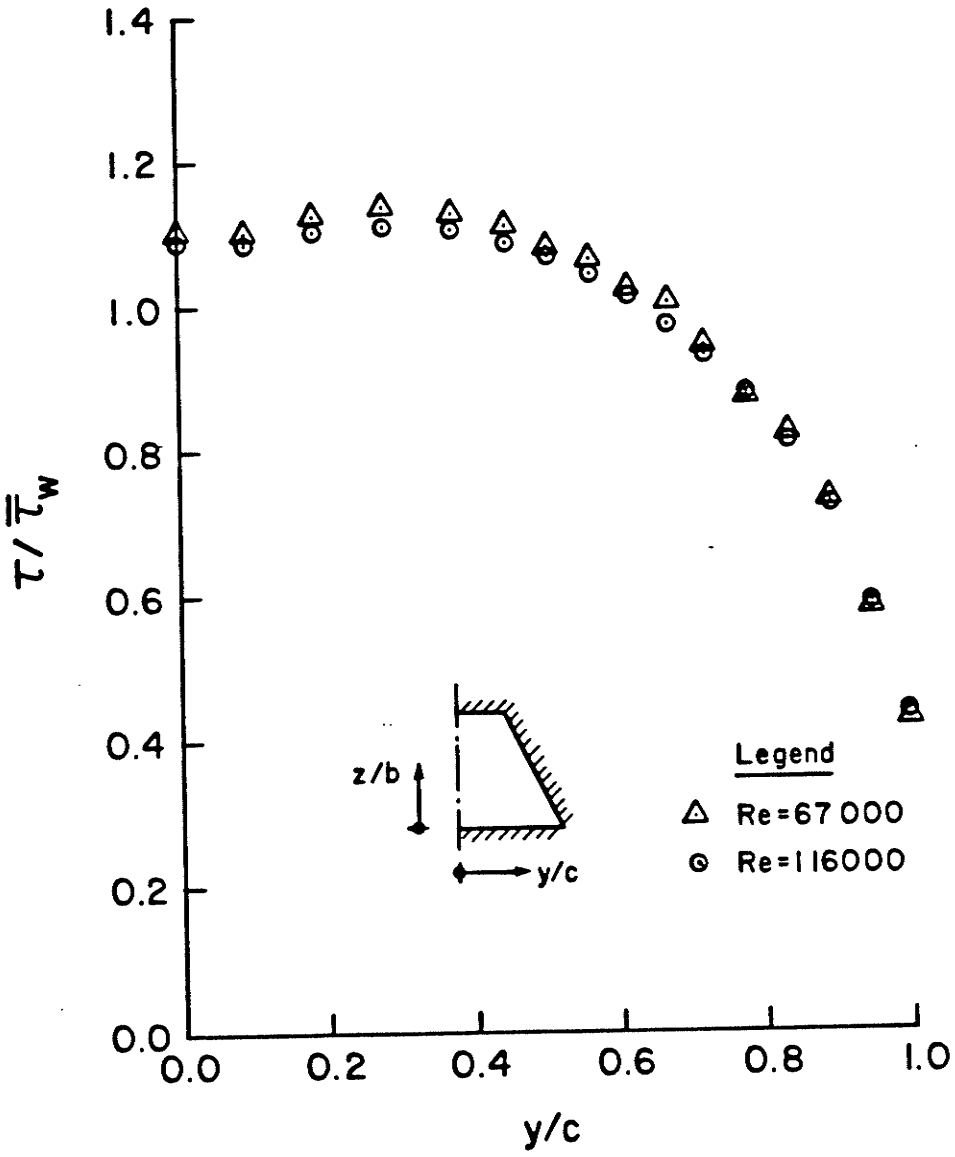

Fig. 7: Wall Shear Stress Distributions for Bottom Wall.

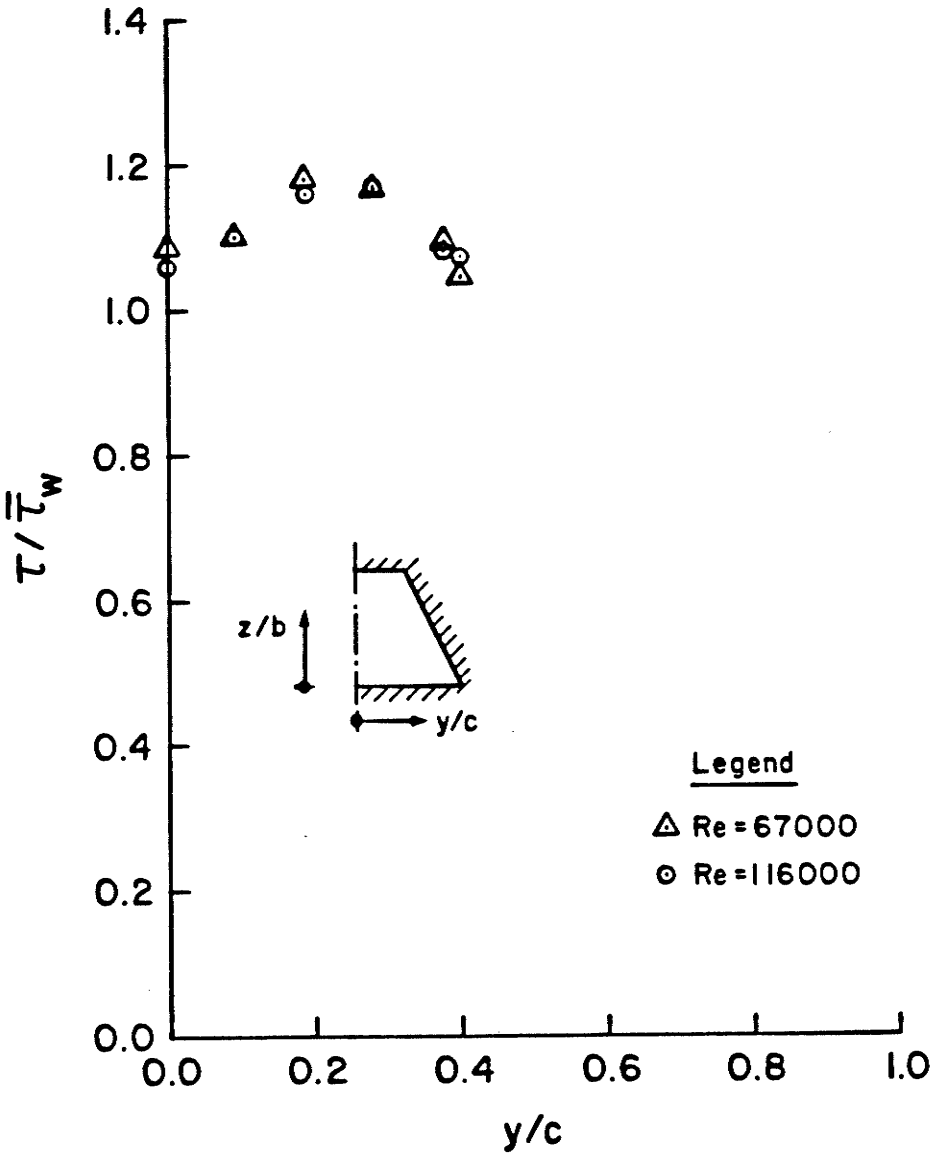

Fig. 8: Wall Shear Stress Distributions for Top Wall.

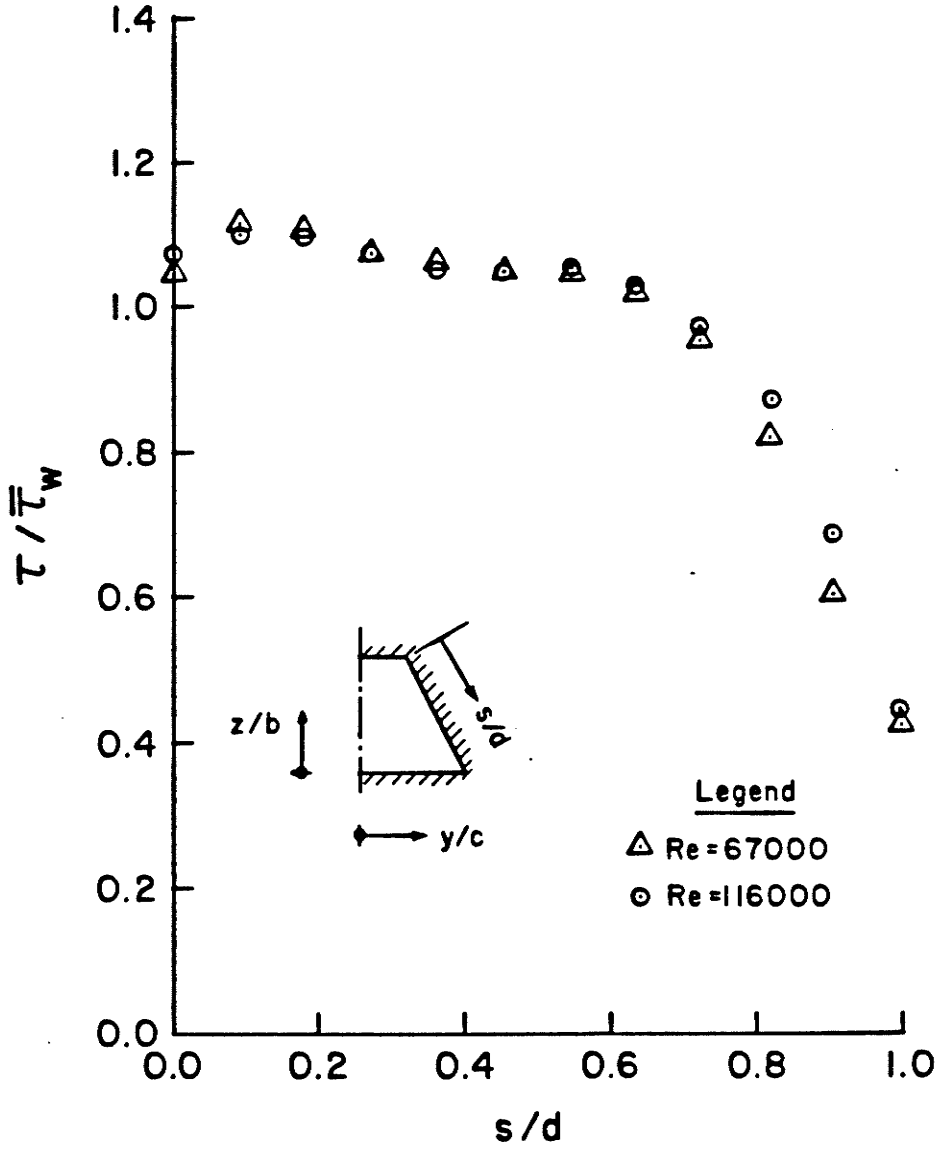

Fig. 9: Wall Shear Stress Distributions for Inclined Wall.

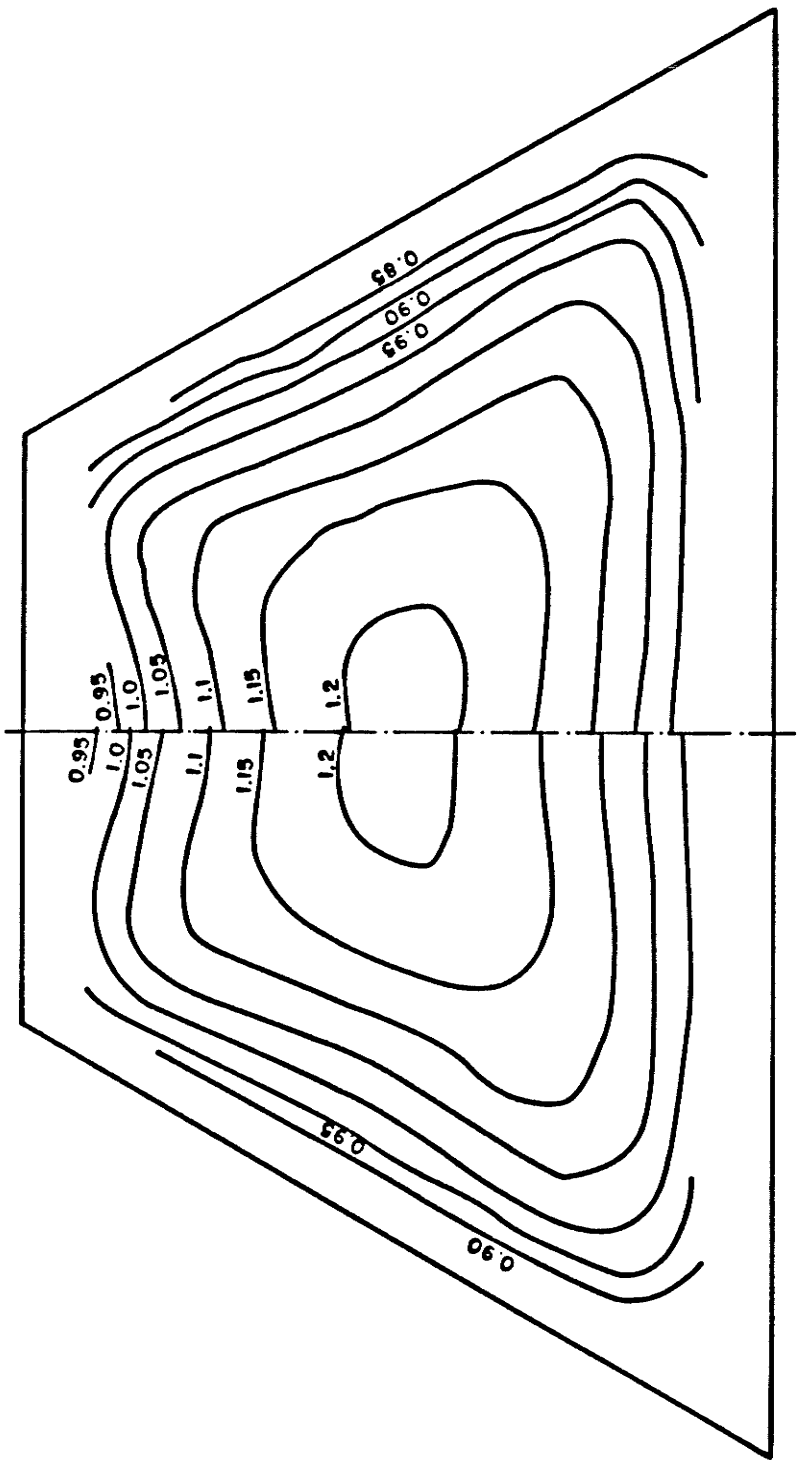

Fig. 10: Contour Plots of Axial Velocity; Re = 99,000
Right: Data Via Single Hot-wire,
Left : Data Via Pitot-tube.

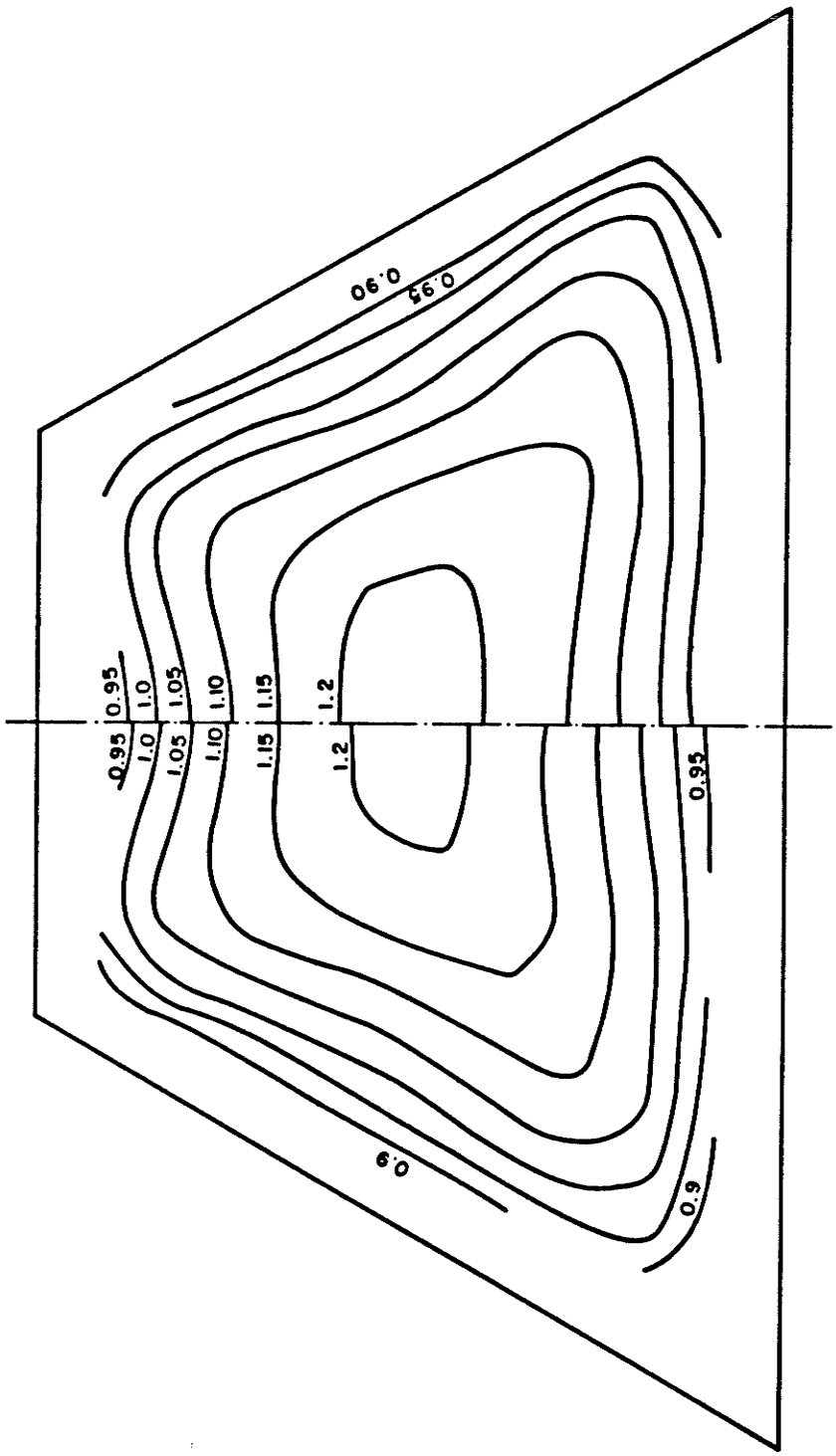

Fig. 11: Contour Plots of Axial Velocity; Data Via Single Hot-wire; Right: Re=79,000; Left: Re=99,000.

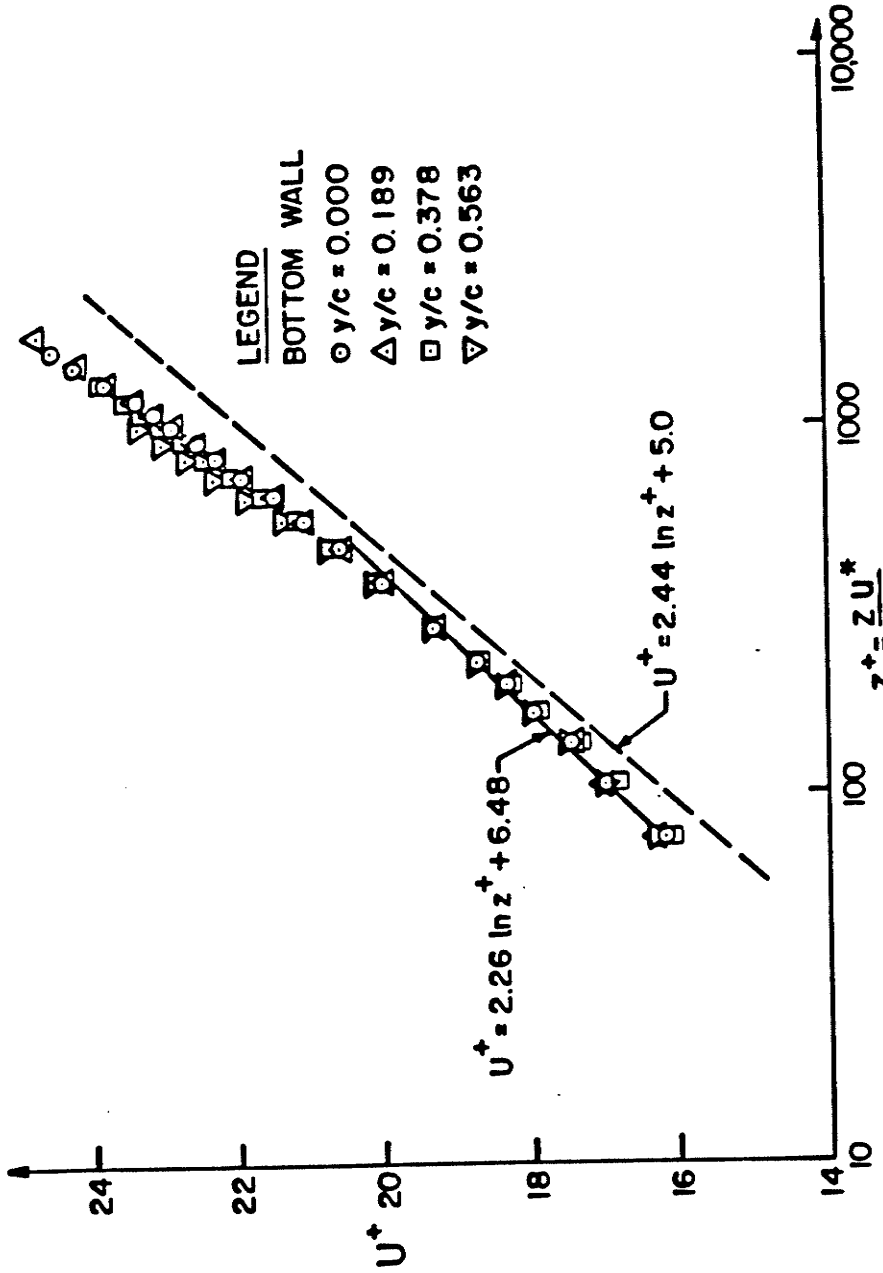

Fig. 12a: Mean Velocity Distributions Near Bottom Wall; Re = 99,000.

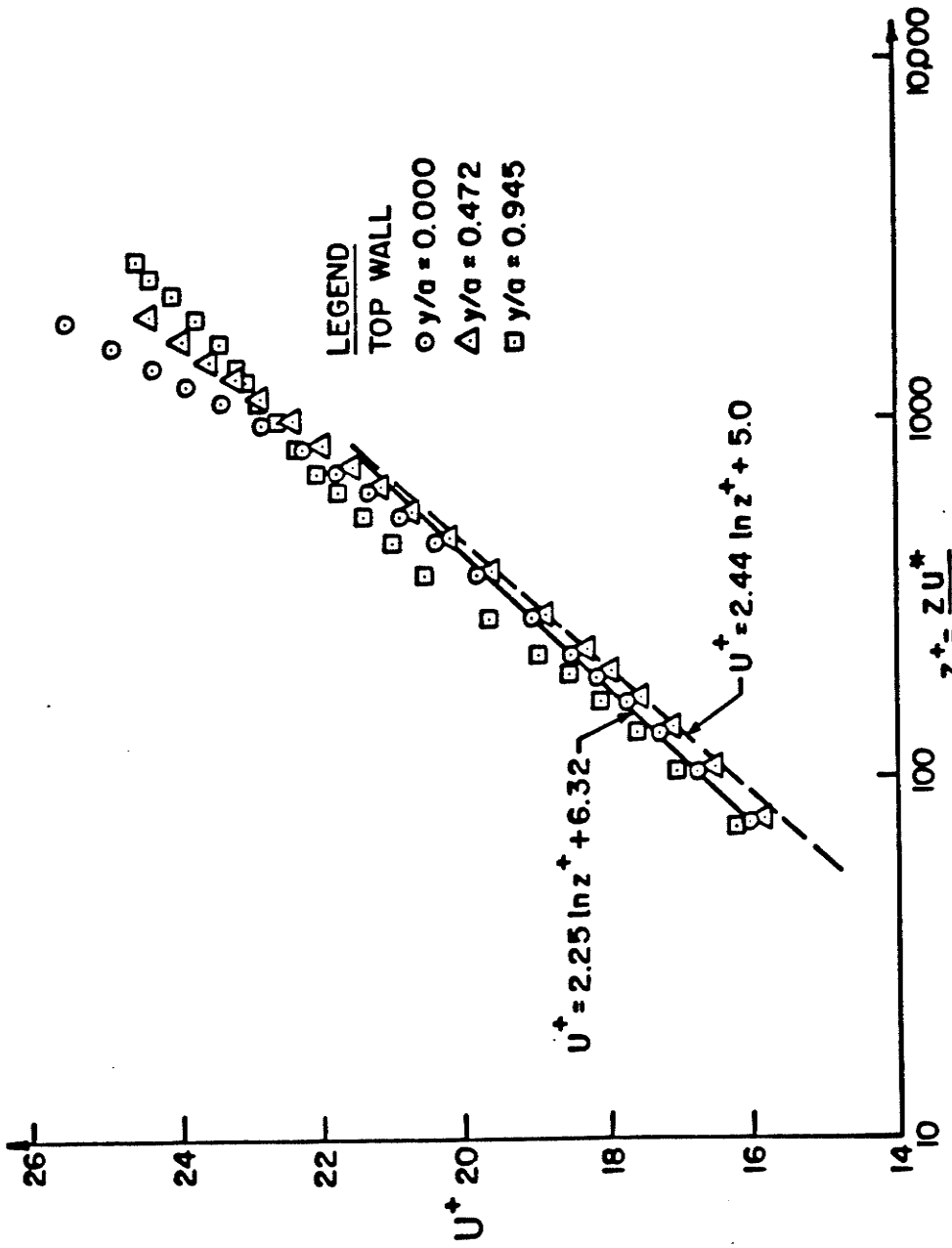

Fig. 12b: Mean Velocity Distributions Near Top Wall; Re = 99,000.

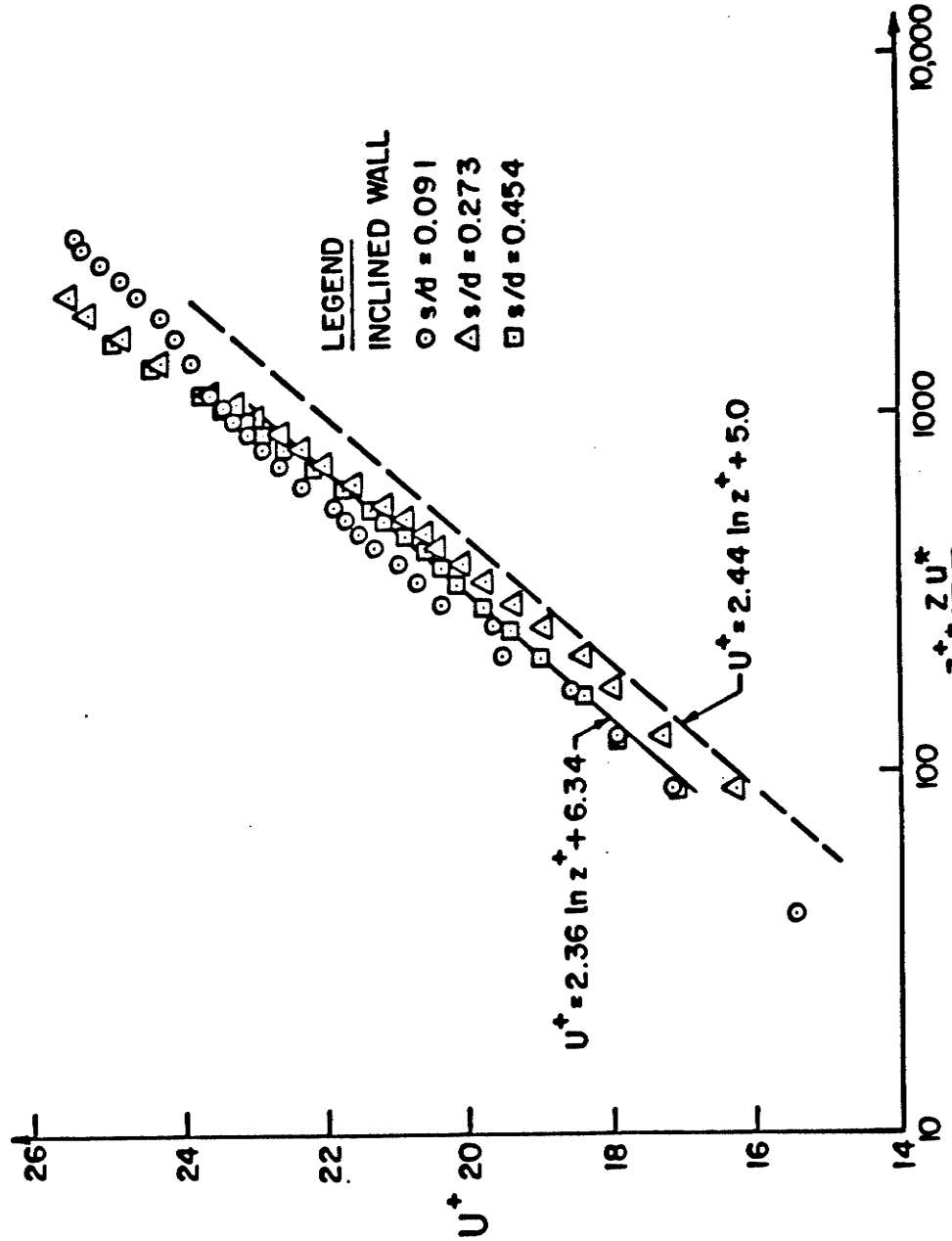

Fig. 12c: Mean Velocity Distributions Near Inclined Wall; Re = 99,000.

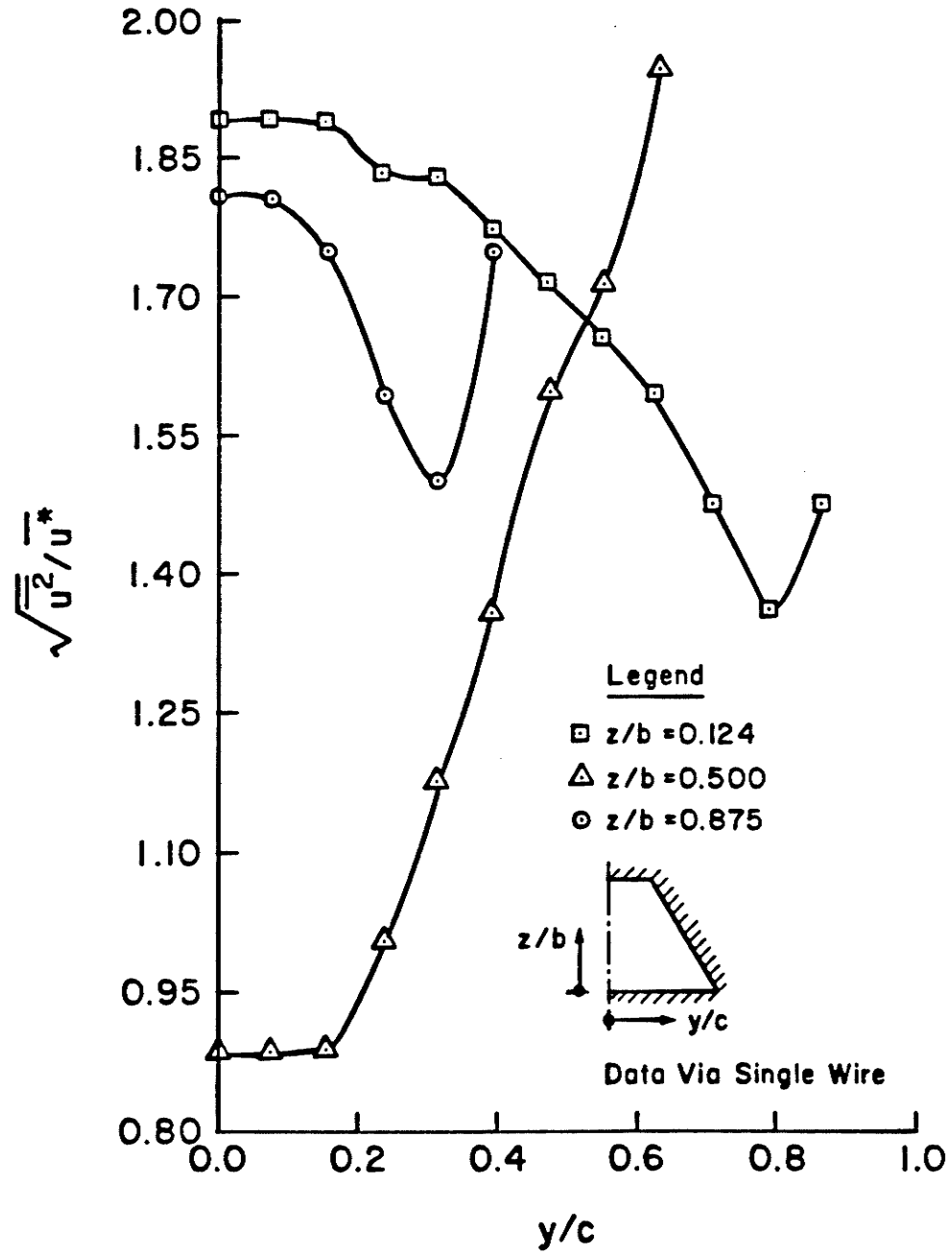

Fig. 13: Distributions of $(\overline{u^2})^{1/2}/\bar{u}^*$ Via Single Hot-wire; Re = 99,000.

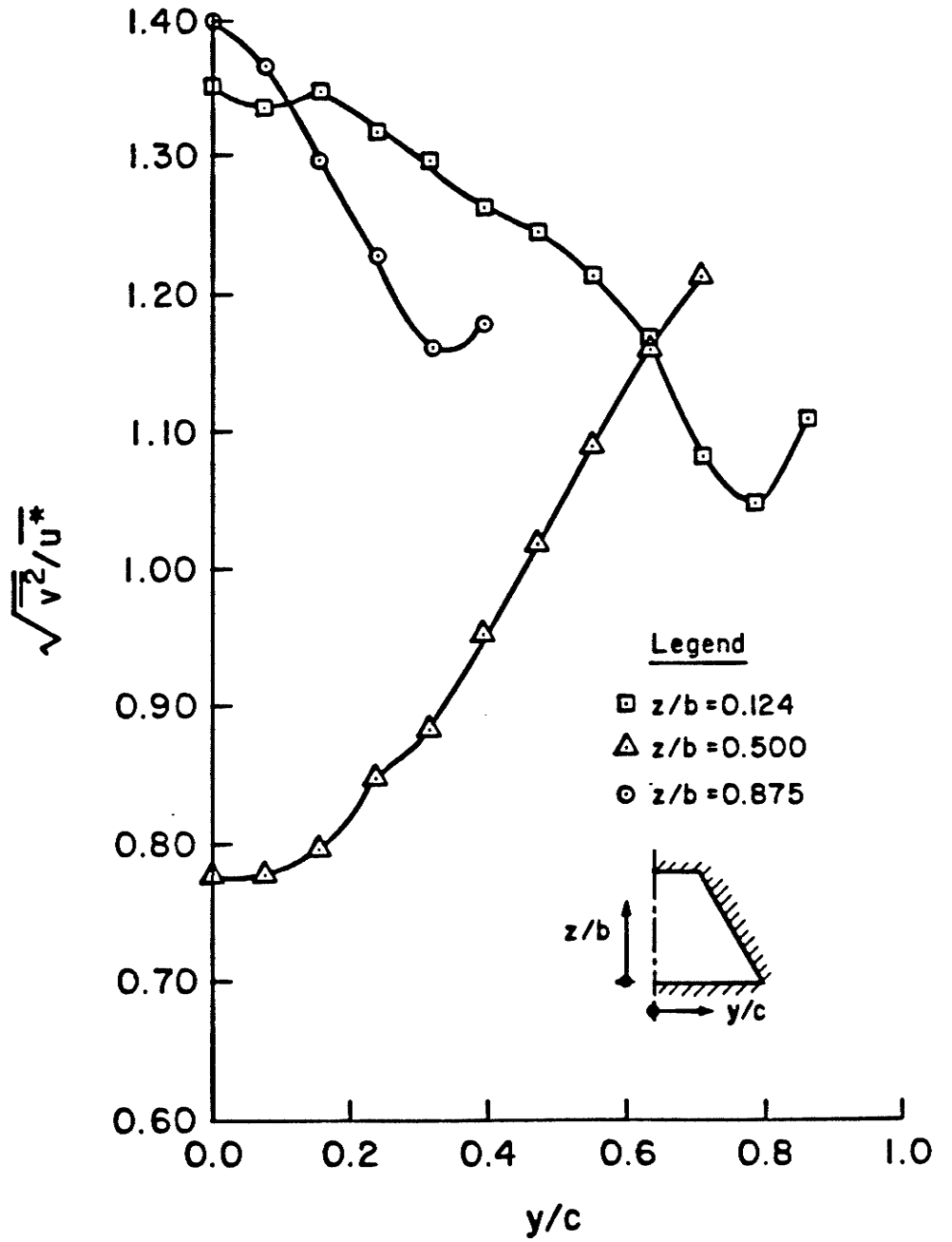

Fig. 14: Distributions of $(\overline{v^2})^{1/2}/\overline{u}^*$; Re= 99,000.

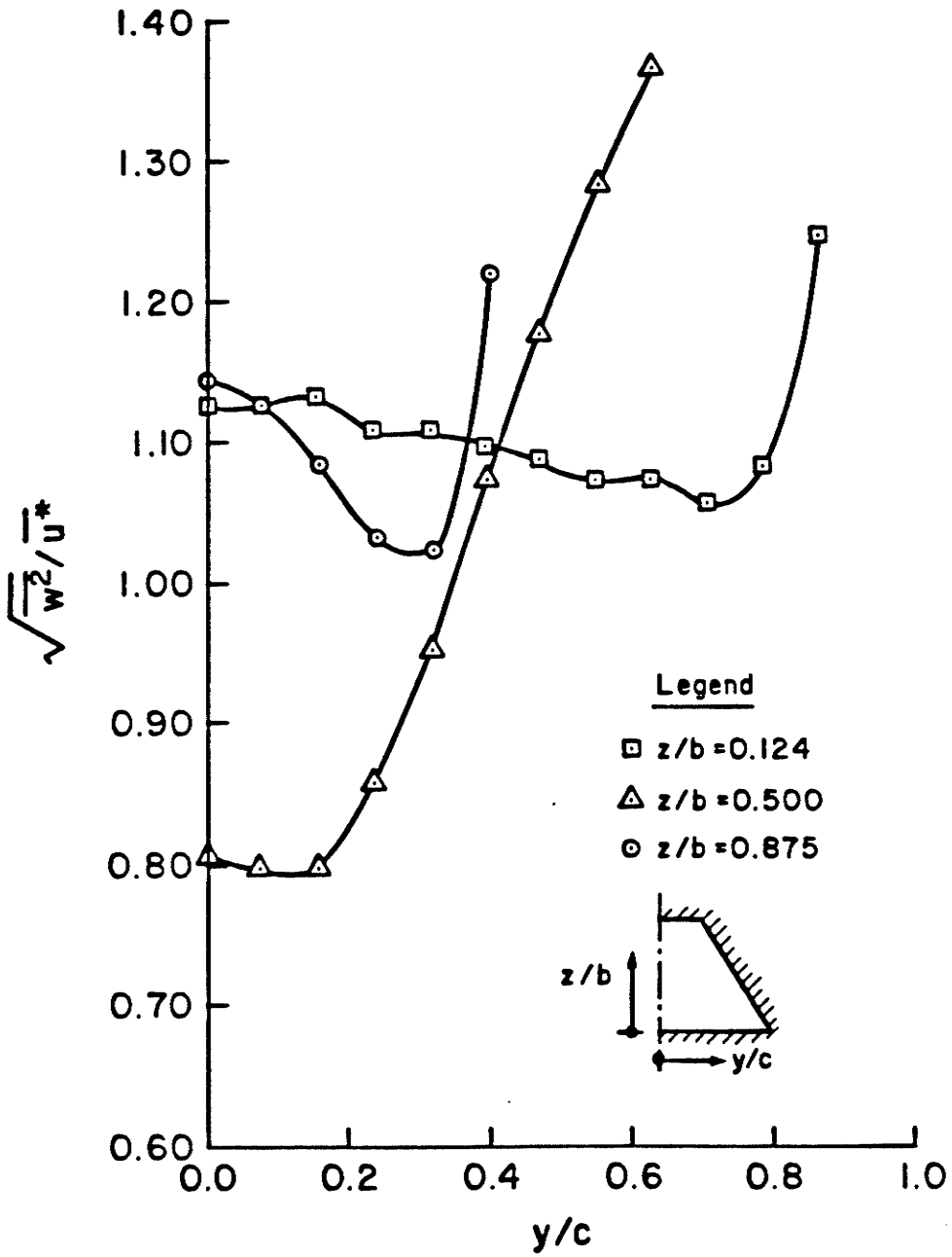

Fig. 15: Distributions of $(\overline{w^2})^{1/2}/\bar{u}^*$; Re= 99,000.

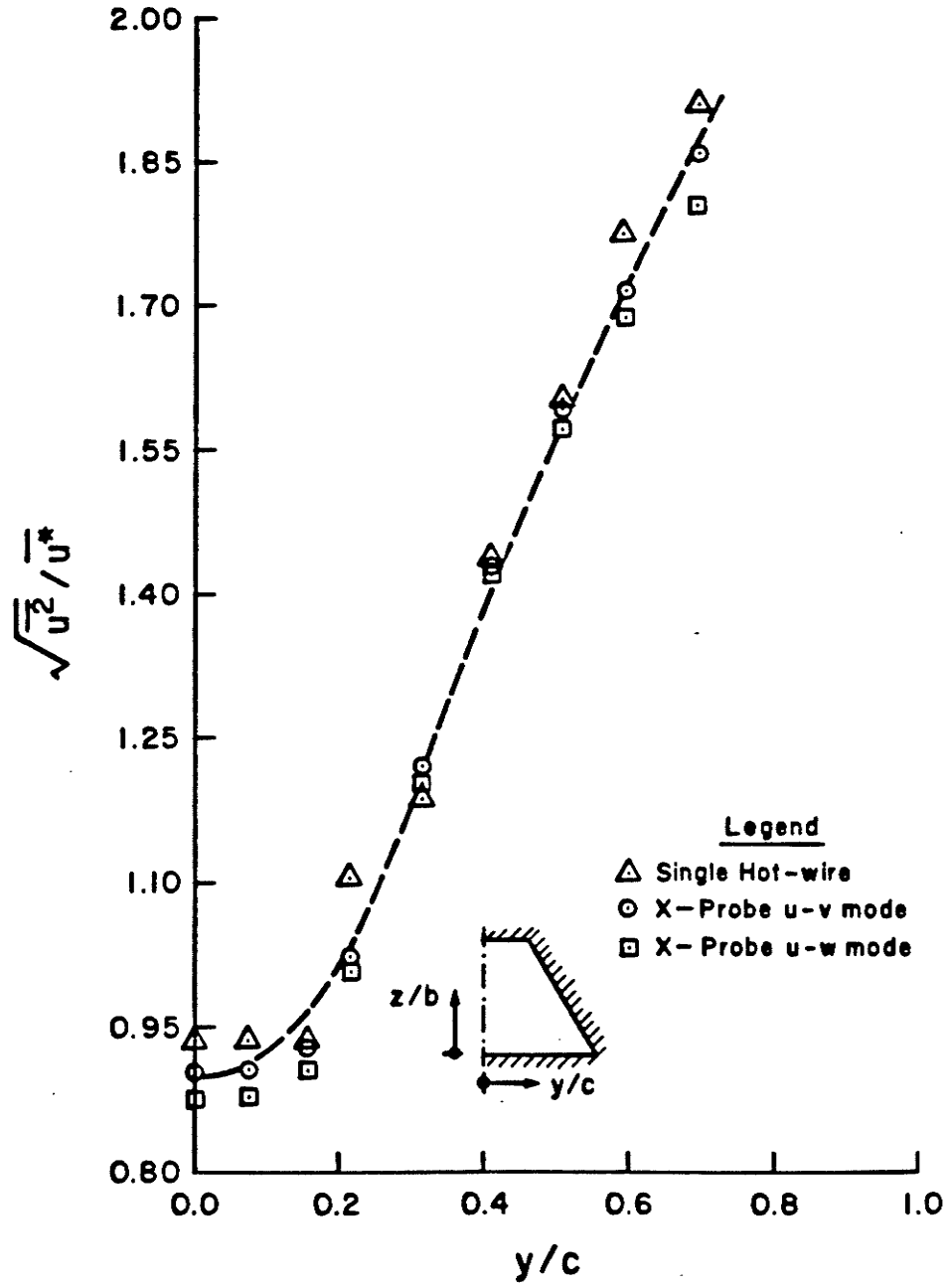

Fig. 16: Distributions of $(\overline{u^2})^{1/2}/\bar{u}^*$ at z/b = 0.5 Using Different Probes; Re = 79,000.

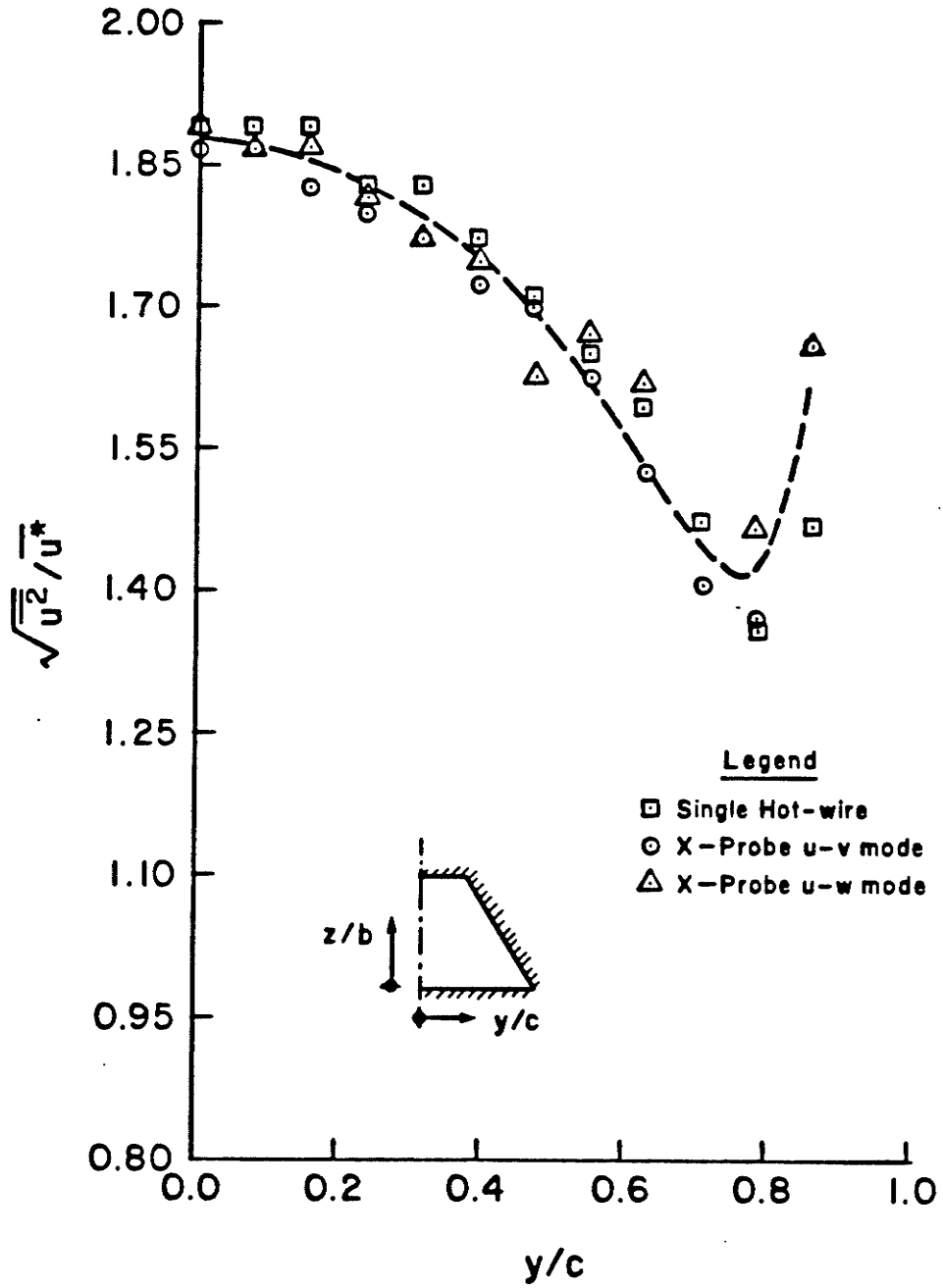

Fig. 17: Distributions of $(\overline{u^2})^{1/2}/\overline{u}^*$ at z/b = 0.124 Using Different Probes; Re = 99,000.

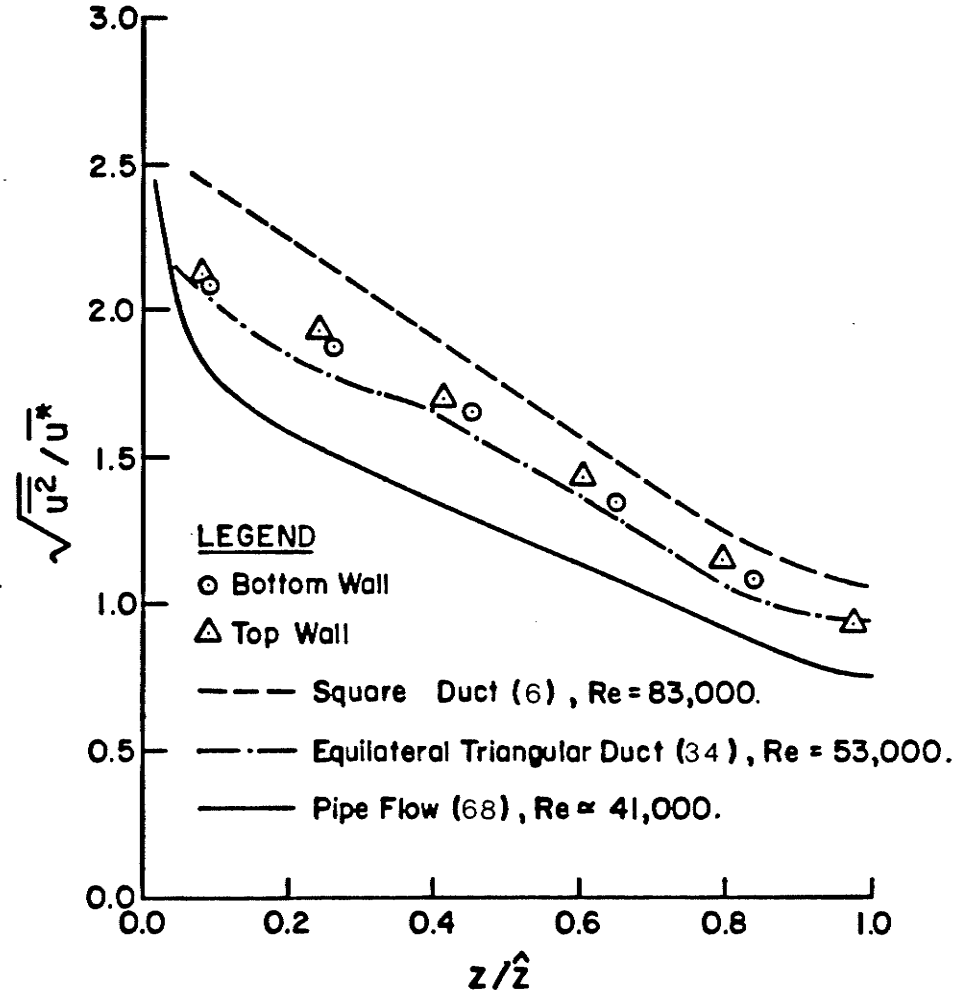

Fig. 18: Distributions of $(\overline{u^2})^{1/2}/\overline{u^*}$ Along Duct Symmetry Line; Re = 99,000.

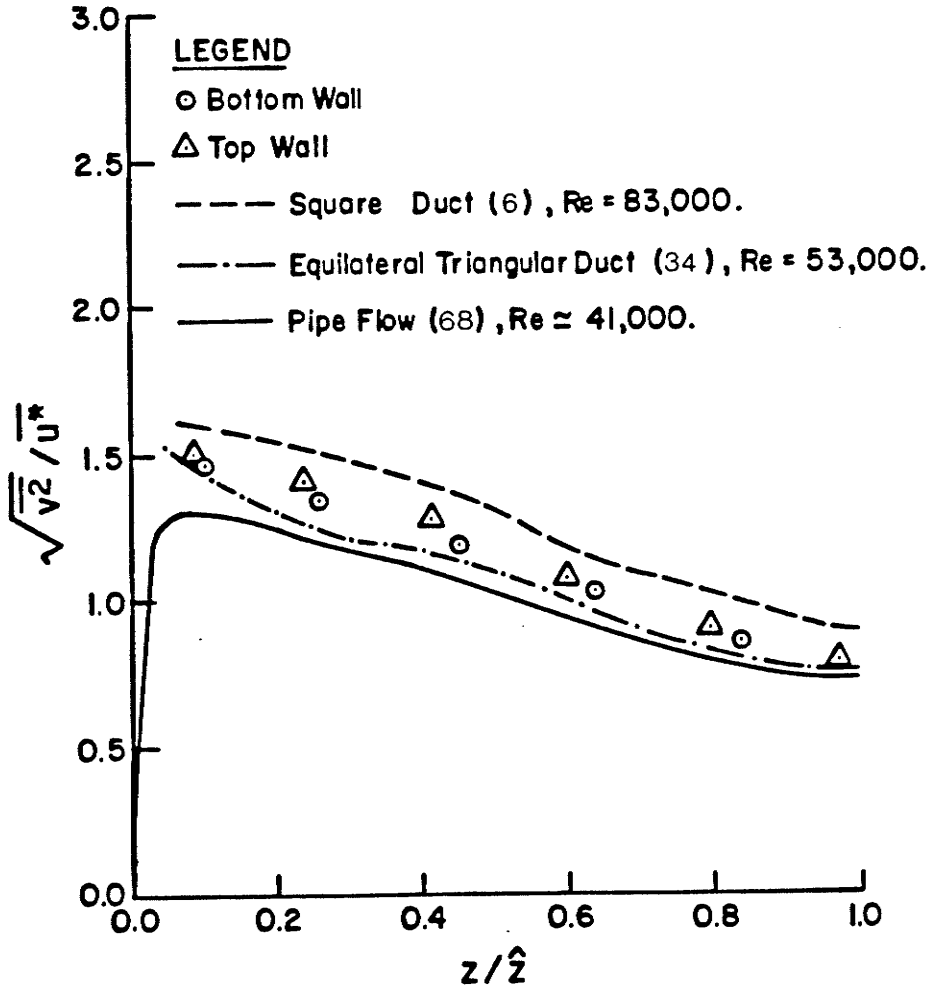

Fig. 19: Distributions of $(\overline{v^2})^{1/2}/\overline{u}^*$ Along Duct Symmetry Line; Re = 99,000.

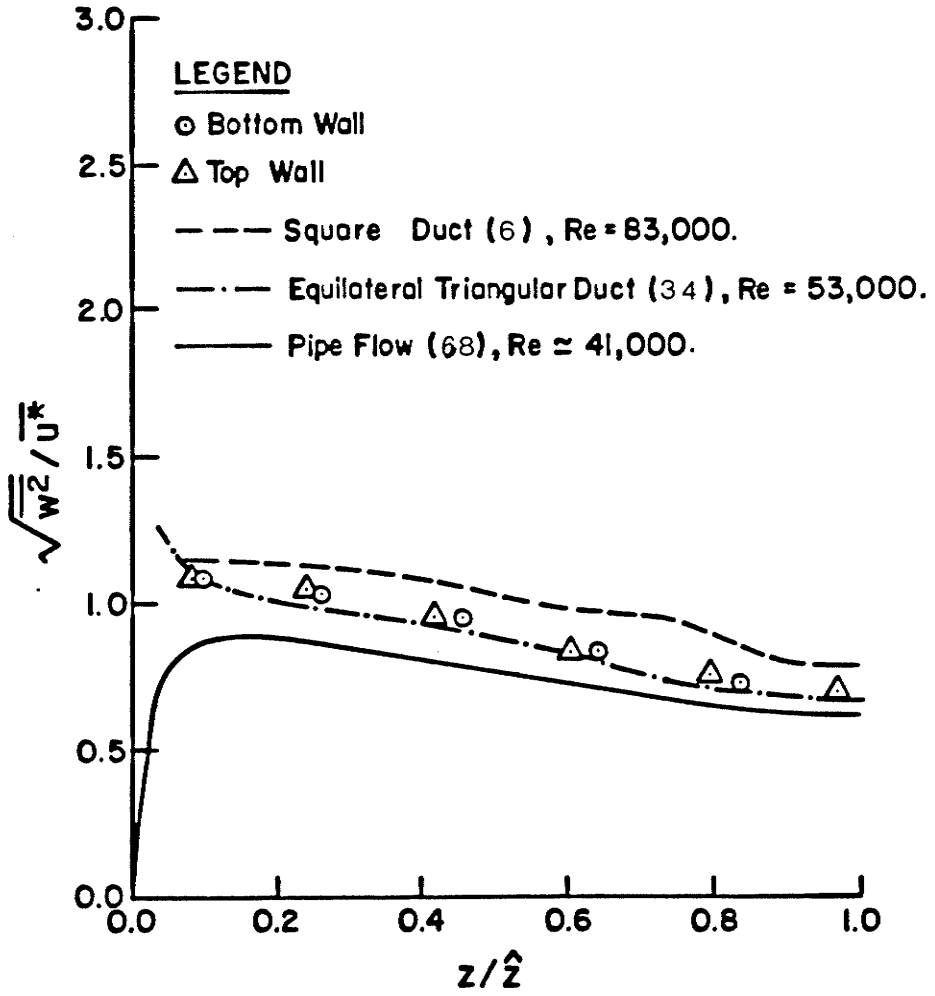

Fig. 20: Distributions of $(\overline{w^2})^{1/2}/\bar{u}^*$ Along Duct Symmetry Line; Re = 99,000.

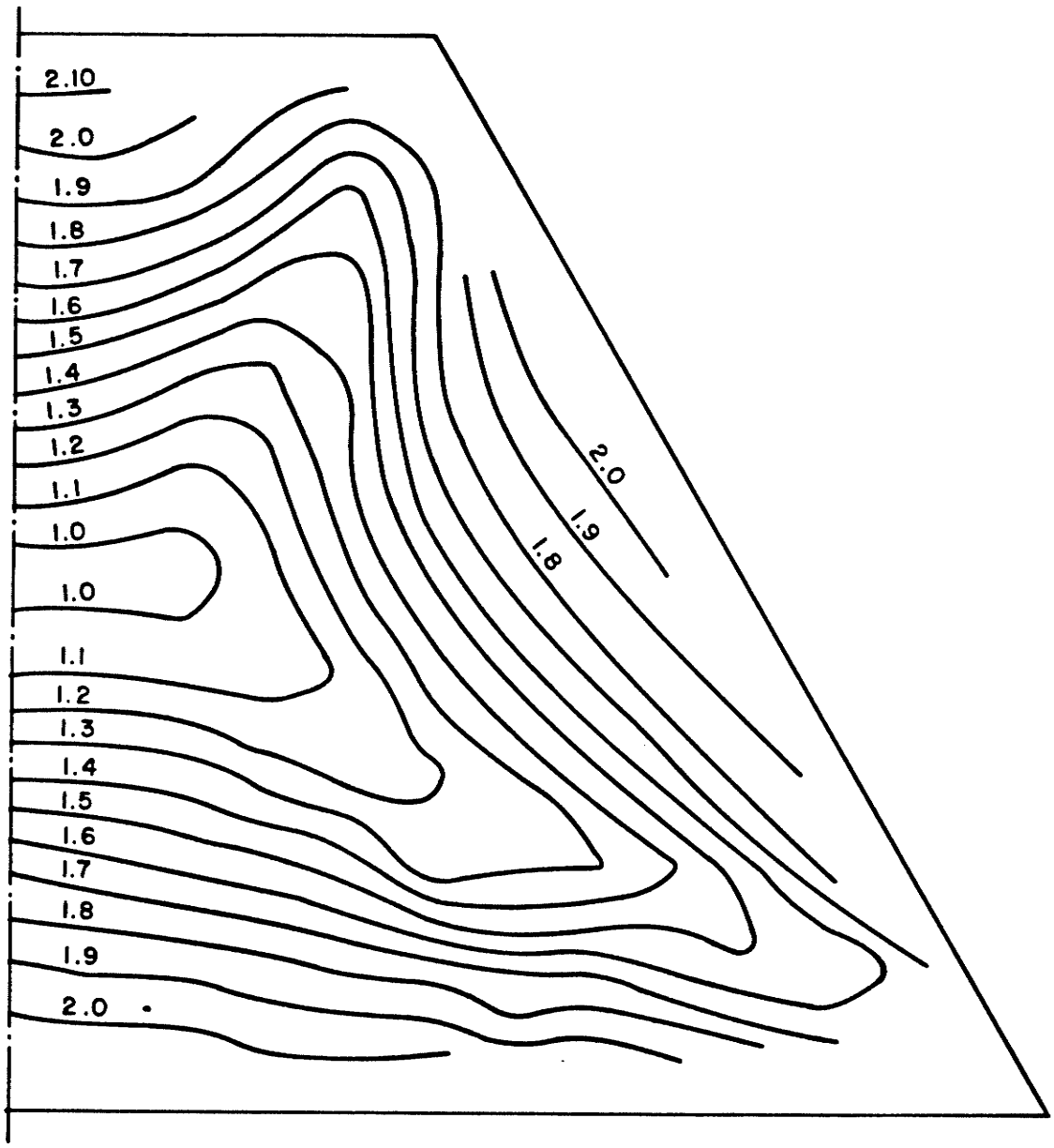

Fig. 21: Contours of $(\overline{u^2})^{1/2}/\bar{u}^*$; Re = 99,000.

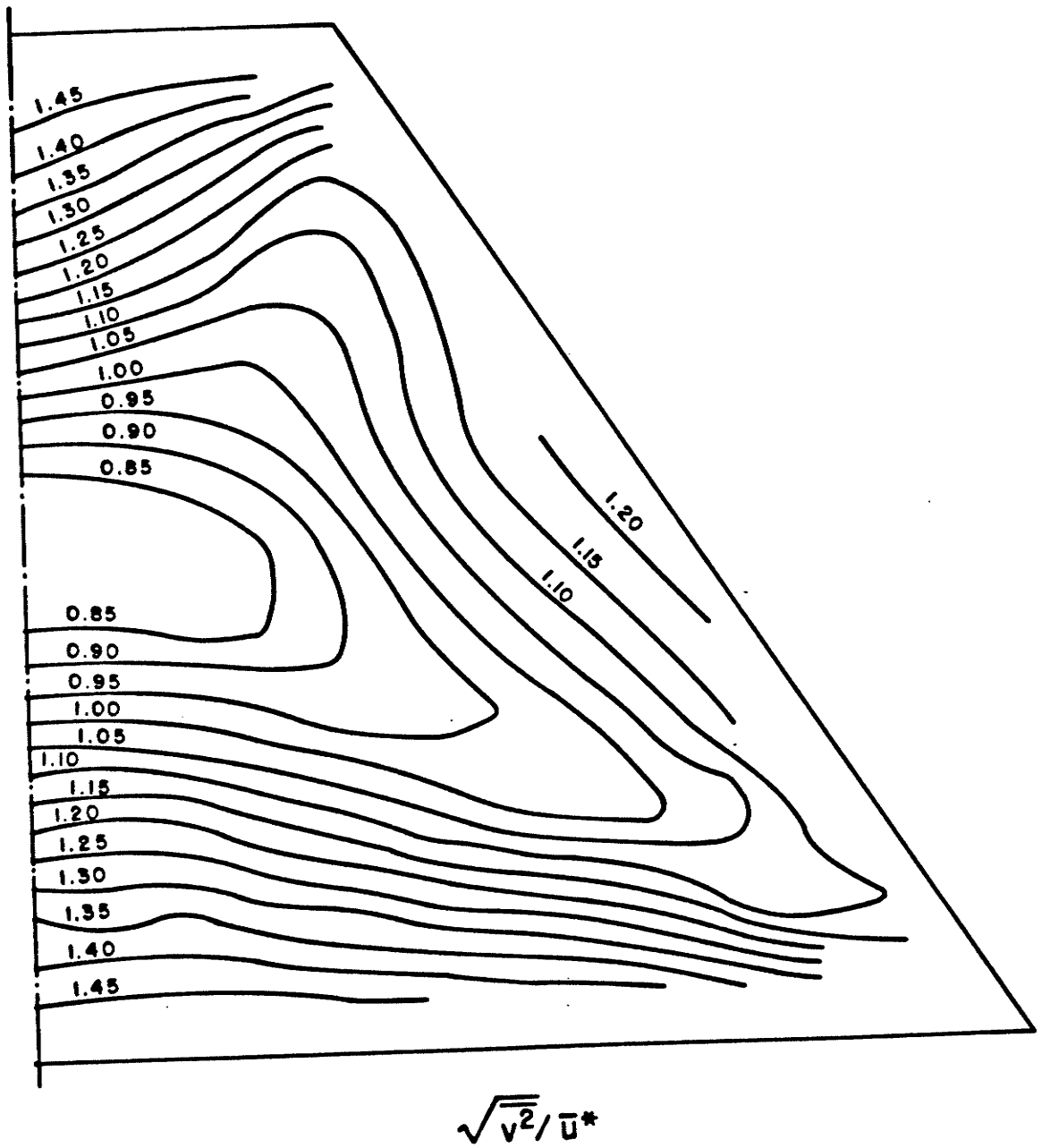

Fig. 22: Contours of $(\overline{v^2})^{1/2}/\bar{u}^*$; Re = 99,000.

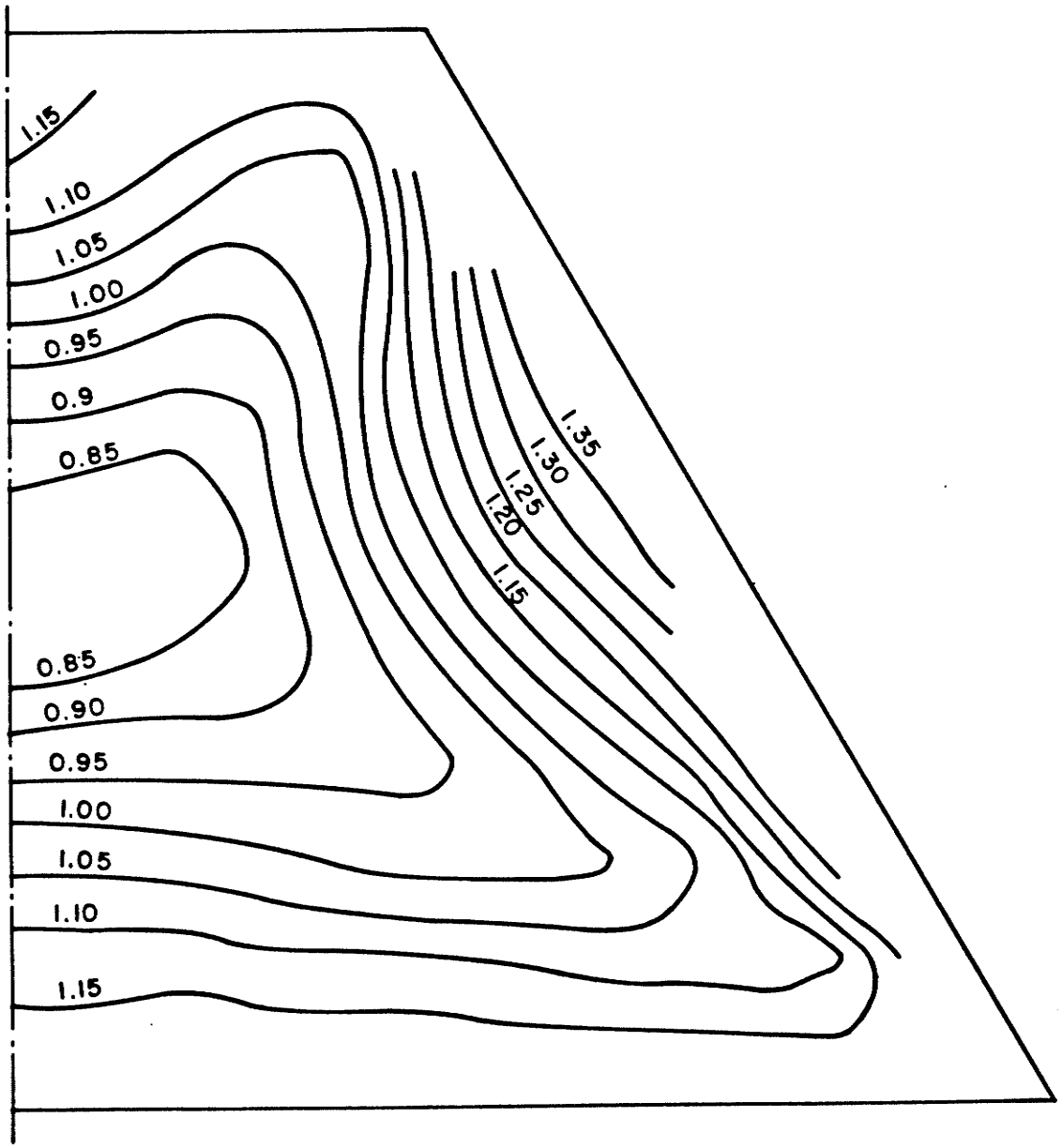

Fig. 23: Contours of $(\overline{w^2})^{1/2}/\bar{u}^*$; Re = 99,000.

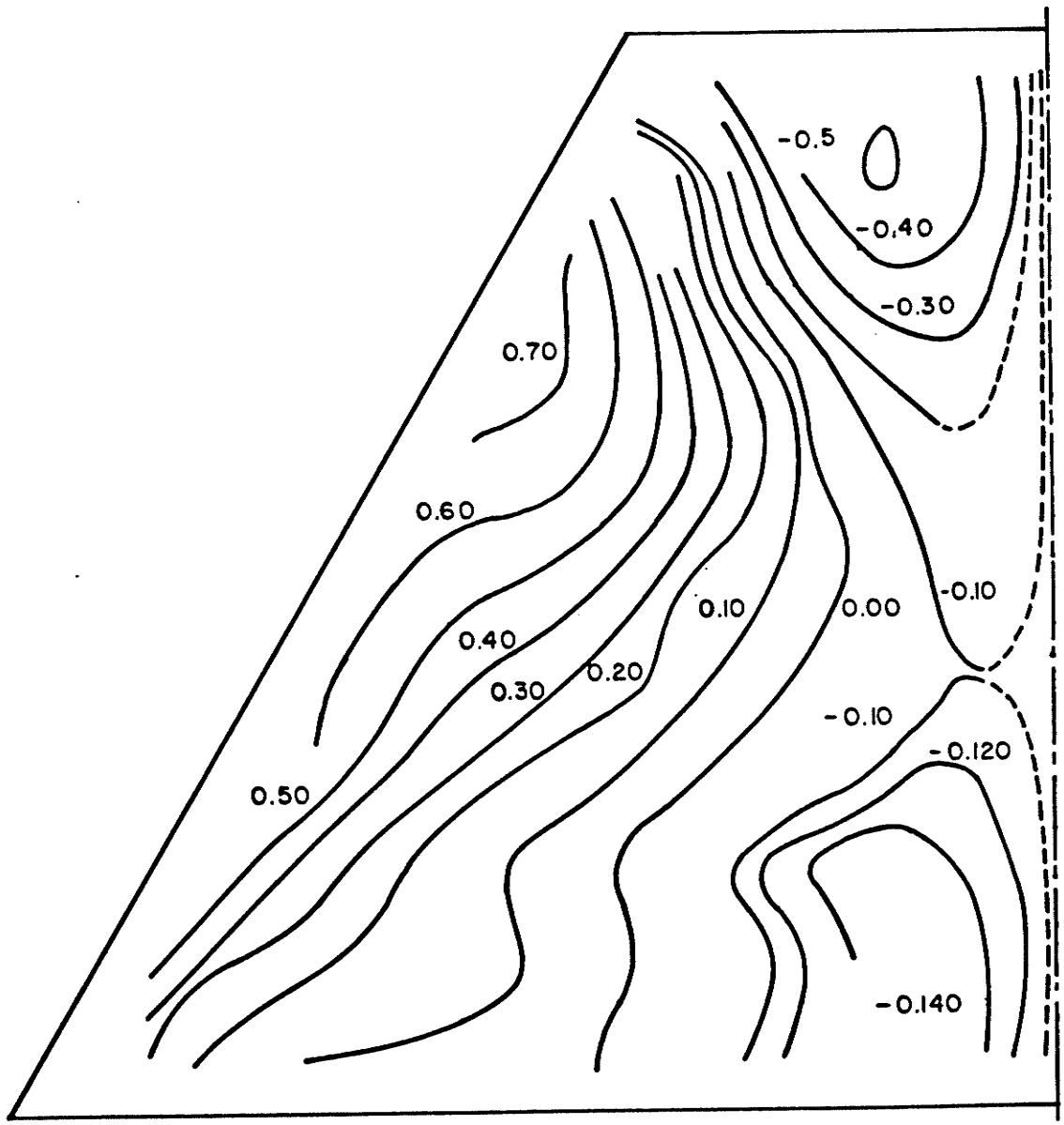

Fig. 24: Contours of $\overline{uv}/(\bar{u}^*)^2$; Re = 99,000.

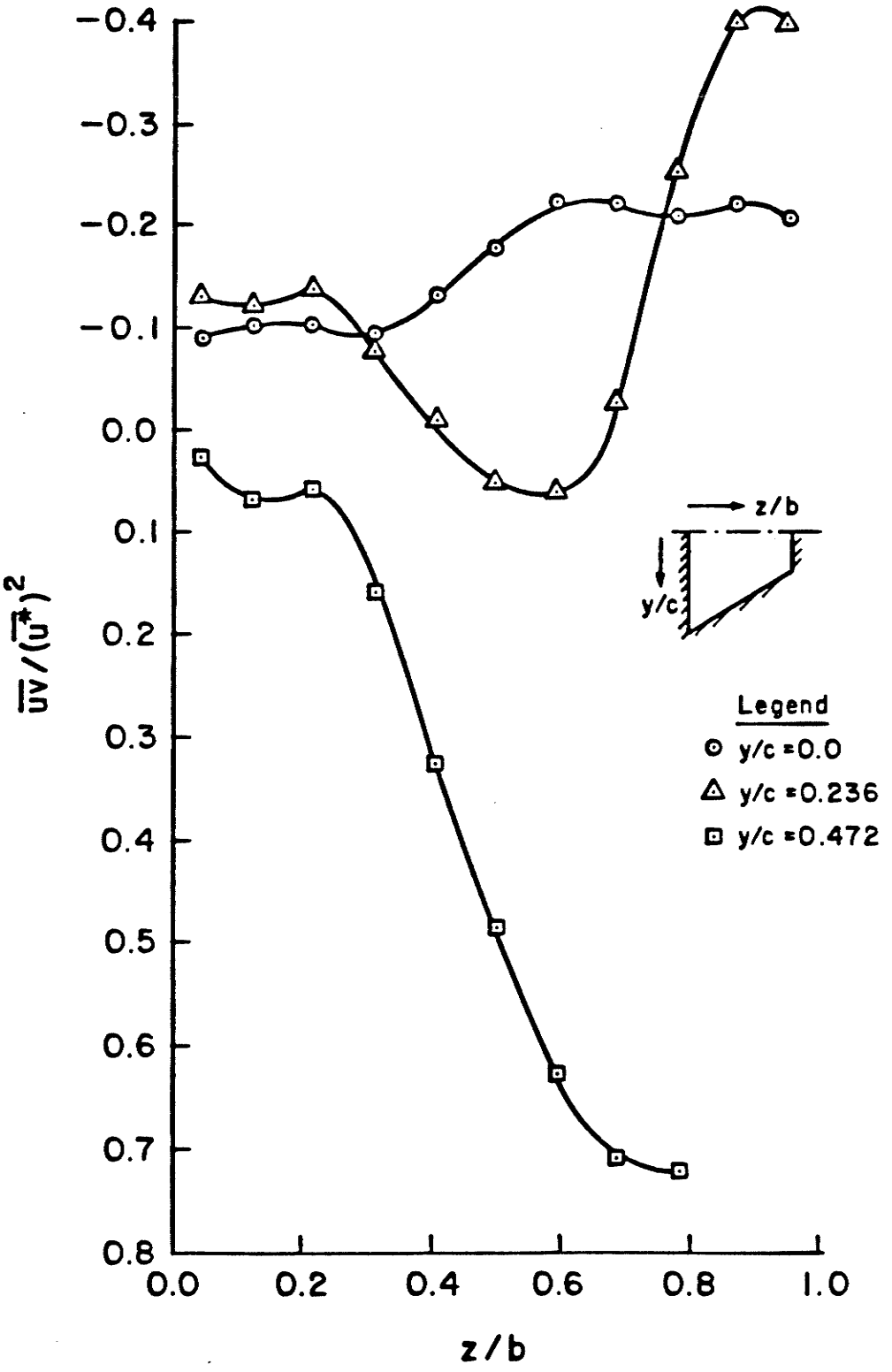

Fig. 25: Distributions of Shear Stress $\rho\overline{uv}$; Re=99,000.

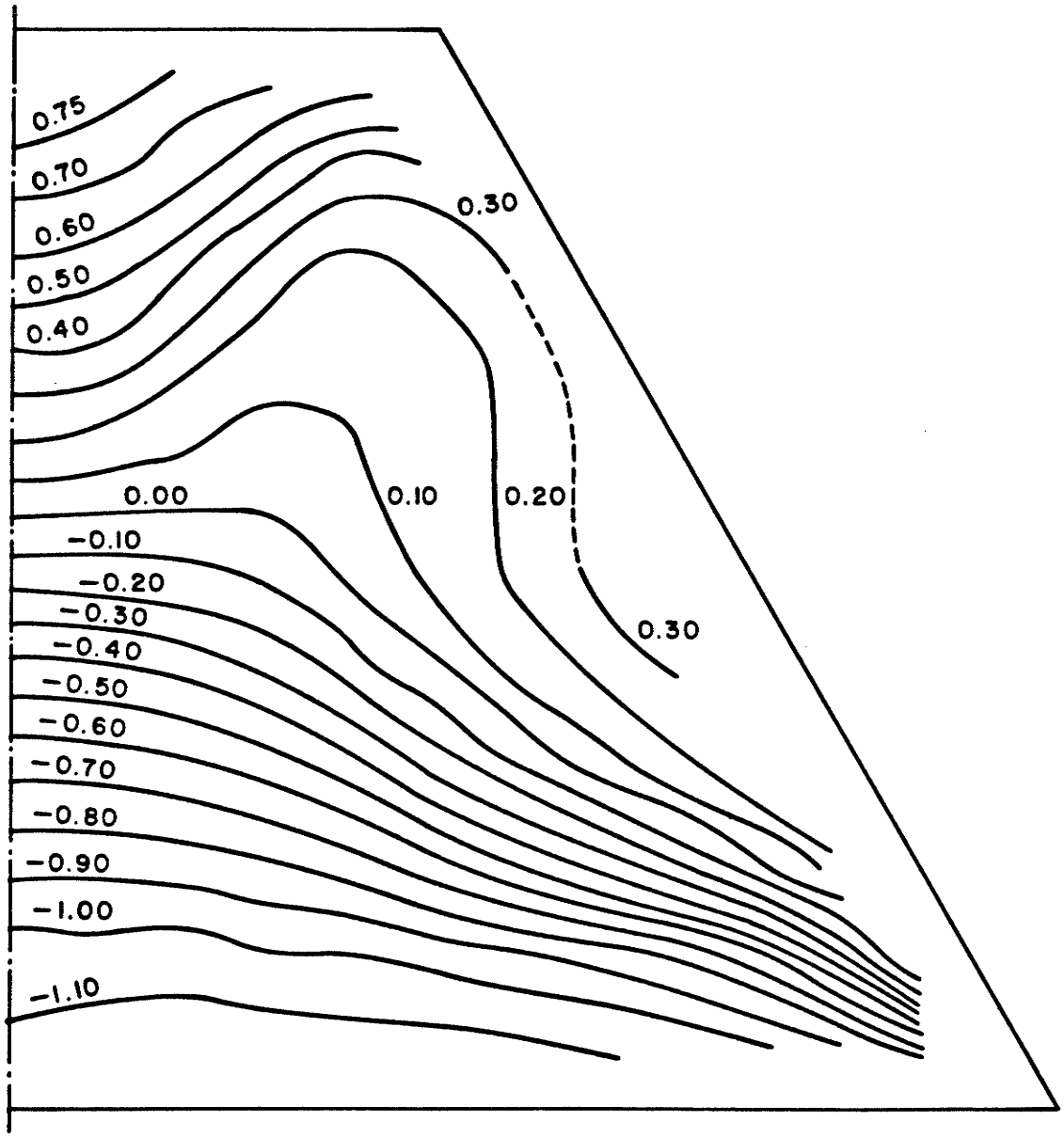

Fig. 26: Contours of $\overline{uw}/(\bar{u}^*)^2$; Re = 99,000.

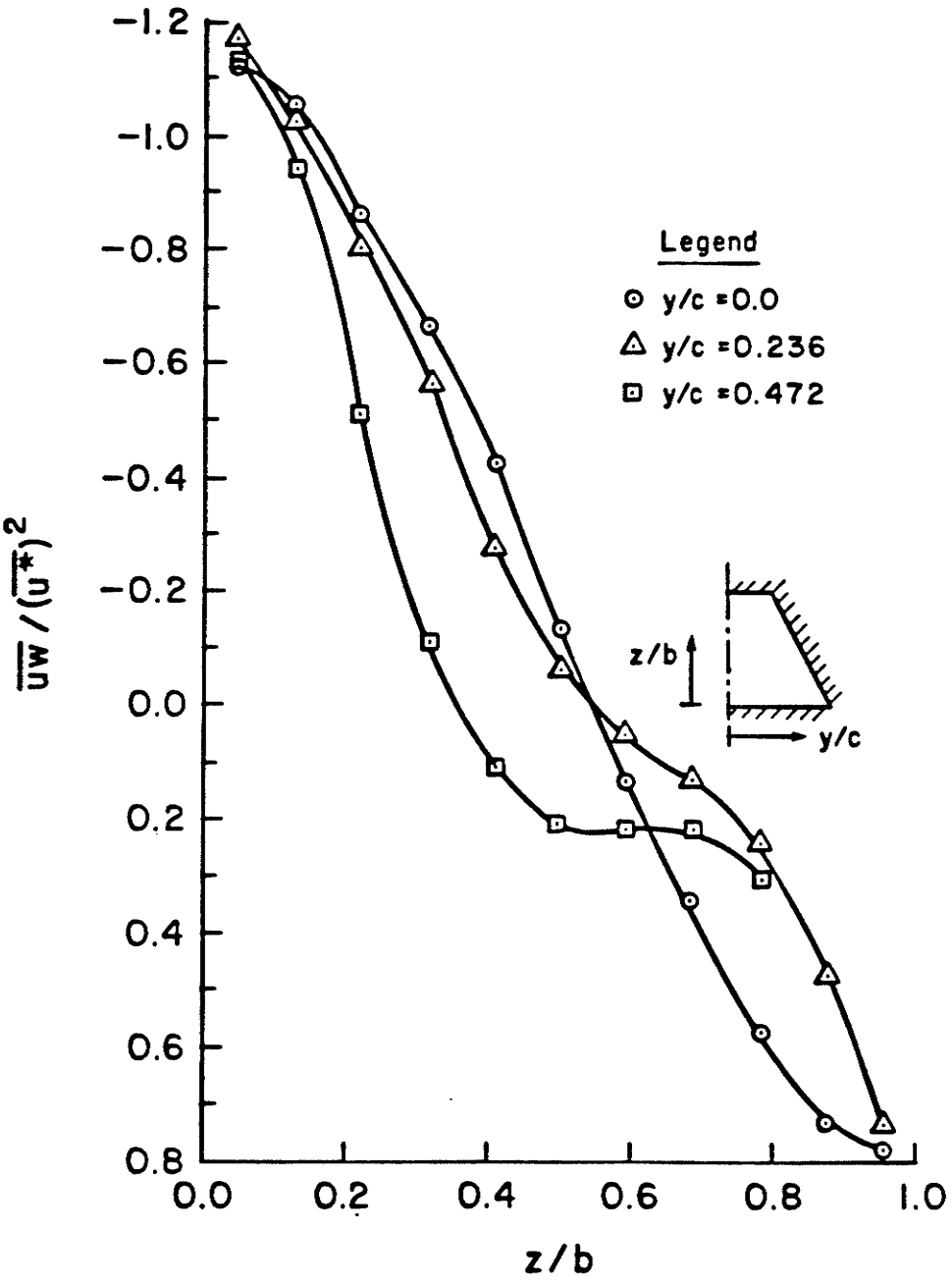

Fig. 27: Distributions of Shear Stress $\rho\overline{uw}$; Re=99,000.

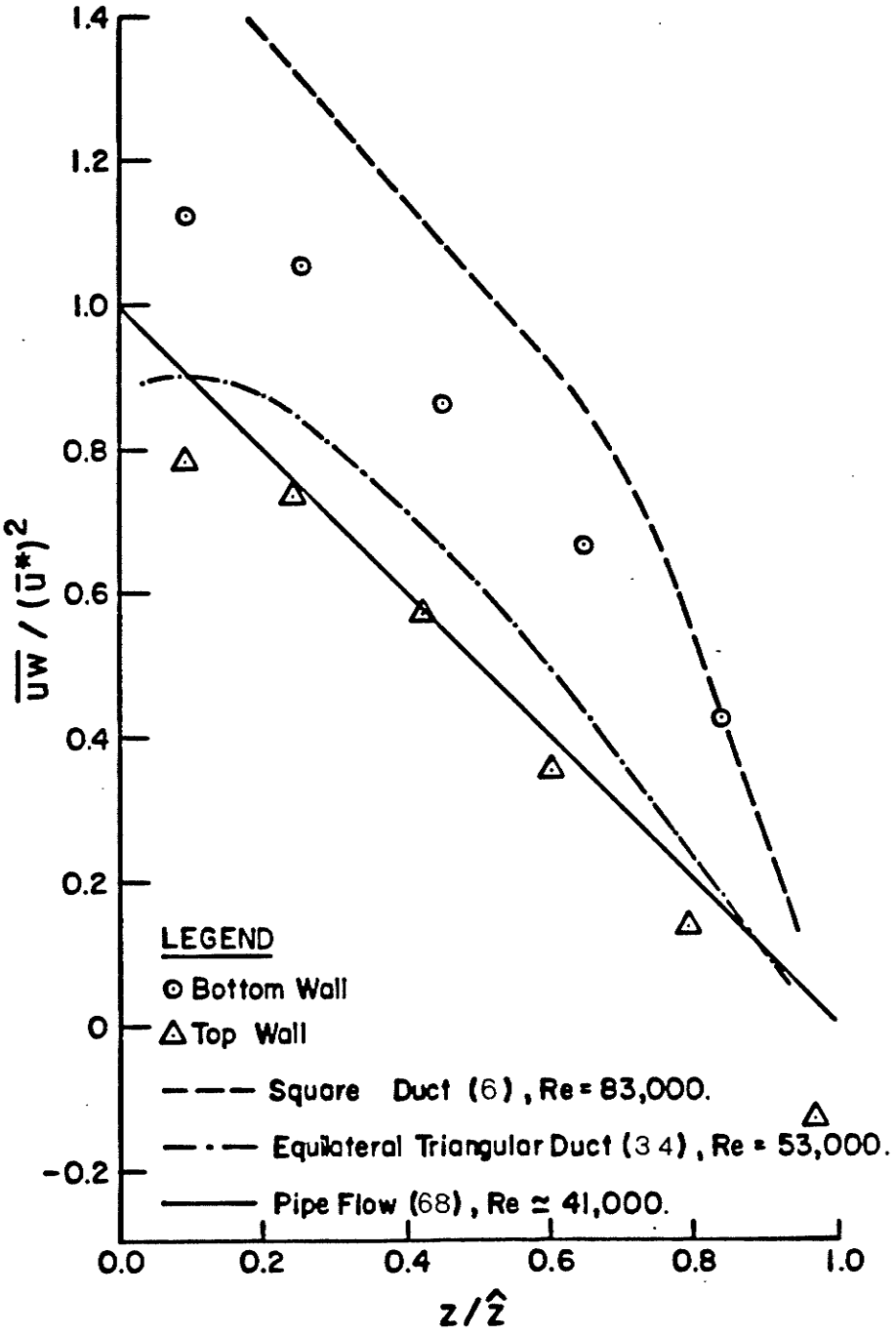

Fig. 28: Distributions of Primary Shear Stress Along Duct Symmetry Line (y = 0); Re = 99,000.

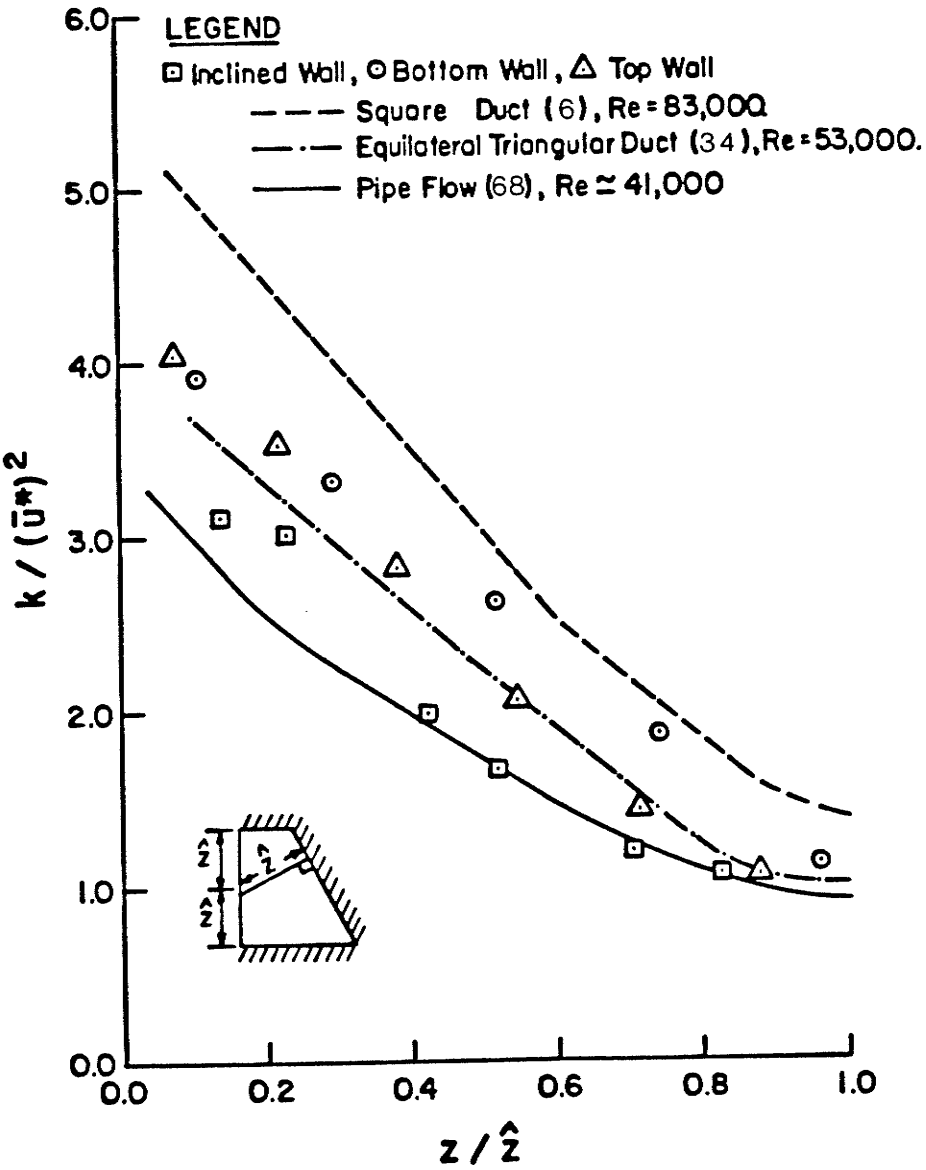

Fig. 29: Distributions of k Normal to Walls; Re=99,000.

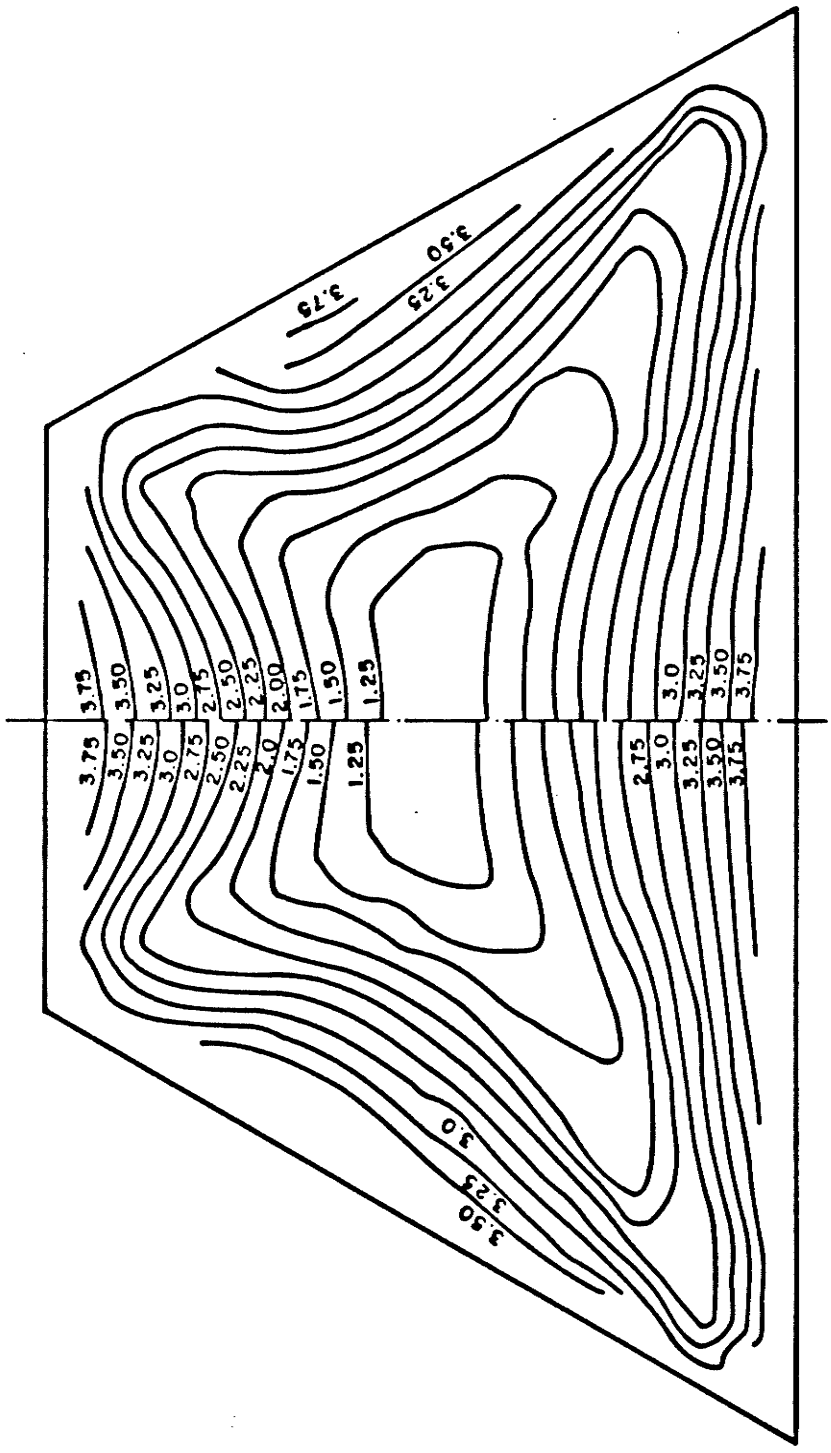

Fig. 30: Contour Plots of $k/(\overline{u}^*)^2$; Right: Re=99,000
Left: Re=79,000.

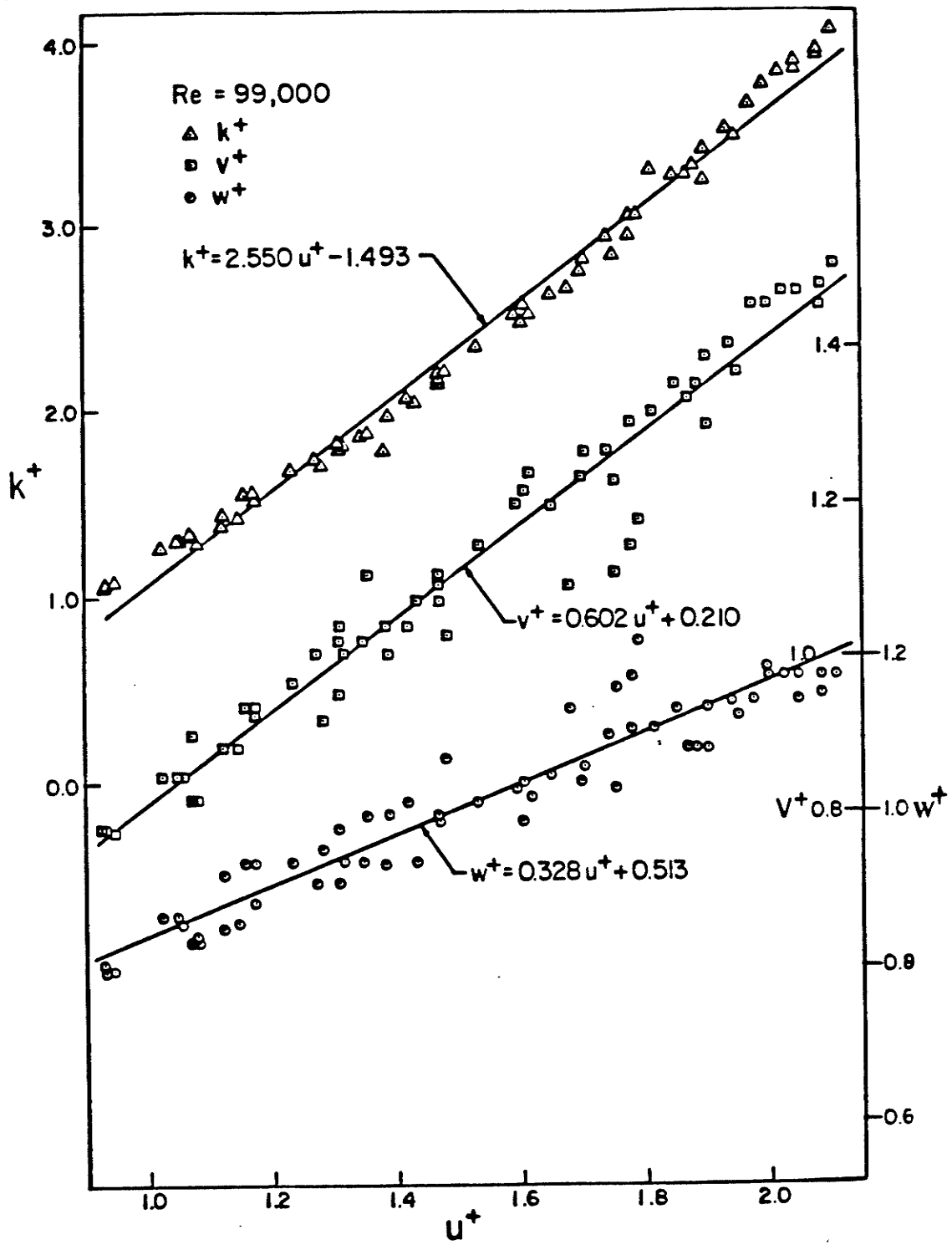

Fig. 31: Relationships Between u^+ and k^+, v^+ and w^+ for the Rectangular Domain : $0 \leq y/a \leq 1$, $0 \leq z/b \leq 1$; Re = 99,000.

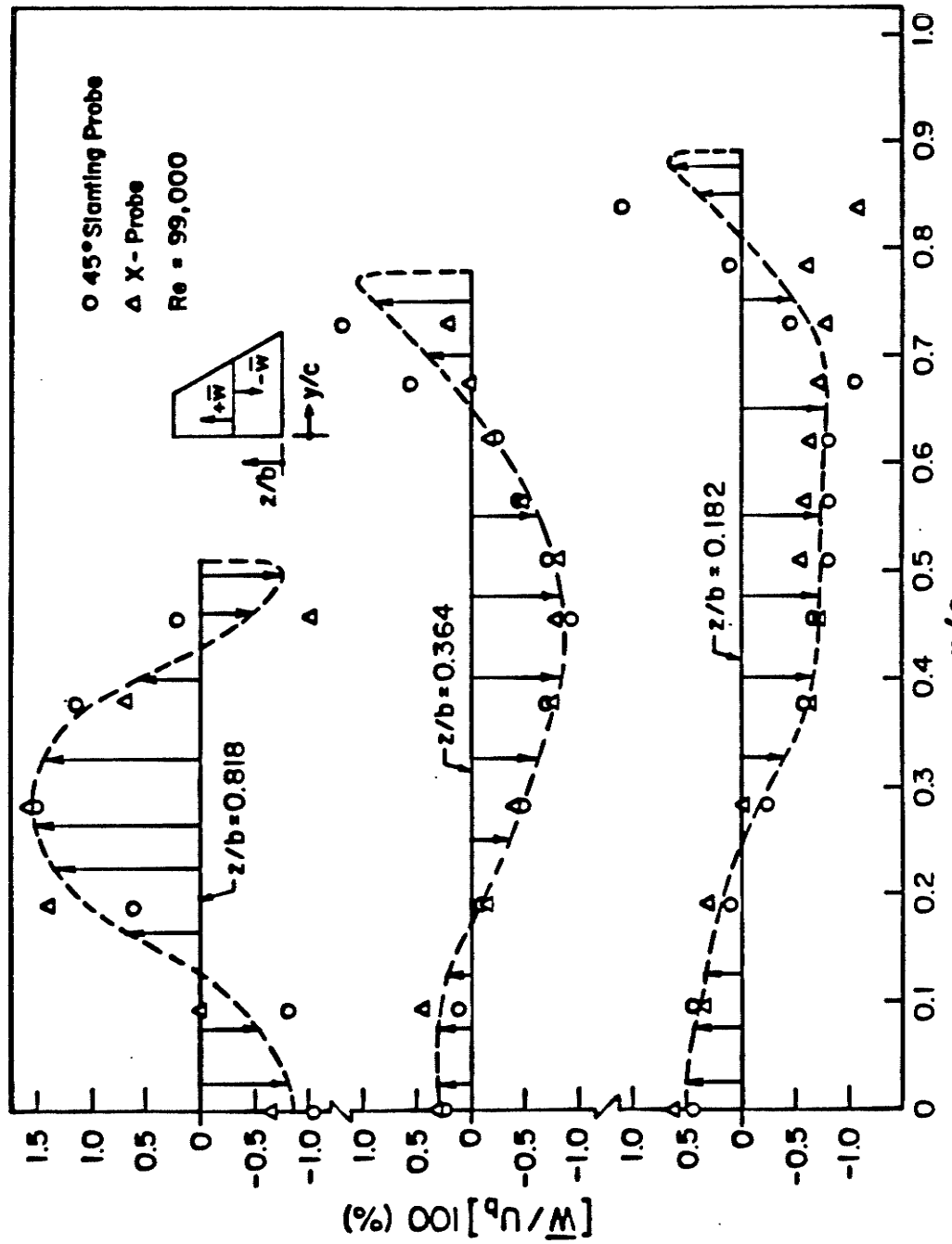

Fig. 32: Distributions of $\overline{W}$ for Three Horizontal Traverses; Re = 99,000.

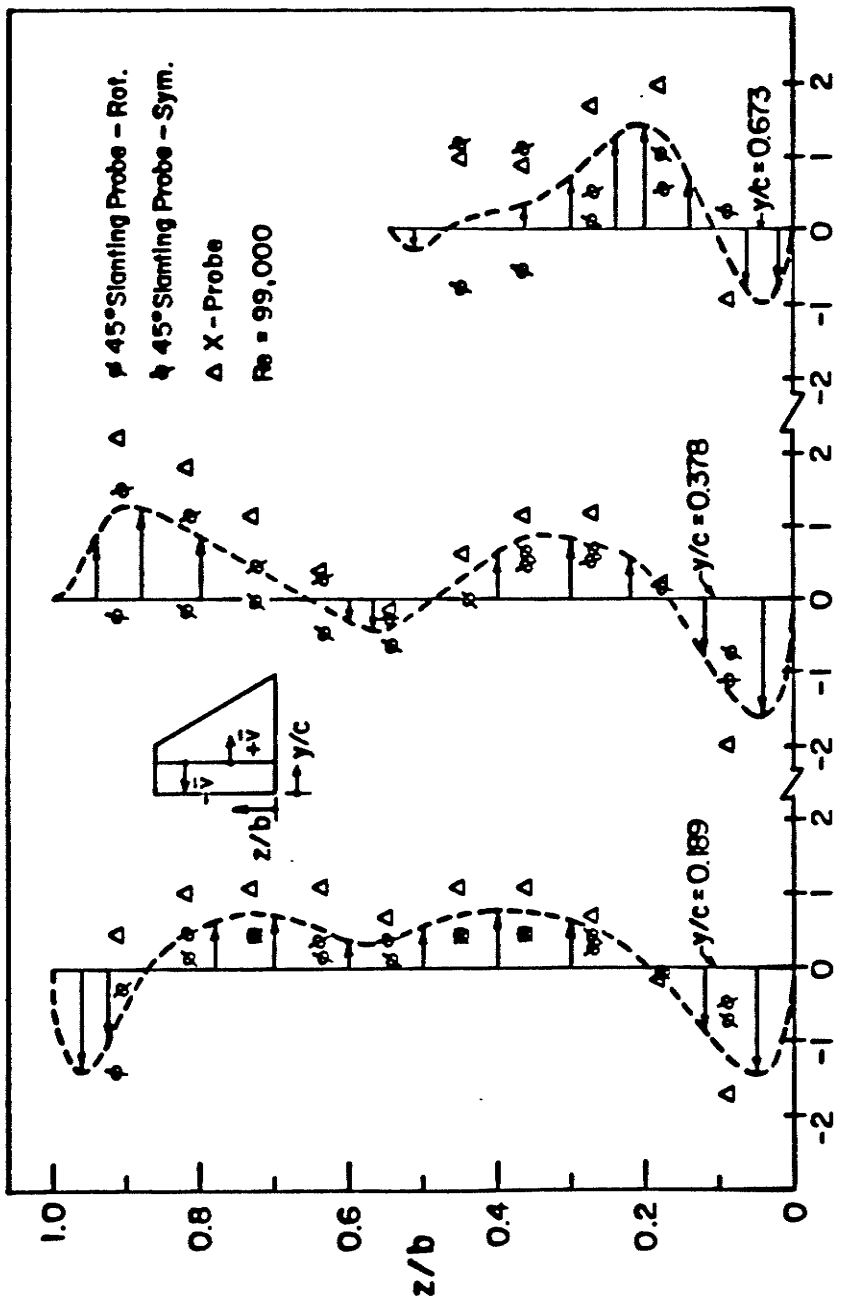

Fig. 33: Distributions of $\bar{V}$ for Three Vertical Traverses; Re = 99,000.

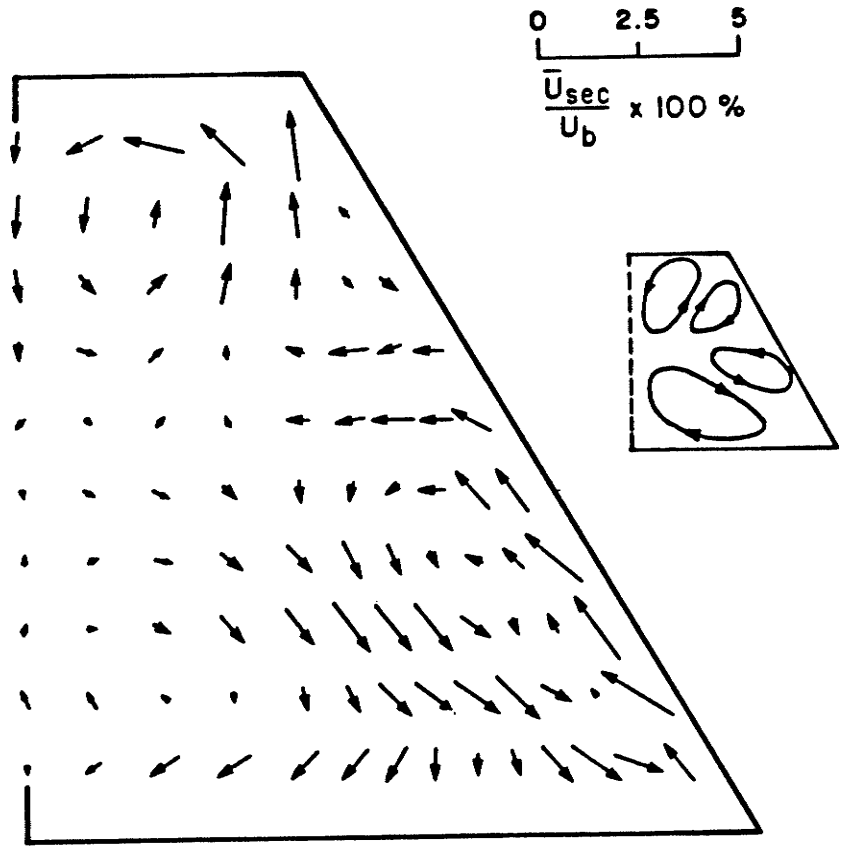

Fig. 34: Secondary Flow in a Trapezoidal Duct; Re=99,000.

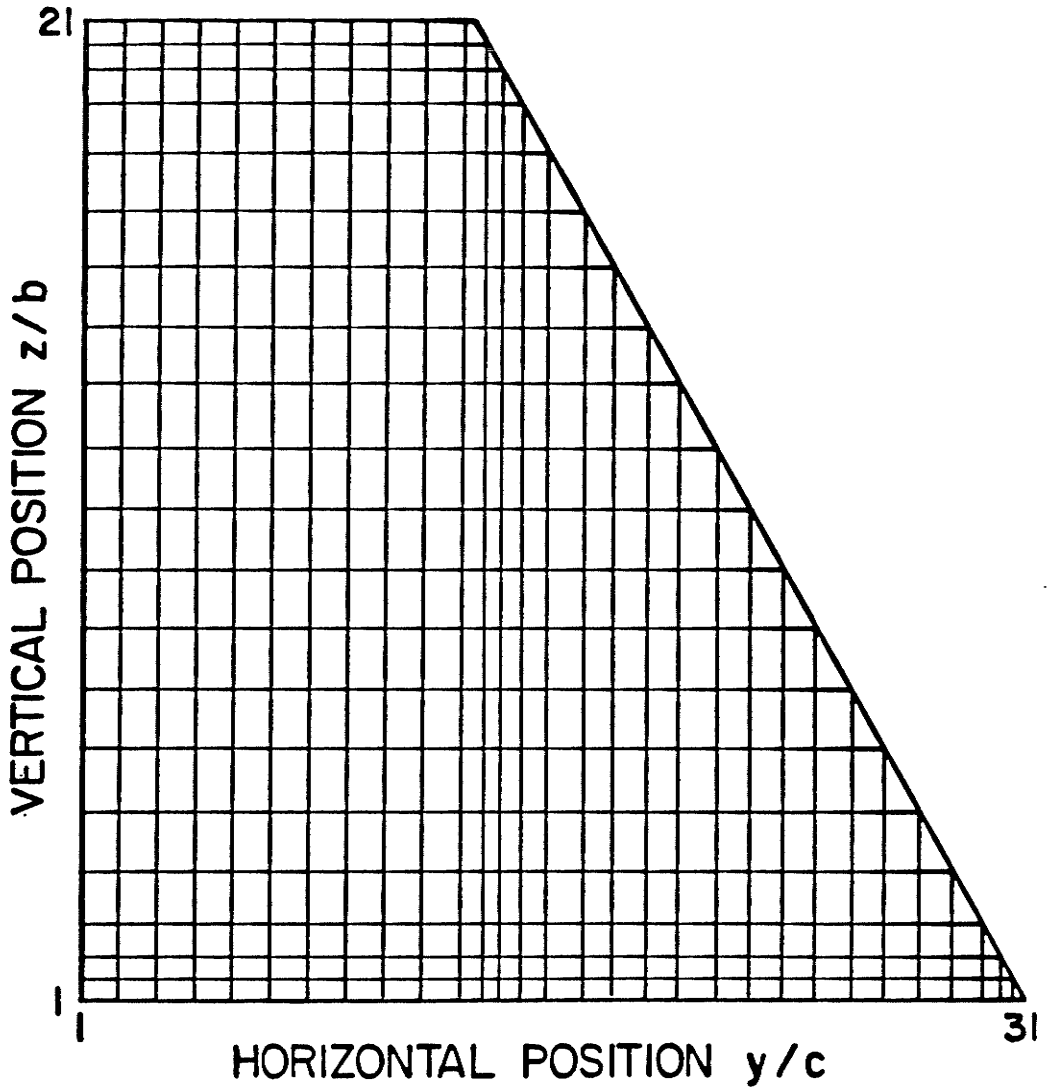

Fig. 35: Finite Difference Grid for Numerical Prediction.

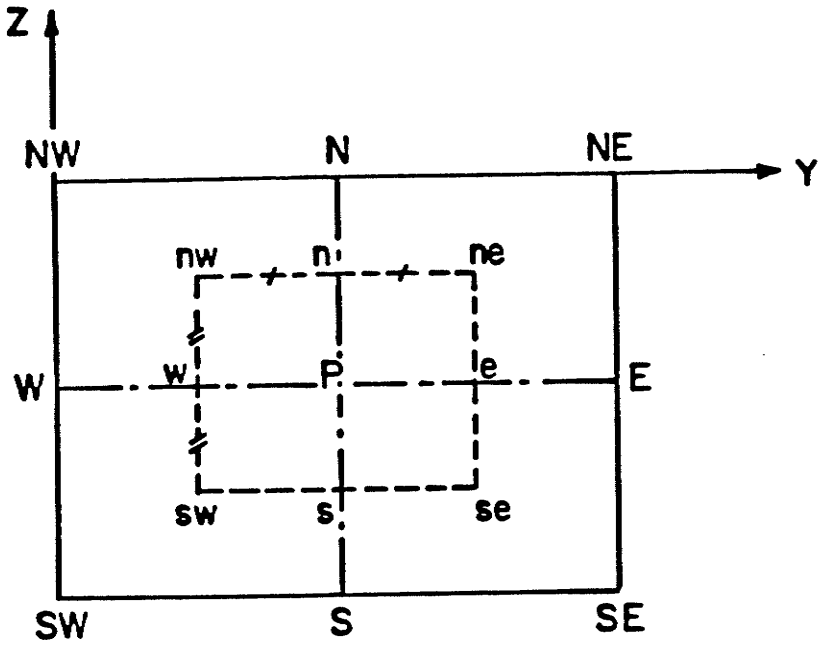

Fig. 36: Finite Difference Area of Integration.

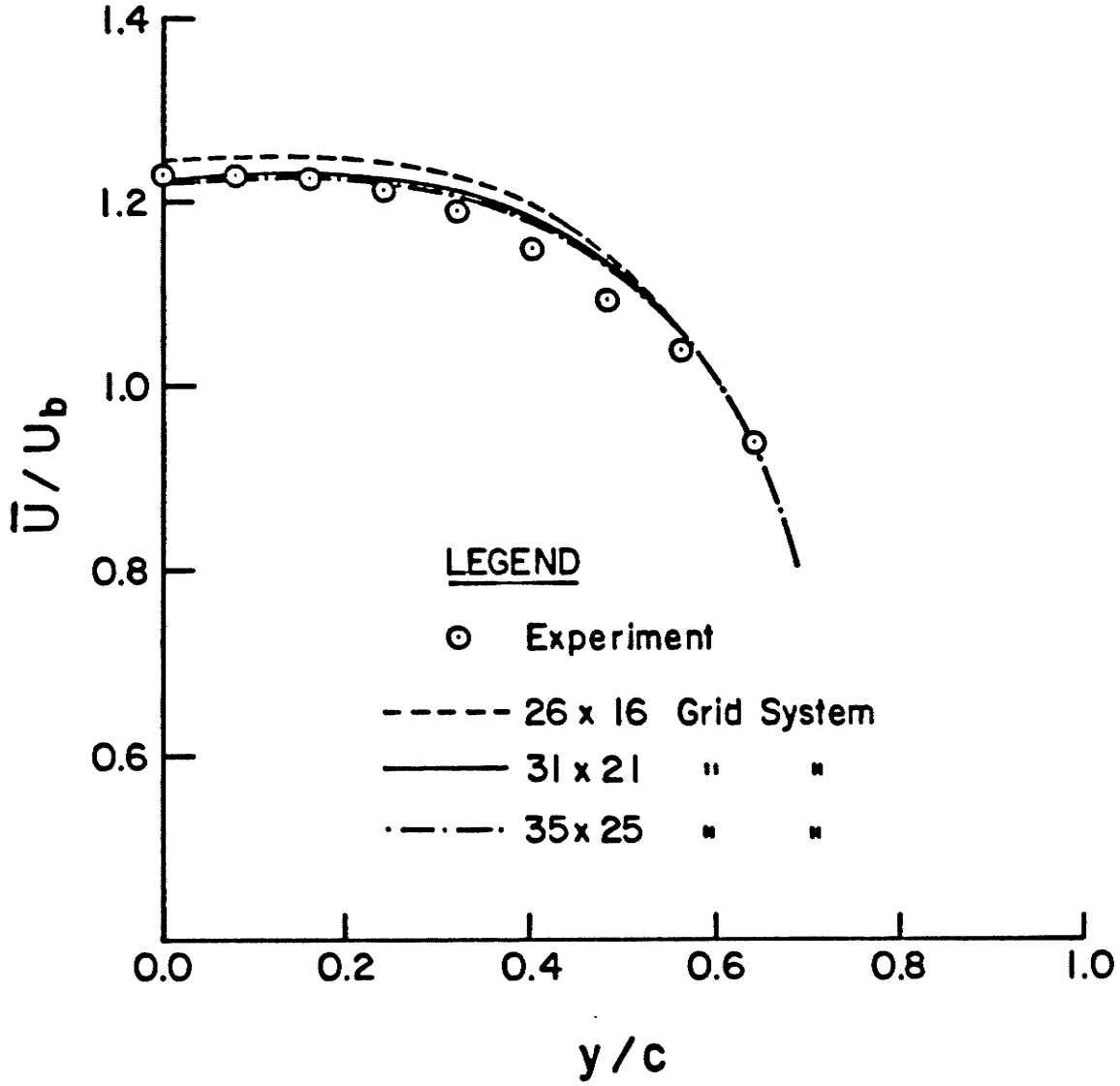

Fig. 37: Predictions of $\bar{U}/U_b$ Using Different Grid Systems at z/b = 0.5; Re = 99,000.

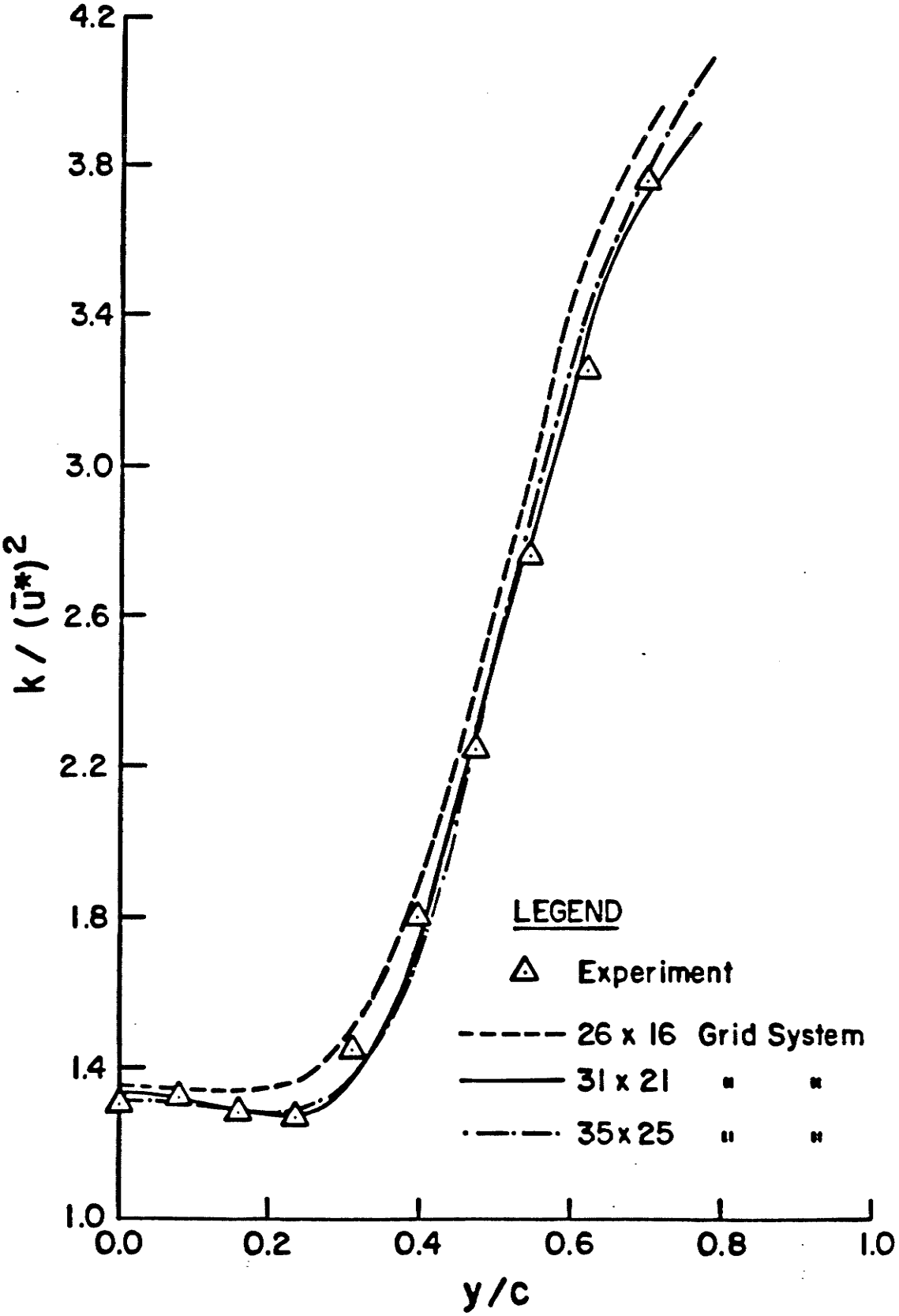

Fig. 38: Predictions of $k/(\bar{u}^*)^2$ Using Different Grid Systems at z/b = 0.406; Re = 99,000.

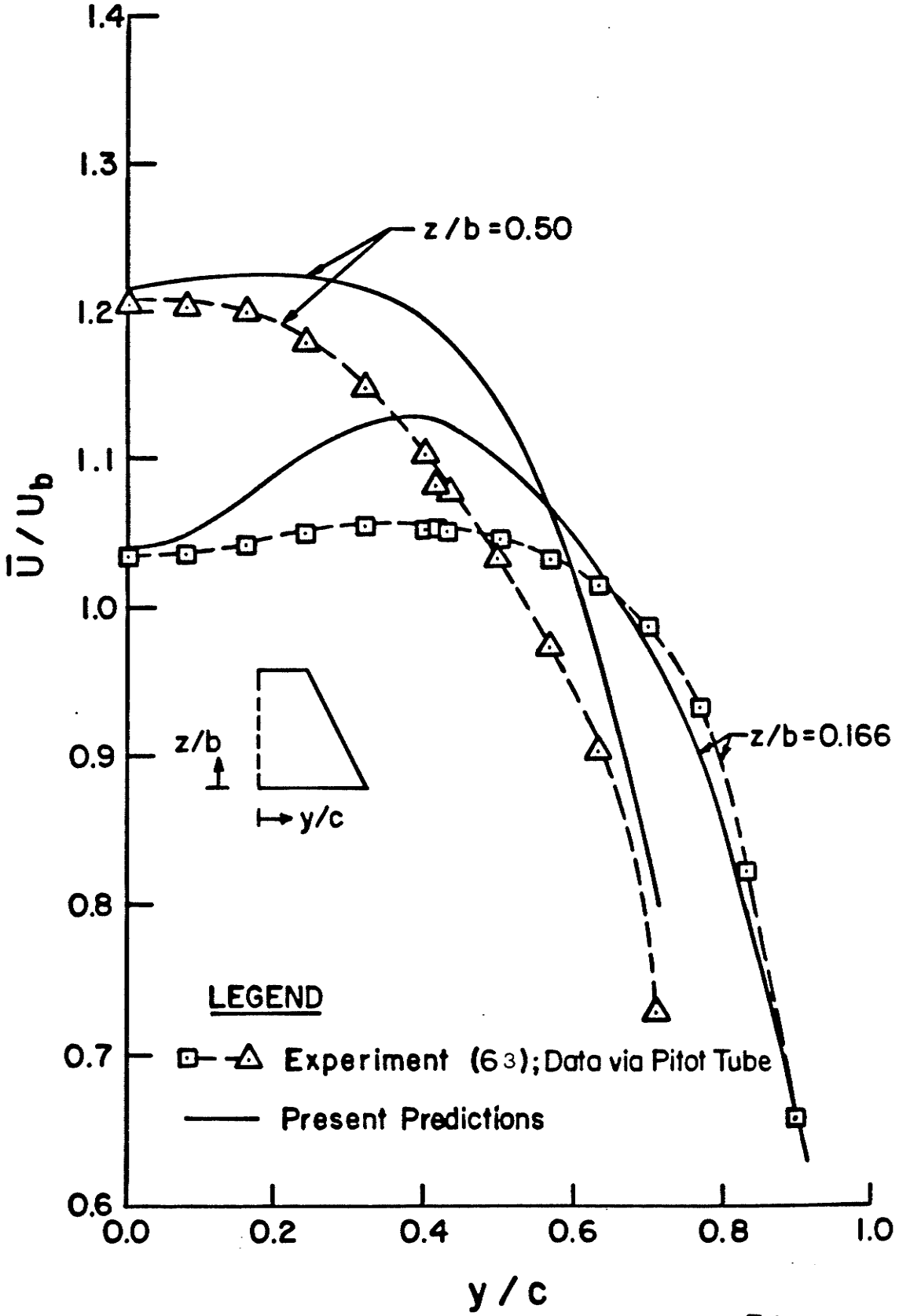

Fig. 39: Comparison of Predicted and Measured $\bar{U}/U_b$ Along Horizontal Traverses; Re=99,000.

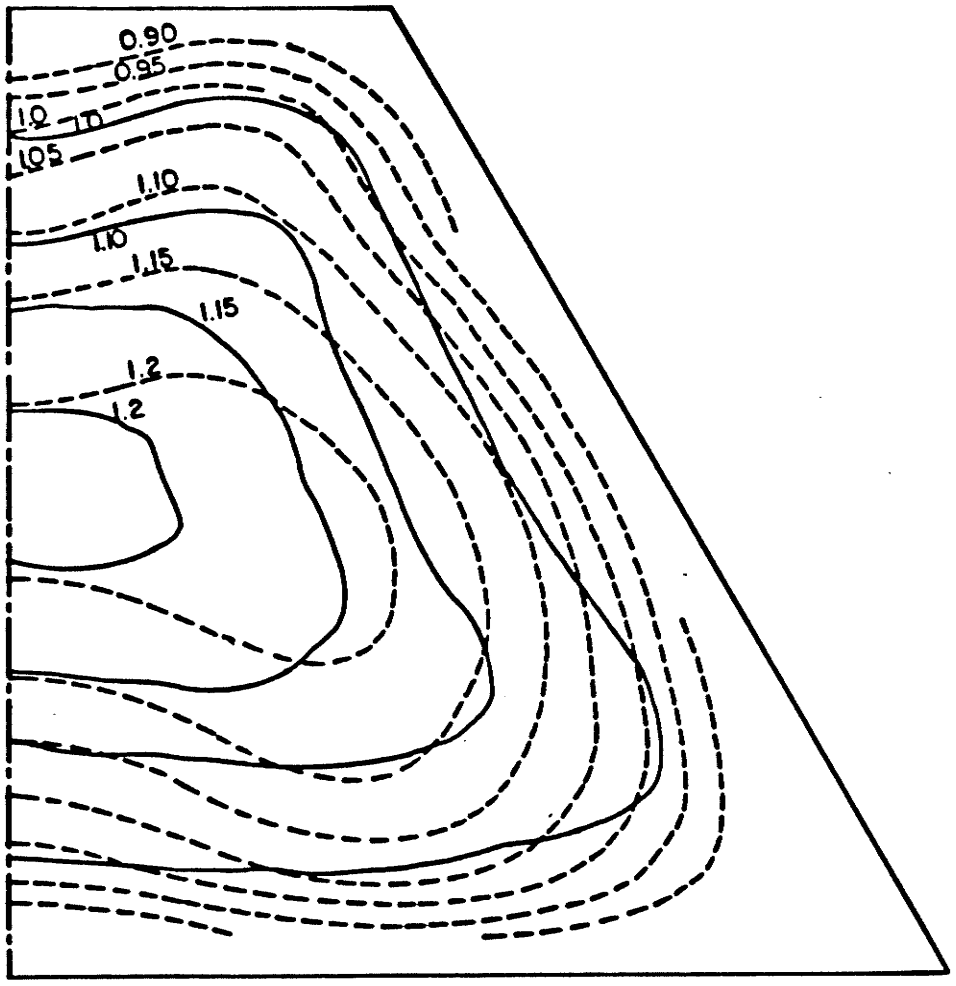

Fig. 40: Comparison of Predicted and Measured $\overline{U}/U_b$; Re = 99,000.

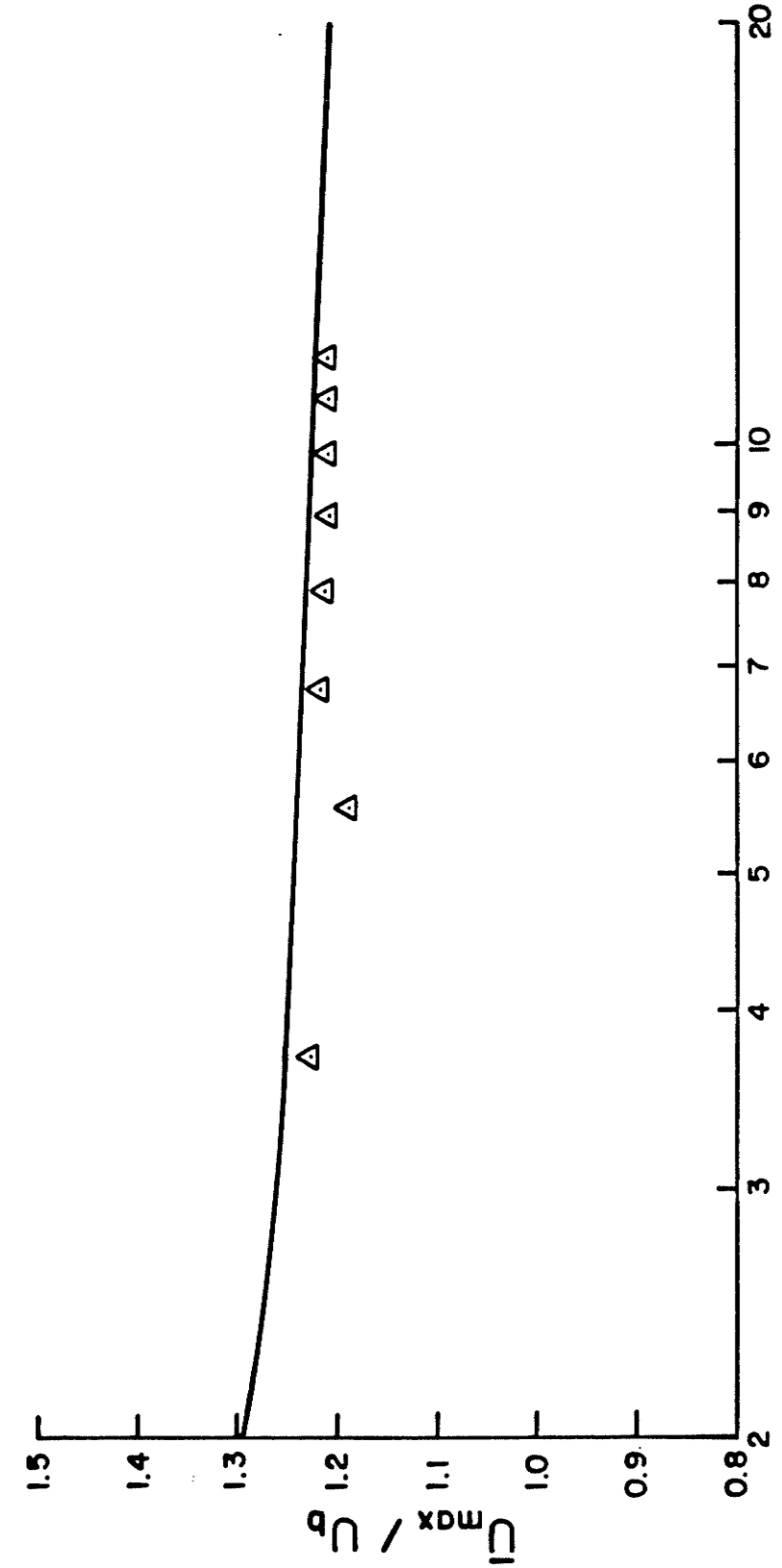

Fig. 41: Variation of Maximum Axial Velocity (U_{max}) With Reynolds Number; △ Experiment, – Predictions.

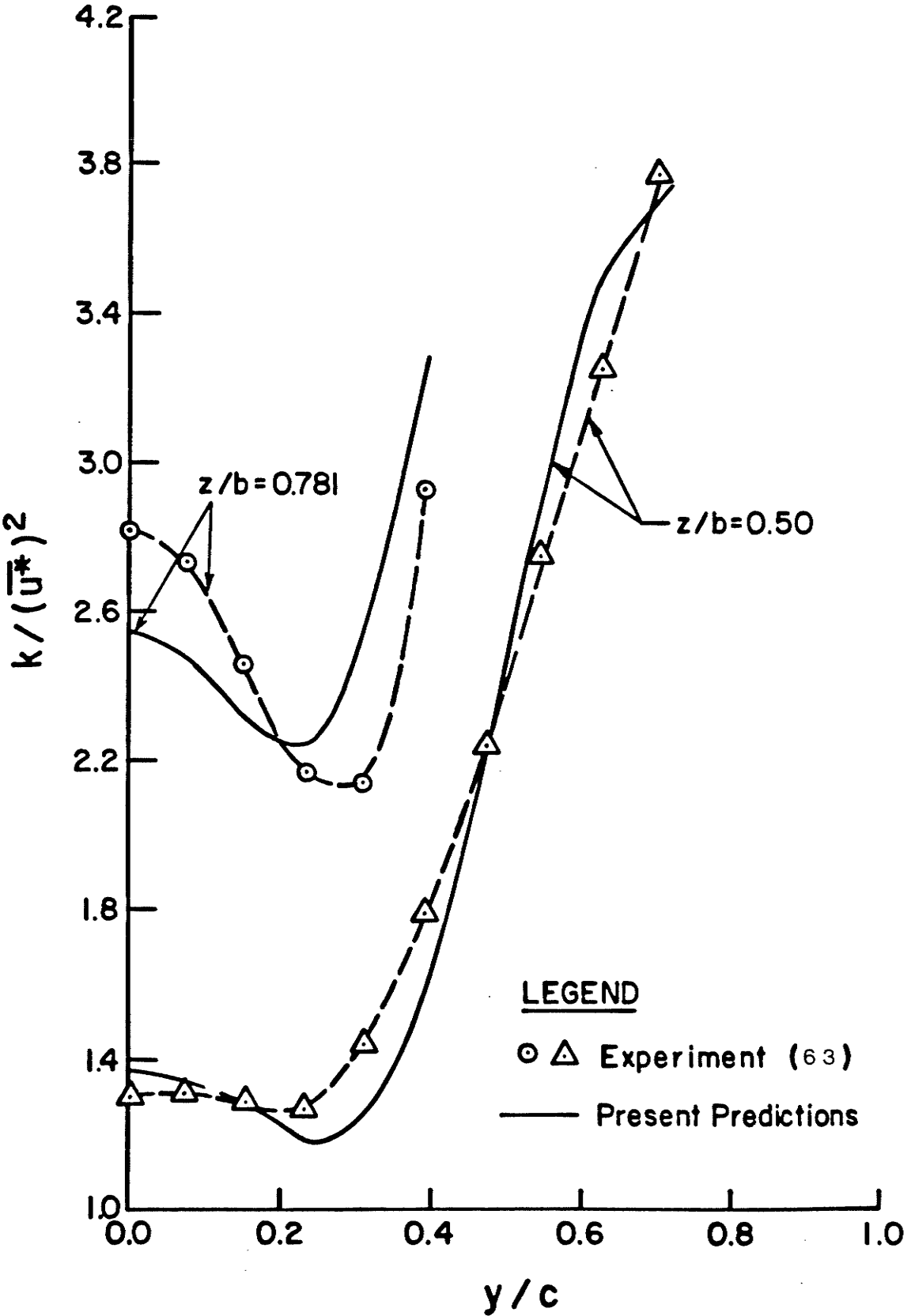

Fig. 42: Comparison of Predicted and Measured $k/(\bar{u}^*)^2$ Along Horizontal Traverses; Re=99,000.

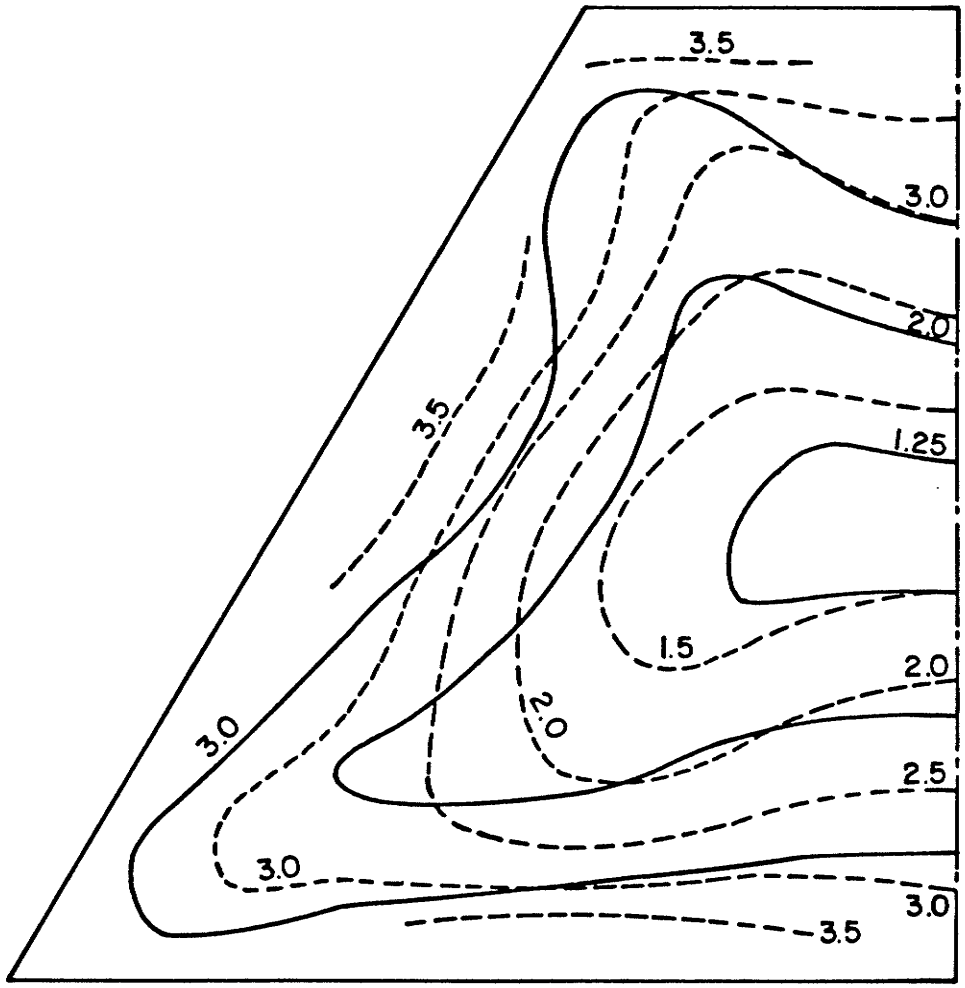

Fig. 43: Comparison of Predicted and Measured $k/(\bar{u}^*)^2$; Re = 99,000.

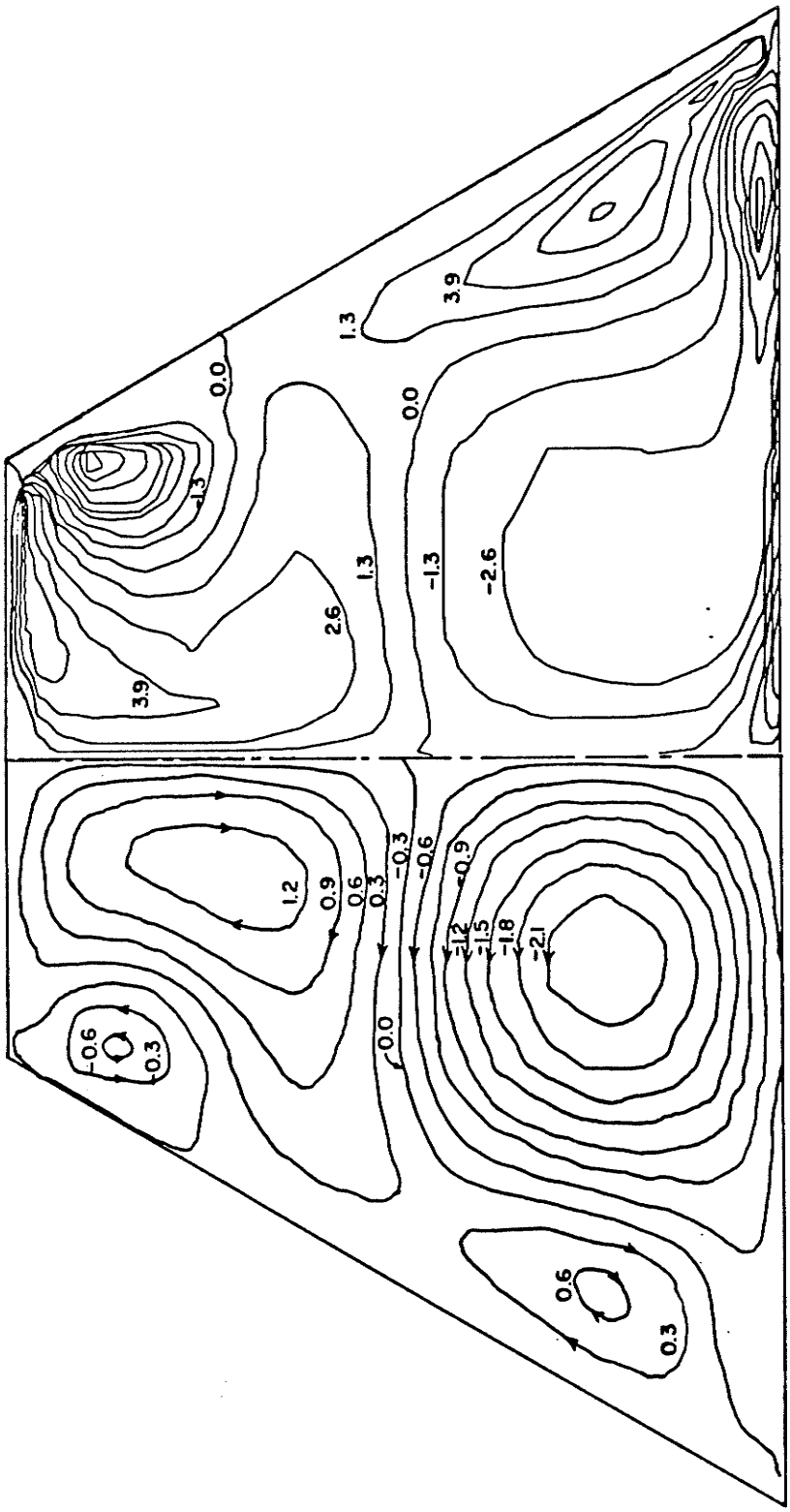

Fig. 44: Contour Plots of Stream Function Ψ and Axial Vorticity ω; Re = 99,000;
Right: $\omega D_h/(\bar{u}^*)$
Left : $\Psi/(\rho U_b D_h) \times 1000$.

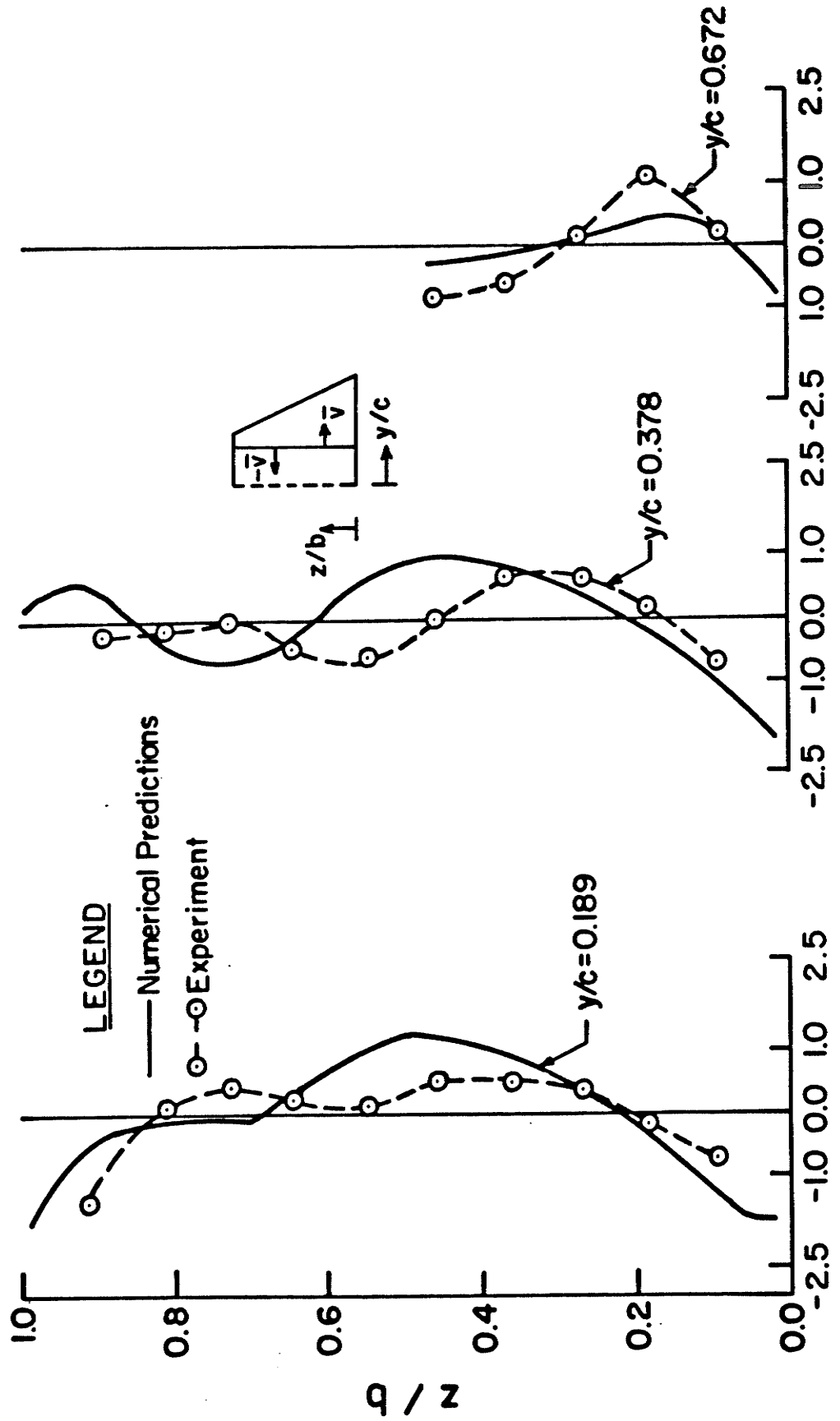

Fig. 45: Comparison of Predicted and Measured Secondary Flow Component $\bar{V}$; Re = 99,000.

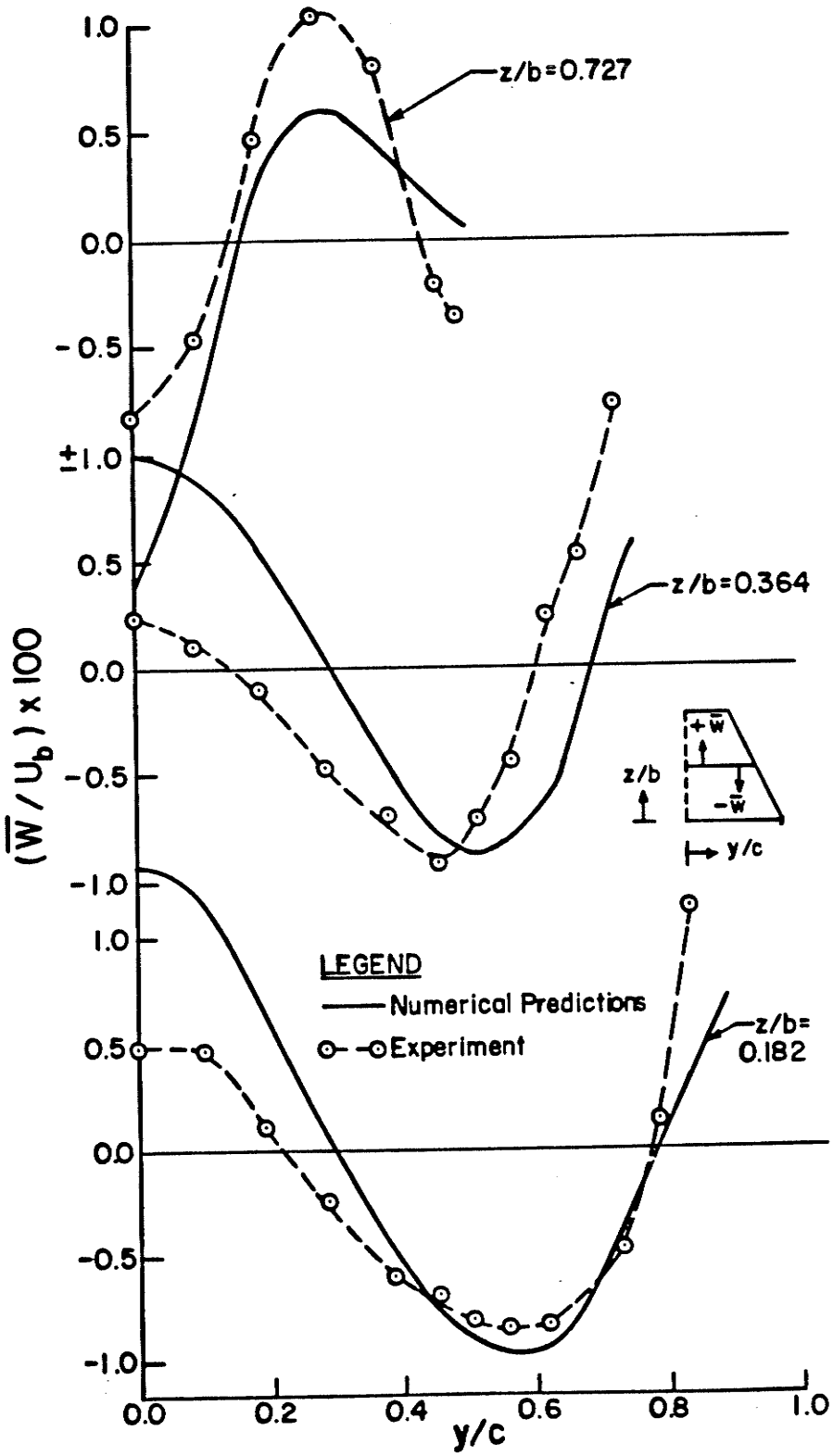

Fig. 46: Comparison of Predicted and Measured Secondary Flow Component $\bar{W}$; Re = 99,000.

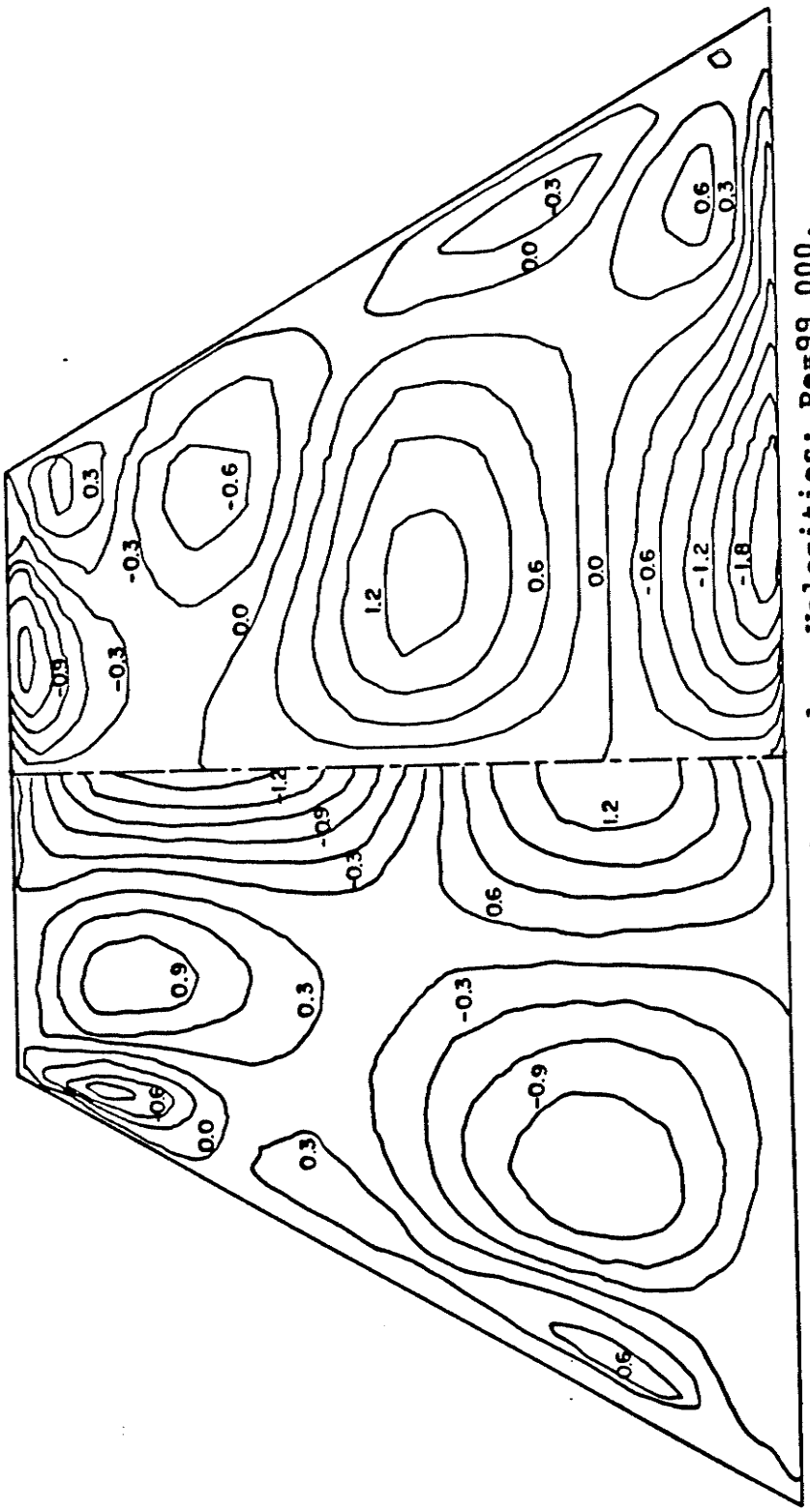

Fig. 47: Contour Plots of Secondary Velocities; Re=99,000.
Right : $(\overline{V}/U_b)\%$
Left : $(\overline{W}/U_b)\%$

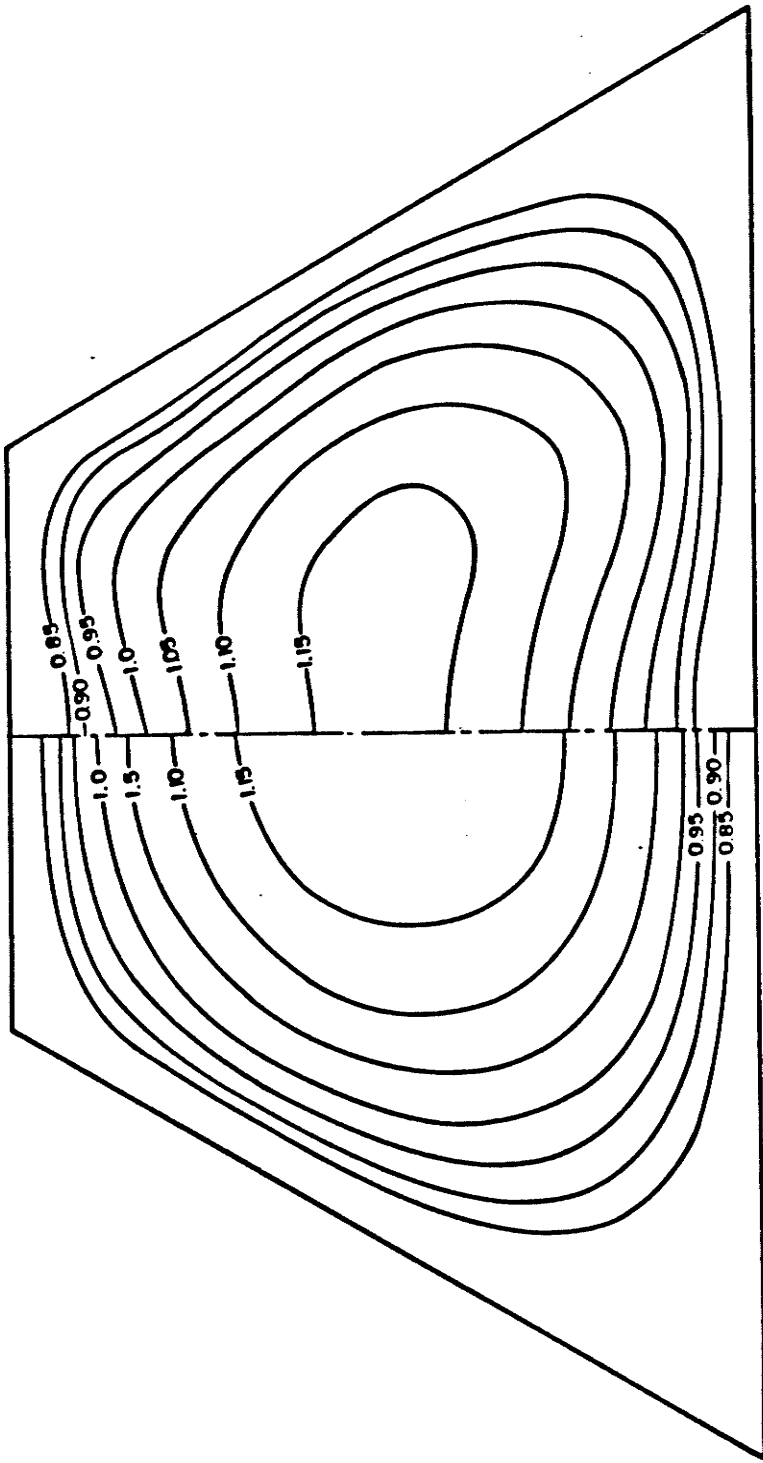

Fig. 48: Contour Plots of Temperature Distribution T*;
Re = 99,000.

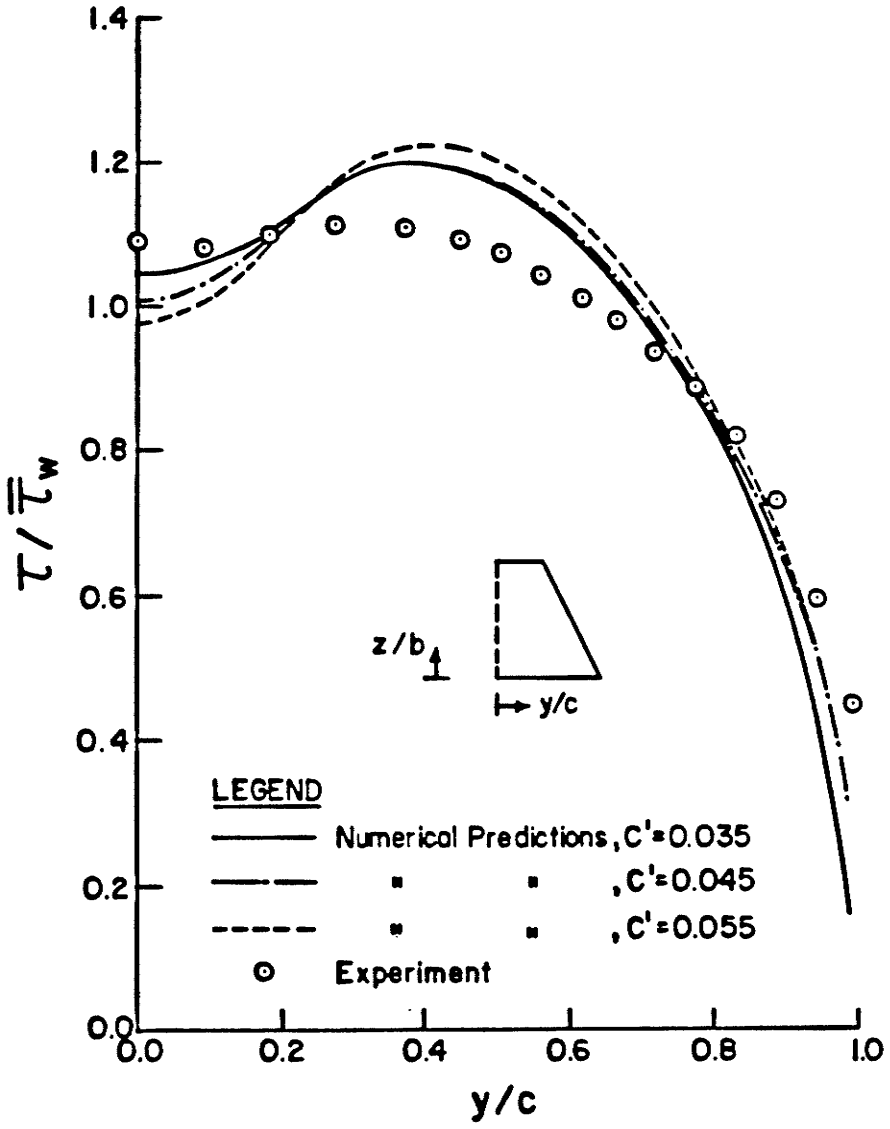

Fig. 49: Comparison of Predicted and Measured Local Wall Shear Stress for Bottom Wall; Re = 116,000.

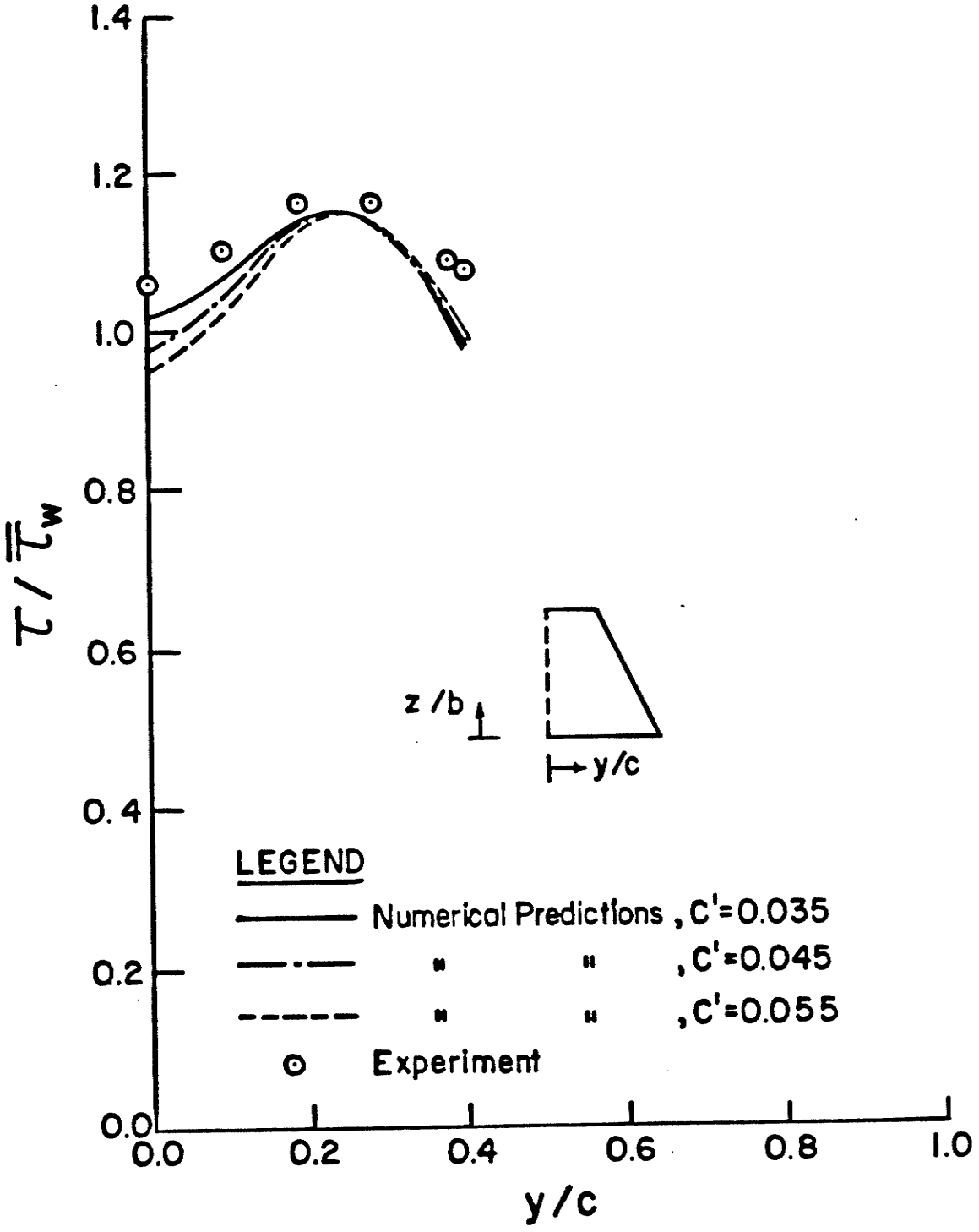

Fig. 50: Comparison of Predicted and Measured Local Wall Shear Stress for Top Wall; Re = 116,000.

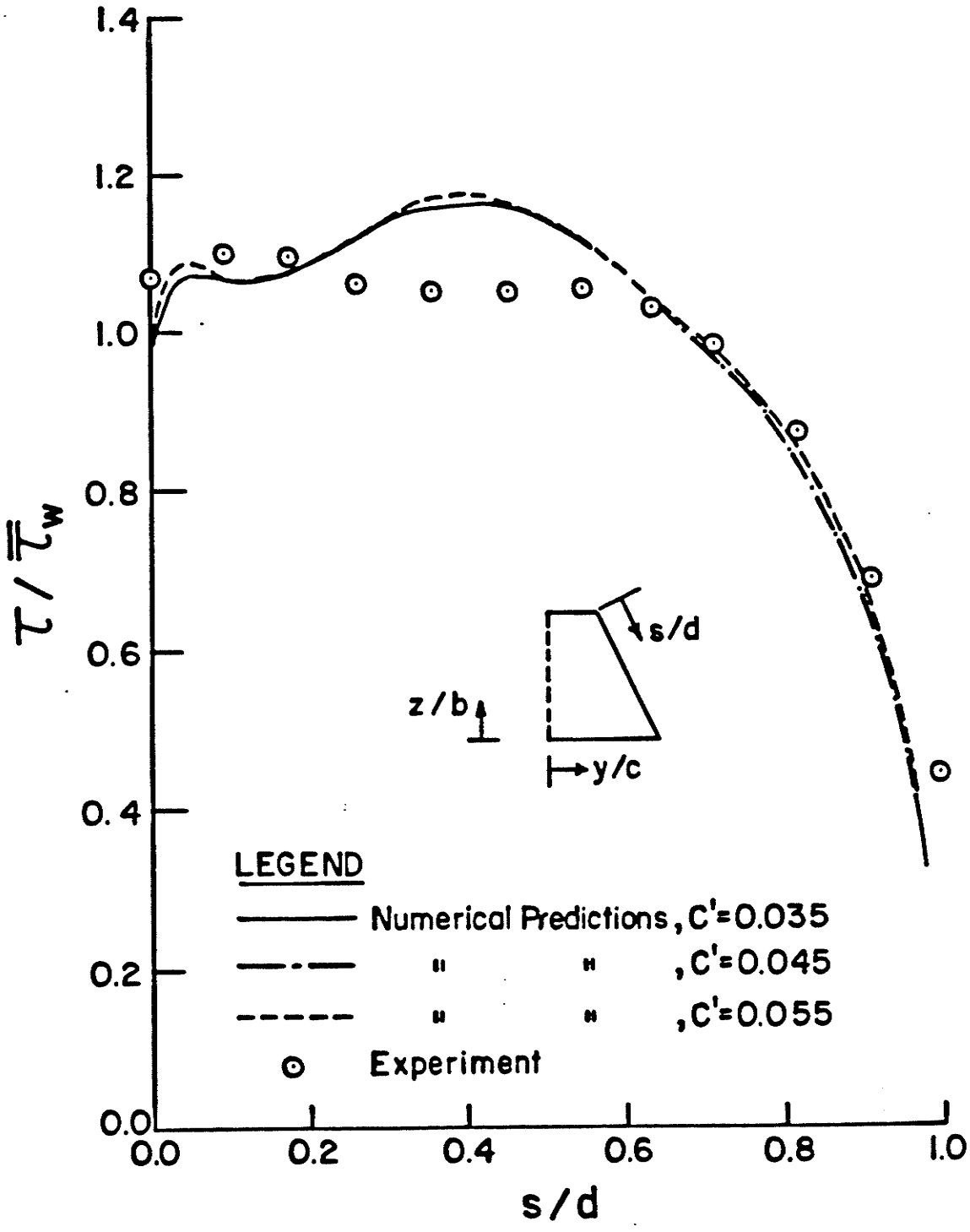

Fig. 51: Comparison of Predicted and Measured Local Wall Shear Stress for Inclined Wall; Re = 116,000.

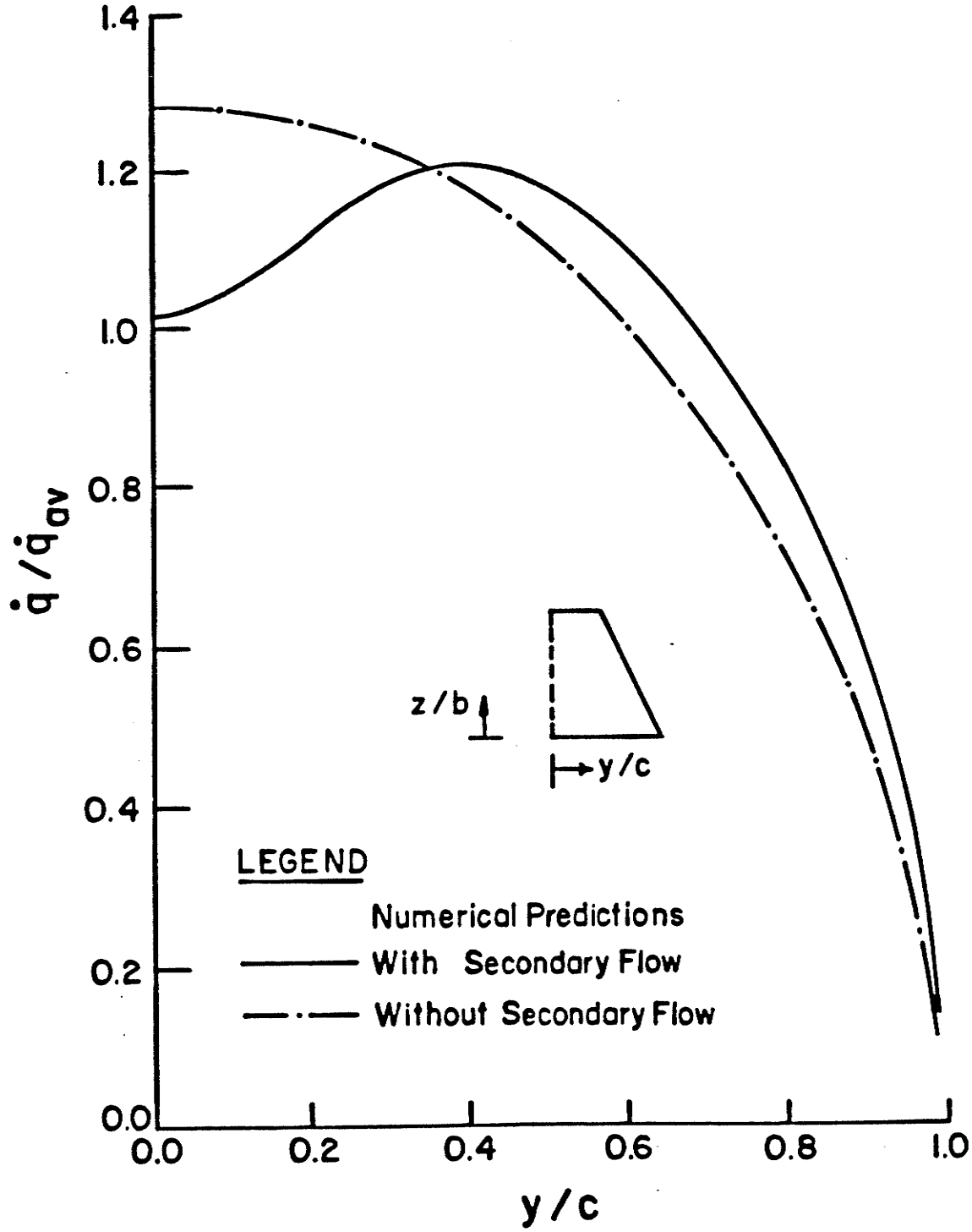

Fig. 52: Local Heat Flux Distribution Along the Bottom Wall; Re = 99,000.

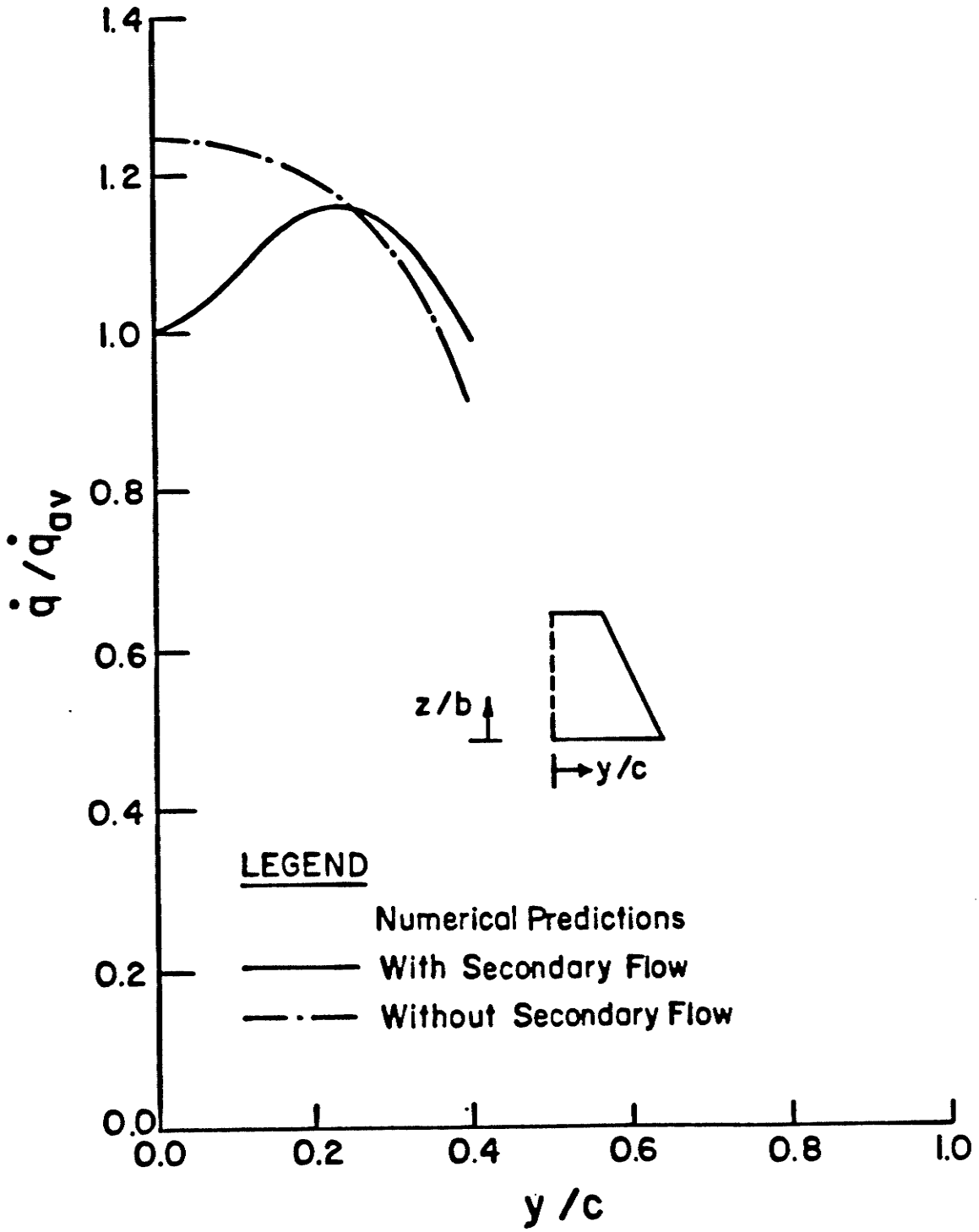

Fig. 53: Local Heat Flux Distribution Along the Top Wall; Re = 99,000.

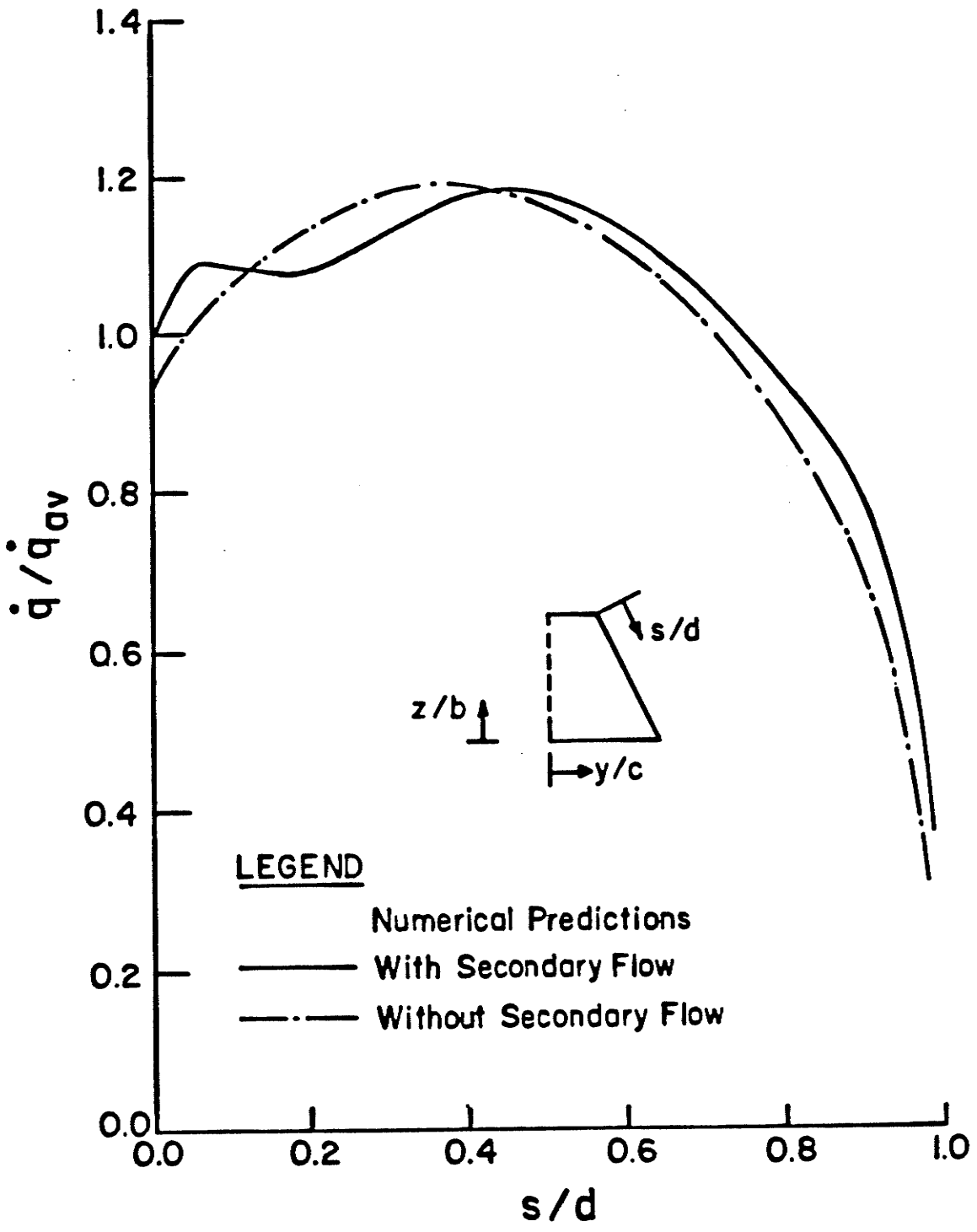

Fig. 54: Local Heat Flux Distribution Along the Inclined Wall; Re = 99,000.

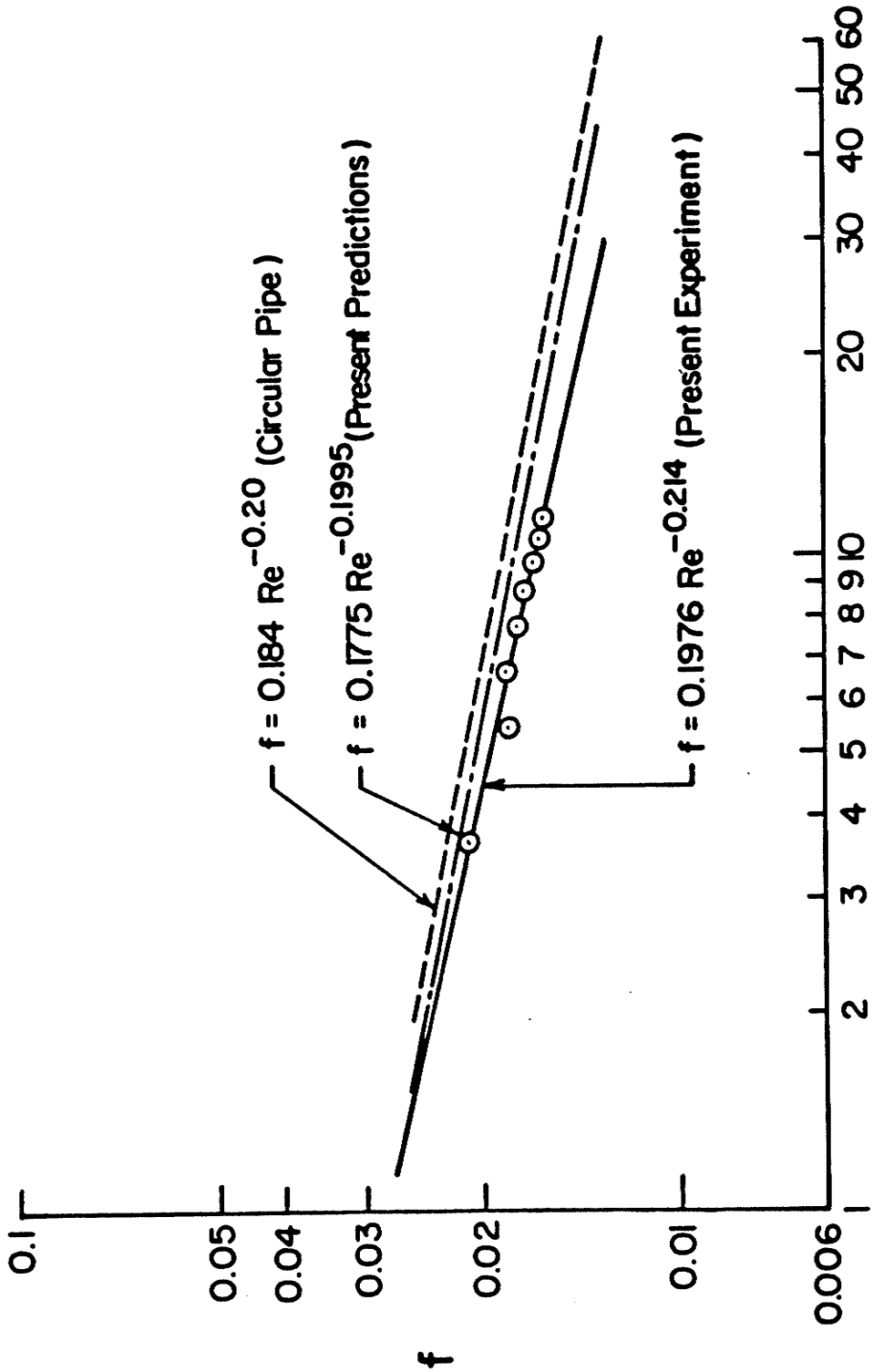

Fig. 55: Comparison of Predicted and Measured Friction Factors

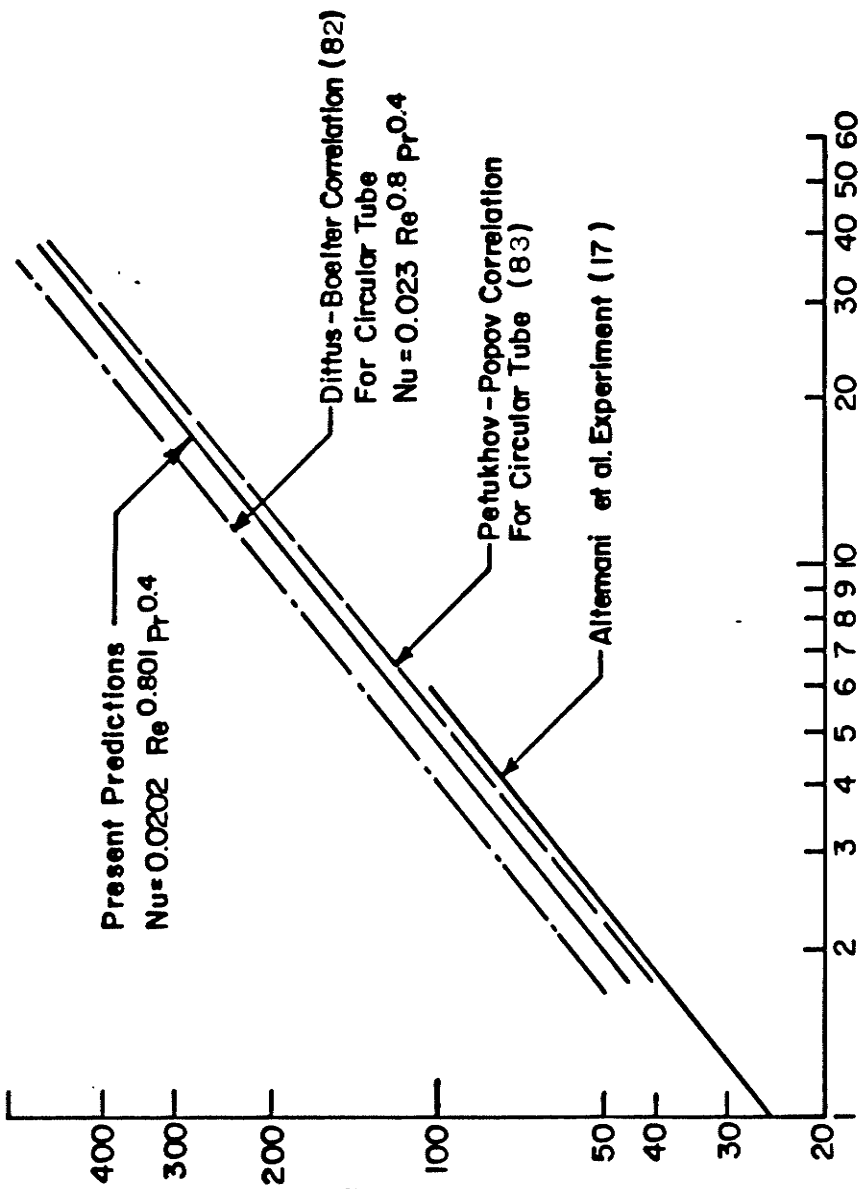

Fig. 56: Average Nusselt Number vs Reynolds Number; Pr = 0.712.

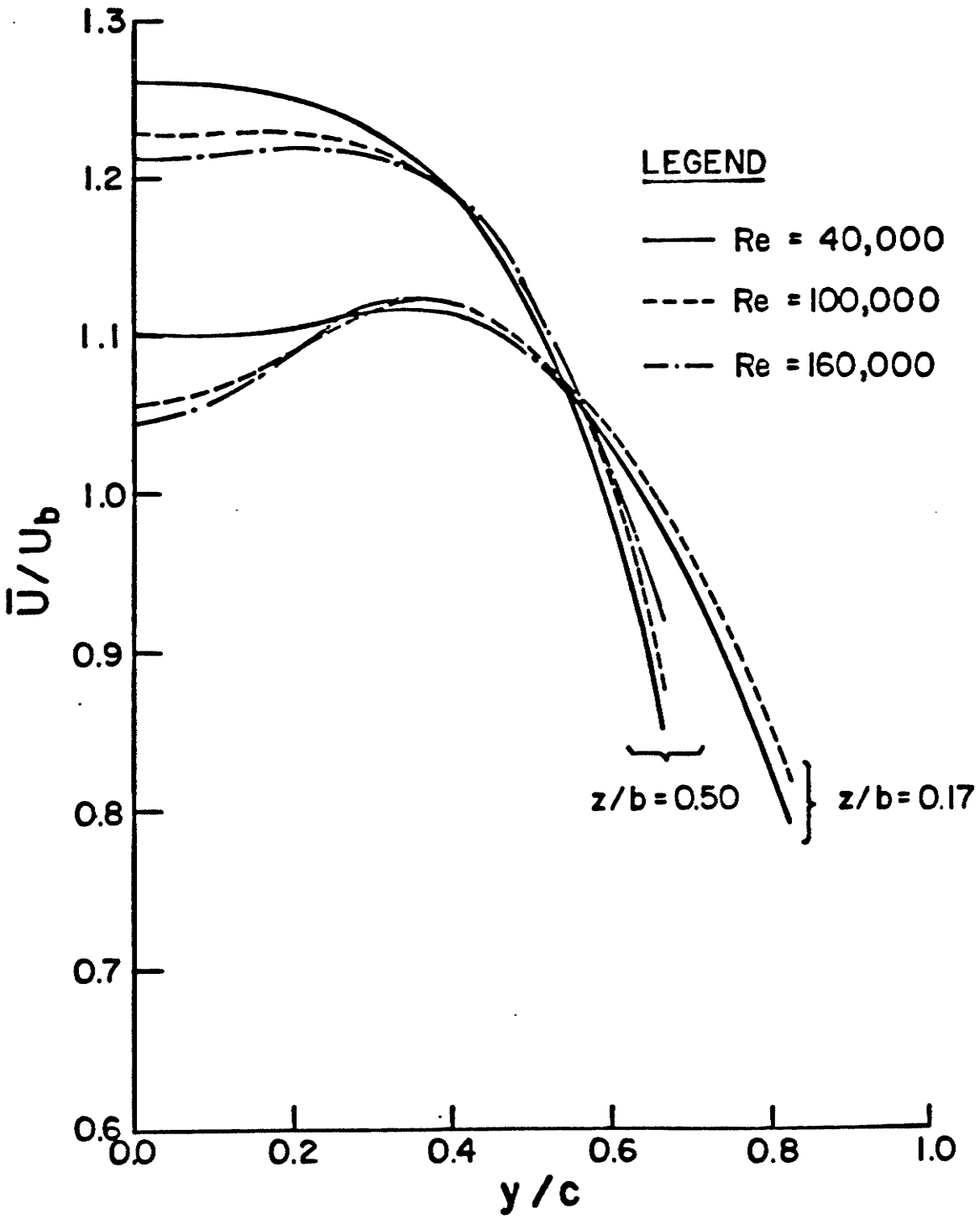

Fig. 57: Effect of Reynolds Number on $\bar{U}/U_b$.

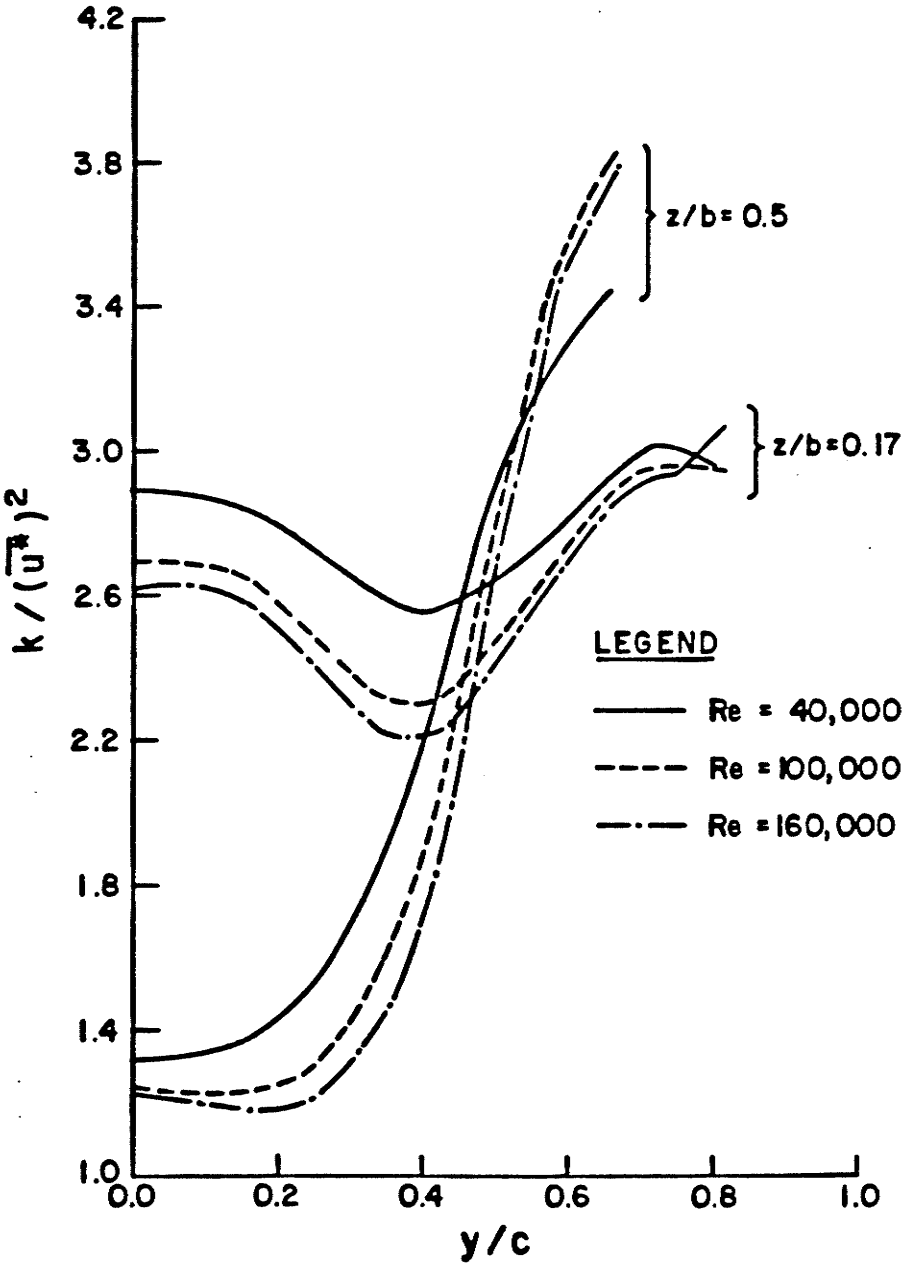

Fig. 58: Effect of Reynolds Number on $k/(\bar{u}^*)^2$.

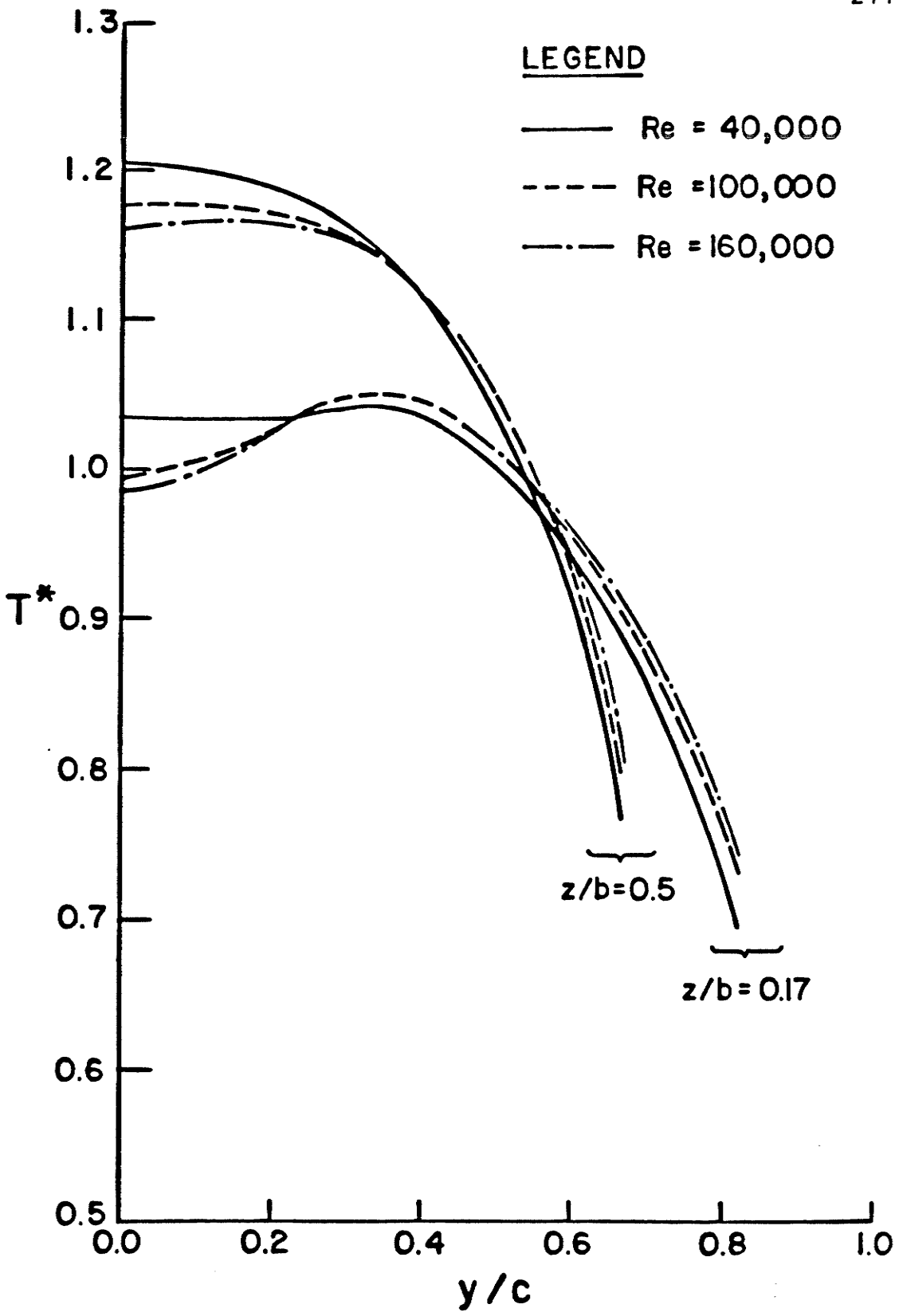

Fig. 59: Effect of Reynolds Number on T*.

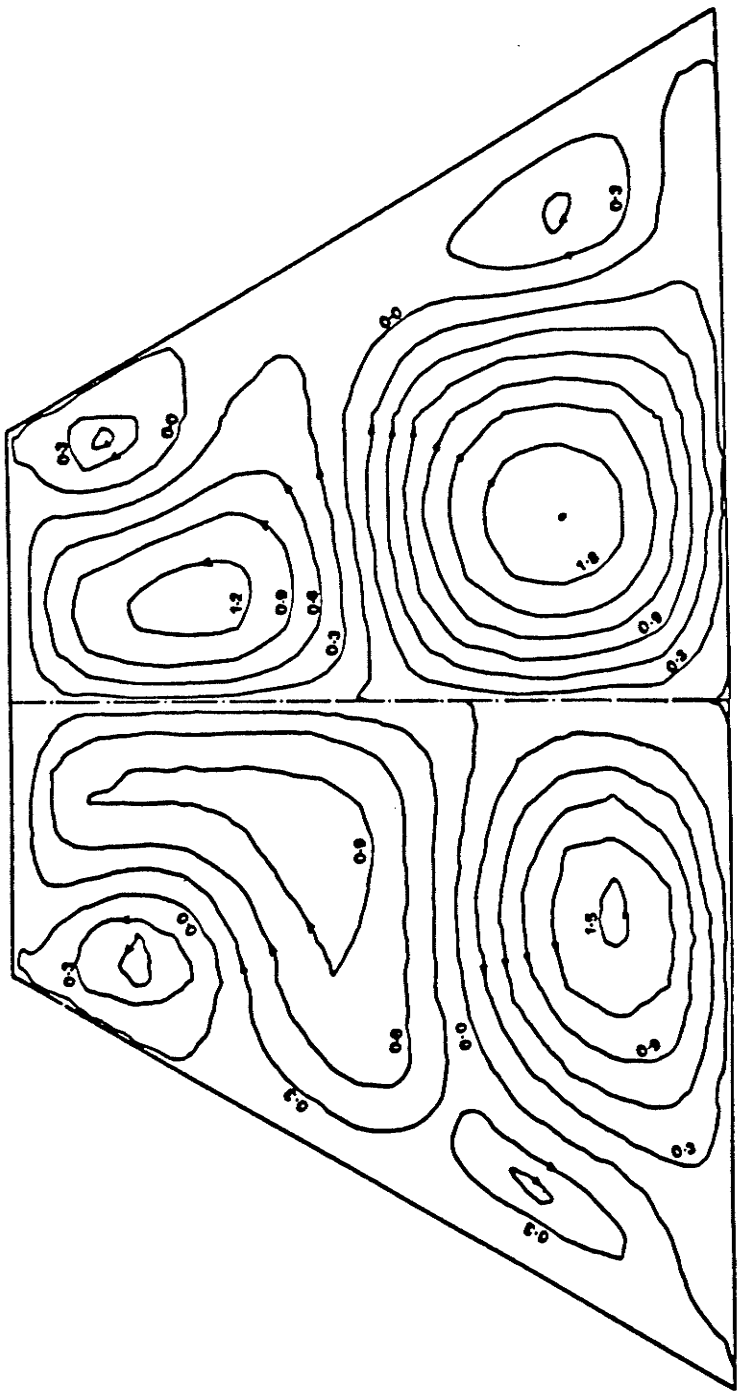

Fig. 60: Contour Plots of $\Psi/(\rho U_b D_h) \times 1000$;
Right : Re = 160,000,
Left : Re = 40,000.

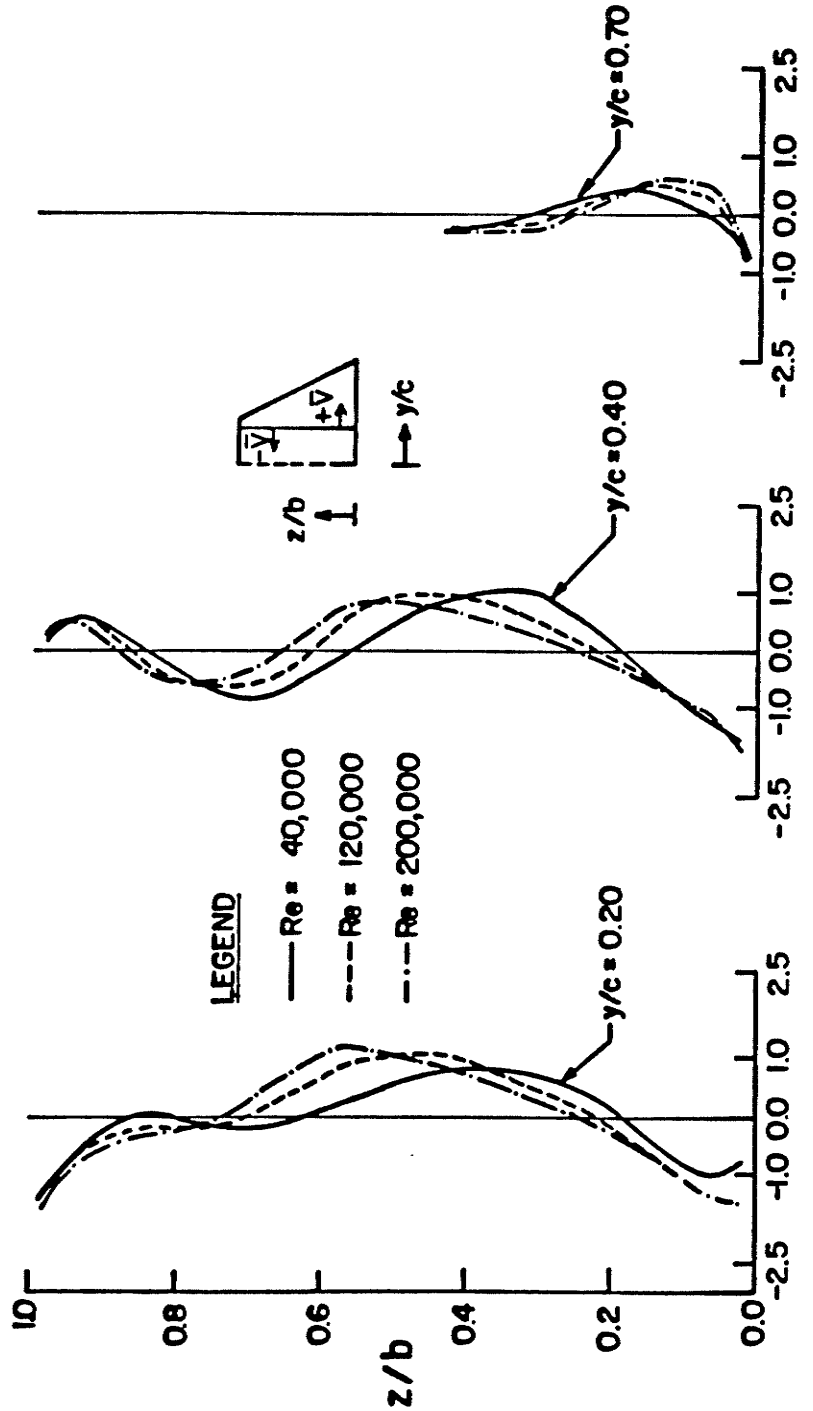

Fig. 61: Effect of Reynolds Number on $\bar{V}/U_b$.

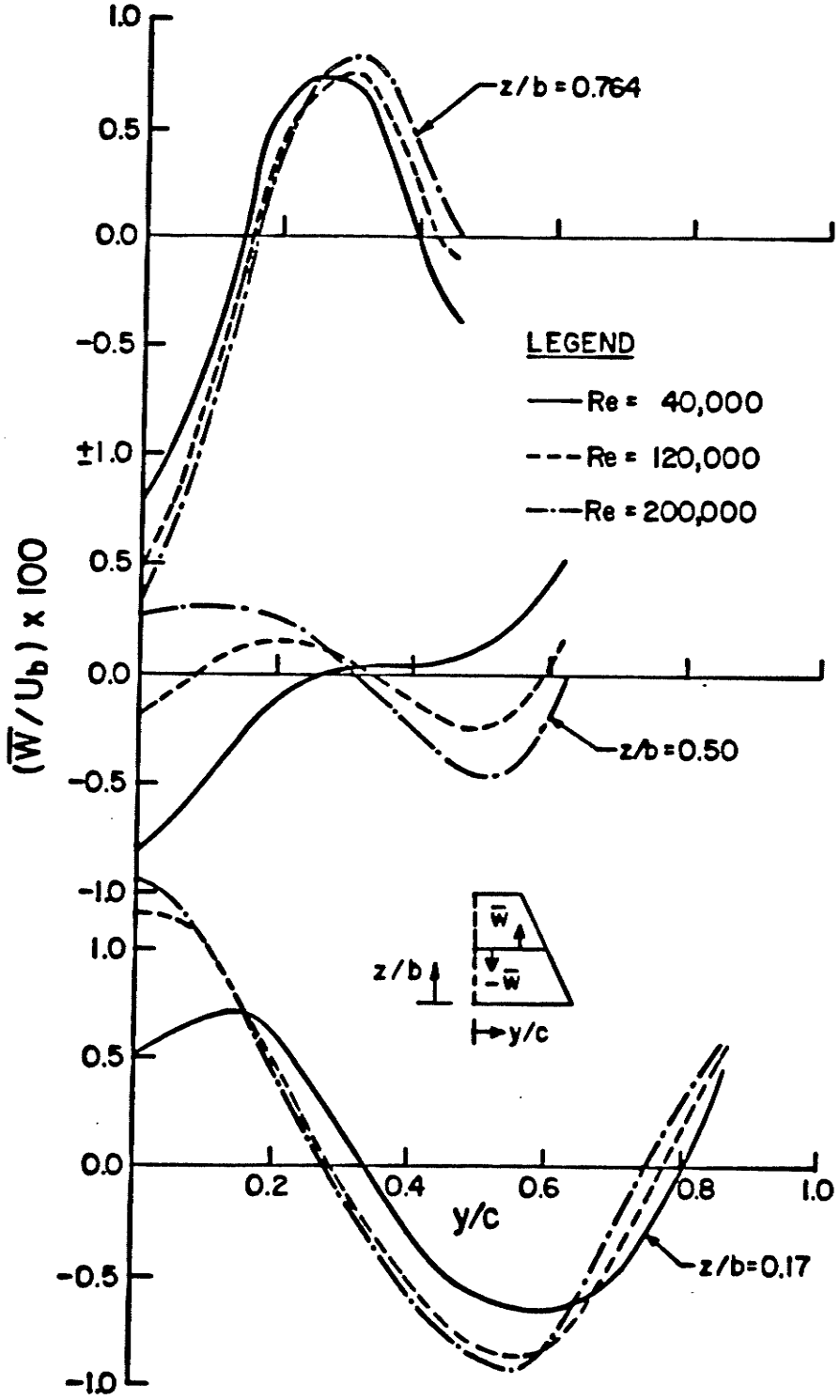

Fig. 62: Effect of Reynolds Number on $\overline{W}/U_b$.

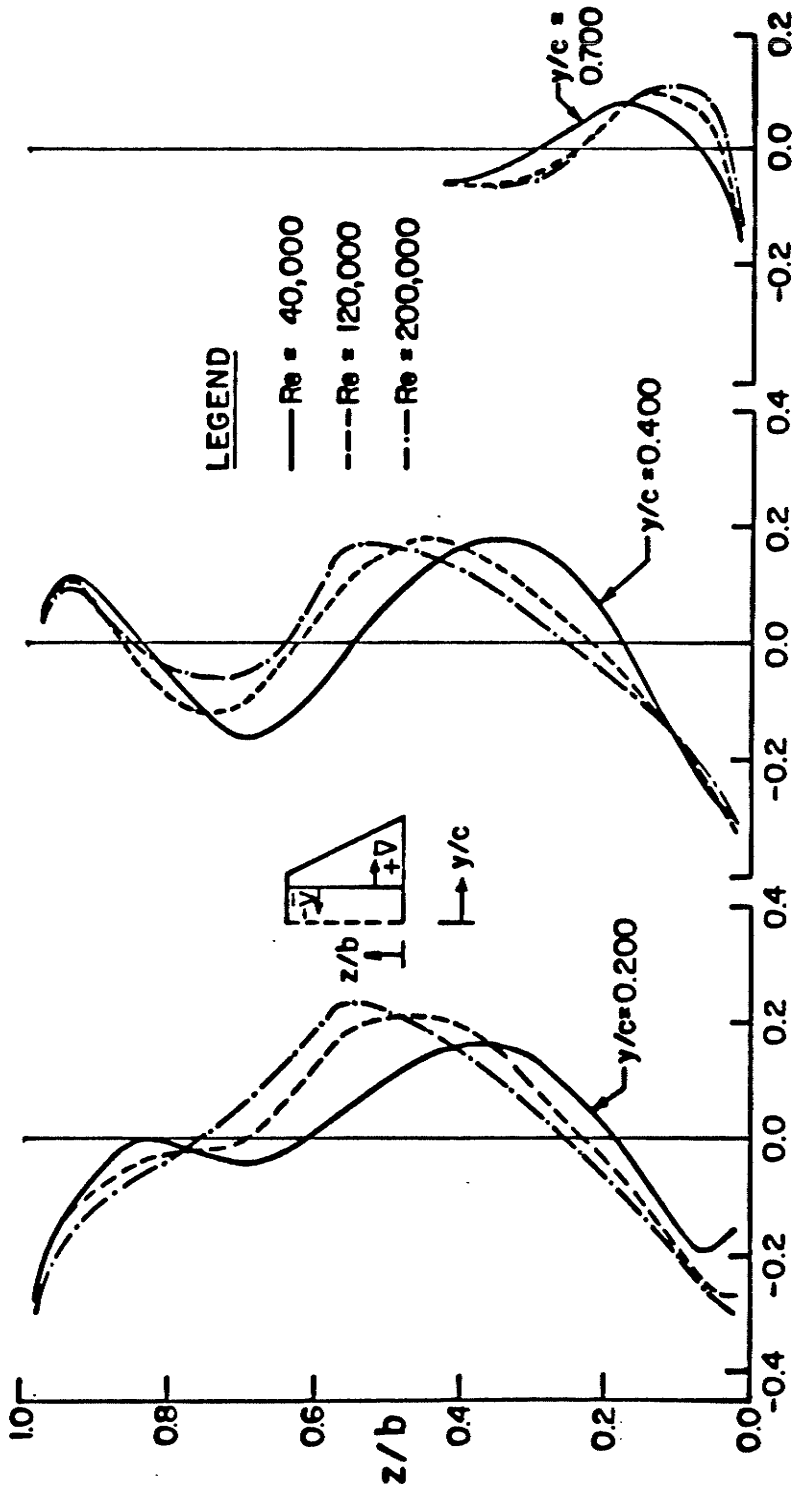

Fig. 63: Effect of Reynolds Number on $\overline{V}/\overline{u^*}$.

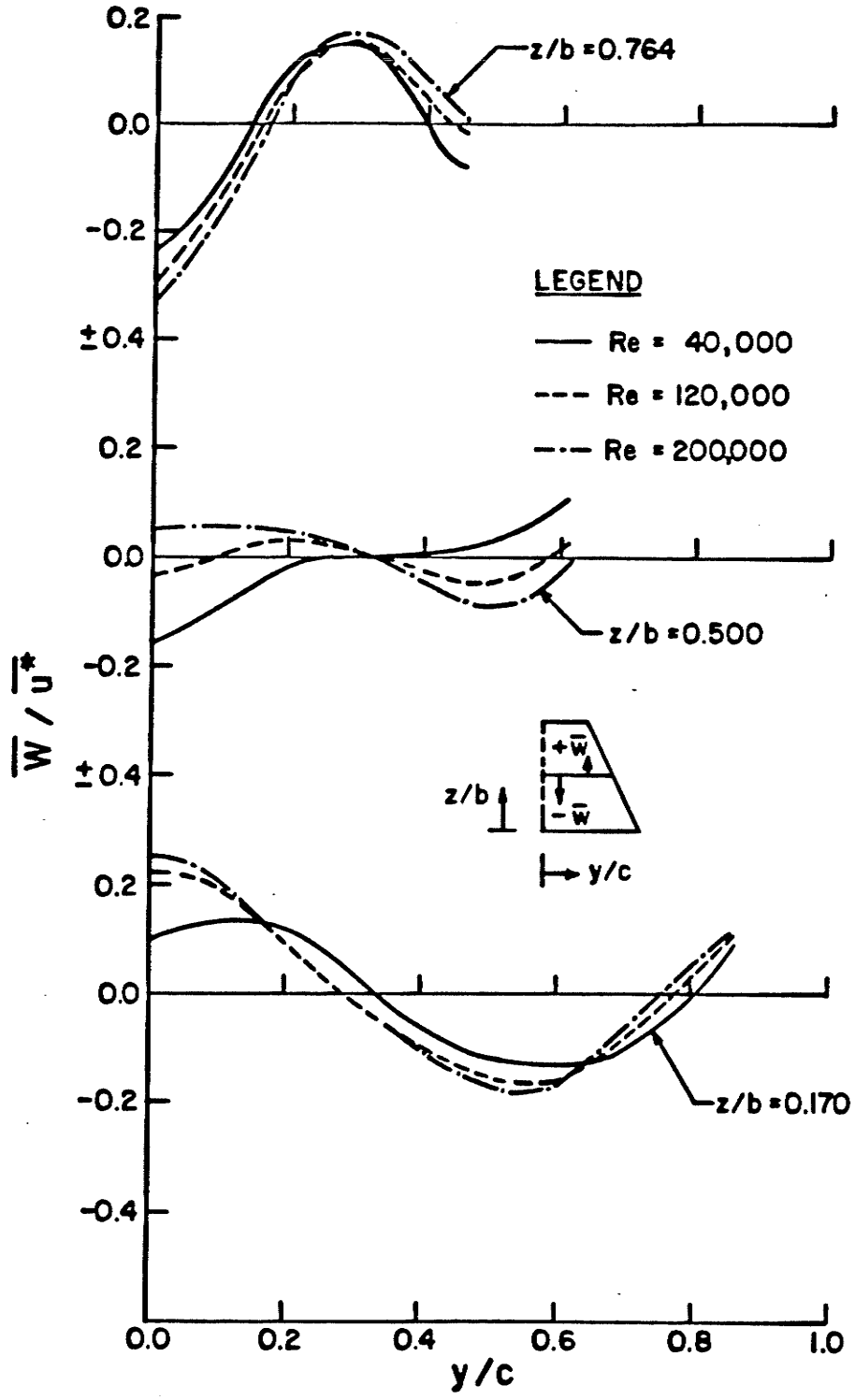

Fig. 64: Effect of Reynolds Number on $\overline{w}/\overline{u}^*$.

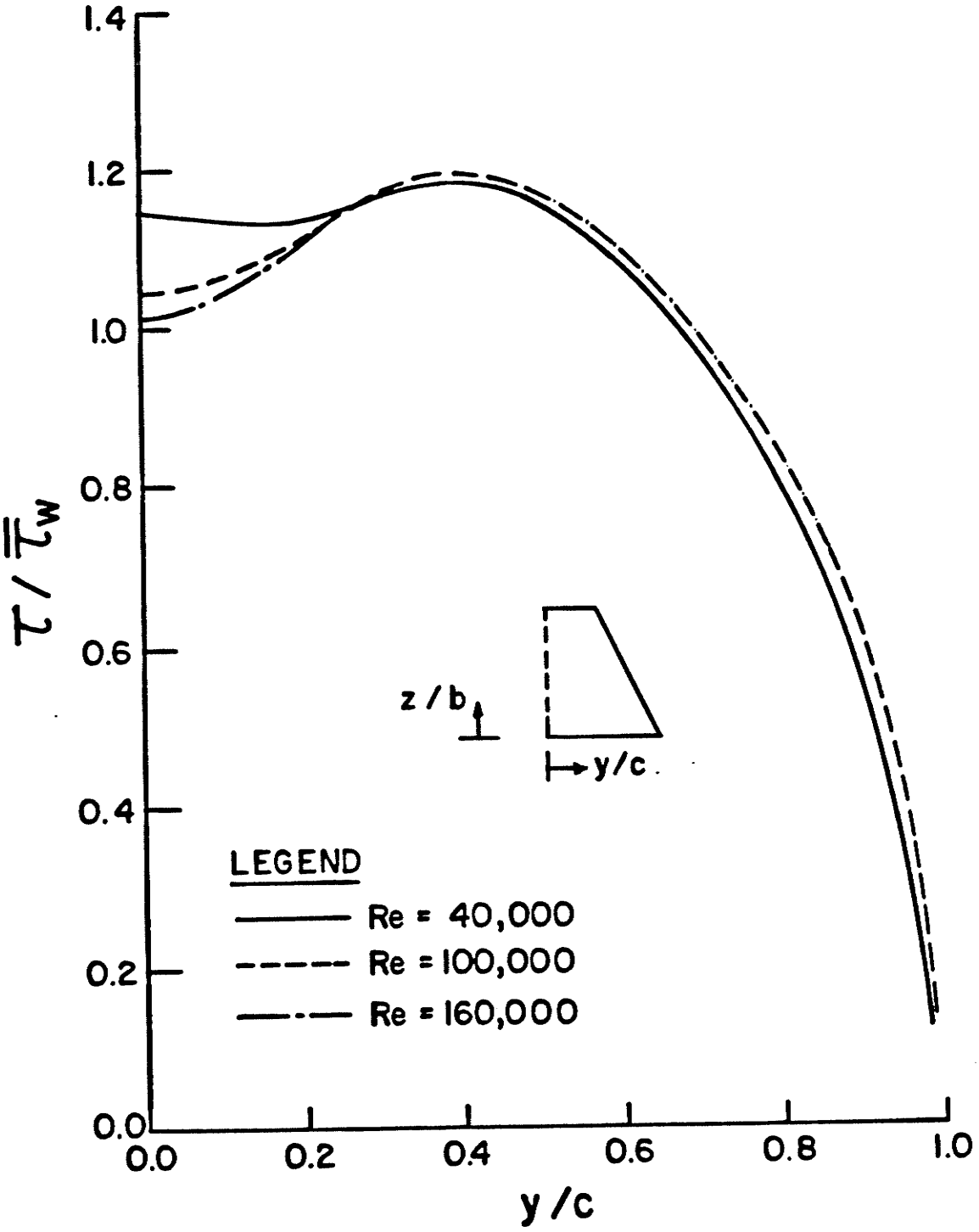

Fig. 65: Effect of Reynolds Number on Local Wall Shear Stress

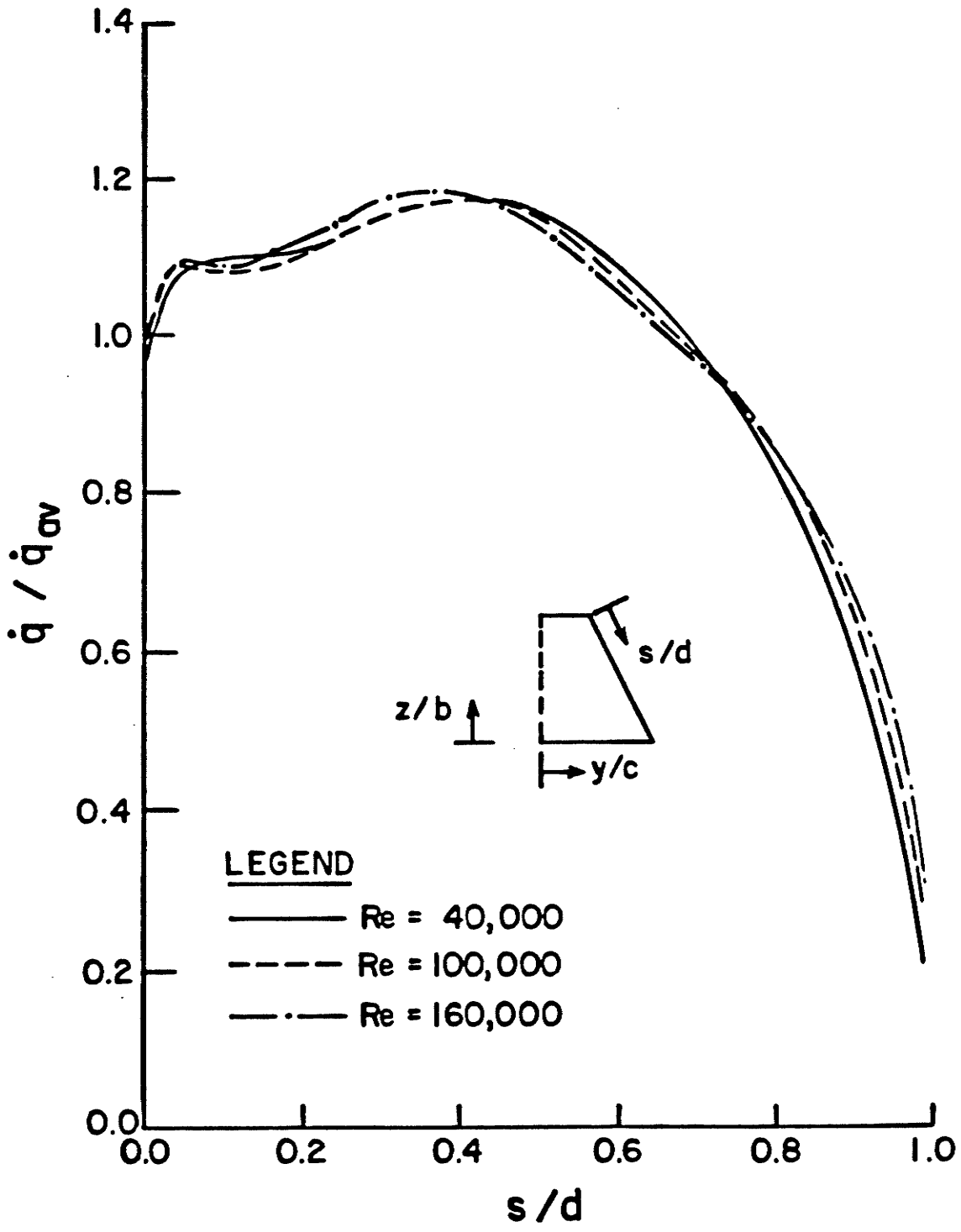

Fig. 66: Effect of Reynolds Number on Local Wall Heat Flux.

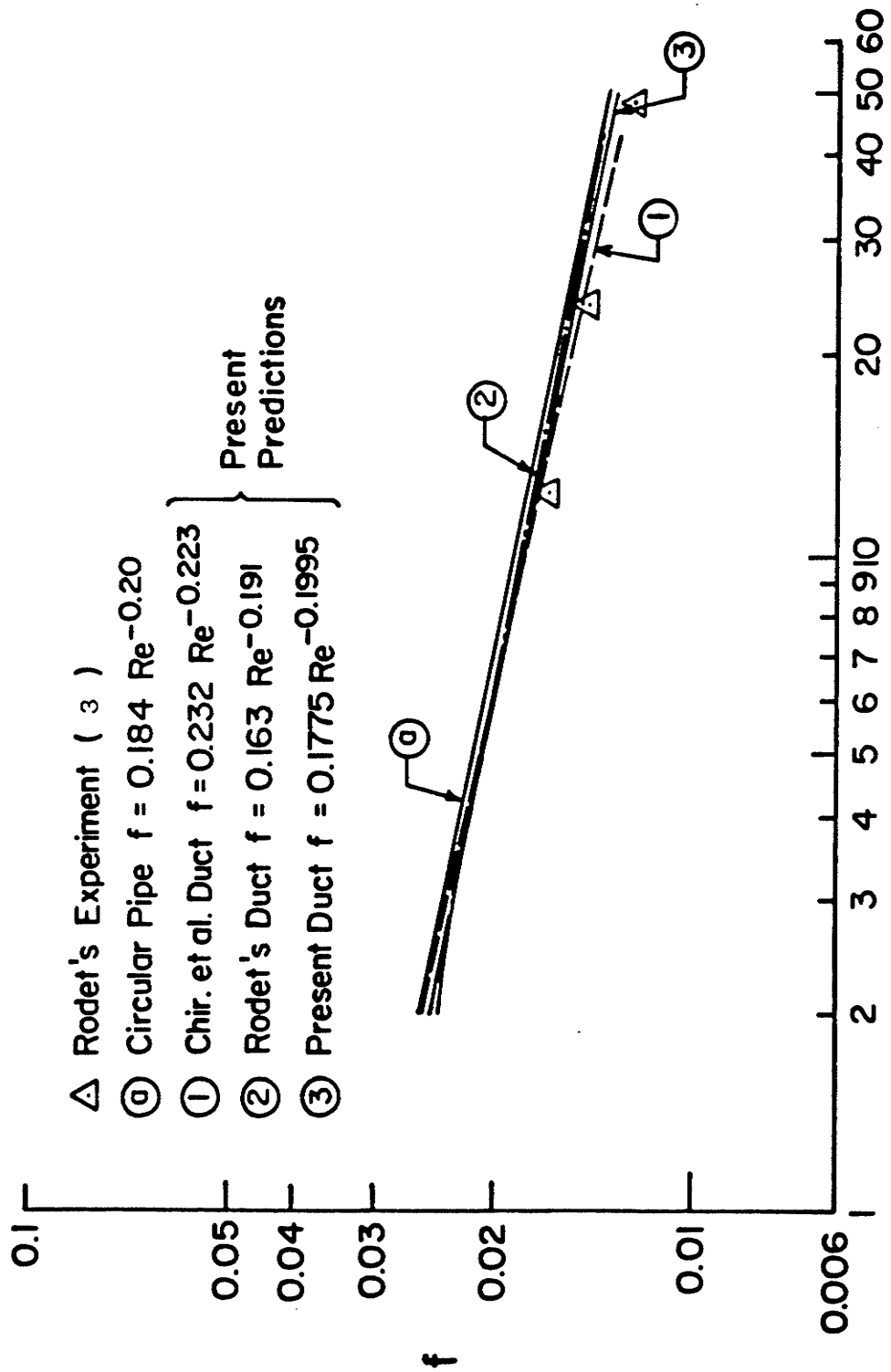

Fig. 67: Comparison of Friction Factors for Three Trapezoidal Ducts.

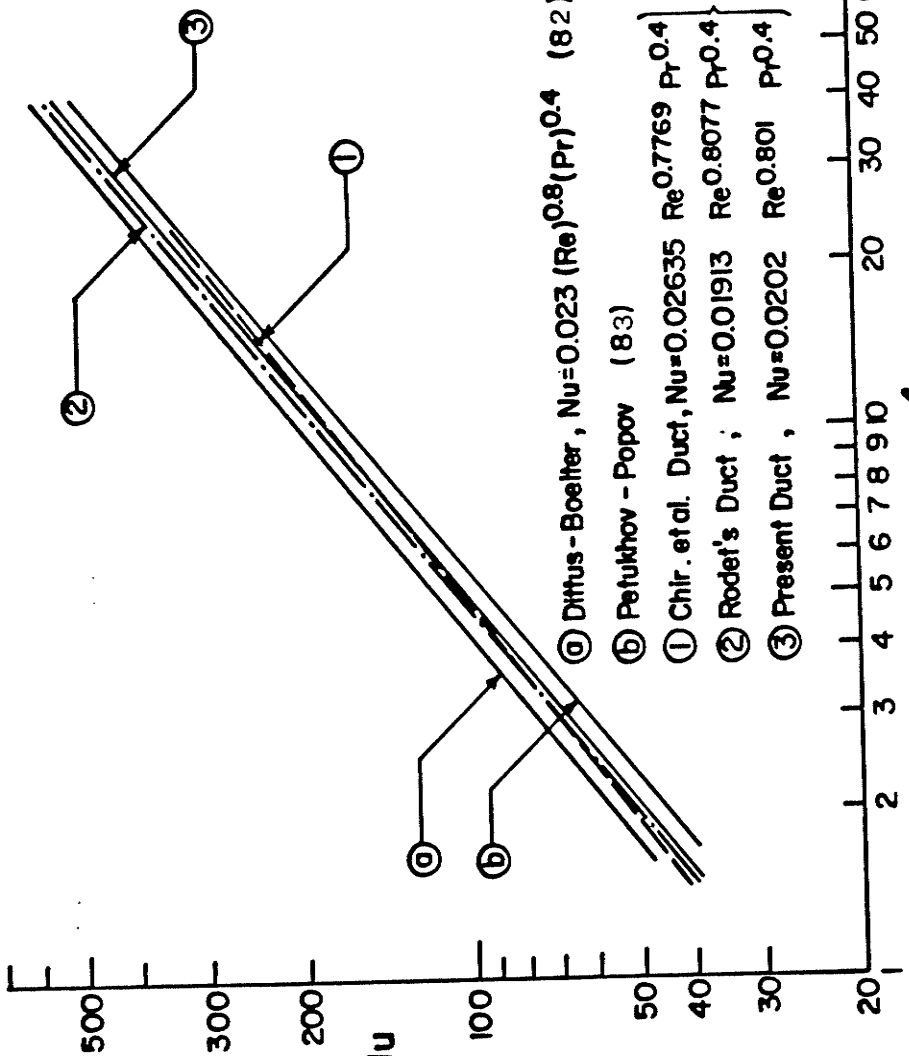

Fig. 68: Comparison of Nusselt Number for Three Trapezoidal Ducts; Pr=0.712.

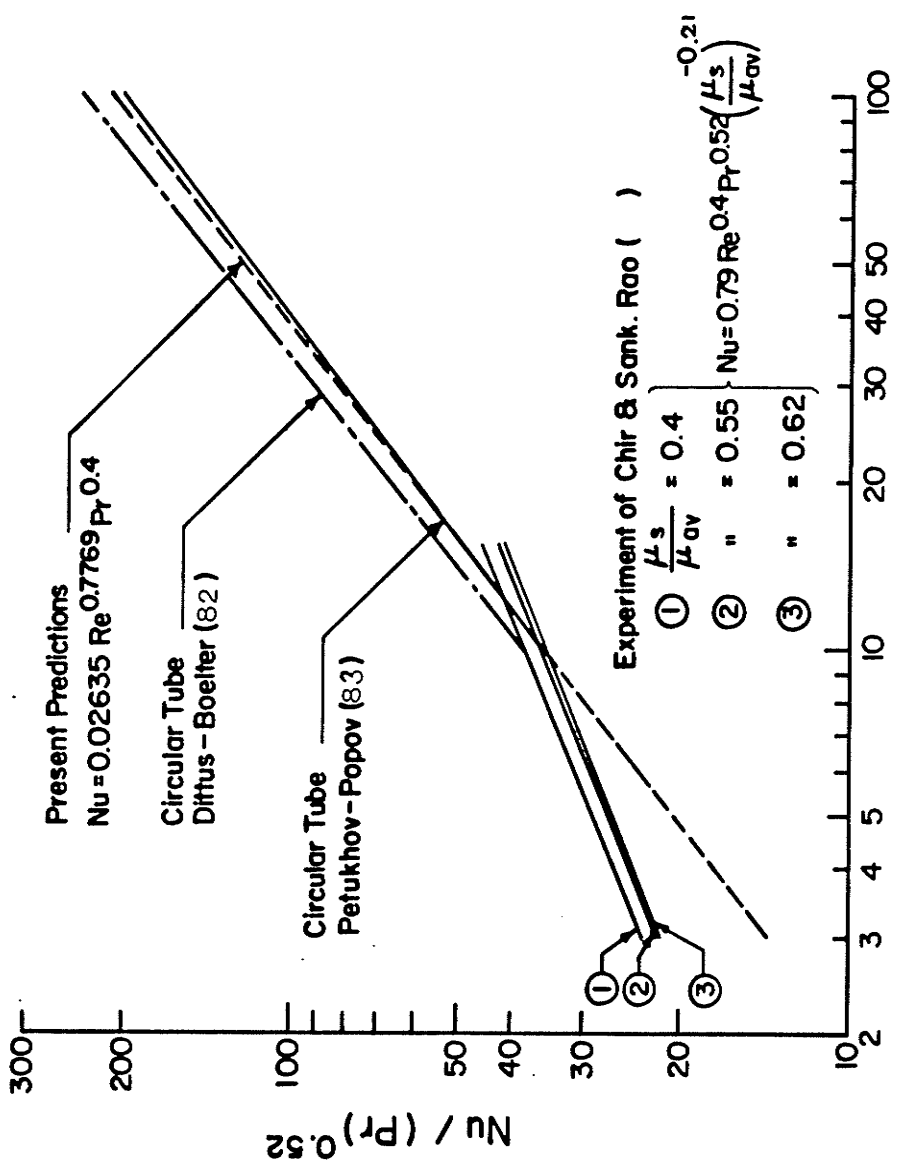

Fig. 69: Comparison of Nusselt Number with Experiment [4]; Pr=0.712.

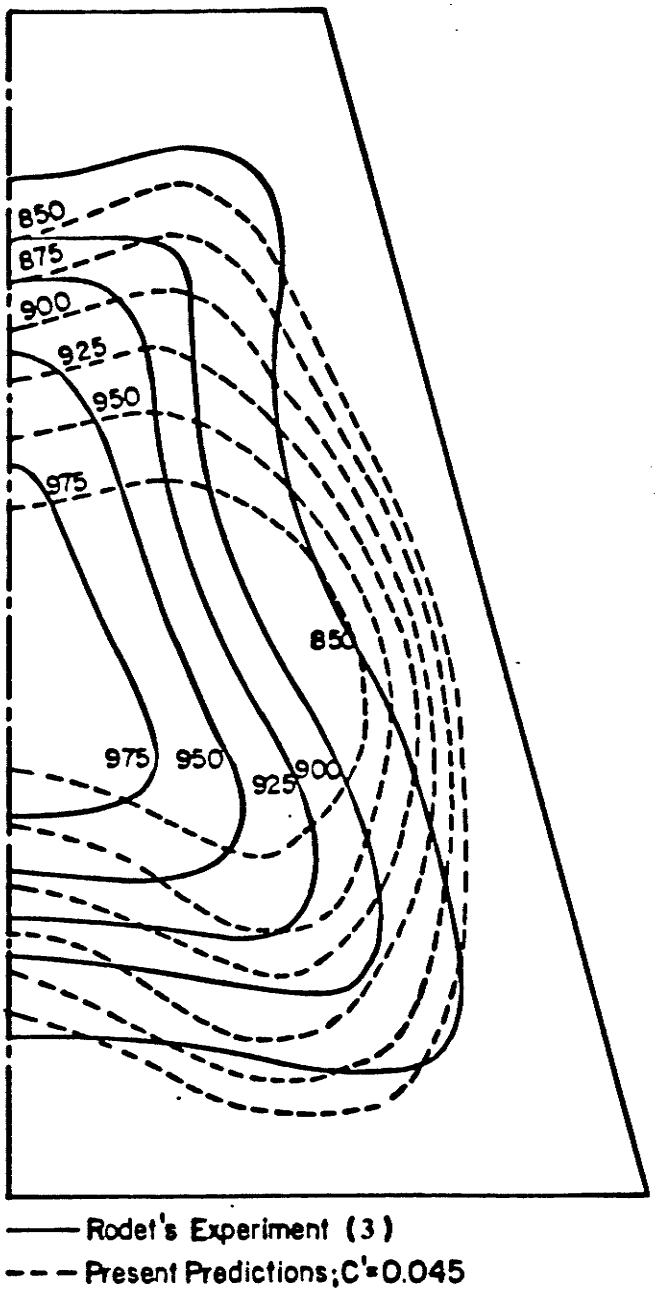

Fig. 70: Contour Plots of $(\bar{U}/\bar{U}_{max})$x1000; Re=240,000.

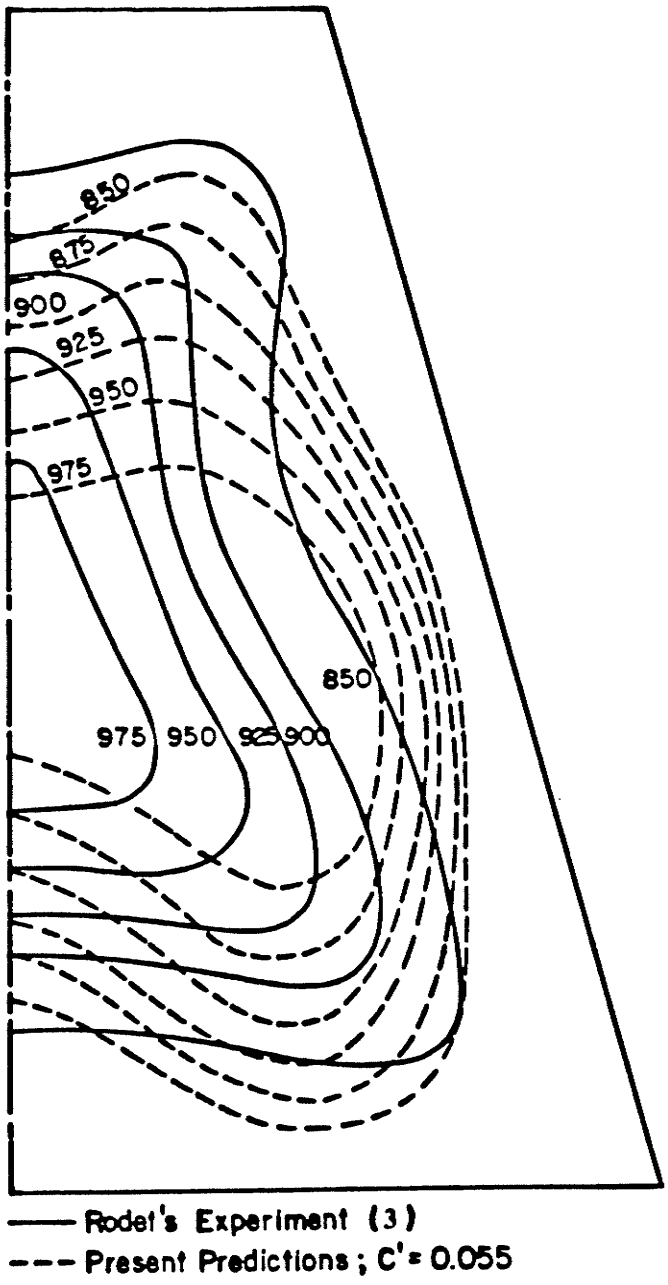

Fig. 71: Contour Plots of $(\bar{U}/\bar{U}_{max})$x1000; Re=240,000.

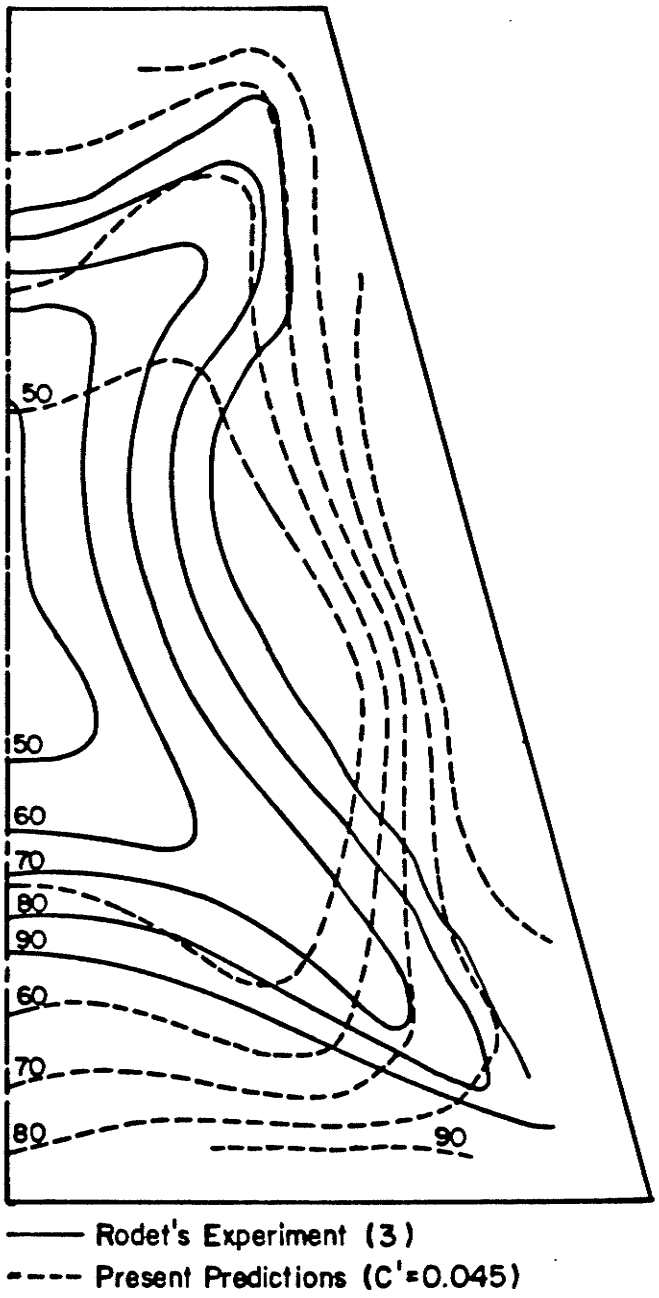

Fig. 72: Contour Plots of $2k/(\bar{U}_{max})^2 \times 10000$; Re=240,000.

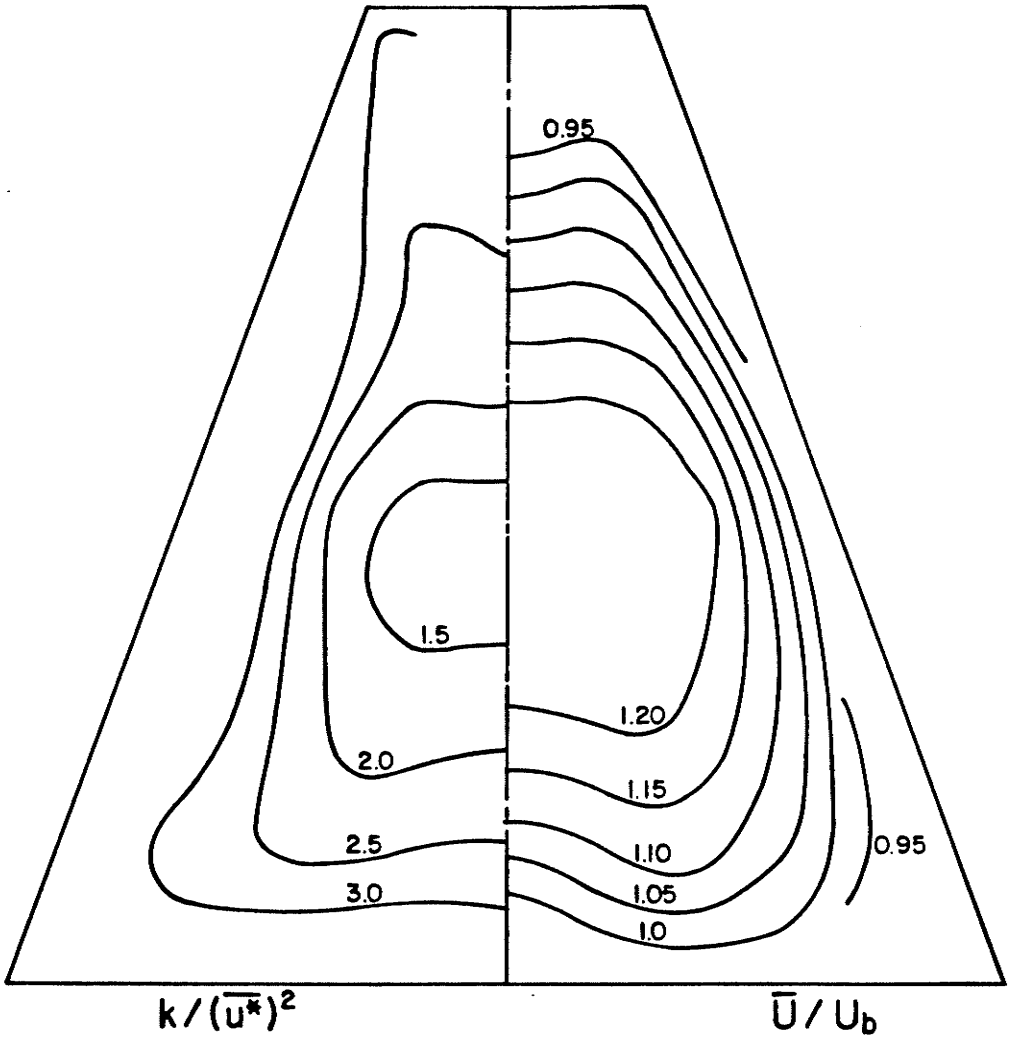

Fig. 73: Contour Plots of $k/(\bar{u}^*)^2$ and $\bar{U}/U_b$ for the Duct of [4]; Re=100,000.

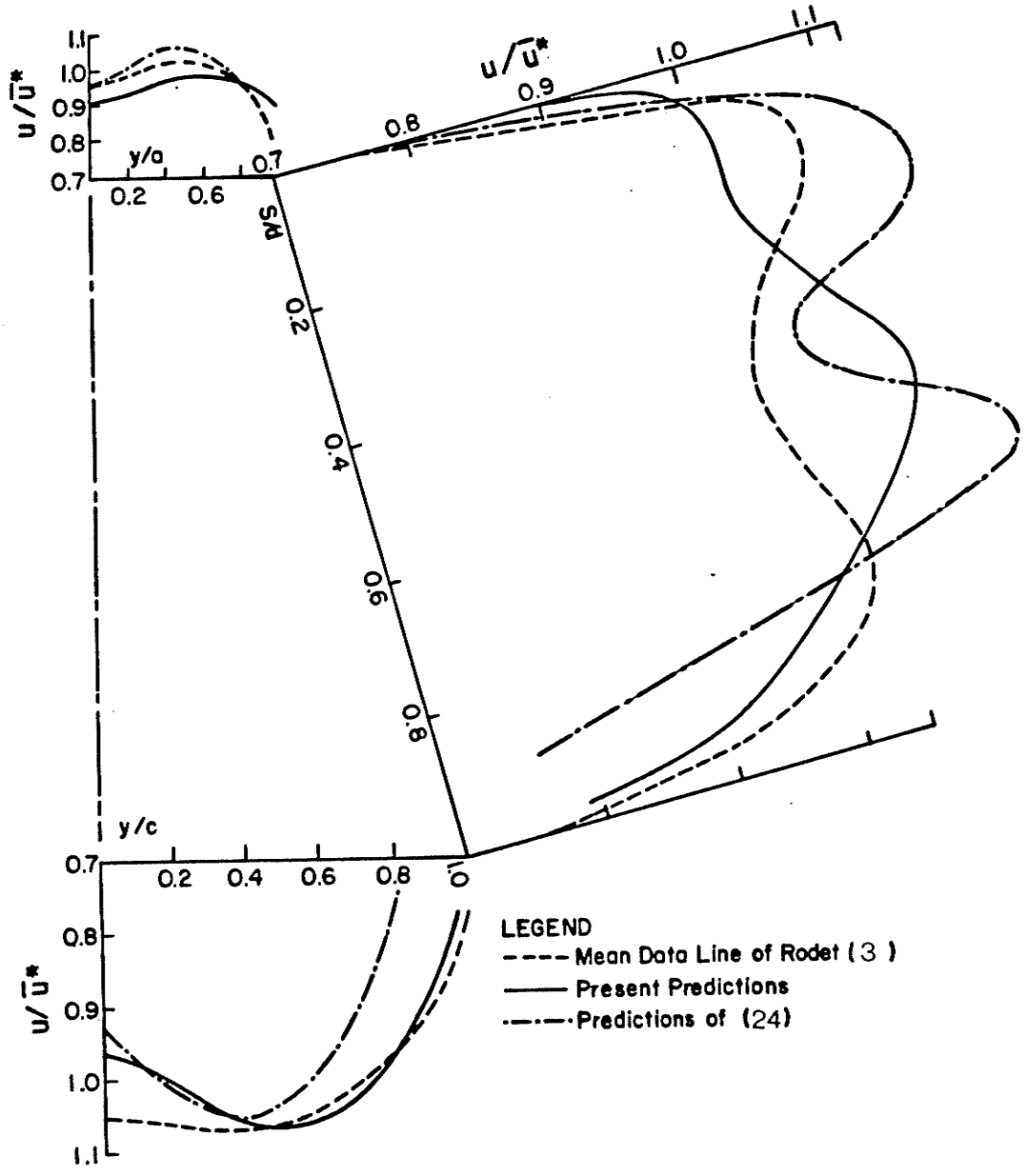

Fig. 74: Comparison of Local Friction Velocity With Experiment [3]; Re=240,000.

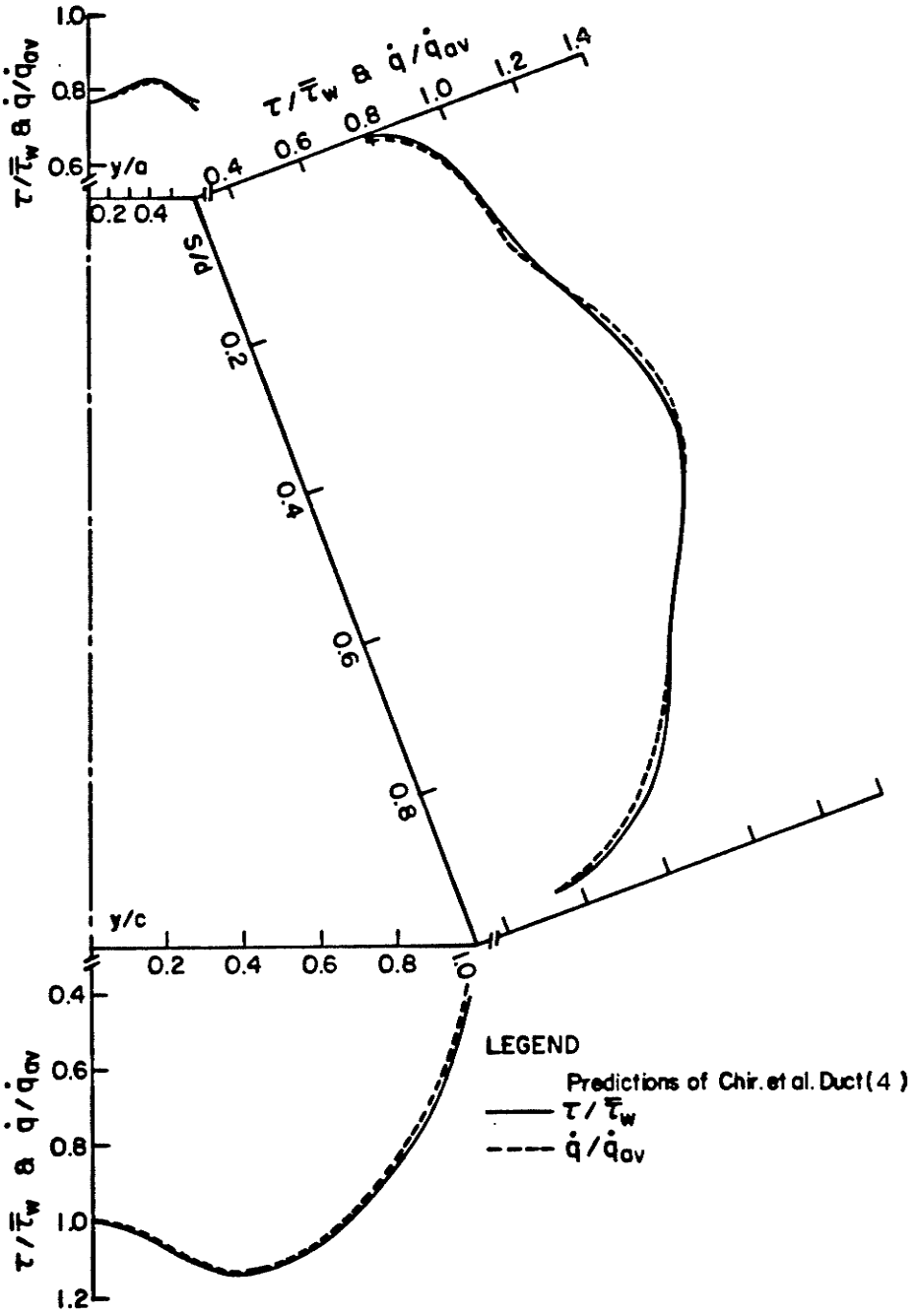

Fig. 75: Local Wall Shear Stress and Heat Flux for the Duct of [4]; Re=100,000.